USE OF FALLING WEIGHT DEFLECTOMETER MULTI-LOAD DATA FOR PAVEMENT STRENGTH ESTIMATION

Final Report
(Report No. FHWA/NC/2002-006)

To North Carolina Department of Transportation
(Research Project No. HWY-00-4)

Submitted by

Y. Richard Kim, Ph.D., P.E.
Campus Box 7908
Department of Civil Engineering
North Carolina State University
Raleigh, NC 27695-7908
Ph: 919-515-7758
Fax: 919-515-7908
E-mail: kim@eos.ncsu.edu

Heemun Park, Ph.D.
Former Graduate Student

Department of Civil Engineering
North Carolina State University
Raleigh, NC

June 2002

Technical Report Documentation Page

1. Report No. FHWA/NC/2002-006	2. Government Accession No.	3. Recipient's Catalog No.
4. Title and Subtitle Use of FWD Multi-Load Data for Pavement Strength Estimation		5. Report Date May 28, 2002 6. Performing Organization Code
7. Author(s) Y. Richard Kim and Heemun Park		8. Performing Organization Report No.
9. Performing Organization Name and Address Campus Box 7908, Department of Civil Engineering North Carolina State University		10. Work Unit No. (TRAIS) 11. Contract or Grant No. HWY-00-04
12. Sponsoring Agency Name and Address North Carolina Department of Transportation		13. Type of Report and Period Covered Final Report July 1999 – June 2001 14. Sponsoring Agency Code
15. Supplementary Notes		

16. Abstract

The objective of this study is to develop a mechanistic-empirical method for assessing pavement layer conditions and estimating the remaining life of flexible pavements using multi-load level Falling Weight Deflectometer (FWD) deflections. A dynamic finite element program, incorporating a stress-dependent soil model, was developed to generate the synthetic deflection database. Based on this synthetic database, the relationships between surface deflections and critical pavement responses, such as stresses and strains in each individual layer, have been established. A condition assessment procedure for asphalt pavements that uses multi-load level FWD deflections has been developed using these relationships. The verification study was conducted using field data. The results indicate that the proposed procedure can estimate the base and subgrade layer conditions. It was found from the study for the nonlinear behavior of a pavement structure that an FWD test with a load of 12 kip or less does not result in any apparent nonlinear behavior of the subgrade in aggregate base pavements. The study also indicated that the deflection ratio obtained from multi-load level deflections may predict the type and quality of the base/subgrade materials. With regard to the condition assessment of the asphalt concrete (AC) layer, the AC layer modulus and the tensile strain at the bottom of the AC layer were found to be better indicators than deflection basin parameters.

The procedures for performance prediction of fatigue cracking and rutting were developed for flexible pavements. The drastically increasing trend in fatigue cracking with time may not be predicted accurately using the proposed procedure. Such trends may be due to the environmental effects and the inconsistent distress measurements. Predicted rut depths using multi-load level deflections show good agreement with measured rut depths over a wide range of rutting. However, the procedure using single load level deflections consistently underpredicts the rut depths. It was concluded that the rutting prediction procedure using multi-load level deflections can estimate an excessive level of rutting quite well and, thus, improve the quality of prediction for rutting potential in flexible pavements.

The layer condition assessment procedure and the remaining life prediction algorithms developed in this project were incorporated into APLCAP (Asphalt Pavement Layer Condition Assessment Program) version 2.0, the VisualBasic program developed under the NCHRP 10-48 project.

17. Key Words FWD, Multi-Load, Pavement Condition, Remaining Life, Fatigue, Rutting, Finite Element Model, APLCAP	18. Distribution Statement		
19. Security Classif. (of this report)	20. Security Classif. (of this page)	21. No. of Pages	22. Price

Form DOT F 1700.7 (8-72) **Reproduction of completed page authorized**

DISCLAIMER

The contents of this report reflect the views of the authors and not necessarily the views of the University. The authors are responsible for the facts and the accuracy of the data presented herein. The contents do not necessarily reflect the official views or policies of either the North Carolina Department of Transportation or the Federal Highway Administration at the time of publication. This report does not constitute a standard, specification, or regulation.

ACKNOWLEDGMENTS

This research was sponsored by the North Carolina Department of Transportation and the Federal Highway Administration. Our Technical Advisory Committee consisted of George Gibson, P.E., Chair; Moy Biswas, Ph.D., P.E.; Judith Corley-Lay, Ph.D., P.E.; and Jim Travis, P.E. These advisors have given invaluable direction and support to us throughout the project. The principal investigator wishes to thank these people for their significant contributions to the research.

TABLE OF CONTENTS

LIST OF TABLES

LIST OF FIGURES

CHAPTER 1

INTRODUCTION

1.1 Background

The Falling Weight Deflectometer (FWD) is an excellent device for evaluating the structural capacity of pavements in service for rehabilitation designs. Because the FWD test is easy to operate and simulates traffic loading quite well, many state highway agencies utilize it widely for assessing pavement conditions.

Generally, surface deflections obtained from FWD testing have been used to backcalculate in situ material properties using an appropriate analysis technique, or to predict the pavement responses and then determine the strength and remaining life of the existing pavement. The typical testing program consists of three drops of the FWD, each with a load of approximately 9 kip although the FWD is capable of imparting multiple load levels ranging from about 4 kip to about 16 kip, with little additional effort in operation.

Multi-load level deflection data could result in significant enhancement of pavement engineers' ability to estimate the strength and remaining life of pavements. To illustrate this point, deflection data under multi-load levels are plotted in Figure 1.1 for US 70 section (5.5 in. thick AC layer and 11 in. thick aggregate base) and Section 20 (9 in. thick AC full depth) of US 421. At the time of FWD testing, the US 70 section was one year old and in good condition, whereas some surface cracks were visible in US 421 Section 20. It was obvious that these two pavements had different strengths and

remaining lives. However, the deflection basins of these two pavements under a 9 kip load were identical. Using the current method based on single-load level (9 kip) data would result in the same overlay thickness being used for both pavements in spite of their different strengths and conditions, if these pavements are subjected to equal traffic volume and truck traffic.

The effect of these different strengths of these two pavements becomes evident when multi-load level data are compared. As shown in Figure 1.1, Section 20 underwent a greater increase in deflections as the load level increased than US 70 section did. It is well known that the elastic moduli of unbound materials are stress dependent. When a 9 kip load is used in FWD testing, the resulting stress and strain levels are low enough to neglect the errors associated with using a stress dependent material model. However, the analysis of higher load level deflections requires consideration of the nonlinear behavior of materials. The nonlinear behavior of pavement material induced by multi-load levels necessitates the use of the finite element method with a stress dependent material model.

It seems clear that this added information would provide another dimension in our pavement analysis and would improve our knowledge of the relative urgency of various pavement rehabilitation projects. Although this information can be obtained at no additional cost in terms of testing time, traffic control requirements for field investigations, and changes to the equipment, the lack of a reliable analysis method of multi-load level data prohibits pavement engineers from taking advantage of this readily available information.

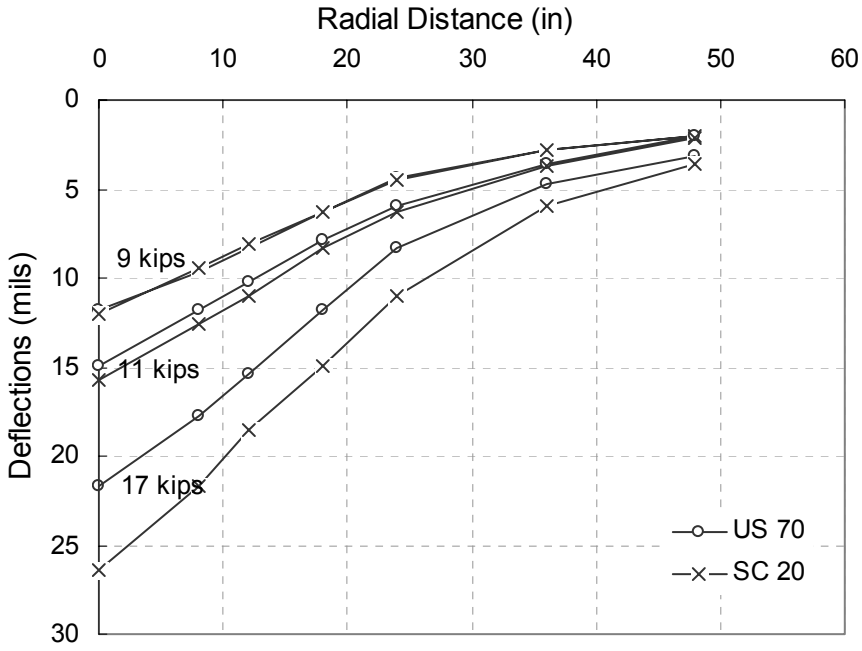

Figure 1.1. Different effects of multi-load levels on deflections from pavements with different strengths.

1.2 Objectives and Scope

The objective of this study is to develop analysis methods for assessing pavement layer conditions and estimating the remaining life of asphalt concrete pavements using multi-load level FWD deflections. The static and dynamic finite element programs incorporating a stress dependent soil model were developed to generate the synthetic deflection database. Based on this synthetic database, the relationships between surface deflections and critical pavement responses, such as stresses and strains in each individual layer (Pavement Response Models), have been established. Pavement response models and field databases such as coring, destructive testing, and visual

distress surveys were employed to develop relationships between critical pavement responses and pavement strength or performance (Pavement Performance Models).

Since the performance and the state of stress of asphalt concrete pavements over a cement-treated base or a Portland cement concrete (PCC) slab are quite different from those of other asphalt concrete pavements, the scope of this study is limited to full-depth asphalt concrete pavement and asphalt concrete pavement with an aggregate base course. Pavement performance characteristics to be investigated in this study include load-related fatigue cracking and permanent deformation.

CHAPTER 2

DEVELOPMENT OF PAVEMENT RESPONSE MODELS

Pavement surface deflections measured using a Falling Weight Deflectometer (FWD) test provide valuable information for the structural evaluation of asphalt concrete pavements. The performance of a pavement structure may be monitored by measuring the surface rut depth and observing the fatigue cracking. The pavement response models presented in this chapter are used to bridge surface deflections and performance of the pavement structure.

There are several pavement responses that have been identified by other researchers as good performance indicators (Garg et al., 1998 and Kim et al., 2000). They include: (1) tensile strain at the bottom of the AC layer for fatigue cracking and vertical compressive strain in the AC layer for permanent deformation; (2) vertical compressive strain on the top of the base layer for permanent deformation; and (3) vertical compressive strain on the top of the subgrade for permanent deformation. To investigate the effectiveness of load level as a determinant of the condition of pavement layers, it was desirable to predict the change in critical pavement responses in each individual layer caused by an increase in load level.

2.1 Existing Pavement Response Models

Deflection basin parameters (DBPs) derived from either the magnitude or shape of the deflection basin under a 9 kip FWD load have been used for pavement condition assessment (Lee, 1997). Several researchers have developed relationships between deflection basin parameters and pavement responses such as stresses and strains. The following sections present the existing pavement response models found in the literature.

2.1.1 Fatigue Cracking

Jung (1988) suggested a method for predicting tensile strain at the bottom of the AC layer using the slope of deflection at the edge of the FWD load plate. This slope is determined by fitting the reciprocal of a deflection bowl into a polynomial equation. The tensile strain at the bottom of the AC layer (ε_{ac}) is determined from the radius of curvature, R, using:

$$\varepsilon_{ac} = \frac{H_{ac}}{2R} \tag{2.1.a}$$

$$R = \frac{-a}{2(D_0 - D_{edge})} \tag{2.1.b}$$

where

H_{ac} = thickness of the AC layer,

a = radius of the FWD load plate,

D_0 = center deflection, and

D_{edge} = deflection at the edge of the load plate calculated from the curve fit to the individual deflection bowl.

Another promising relationship for the determination of ε_{ac} for full depth pavements and aggregate base pavements was developed by Thompson (1989, 1995) using the Area Under the Pavement Profile (*AUPP*). Figure 2.1 defines the *AUPP* as follows:

$$AUPP = \frac{1}{2}(5D_0 - 2D_1 - 2D_2 - D_3) \tag{2.2}$$

where

D_0 = deflection at the center of the loading plate in mils,

D_1 = deflection at 12 in. from the center of the loading plate in mils,

D_2 = deflection at 24 in. from the center of the loading plate in mils, and

D_3 = deflection at 36 in. from the center of the loading plate in mils.

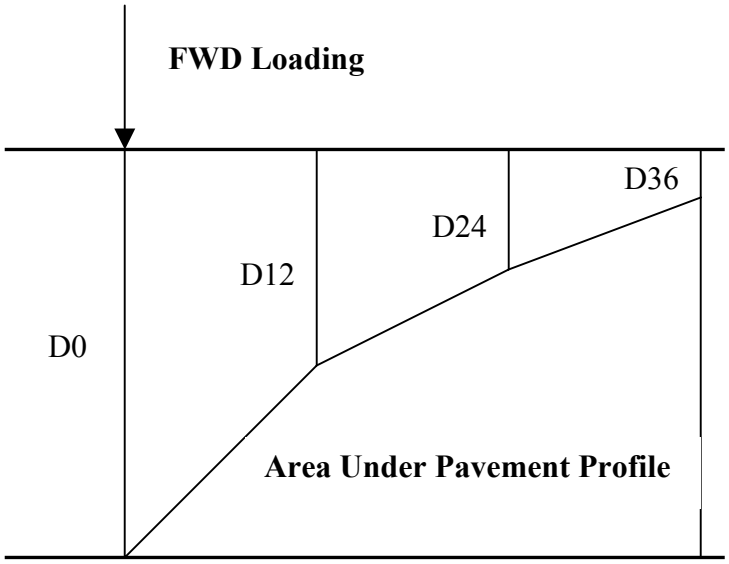

Figure 2.1. Area Under Pavement Profile.

For full-depth asphalt pavements, the ε_{ac} is calculated from:

$$\log(\varepsilon_{ac}) = 1.024 \log(AUPP) + 1.001 \quad (2.3)$$

For aggregate base pavements, the relationship between ε_{ac} and the AUPP is as follows:

$$\log(\varepsilon_{ac}) = 0.821 \log(AUPP) + 1.210 \quad (2.4)$$

The study for Mn/Road test sections by Garg and Thompson (1998) concluded that the AUPP is an important deflection basin parameter that can be used to predict the tensile strain at the bottom of the AC layer quite accurately. Since the AUPP is a geometric property of the deflection basin, the use of the AUPP for the prediction of ε_{ac} is not affected by the type of subgrade and pavement.

2.1.2 Rutting

Thompson (1989) developed a parameter called Subgrade Stress Ratio (SSR) that can be used to estimate the rutting potential of a pavement system. The SSR is defined by

$$SSR = \frac{\sigma_{dsg}}{q_u} \quad (2.5)$$

where

SSR = Subgrade Stress Ratio,

σ_{dsg} = subgrade deviator stress, and

q_u = subgrade unconfined compressive strength.

Using the synthetic database developed by the ILLIPAVE finite element program, the following regression equation in determining the SSR was established for flexible pavements with an aggregate base layer:

$$\log(SSR) = 1.671 \log(D_0) - 2.876 \quad (2.6)$$

A list of SSR design criteria developed during the most critical season, spring, is shown in Table 2.1. These criteria provide a limit for an acceptable level of the total anticipated surface rutting for design traffic volume.

Table 2.1. SSR Design Criteria during Critical Period (after Thompson, 1989)

Type of Pavement	Permissible SSR
Full Depth AC	0.5
AC + Granular Base	0.5
Surface Treated + Granular Base	0.75 (< 20k ESALs)
	0.70 (20k – 40k ESALs)
	0.65 (40k – 80k ESALs)

2.2 Synthetic Pavement Response Databases

Synthetic pavement responses were computed using the NCPAVE for the static analysis and the ABAQUS finite element commercial software package for the dynamic analysis in full depth and aggregate base pavements. The 9, 12, and 15 kips of load level were used for synthetic database generation. After surveying the database in DataPave 2.0, the range of thickness of each pavement type was determined to cover as many existing pavements as possible.

To simulate the nonlinear behavior in base and subgrade materials, the universal soil model was implemented in these two finite element programs. The model constants for granular materials in the base layer were selected using information from the research of Garg and Thompson (1998), and the model constants for subgrade soils were adopted from Santha (1994).

In this study, the synthetic database generated by the ABAQUS program was used in developing the pavement response models. Table 2.2 illustrates the range of layer

thicknesses and moduli of pavement materials used in creating the nonlinear elastic synthetic database. A total of 2,000 cases for full-depth pavements and 8,000 cases for aggregate base pavements was generated using the random selection approach.

Table 2.2. Nonlinear Elastic Synthetic Database Structures

Pavement Type	Pavement Layer	Thickness (in)	Modulus (ksi)
Aggregate Base Pavement	Asphalt Concrete	2 – 24	100-1600
	Aggregate Base	6 – 24	*
	Subgrade	30 – 240	**
Full Depth Pavement	Asphalt Concrete	2 – 28	100-2400
	Subgrade	30 – 240	**

* after Garg and Thompson, 1998
** after Santha, 1994

The nonlinear elastic synthetic database includes the surface deflections at various offset distances from the center of the loading plate, and stresses and strains at specific locations in each individual layer. The statistical regression approach was adopted to find the correlations between deflection basin parameters and critical pavement responses for each pavement layer using a wide range of synthetic databases.

2.3 Parametric Sensitivity Analysis of Pavement Responses

The synthetic database mentioned in the previous section was analyzed to identify deflection basin parameters that have a significant influence in the prediction of critical pavement responses in flexible pavements. All the deflection basin parameters used in this study are summarized in Table 2.3 and, among these, deflection basin parameters under a 9 kip load level were used in a parametric sensitivity analysis.

Table 2.3. Deflection Basin Parameters

Deflection Parameter	Formula
Area Under Pavement Profile	$AUPP = \frac{5D_0 - 2D_{12} - 2D_{24} - D_{36}}{2}$
Surface Curvature Index	$SCI = D_0 - D_{12}$
Base Damage Index	$BDI = D_{12} - D_{24}$
Base Curvature Index	$BCI = D_{24} - D_{36}$
Difference of BDI	$DBDI = BDI_{15kips} - BDI_{9kips}$
Difference of BCI	$DBCI = BCI_{15kips} - BCI_{9kips}$
Slope Difference	$SD = (D_{36}\text{-}D_{60})_{15kips} - (D_{36}\text{-}D_{60})_{9kips}$

The correlations between DBPs and critical pavement responses were analyzed and Root Mean Square Error (RMSE) values were calculated for each DBP. Tables 2.4 and 2.5 show the results of the parametric sensitivity analysis for the full-depth pavement and the aggregate base pavement, respectively. The DBPs with the highest RMSEs marked in these tables were considered the best parameters for critical pavement response prediction.

Table 2.4. Parametric Analysis Results for Full-Depth Pavements

Distress Type	Critical Response	DBP's	R Square
Fatigue Cracking	Tensile Strain at Bottom of AC layer	**BDI√**	**0.9858**
		AUPP√	**0.9530**
		BCI	0.9366
		SCI	0.8561
Rutting	Average Compressive Strain in AC layer	**SCI√**	**0.9110**
		AUPP	0.7476
		BDI	0.5206
		BCI	0.4182
	Compressive Strain on Top of Subgrade	**BDI√**	**0.9787**
		AUPP	0.9384
		BCI	0.9158
		SCI	0.8442
		D_{36}-D_{60}	0.5574

Table 2.5. Parametric Analysis Results for Aggregate Base Pavements

Distress Type	Critical Response	DBP's	R Square
Fatigue Cracking	Tensile Strain at Bottom of AC layer	**BDI√**	**0.9808**
		AUPP√	**0.9319**
		BCI	0.9302
		SCI	0.8458
Rutting	Average Compressive Strain in AC layer	**SCI√**	**0.9110**
		AUPP	0.7476
		BDI	0.5206
		BCI	0.4182
	Compressive Strain on Top of Base Layer	**BDI√**	**0.9675**
		BCI	0.908
		AUPP	0.8824
		SCI	0.7830
		D_{36}-D_{60}	0.5155
	Compressive Strain on Top of Subgrade	**BCI√**	**0.7461**
		BDI	0.7157
		D_{36}-D_{60}	0.6240
		SCI	0.5320
		AUPP	0.4977

2.4 Pavement Response Model for Fatigue Cracking Potential

Two approaches were used in this study to predict the horizontal tensile strain at the bottom of the AC layer (ε_{ac}) from FWD measurements. The first approach uses a statistical regression method to relate ε_{ac} and Base Damage Index (BDI) values. As was described in the previous section, the tensile strain at the bottom of the AC layer is highly correlated with the BDI value (Figure 2.2). To investigate the effect of load level on this correlation, the difference in ε_{ac} values at 9 and 15 kip loads, $d\varepsilon_{ac}$, was predicted using the difference in BDI values at 9 and 15 kip loads. The thickness of the AC layer was

also input to regression equations in predicting ε_{ac} and $d\varepsilon_{ac}$ values. For full depth pavements, the ε_{ac} and $d\varepsilon_{ac}$ values can be determined by using the following equations:

$$\log(\varepsilon_{ac}) = 1.069 \log(BDI) + 0.175 \log(H_{ac}) + 1.514 \quad (2.7.a)$$

$$R^2 = 0.987 \qquad SEE = 0.065$$

$$\log(d\varepsilon_{ac}) = 1.085 \log(DBDI) + 0.237 \log(H_{ac}) + 1.462 \quad (2.7.b)$$

$$R^2 = 0.988 \qquad SEE = 0.064$$

where H_{ac} is the thickness of the AC layer in inches.

For aggregate base pavements, the ε_{ac} and $d\varepsilon_{ac}$ values are calculated from the following equations:

$$\log(\varepsilon_{ac}) = 1.082 \log(BDI) + 0.259 \log(H_{ac}) + 1.409 \quad (2.8.a)$$

$$R^2 = 0.987 \qquad SEE = 0.043$$

$$\log(d\varepsilon_{ac}) = 1.089 \log(\mathrm{D}BDI) + 0.326 \log(H_{ac}) + 1.353 \quad (2.8.b)$$

$$R^2 = 0.977 \qquad SEE = 0.053$$

Another method to predict the ε_{ac} is to use the AUPP value. The predicted ε_{ac} values are plotted in Figure 2.3 against the AUPP values for full depth pavements, and can be expressed as:

$$\log(\varepsilon_{ac}) = 1.075 \log(AUPP) + 0.910 \quad (2.9)$$

$$R^2 = 0.975 \qquad SEE = 0.091$$

For aggregate base pavements,

$$\log(\varepsilon_{ac}) = 1.034 \log(AUPP) + 0.932 \quad (2.10)$$

$$R^2 = 0.934 \qquad SEE = 0.099$$

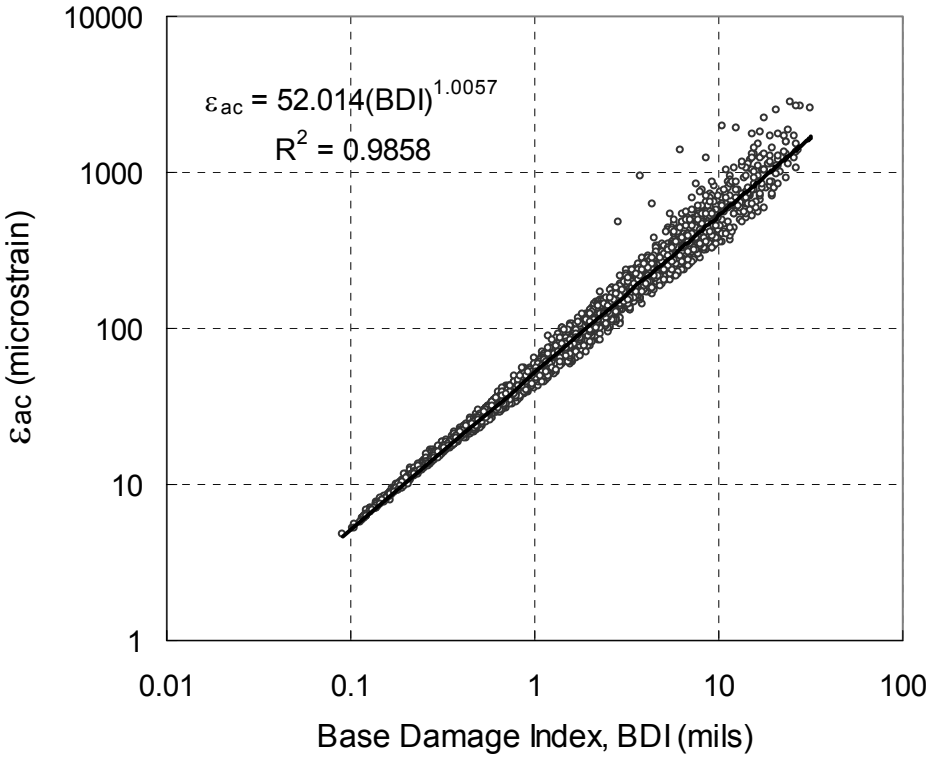

Figure 2.2. The relationship between the tensile strain at the bottom of the AC layer and

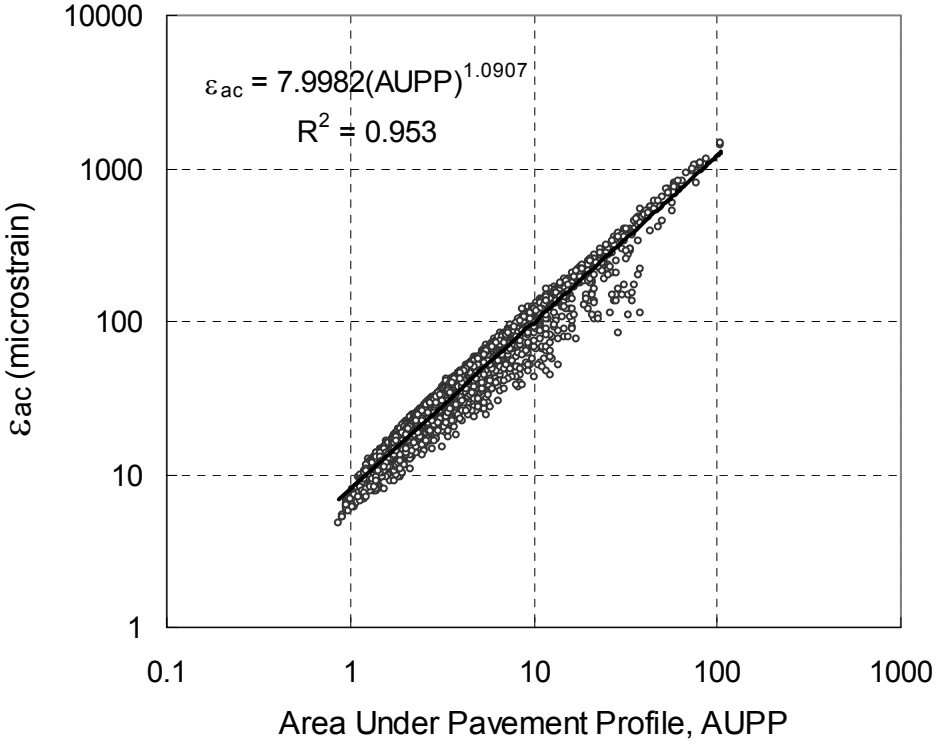

Figure 2.3. The relationship between the tensile strain at the bottom of the AC layer and the AUPP (9 kip load level).

Figure 2.4 shows the comparison of ε_{ac} predictions using the BDI- and AUPP-based approaches for aggregate base pavements. There is not a significant difference in the predicted ε_{ac} values using the BDI- or the AUPP-based approach. However, the AUPP-based approach seems to yield a higher tensile strain value at a larger than 500 microstrain than the BDI-based approach.

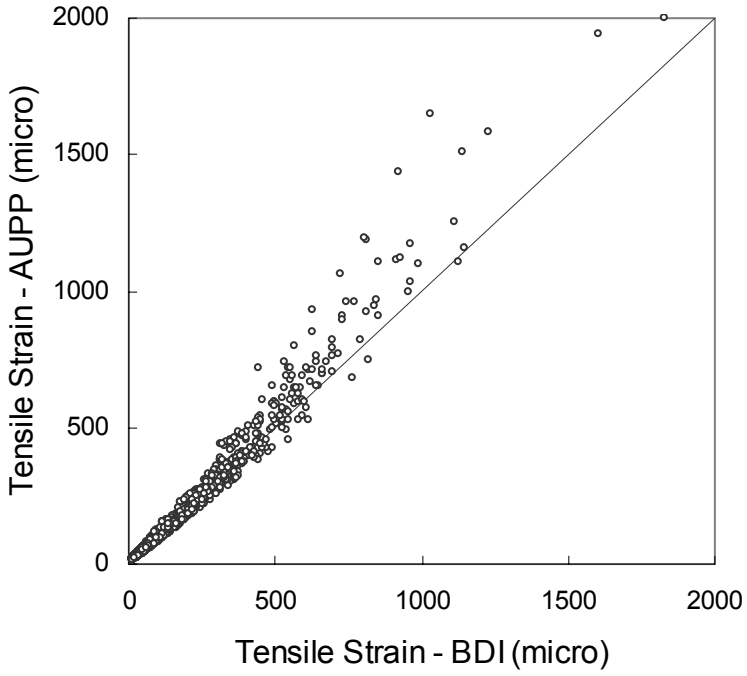

Figure 2.4. Comparison of ε_{ac} predictions from the BDI and AUPP for asphalt concrete pavements.

2.5 Pavement Response Model for Rutting Potential

The compressive strain in the AC layer (ε_{cac}) on top of the base layer (ε_{base}) and on top of the subgrade (ε_{sg}) have been used to represent rutting potential in flexible pavements. The ε_{cac} values can be determined by dividing the difference in deflections on the top and at the bottom of the AC layer by the AC layer thickness. It is noted that ε_{cac} is the average strain value across of the thickness of the AC layer. The ε_{cac} values are obtained from the following equation developed from the nonlinear synthetic database:

$$\log(\varepsilon_{cac}) = 1.076 \log(SCI)+1.122 \log(H_{ac}) + 0.175 \qquad (2.11)$$

$$R^2 = 0.911 \qquad SEE = 0.061$$

According to Kim et al. (2000), the base materials influence only a small portion of pavement surface deflections. However, the condition of the base layer has a significant effect on the long-term performance of flexible pavements. For aggregate base pavements, it was found from the sensitivity analysis that the BDI is the most critical deflection parameter for the prediction of ε_{abc}. Figure 2.5 presents the relationship between ε_{abc} and BDI under a 9 kip load level. In addition, the difference in ε_{abc} values under 9 and 15 kip loads was also predicted using difference in BDI values (DBDI) values. The pavement response models for ε_{abc} and $d\varepsilon_{abc}$ are expressed as:

$$\log(\varepsilon_{abc}) = 0.938 \log(BDI) - 0.079 \log(H_{ac}) + 0.045 \log(H_{base}) + 2.221 \qquad (2.12.a)$$

$$R^2 = 0.970 \qquad SEE = 0.066$$

$$\log(d\varepsilon_{abc}) = 0.918 \log(DBDI) + 0.007 \log(H_{ac}) + 0.071 \log(H_{base}) + 2.035 \qquad (2.12.b)$$

$$R^2 = 0.961 \qquad SEE = 0.067$$

where H_{base} is the thickness of the base layer in inches.

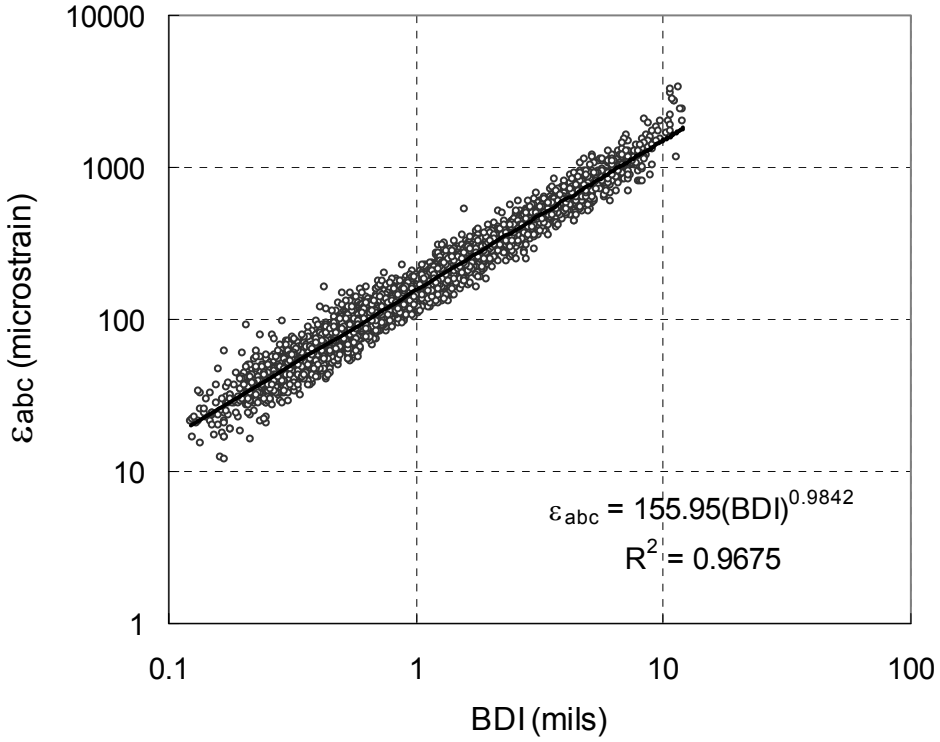

Figure 2.5. The relationship between the compressive strain on the top of the base layer and the BDI for aggregate base pavements (9 kip load level).

In the AASHTO 93 Guide (1993) a simple formula is presented for backcalculating the subgrade modulus from a single deflection measured from an outer-most sensor and the load magnitude. However, this approach may not be suitable for an accurate prediction of the stiffness of the subgrade because the load spreadability is a function of layer stiffness, distress condition, and thickness (Lee, 1997). For example, since there are no intermediate support layers in full depth pavements, the BDI and DBDI were found to be critical deflection basin parameters in predicting the compressive strain on the top of the subgrade, ε_{sg}, and the difference of ε_{sg} due to load level, $d\varepsilon_{sg}$, respectively. Figure 2.6 shows the relationship between predicted ε_{sg} values and the BDI

values under a 9 kip load level. It indicates a high correlation between ε_{sg} and BDI. For full depth pavements, the ε_{sg} and $d\varepsilon_{sg}$ may be predicted using the following equations:

$$\log(\varepsilon_{sg}) = 0.999 \log(BDI) + 0.063 \log(H_{ac}) + 2.077 \qquad (2.13.a)$$

$$R^2 = 0.979 \qquad SEE = 0.061$$

$$\log(d\varepsilon_{sg}) = 1.000 \log(DBDI) + 0.103 \log(H_{ac}) + 2.032 \qquad (2.13.b)$$

$$R^2 = 0.978 \qquad SEE = 0.062$$

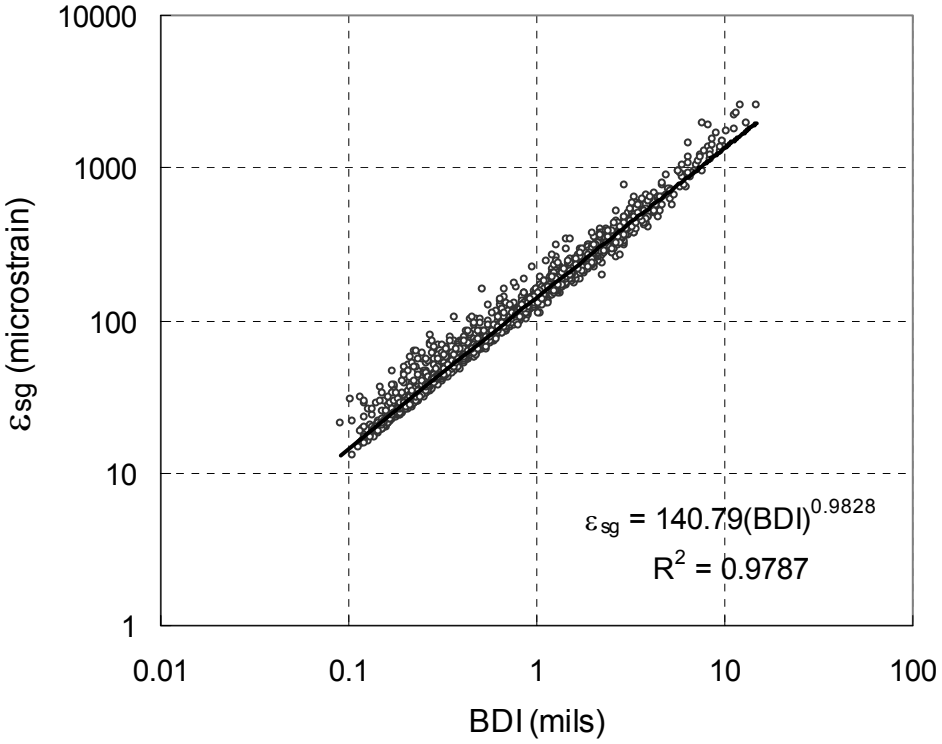

Figure 2.6. The relationship between the compressive strain on the top of the subgrade and the BDI for full depth pavements (9 kip load level).

According to the parametric sensitivity study, instead of deflection at the outer-most sensor location, the Base Curvature Index (BCI) was found to be a good indicator of the condition of the subgrade for aggregate base pavements. The BCI is defined as the difference in deflections at 24 and 36 in. of the radial distance from the center of the load

plate. The relationship between the ε_{sg} versus BCI is shown in Figure 2.7. The BCI value and the thicknesses of the AC and base layers were input to the pavement response model to predict the ε_{sg} value for aggregate base pavements. The difference of BCI values, the DBCI, obtained from deflections under different load levels also was investigated to predict the difference of ε_{sg} due to load level ($d\varepsilon_{sg}$). Similar to the full depth pavement, the ε_{sg} and $d\varepsilon_{sg}$ for aggregate base pavements can be calculated using the following equations:

$$\log(\varepsilon_{sg}) = 1.017 \log(BCI) - 0.042 \log(H_{ac}) - 0.494 \log(H_{base}) + 2.624 \qquad (2.14.a)$$

$$R^2 = 0.903 \qquad SEE = 0.125$$

$$\log(d\varepsilon_{sg}) = 1.023 \log(DBCI) - 0.045 \log(H_{ac}) - 0.445 \log(H_{base}) + 2.604 \qquad (2.14.b)$$

$$R^2 = 0.909 \qquad SEE = 0.115$$

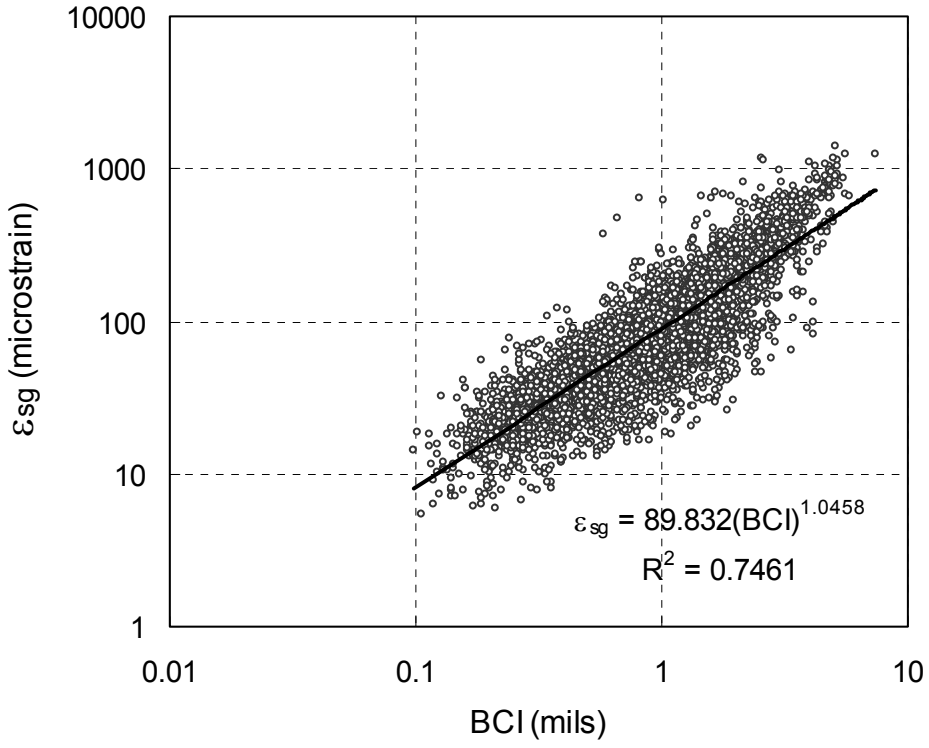

Figure 2.7. The relationship between the compressive strain on the top of the subgrade and the BCI for aggregate base pavements (9 kip load level).

CHAPTER 3

DEVELOPMENT OF TEMPERATURE CORRECTION FACTORS

The Falling Weight Deflectometer (FWD) is an excellent means of evaluating the structural capacity of pavements in service for rehabilitation design. Deflection measurements in flexible pavements must be corrected to a particular type of loading system and to a predefined environmental condition. The loading system factor is dependent on the type of nondestructive testing device, the frequency of loading, and the load level. It is also well known that the most critical environmental factor affecting deflections in flexible pavements is the temperature of the asphalt concrete layer.

The general procedure for temperature correction of FWD deflections and backcalculated asphalt concrete moduli is presented in the 1993 AASHTO Guide for Design of Pavement Structure. Chen et al. (2000) recently developed a universal temperature correction equation for deflection and moduli for flexible pavements in Texas. Their study shows that only the deflections at a radial distance of 0 and 8 in. are significantly affected by temperature.

Deflections at variable offset distances and deflection basin parameters have been used to perform the pavement condition evaluation and to predict the remaining life of a pavements in service (Kim et al., 2001). Many temperature correction procedures for deflections may be applied only to the center deflection (Kim et al., 1995 and 1996). Also, these procedures are applicable only to a 9 kip FWD load. In this report, a new temperature correction procedure for flexible pavements in North Carolina (NC) is

presented. This procedure provides deflection correction factors at varying radial distances from the center of the FWD load as well as at different FWD load levels. Temperatures and deflections measured from 11 pavement sections in North Carolina were used in developing this procedure.

Recently, Lukanen et al. (2000) developed new temperature prediction and deflection correction procedures using data collected from the LTPP study. Since these procedures were developed from the national database, it was deemed important to verify the LTPP procedure against local data. The temperature and deflection data measured from the 11 NC pavements were used in checking the accuracy of the LTPP temperature prediction and deflection correction procedures.

3.1 Selection of Pavement Sections

Kim et al. (1995) developed a temperature correction procedure for center deflection using data collected in the central region of North Carolina. To improve the accuracy of the temperature-deflection correction procedure for various types of pavement in all climatic regions of North Carolina, a total of 11 pavement sites were selected for temperature correction of deflections in another study (Kim et al., 1996): 3 in the eastern, 5 in the central, and 3 in the western region. Characteristics of the selected sections are summarized in Table 3.1.

Table 3.1. Pavement Test Sections

Region	Route	Thickness (in.)				
		Surface Course	Binder Course	Asphalt Base	Aggregate Base	Total AC Layer
Eastern	US 264	2.5	2.0	-[b]	8.0	4.5
	NC 24	2.5	1.7	4.8	-	9.0
	US 17	2.5	4.5	5.0	-	12.0
Central	NC 54	2.5	4.5	3.0	-	10.0
	US 421 (13[a])	2.0	1.5	4.0	-	7.5
	US 421 (17[a])	2.0	1.5	-	8.0	3.5
	US 421 (20[a])	2.0	1.5	5.5	-	9.0
	US 70	2.0	3.5	-	11.0	5.5
Western	US 74	2.5	4.0	-	8.0	6.5
	US 25	2.5	5.5	-	12.0	8.0
	US 421	2.5	3.0	4.0	-	9.5

[a]Section number.
[b]Data not applicable.

3.2 Implementation of Temperature Gauge

To measure pavement temperatures at varying depths, thermocouples were installed through a 6 in. diameter hole drilled to a depth of 6.5 ft below the bottom of the AC layer. After compacting base and subgrade materials, thermocouples in the asphalt concrete layers were installed by drilling horizontal holes to the core wall using a drill with a pivoting nose. Epoxy was injected into each horizontal hole followed by a thermocouple attached to strands of insulated wire. The wires from the plastic tube and thermocouples in the AC layers were taken across the pavement through a trench slit cut transversely from the core hole to the pavement edge. The core hole was backfilled with hot mix and the trench in the pavement was filled with epoxy.

The wire connections were plugged into a junction box and automatic data logger that displays the temperatures given by each thermocouple. The use of the data logger allowed continuous temperature measurements without an operator.

3.3 Mid-Depth Temperature Prediction

In order to correct the measured deflection at a FWD testing temperature to the deflection at a reference temperature, the effective temperature of the AC layer must be determined. The temperature at the mid-depth of the AC layer was selected as the effective temperature in this study. The BELLS3 equation developed by FHWA was used to predict the mid-depth temperature. Infrared surface temperature, average air temperature the day before testing, and time of FWD testing from the NCDOT database were input to the BELLS3 prediction equation; predicted versus measured mid-depth temperatures are plotted in Figure 3.1. The predicted temperatures agree quite well with the measured temperatures at a wide range of temperatures, considering that the prediction procedure was developed from the national database and that the data used in Figure 3.1 were obtained from NC pavements. The variation of AC material from one location to another does not seem to affect the heat transfer characteristics in flexible pavements.

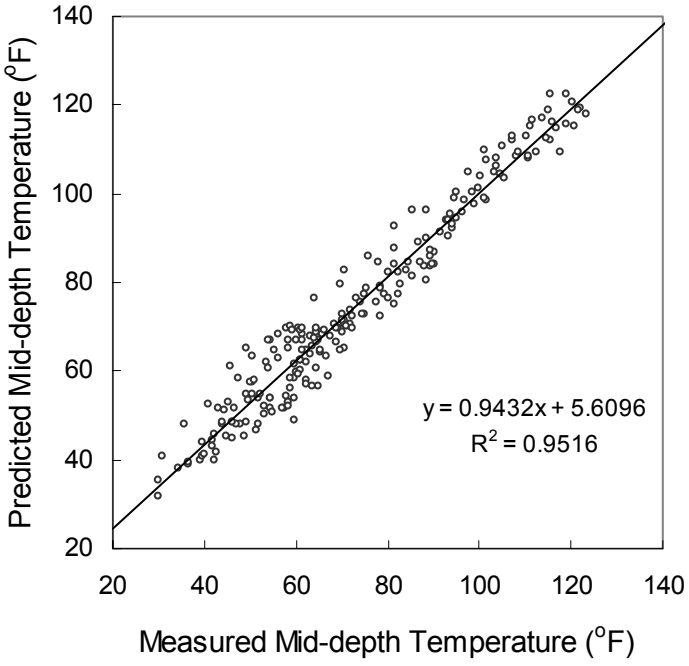

Figure 3.1. Predicted mid-depth temperature versus measured mid-depth temperature.

3.4 Effect of Load Level on Temperature Correction of FWD Deflections

Many temperature correction procedures for FWD deflections have been developed using deflection data under a 9 kip load level. Since the applicability of deflection correction factors based on a 9 kip load to multi-load level deflection is questionable, the effect of the load level on the temperature dependence of the deflection was examined in this study.

The center deflections under four different load levels measured from US 264 are plotted in Figure 3.2 against the measured mid-depth temperature on semi-log scale. It can be observed from this figure that the slopes in deflection-AC mid-depth temperature plotted on a semi-logarithm scale (n value) are relatively the same at all load levels. To verify this visual observation, a paired T test was performed on the data from all 11 pavement sections. The null hypothesis tested was that the n values from the 6 and 9 kip load are the same. A similar null hypothesis was also established when the load changes from 9 to 12 kip and from 9 to 15 kip. In order to reject the null hypothesis at the 95% significant level, the t-stat must be larger than the t critical ($T_{0.95,10} = 1.81$), or the P value must be less than 0.05. Details on the T test results are shown in Table 3.2. It is concluded from the results of the T test that the null hypothesis at all the load levels cannot be rejected, and that the temperature dependence of deflection under the FWD load levels between 6 and 15 kip is statistically the same.

Table 3.2. Results of T Test

Load Level (kips)	t-stat	P value
6	-1.3219	0.2156
12	-0.6245	0.5462
15	0.6073	0.5571

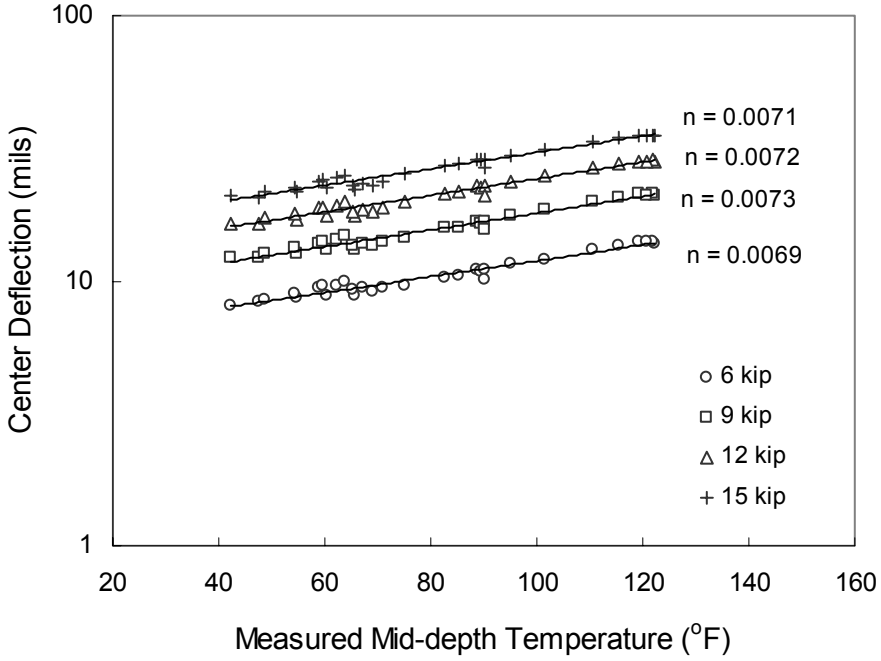

Figure 3.2. Effect of multi load level on temperature-dependency of deflections for US 264.

3.5 The Effective Radial Distance for Temperature Correction of FWD Deflections

In order to find the characteristics of temperature dependence on deflection, the measured deflections under a 9 kip load level are plotted in Figure 3.3 against various AC mid-depth temperatures for US 264 and US 17. Because the total thicknesses of the AC layer in US 264 and US 17 are quite different in the same climatic region (Eastern), these two test sections were selected for use in this figure. It can be observed from Figure 3.3 that only deflections at 0 and 8 in. at US 264 are affected by the mid-depth temperature, whereas deflections up to 36 in. at US 17 are influenced by the mid-depth temperature. It was found that the radial distance in which the AC mid-depth temperature affects deflection increases as the total thickness of the AC layer increases. This phenomenon is

due to the fact that the radial distance influenced by load-induced stress within the AC layer increases with increasing thickness of the AC layer, and necessitates that the temperature correction factors be expressed as a function of sensor location.

To provide a more accurate means of temperature correction of surface deflections at variable offset distances, the effective radial distance for temperature correction (D_{eff}) was adopted in this study. The D_{eff} is defined as the radial distance within which the change of temperature affects the FWD deflections. Where the slope in the AC mid-depth temperature versus deflection plotted on the semi-log scale changes from a positive value to a negative value, the deflection is considered to be independent of the AC mid-depth temperature; then the D_{eff} can be determined. The D_{eff} is plotted against the thickness of the AC layer in Figure 3.4. The slope in this plot is found to be 0.18, and the following relationship was developed from the data:

$$D_{eff} = 5.5\ H_{ac} - 22.2 \qquad (3.1)$$

where

D_{eff} = effective radial distance for temperature correction in inches, and

H_{ac} = AC layer thickness in inches.

Deflection values within the D_{eff} need to be corrected to a reference temperature using temperature correction factors.

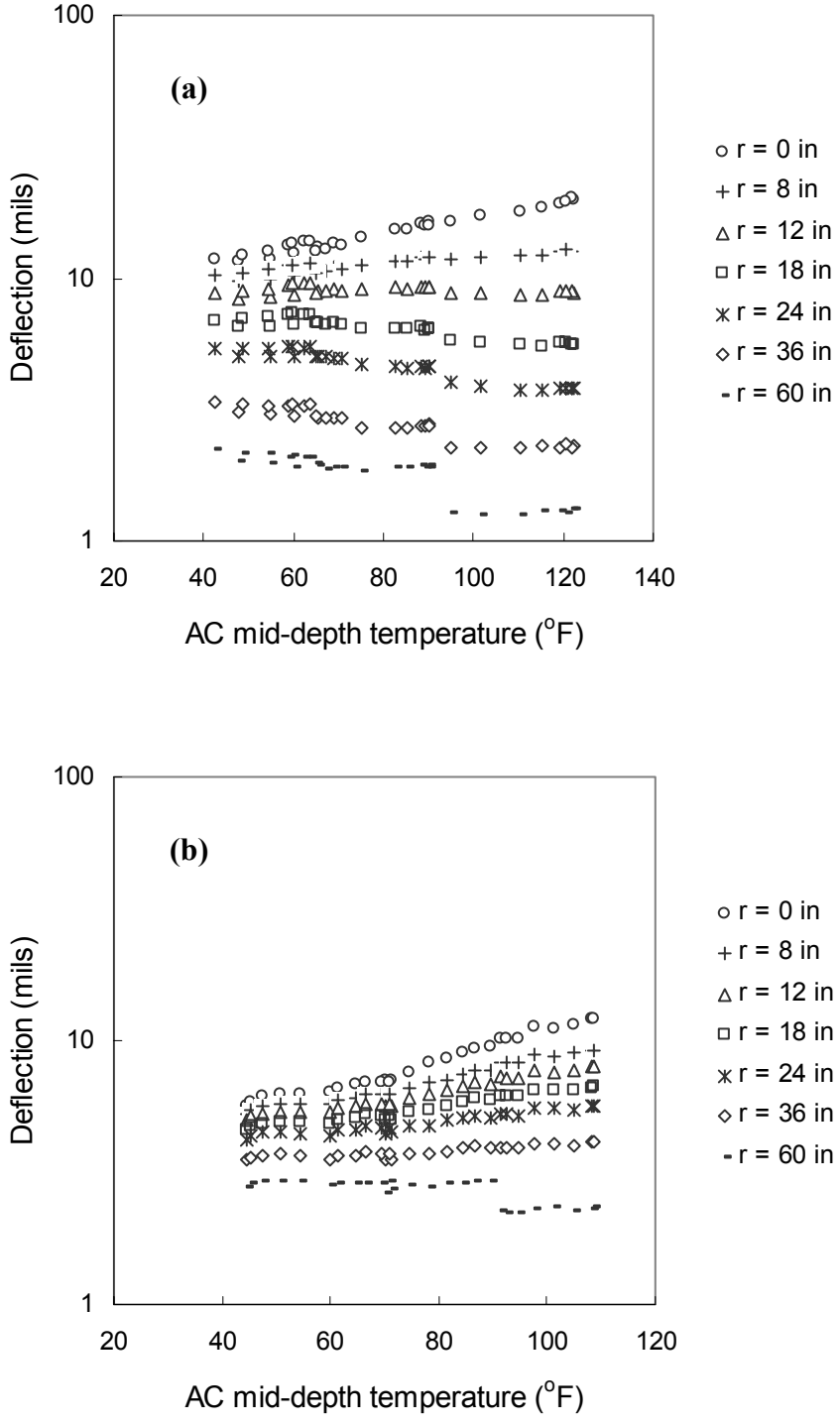

Figure 3.3. Deflection versus mid-depth temperature for: (a) US 264; (b) US 17.

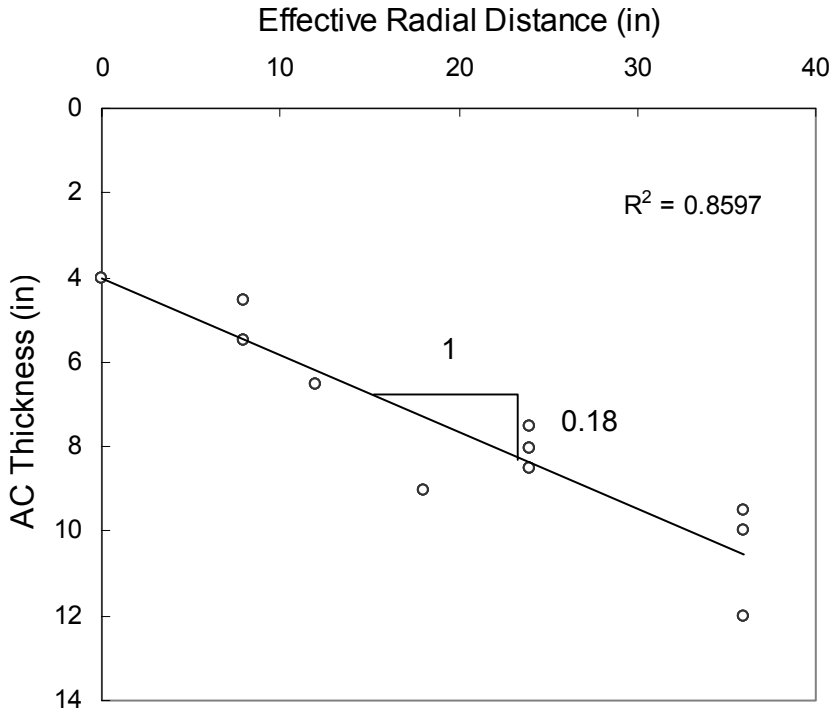

Figure 3.4. Effective radial distance versus AC layer thickness for all pavement sites.

3.6 Temperature Correction of Deflections at Radial Offset Distance

Temperature correction factors for FWD deflections may be developed by calculating the deflection ratios by dividing the measured deflection at a specific temperature (T) by the deflection at a reference temperature (T_0, 68°F). That is,

$$\lambda_w = \frac{w_{T_0}}{w_T} \tag{3.2}$$

where

w_{T0} = the deflection corrected to temperature T_0,

w_T = the deflection at temperature T, and

λw = the temperature correction factor.

Kim et al. (1996) proposed a deflection correction model based on a statistical analysis of measured deflections and temperatures in North Carolina. They suggested that the deflection-temperature relationship is better expressed as a linear function between log *w* and *T*. The linear form of log *w* versus *T* relationship is given by:

$$\log w = b + nT \tag{3.3}$$

where *b* is the log *w* axis intercept and *n* is the slope in the log *w* versus *T* plot. Rewriting Equation 3.3,

$$w = 10^{b+nT} \tag{3.4}$$

Substituting Equation 3.4 into Equation 3.2, one can obtain the correction factor in terms of *n* as follows:

$$\lambda_w = 10^{-n(T-T_0)} \tag{3.5}$$

It was also found that the n-value is an increasing function of the AC layer thickness. Finally, the deflection correction factor (λ_w) for center deflections measured under a 9 kip FWD load can be expressed as:

$$\lambda_w = 10^{-C(H_{ac})(T-T_0)} \tag{3.6}$$

where

H_{ac} = AC layer thickness in inches, and

C = regression constant.

To provide temperature correction factors at variable offset distances, an empirical model was developed based on a statistical analysis of the temperature-deflection data. Because the degree of temperature dependency of deflections linearly decreases as the radial distance increases, the *C* value at a given offset distance may be determined using the following equation:

$$C = -Ar + C_0 \quad (3.7)$$

where r is the radial distance from the center of the load plate. The C_0 values and A values for each of the three regions and for the entire state are summarized in Table 3.3.

Table 3.3. C_0-value for Each Region and the State

Regions	C_0 values	Statewide C_0 value	A value	Statewide A value
East	3.61E-5	4.65E-5	-5.72E-08	-5.47E-08
Central	5.80E-5		-5.62E-08	
West	4.32E-5		-5.07E-08	

Figure 3.5 shows the corrected deflections using the above NCDOT procedure as a function of AC mid-depth temperature for US 264 and US 17. Overall, the corrections appear to be good except for the last sensor. At a radial distance of 60 in., the deflection at a low temperature is larger than that at a high temperature. It is surmised that this phenomenon is due to the reduction of stiffness of the AC layer at high temperatures which thus cause reduction in the lateral spread of the stress distribution.

3.7 Verification of the LTPP Temperature Correction Procedure Using North Carolina Data

Recently, Lukanen et al. (2000) developed procedures for the prediction of AC effective temperature and the correction of FWD deflections using the LTPP data. They found that a temperature correction procedure for FWD deflections requires the AC surface temperature, thickness of the asphalt layer, stiffness of the subgrade, and the latitude of site location. As an indicator of the stiffness of the subgrade, they selected the deflection at a radial distance of 36 in. To explain the effect of asphalt mix characteristics on the

temperature correction, the latitude of the site was also included as an indicator of asphalt stiffness in this procedure.

The corrected center deflections using the NCDOT procedure against mid-depth temperature for pavements in all climatic regions are plotted in Figure 3.6. The LTPP correction procedure was also applied to the same North Carolina data, and the results are plotted in Figure 3.7. In general, the results in Figure 3.6 show relatively constant corrected deflection values at varying mid-depth temperatures. However, in Figure 3.7, the increasing trends of the center deflection versus the mid-depth temperature were observed in US 17, NC 54, and US 421. The thicknesses of the asphalt layers in these pavements are 12, 10, and 9.5 in., respectively. It seems that the LTPP temperature correction procedure undercorrects the deflections at higher temperatures in pavements with an AC layer thicker than 9 in. To describe the correction quality, the distribution of slope (n value) in the AC mid-depth temperature versus temperature corrected deflection plotted on a semi-log scale is shown in Figure 3.8, obtained using the LTPP procedure. It was found that 37% of the n-values from the LTPP procedure fall between –0.004 and +0.004. This result demonstrates that the LTPP procedure is not satisfactory for temperature correction of deflection in North Carolina pavements. The main reason for this deficiency is that the LTPP procedure was developed from the national databases and cannot fully consider the local variation in mixture characteristics.

Since the NCDOT temperature correction procedure used the same temperature and deflections data for model development and validation, a better quality of correction was found. To compare the accuracy of the LTPP and NCDOT procedures fairly, an independent set of temperature and deflection data is needed.

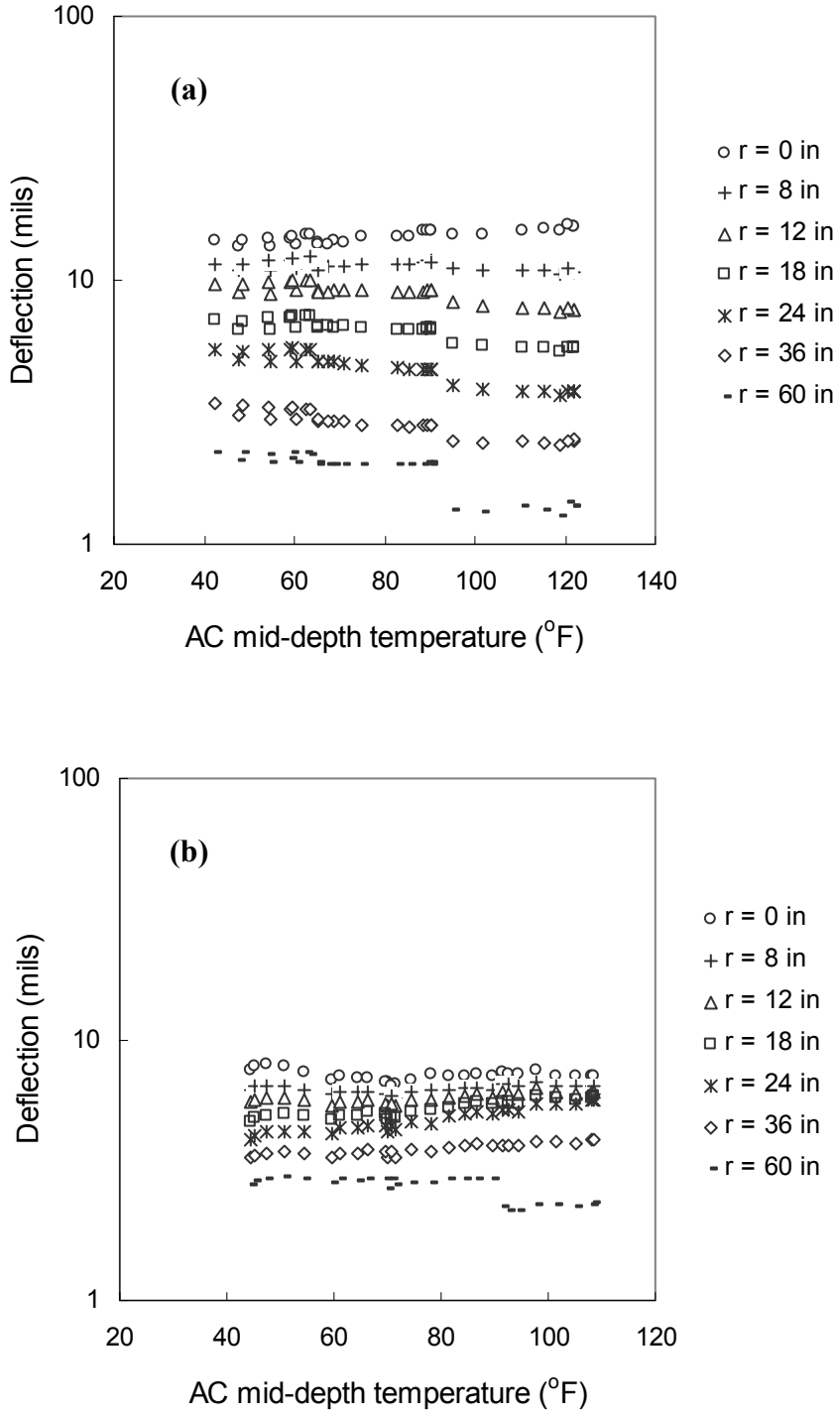

Figure 3.5. NCDOT corrected deflection versus mid-depth temperature for: (a) US 264; (b) US 17.

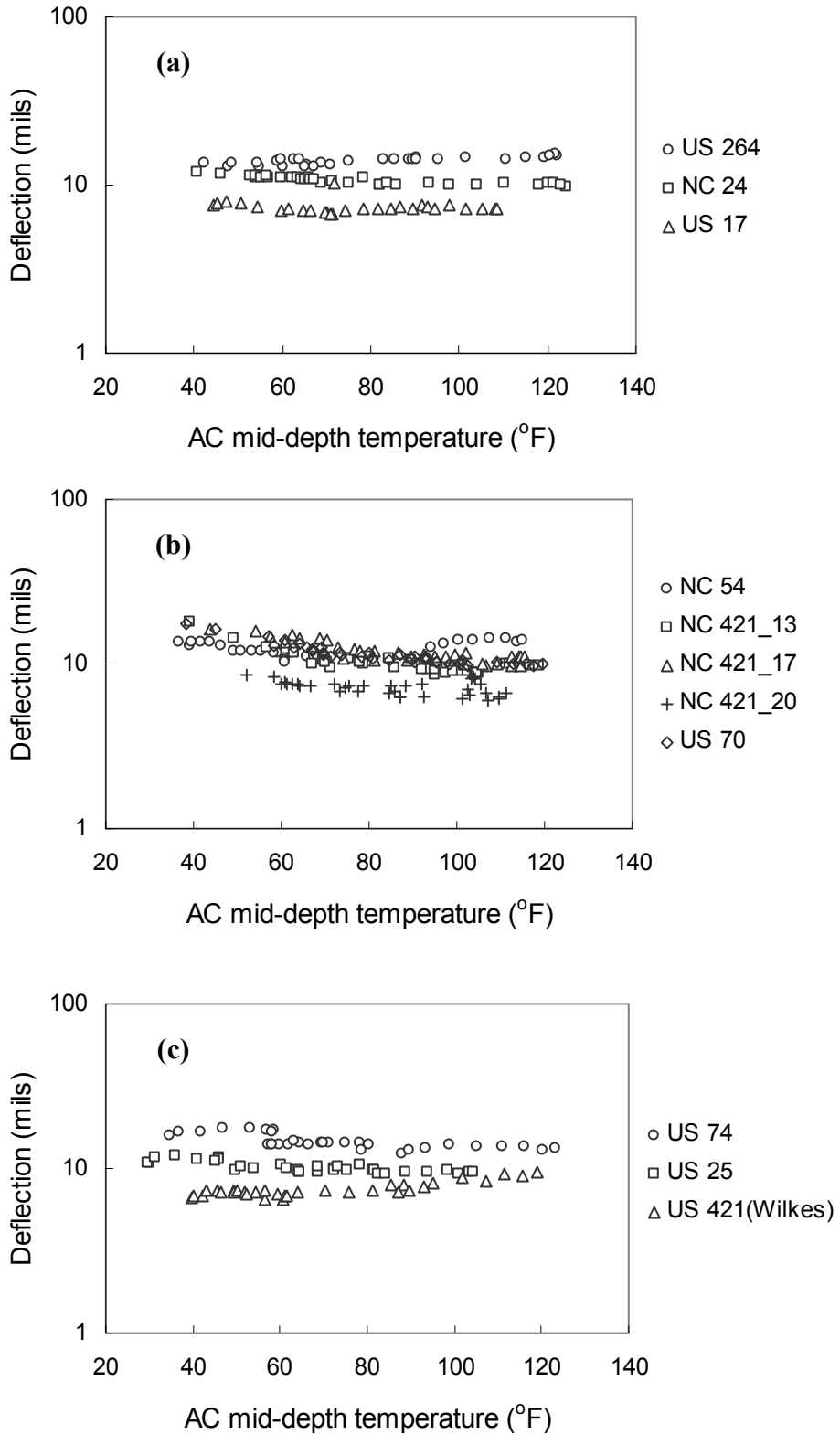

Figure 3.6. NCDOT corrected center deflection versus mid-depth temperature for: (a) eastern region; (b) central region; (c) western region.

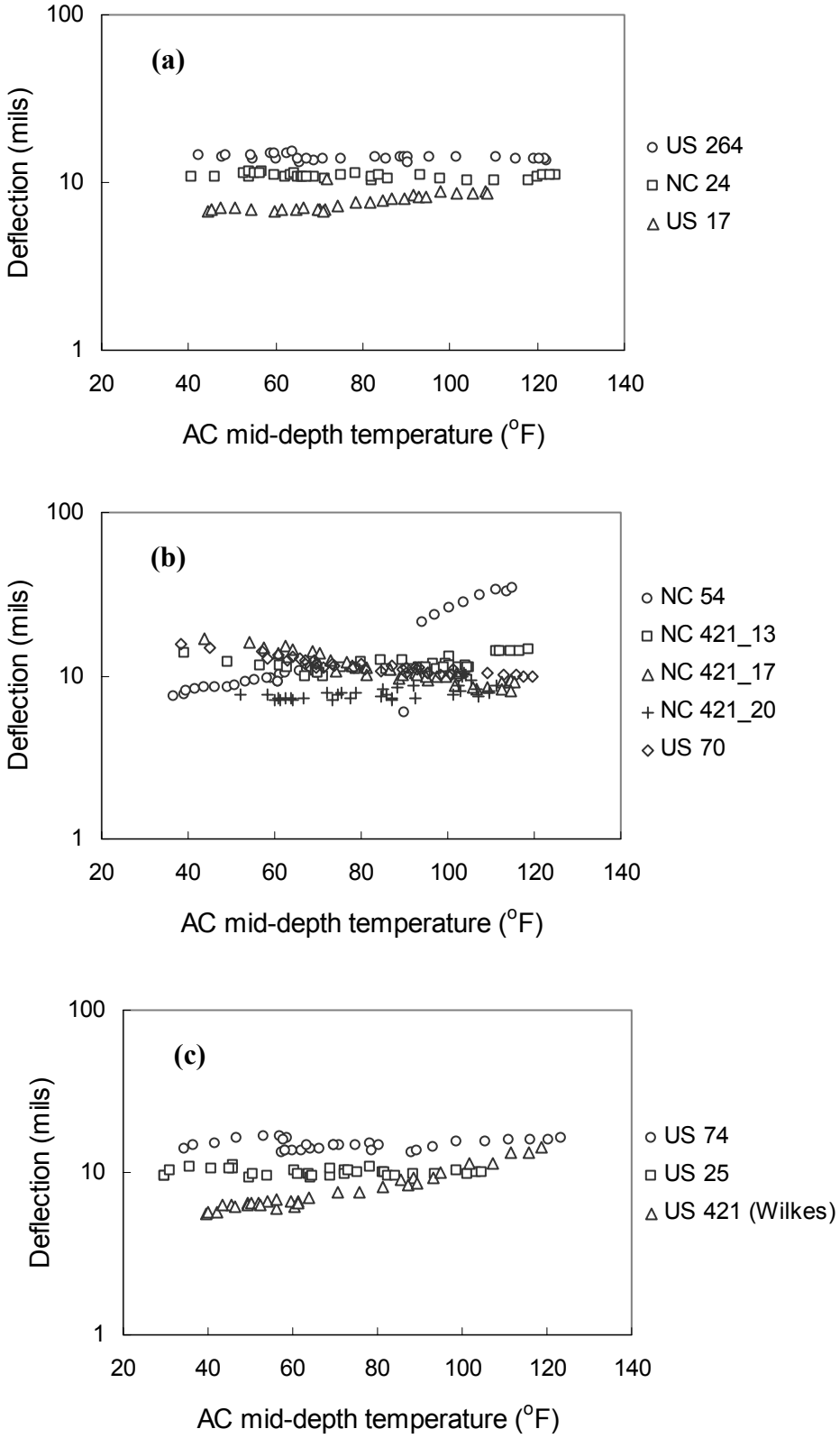

Figure 3.7. LTPP corrected center deflection versus mid-depth temperature for: (a) eastern region; (b) central region; (c) western region.

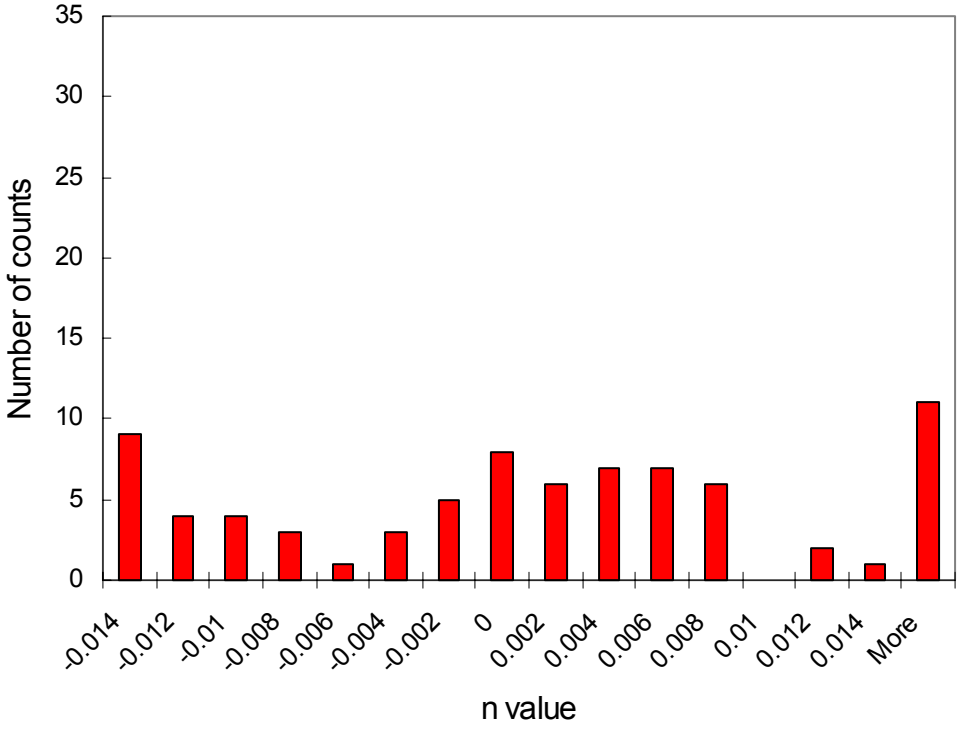

Figure 3.8. The distribution of n value for LTPP temperature correction procedure.

CHAPTER 4

CONDITION ASSESSMENT OF PAVEMENT LAYERS USING MULTI-LOAD LEVEL FWD DEFLECTIONS

FWD deflection basin parameters have been successfully used to estimate the pavement structural capacity and the current condition of existing pavements. In addition to the deflection basin parameters, the pavement responses at critical locations in each individual layer have proven to be good condition indicators for various distresses. As discussed in Chapter 2, these responses can be predicted from the deflection basin parameters and layer thicknesses based on the statistical regression approach using the synthetic database developed by the dynamic finite element program.

This chapter presents the general procedure for condition assessment of pavement layers using multi-load level FWD deflections. Pavement performance data, Dynamic Cone Penetrometer (DCP) testing results, and multi-load level deflection data used in developing this procedure were collected from flexible pavements in North Carolina and in the DataPave 2.0 field database. The multi-load level deflection basin parameters were adopted in this study to evaluate the effect of load level on the estimation of the pavement layer condition.

4.1 Full Depth Pavements

The following section describes the procedure for predicting the condition of the subgrade layer in full depth pavements using multi-load level FWD deflection data.

Since detailed information about the condition of the AC layer for full depth pavements is unavailable in the field database, the procedure for condition assessment of the AC layer is not included in this section.

4.1.1 Subgrade

Indicators for Subgrade Condition Evaluation

For full depth pavements, it was found from the parametric sensitivity study that the base damage index (BDI) is a critical deflection basin parameter for subgrade condition evaluation. The nonlinear behavior of subgrade soils can be observed from the relationship between applied load and surface deflections at various offset distances. For subgrade soils with softening behavior, the deviatoric stress in the subgrade layer increases with loads varying from 6 to 15 kip, after which the magnitude of stiffness tends to decrease. To characterize this nonlinear behavior of subgrade soils in full depth pavements, the difference in the BDI values (DBDI) calculated from deflections under a 6 to 15 kip load level was used.

It is well known that the compressive strain on top of the subgrade (ε_{sg}) is used to represent the subgrade rutting potential, which is closely related to the stiffness of subgrade soils. In addition to deflection basin parameters, the relationships between the pavement responses such as ε_{sg} and the difference of strains due to load level, $d\varepsilon_{sg}$, and subgrade condition were also investigated in this study. The ε_{sg} and $d\varepsilon_{sg}$ for full depth pavements can be predicted using Equations 2.13.a and 2.13.b, as previously described.

Structural Correction Procedure for Subgrade Condition Assessment

Although the BDI, DBDI, $\varepsilon_{sg,}$ and $d\varepsilon_{sg}$ are strongly related to subgrade condition, their values are also dependent on structural and material properties in a flexible pavement. Kim et al. (2000) proposed the structural correction procedure that normalizes these condition indicator values to a standard pavement structure. The standard full depth pavement is assumed to be a pavement structure with E_{ac} = 500 ksi, H_{ac} = 8 in., and H_{sg} = infinity. The condition indicators are described using structural and material properties of a flexible pavement. Using the synthetic database, the following regression equations can be obtained:

$$\log (BDI) = -1.864 \log(H_{ac}) - 0.710 \log (E_{ac}) + 0.045 \log(E_{ri}) + 3.994 \qquad (4.1)$$

$$R^2 = 0.983 \qquad SEE = 0.055$$

$$\log (DBDI) = -1.910 \log(H_{ac}) - 0.724 \log (E_{ac}) + 0.040 \log(E_{ri}) + 3.944 \qquad (4.2)$$

$$R^2 = 0.986 \qquad SEE = 0.051$$

$$\log (\varepsilon_{sg}) = -1.782 \log(H_{ac}) - 0.750 \log (E_{ac}) + 0.035 \log(E_{ri}) + 6.202 \qquad (4.3)$$

$$R^2 = 0.985 \qquad SEE = 0.053$$

$$\log (d\varepsilon_{sg}) = -1.812 \log(H_{ac}) - 0.766 \log (E_{ac}) + 0.028 \log(E_{ri}) + 6.150 \qquad (4.4)$$

$$R^2 = 0.984 \qquad SEE = 0.055$$

where

E_{ac} = the elastic modulus of asphalt concrete in ksi, and

E_{ri} = the subgrade modulus at 6 psi of deviatoric stress in ksi.

For example, the adjusted BDI value corresponding to a standard pavement structure can be obtained by dividing the BDI value obtained from an actual pavement by a structural correction factor.

$$Adjusted \quad BDI = \frac{Estimated \quad BDI}{\beta_1} \tag{4.5}$$

The structural correction factor, β_1, can be defined as

$$\beta_1 = \frac{BDI_m}{BDI_r} \tag{4.6}$$

where

BDI_r = the BDI value at a standard pavement structure, and

BDI_m = the BDI value at an actual pavement structure.

The elastic modulus of the AC layer, predicted by using the following equation, and the thickness of the AC layer were input to Equations 4.1 through 4.4 to determine the BDI_m and BDI_r values:

$$\log (E_{ac}) = -1.059 \log(SCI) - 1.009 \log (H_{ac}) + 4.176 \tag{4.7}$$

where the surface curvature index (SCI) is defined as the difference in deflections at 0 and 12 in. of the radial distance from the center of the load plate.

It is noted that the sum of logarithmic terms in Equations 4.1 through 4.4 can be expressed as the product of power terms. Since the E_{ri} values for actual and reference structures are the same, the E_{ri} terms in BDI_m and BDI_r in Equation 4.6 cancel out. Therefore, the E_{ri} value is not necessary for the structural correction procedure described above.

Validation of Condition Assessment Procedure for Full Depth Pavements

Multi-load level FWD deflections and DCP testing results were collected from several test sections in North Carolina. The load level used in FWD testing ranges from 6 to 12 kip. Results of DCP testing contain the number of weight drops and the penetration

depth in the base and subgrade layers. The California Bearing Ratio (CBR) value for each individual layer was estimated from the penetration depth per drop (PD) based on the empirical correlation developed by the NCDOT, as follows

$$\log(CBR) = 2.6 - 1.07 \log(PD) \quad (4.8)$$

To determine the thickness of the AC layer, coring was also performed by the NCDOT. A summary of the coring results is given in Table 4.1.

Table 4.1. Results of Coring for Full Depth Pavements

Road Number	Test Date	No. of Cores	AC Thickness (in)[1]
SR 1125	2/8/01	6	4.9
SR 1007	5/24/00	2	5.7
SR 1706	2/15/00	4	3.2
NC 2427[2]	1/4/00	5	7.0

[1] Average AC layer thickness
[2] NCHRP 10-48 database

Surface deflections and subgrade CBR values obtained from these pavement sections were incorporated to validate the procedure for condition assessment of the subgrade in full depth pavements. To evaluate the validity of this procedure, the subgrade CBR values were compared against the predicted subgrade condition indicators. The relationships between adjusted BDI and DBDI values, and the subgrade CBR values, are shown in Figures 4.1 and 4.2. Since there are no multi-load level deflection data for full depth pavements with a very poor subgrade condition (where the subgrade CBR value is less than 10), the deflection data under a 9 kip load level and DCP testing results in the NC 2427 section used in NCHRP 10-48 project were adopted to this validation procedure, as shown in Figure 4.1. However, the multi-load deflection data was not available from this pavement. The first point to be made from these figures is the decreasing trend of the subgrade CBR values as the adjusted BDI and DBDI values

increase. This finding is significant because the subgrade strength can be determined based on unique BDI/DBDI – subgrade CBR relationships. Another observation may be made by comparing the degree of correlation between the adjusted BDI and DBDI, and the subgrade CBR value. The degree of correlation for the DBDI is slightly better than that for the BDI. This finding indicates that the deflections under a 12 kip load level is not large enough to cause the significant nonlinearity in the behavior of subgrade soils and to assess the subgrade condition. Therefore, it is desirable to use higher load level deflection data for a more accurate condition assessment of the subgrade.

The predicted ε_{sg} and $d\varepsilon_{sg}$ values are plotted in Figures 4.3 and 4.4 against the subgrade CBR values. Similar trends to those indicated above were observed for deflection basin parameters. Although the $d\varepsilon_{sg}$ slightly improves the degree of correlation, the use of deflections under a 12 kip load level is still not satisfactory. This validation concludes that a higher FWD load (greater than 12 kip) is necessary to improve the accuracy in estimating the subgrade condition.

Poor layer condition must be considered in order to establish criteria for condition indicators. Assuming that a subgrade CBR value (estimated from the DCP testing) of less than 10 is considered to be an indication of a very poor subgrade condition, a critical value for each condition indicator can be determined, as shown in Table 4.2.

Table 4.2. Criteria for Poor Subgrade in Full Depth Pavements

Subgrade Condition Indicators	Criteria for Poor Subgrade
Adjusted BDI	4.7 mils
Adjusted DBDI	5.5 mils
Adjusted ε_{sg}	680 microstrain
Adjusted $d\varepsilon_{sg}$	950 microstrain

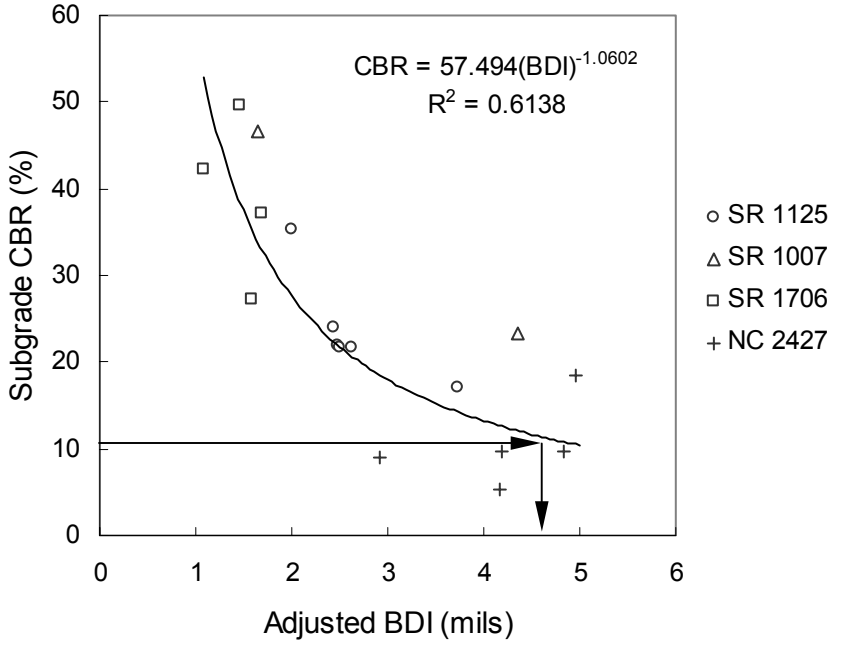

Figure 4.1. Adjusted BDI as a subgrade condition indicator for full depth pavements.

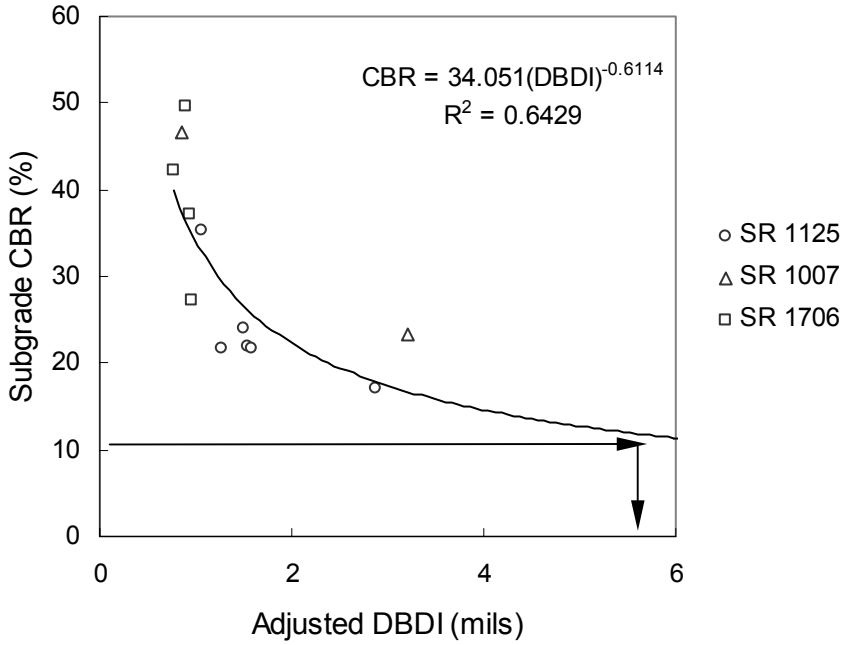

Figure 4.2. Adjusted DBDI as a subgrade condition indicator for full depth pavements.

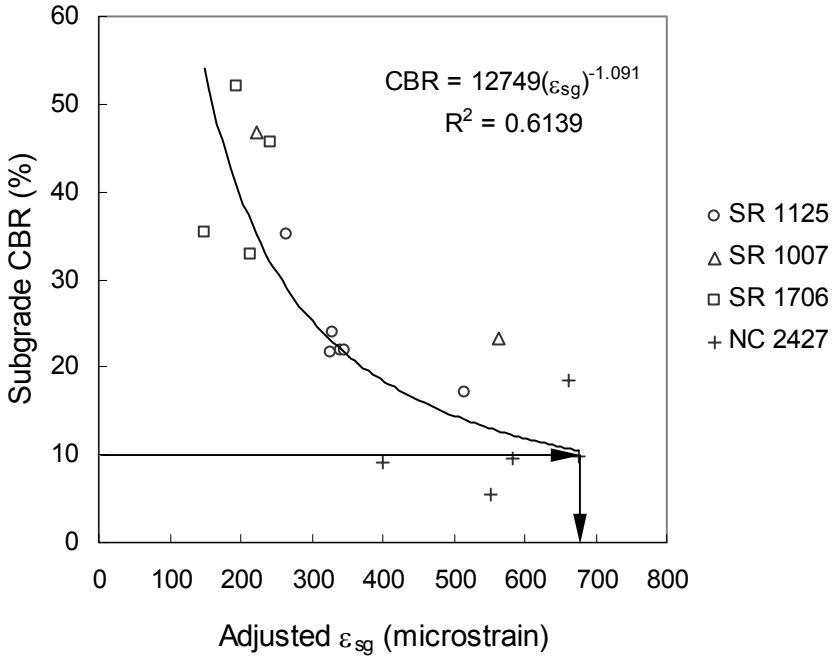

Figure 4.3. Adjusted ε_{sg} as a subgrade condition indicator for full depth pavements.

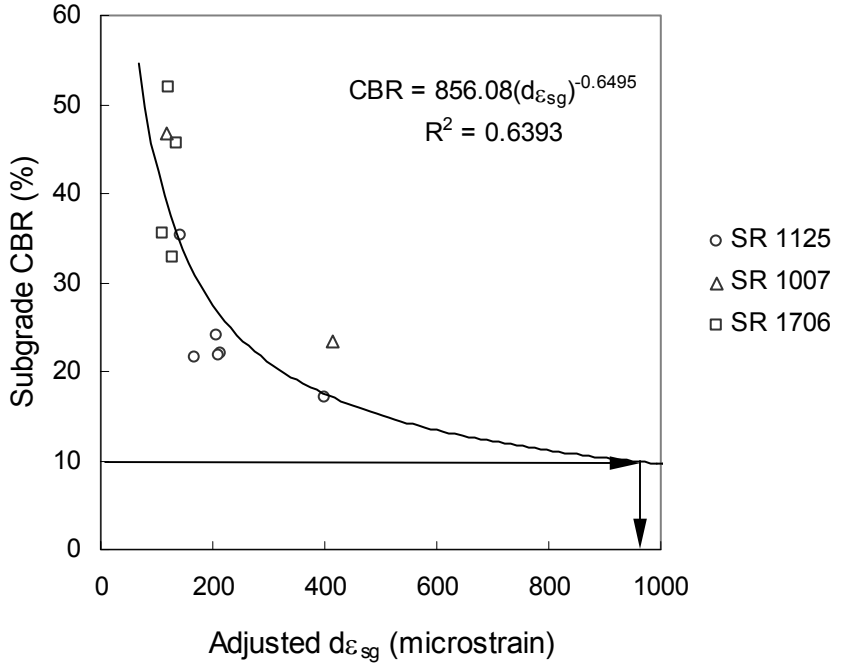

Figure 4.4. Adjusted $d\varepsilon_{sg}$ as a subgrade condition indicator for full depth pavements.

4.2 Aggregate Base Pavements

The following sections focus on the determination of the condition of the asphalt layer, the base layer, and the subgrade layer in aggregate base pavements using multi-load level FWD deflection data. The condition indicators for each layer were chosen based on the parametric sensitivity study discussed in Chapter 2.

4.2.1 Asphalt Layer

Indicators for AC Layer Condition Evaluation

Cracking at the top and bottom of the AC layer reduces the stiffness of the AC layer and then causes other distresses in flexible pavements. One possible method to detect the cracking potential in the AC layer is to use deflection basin parameters such as the SCI and the difference of the SCI (DSCI) due to the change in the load level as condition indicators. The parametric sensitivity analysis demonstrates that the SCI is the most sensitive indicator for the stiffness of the AC layer. Based on the synthetic database developed from dynamic, nonlinear finite element analysis, the following regression equation was derived to predict the E_{ac} value for aggregate base pavements.

$$\log(E_{ac}) = -1.183 \log(H_{ac}) - 1.103 \log(SCI) + 4.356 \quad (4.9)$$

Another approach is to use the value of the AC modulus and the horizontal tensile strain at the bottom of the AC layer, ε_{ac}, and the difference in ε_{ac} values at the highest and lowest load levels, $d\varepsilon_{ac}$. According to the pavement response models in Equations 2.8.a and 2.8.b, the ε_{ac} and $d\varepsilon_{ac}$ can be predicted as a function of the BDI and AC thickness.

Validation of Condition Assessment Procedure for the AC layer

The Long Term Pavement Performance (LTPP) data in DataPave 2.0 were used to validate the proposed procedure in assessing fatigue cracking potential in the AC layer. The LTPP pavement sections used here were selected from the Seasonal Monitoring Program (SMP) of the LTPP data. The LTPP data include temperature measurements within the AC layer, traffic monitoring data, multi-load level FWD deflection data, and distress survey results. All the test sections are located in wet no-freeze and wet freeze regions. Characteristics of the selected test sections are summarized in Table 4.3.

Table 4.3. Characteristics of Pavement Test Sections in LTPP Data

State	SHRP ID	Thickness (in)			Material Type		
		AC	Base	Subbase	Base	Subbase	Subgrade
NC (37)[1]	1028	10.5	5.5	-	Silty Sand	-	SM
TX (48)[1]	1077	5.1	10.4	-	Cr. Stone	-	ML
TX (48)[1]	1068	10.9	6.0	8.0	Cr. Stone	Lime-Tr Soil	CL
TX (48)[1]	1060	7.5	12.3	6.0	Cr. Stone	Lime-Tr Soil	SM
AL (1)[1]	0102	4.0	12.0		Cr. Stone		CL
CT (9)[2]	1803	7.2	12.0	-	Gravel	-	ML
MA (25)[2]	1002	7.8	4.0	8.4	Cr. Gravel	Soil Agg.	SP
MN (27)[2]	6251	7.4	10.2	-	Gravel	-	SP
NE (31)[2]	0114	7.0	12.0	-	Agg.		CL
NH (33)[2]	1001	8.4	19.3	14.4	Gravel	Soil Agg.	SP
OK (40)[2]	4165	2.7	5.4	-	HMAC	-	SM

[1]Wet no-freeze region
[2]Wet freeze region

Because the AC mixture characteristics are different based on the climatic region defined in the LTPP study, the validation was performed on wet no-freeze and wet freeze regions separately. All the deflection data used in this study were collected at the final year of the distress survey. Measured AC mid-depth temperature data were used for this condition evaluation. Different damage levels are expected to contribute to the magnitude and variation of pavement condition indicators with respect to the AC mid-depth temperature. Compared with the intact AC layers, the excessively damaged AC layers show a high magnitude of deflection basin parameters and pavement responses, and a low magnitude of the AC modulus. It also attributes to the large deviation from the pavement condition indicators versus the AC mid-depth temperature relationship in an intact pavement.

Figures 4.5 to 4.8 show the plots of the SCI and DSCI values versus the AC mid-depth temperatures for the LTPP test sections. Table 4.4 shows the area with fatigue cracking and length of longitudinal cracking for LTPP test sections. Note that filled symbols represent the excessive level of fatigue cracking, crossed symbols represent the moderate level of fatigue cracking, and empty symbols represent the nominal level of fatigue cracking. As shown in Figures 4.5 and 4.7, the SCI and DSCI values in the 48-1077 section with moderate cracking are higher than those in the 37-1028 and 48-1068 sections with excessive cracking. This result indicates that the deflection basin parameters may not be good indicators for detecting the fatigue cracking in the AC layer because the measured SCI and DSCI values cannot distinguish between intact and damaged pavements.

Table 4.4. Area with Fatigue Cracking in LTPP Test Sections

Region	State	SHRP ID	Survey Date	Area with Fatigue Cracking (ft^2)	Length of Longitudinal Cracking (ft)
Wet no Freeze	NC (37)	1028	9/29/98	1865.6	666.7
	TX (48)	1068	9/17/97	1076.7	300.0
	TX (48)	1077	7/2/97	57.8	233.3
	TX (48)	1060	7/10/97	12.2	33.3
Wet Freeze	CT (9)	1803	9/11/97	351.1	333.3
	MA (25)	1002	5/7/97	1953.3	566.7
	MN (27)	6251	6/11/97	271.1	166.7
	NH (33)	1001	10/22/97	1302.2	33.3
	OK (40)	4165	9/11/97	41.1	50.0

Further investigation of the AC layer condition assessment was carried out using pavement responses and the elastic modulus of the AC layer. Figures 4.9 to 4.12 display the changes in ε_{ac} and $d\varepsilon_{ac}$ as a function of the AC mid-depth temperatures. Overall, the magnitudes of ε_{ac} and $d\varepsilon_{ac}$ in pavements with high levels of severe fatigue cracking are higher than those in pavements with low levels of severe fatigue cracking at a wide range of temperatures. For pavements in a wet freeze region, there is a definite difference in pavement responses among pavements with excessive and moderate fatigue cracking. The largest variation in the AC modulus-AC mid-depth temperature relationship was observed from section 33-1011. The primary reason for this variation may be the existence of fatigue or longitudinal cracking in the pavement section.

The predicted E_{ac} values are plotted in Figures 4.13 and 4.14 against the AC mid-depth temperatures for the LTPP test sections. As expected, the predicted E_{ac} values in pavements with high levels of severe fatigue cracking are lower than those in pavements with low levels of severe fatigue cracking. The recent study by Xu (2000) concludes that a distressed AC layer shows a larger deviation of the AC modulus value than that

represented in the AC modulus versus the AC mid-depth temperature relationship for intact pavements. It can be seen that pavement in section 33-1001 shows a large deviation in the predicted E_{ac} - AC mid-depth temperature relationship, which supports the possible existence of high or moderate levels of severe fatigue cracking in the AC layer. The conclusion drawn from these observations is that the E_{ac}, ε_{ac}, and $d\varepsilon_{ac}$ are capable of evaluating the condition of the AC layer.

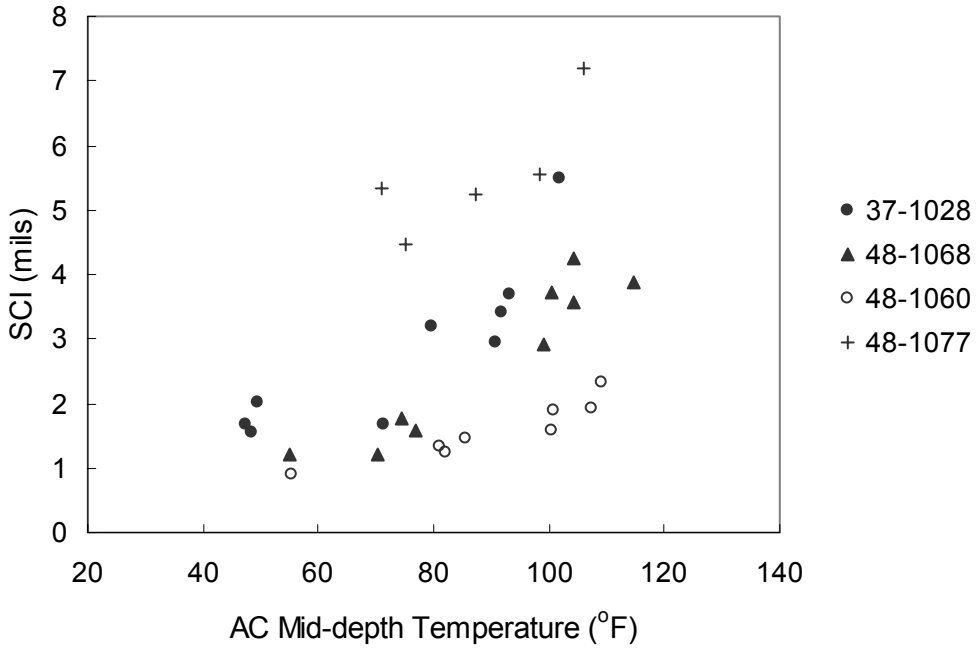

Figure 4.5. SCI versus AC mid-depth temperature for LTPP test sections in a wet no-freeze region.

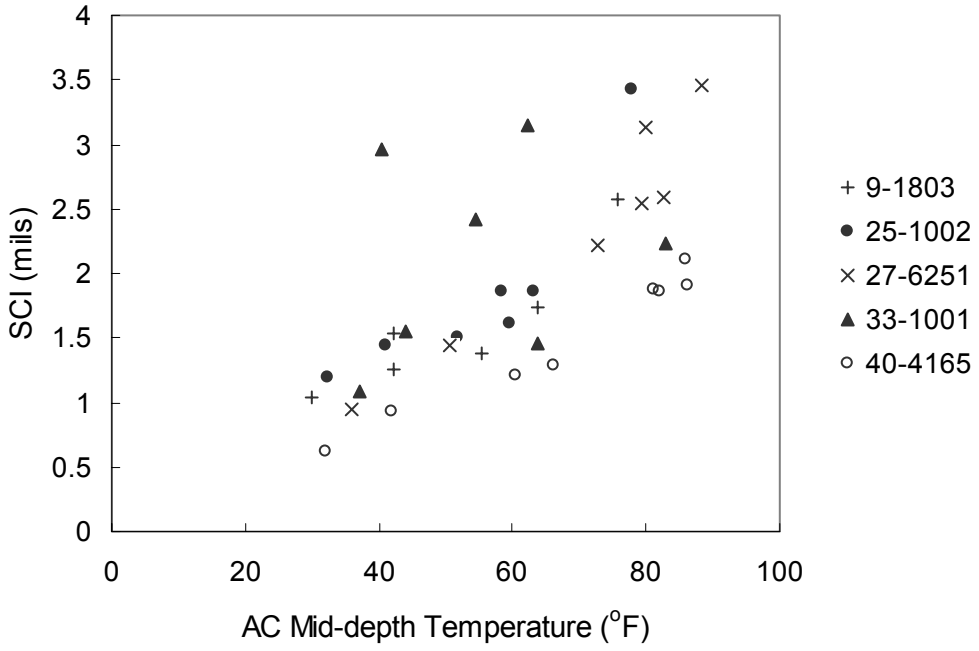

Figure 4.6. SCI versus AC mid-depth temperature for LTPP test sections in a wet freeze region.

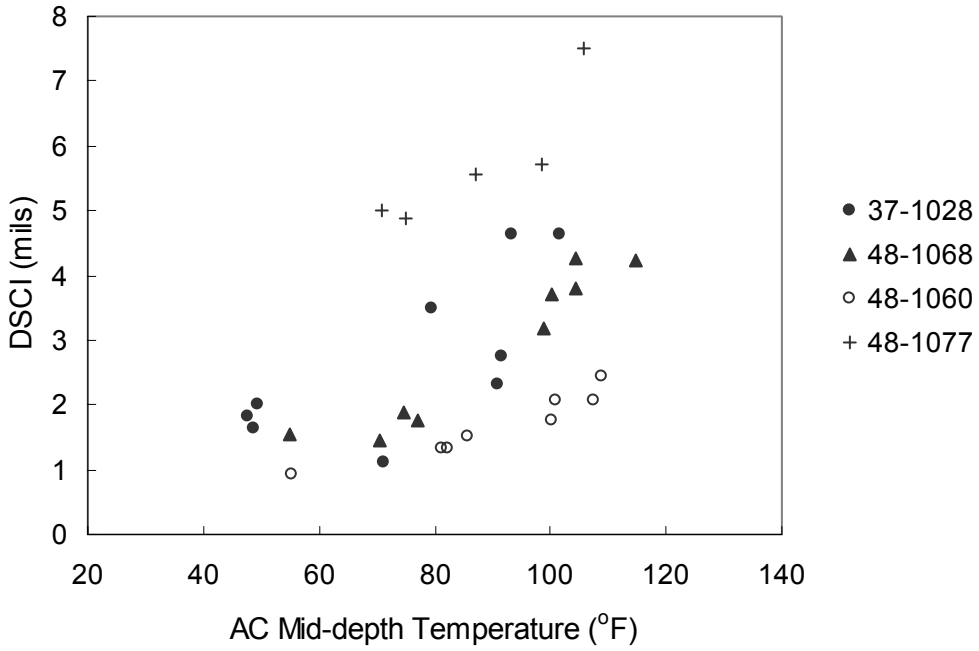

Figure 4.7. DSCI versus AC mid-depth temperature for LTPP test sections in a wet no-freeze region.

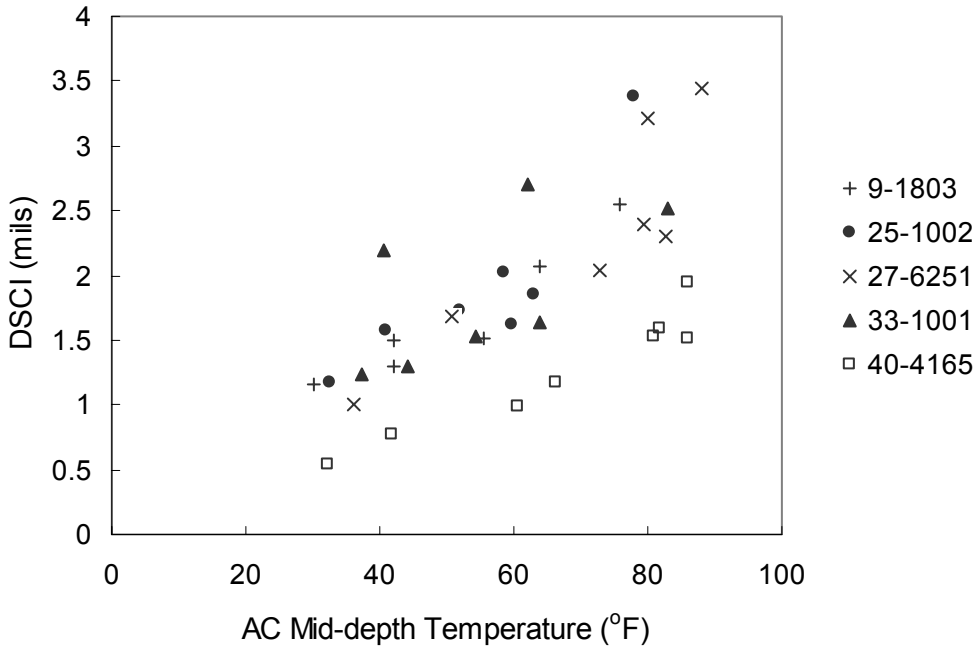

Figure 4.8. DSCI versus AC mid-depth temperature for LTPP test sections in a wet freeze region.

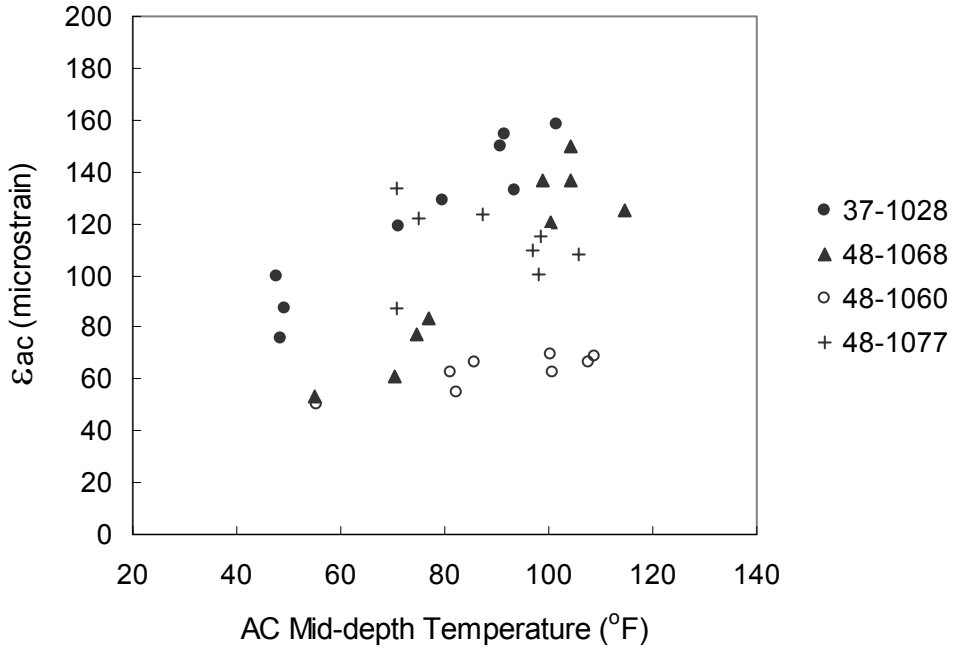

Figure 4.9. ε_{ac} versus AC mid-depth temperature for LTPP test sections in a wet no-freeze region.

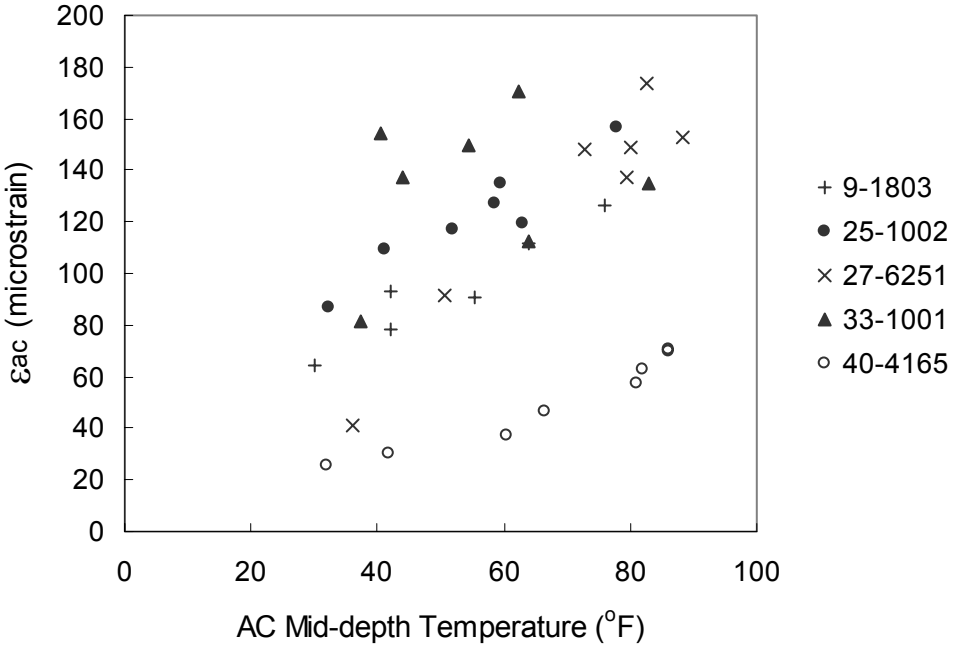

Figure 4.10. ε_{ac} versus AC mid-depth temperature for LTPP test sections in a wet freeze region.

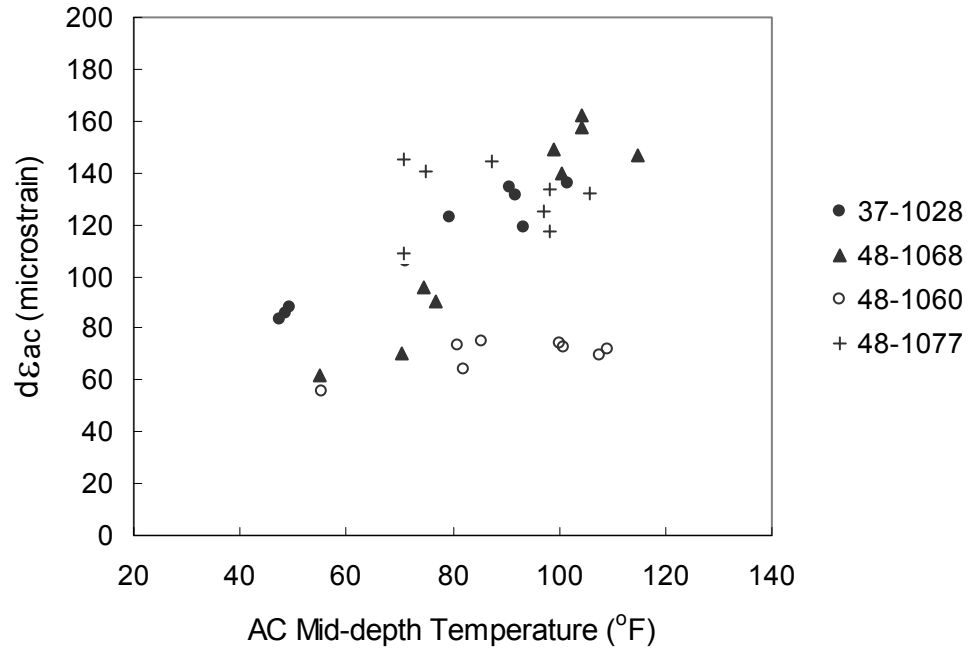

Figure 4.11. $d\varepsilon_{ac}$ versus AC mid-depth temperature for LTPP test sections in a wet no-freeze region.

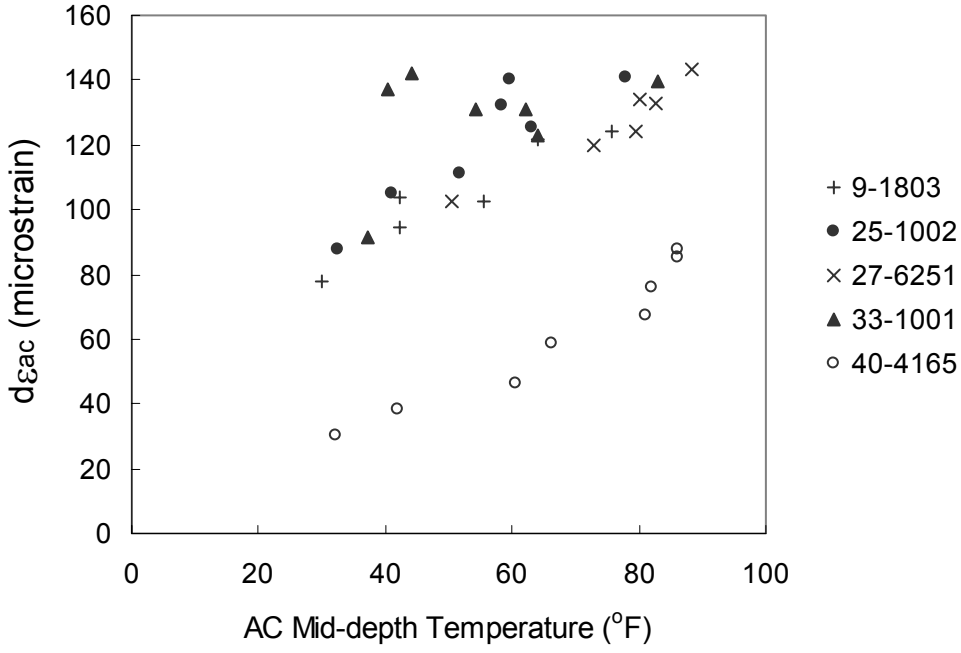

Figure 4.12. $d\varepsilon_{ac}$ versus AC mid-depth temperature for LTPP test sections in a wet freeze region.

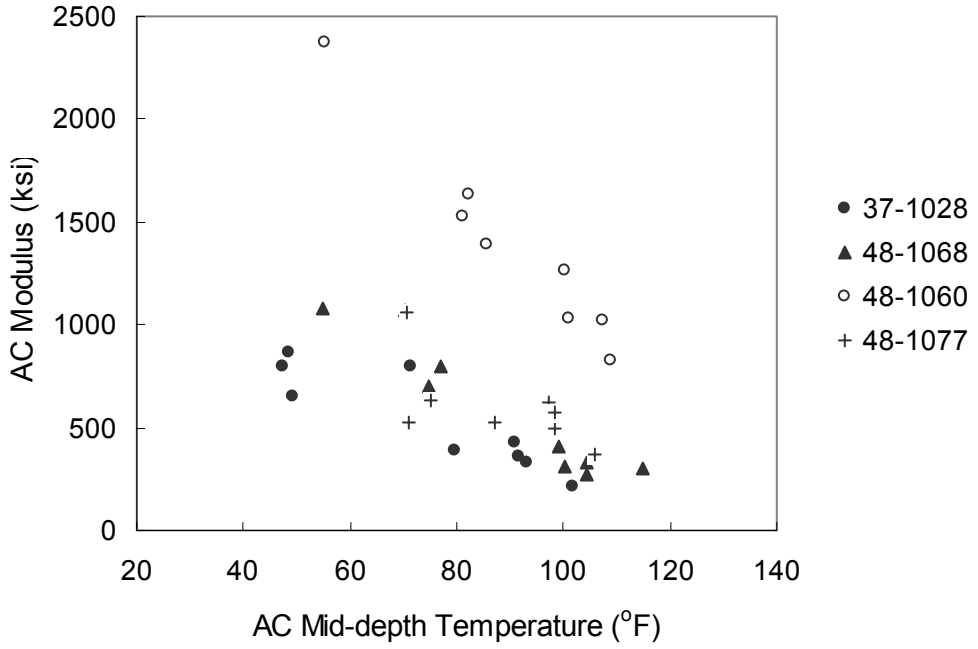

Figure 4.13. E_{ac} versus AC mid-depth temperature for LTPP test sections in a wet no-freeze region.

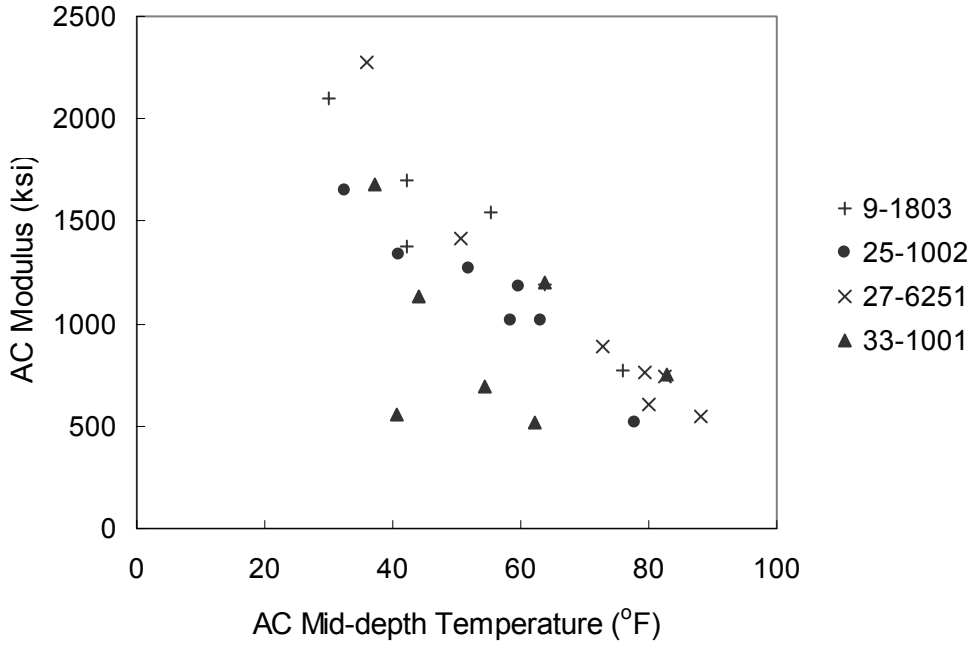

Figure 4.14. E_{ac} versus AC mid-depth temperature for LTPP test sections in wet no-freeze region.

4.2.2 Base Layer

Indicators for Base Layer Condition Evaluation

For base layer condition evaluation, the BDI, DBDI, compressive strain on the top of the base layer, ε_{abc}, and the difference of ε_{abc} due to load level, $d\varepsilon_{abc}$, were selected as critical indicators based on the parametric sensitivity analysis. The pavement response models presented in Equations 2.12.a and 2.12.b were used to calculate ε_{abc} and $d\varepsilon_{abc}$ values.

Structural Correction Procedure for Base Layer Condition Assessment

For the structural correction procedure the nonlinear synthetic database was used to represent these indicators in terms of structural and material parameters as follows

$$\log(BDI) = -1.549 \log(H_{ac}) - 0.095 \log(H_{base}) - 0.572 \log(E_{ac}) - 0.013 \log(E_{ri}) + 3.535$$

$$R^2 = 0.947 \qquad SEE = 0.090 \tag{4.10}$$

$$\log(DBDI) = -1.476 \log(H_{ac}) - 0.112 \log(H_{base}) - 0.559 \log(E_{ac}) - 0.018 \log(E_{ri}) + 3.287$$

$$R^2 = 0.935 \qquad SEE = 0.097 \tag{4.11}$$

$$\log(\varepsilon_{abc}) = -1.583 \log(H_{ac}) + 0.001 \log(H_{base}) - 0.591 \log(E_{ac}) + 0.146 \log(E_{ri}) + 5.031$$

$$R^2 = 0.940 \qquad SEE = 0.100 \tag{4.12}$$

$$\log(d\varepsilon_{abc}) = -1.362 \log(H_{ac}) + 0.010 \log(H_{base}) - 0.536 \log(E_{ac}) + 0.145 \log(E_{ri}) + 4.413$$

$$R^2 = 0.900 \qquad SEE = 0.124 \tag{4.13}$$

Using these regression equations, the condition indicators for the pavement structure in question can be corrected for a standard structure. The standard structure used in this study is as follows: H_{ac} = 6 in., E_{ac} = 500 ksi, H_{base} = 10 in., and H_{sg} = infinity. Using a similar correction procedure in full depth pavements, an adjusted condition indicator for a standard structure can be determined.

Validation of Condition Assessment Procedure for Aggregate Base Layer

Multi-load level FWD deflection data and DCP testing results were used to check the accuracy of the condition assessment of the base layer in aggregate base pavements. Figure 4.15 presents the results of DCP testing performed on SR 2026. As shown in this figure, the thickness of the base layer was considered to be a breakpoint in the number of blows versus penetration depth plot. A summary of the coring and DCP testing results is given in Table 4.5.

Table 4.5. A Summary of Coring and DCP Testing for Aggregate Base Pavements

Road	Test Date	No. of Cores	AC Thickness (in)	Base Thickness (in)
SR 1128	12/12/00	3	5.8	6.0
SR 1600	1/31/01	4	3.9	5.4
SR 1901	1/4/00	2	4.3	6.0
SR 2026	2/16/00	3	4.0	10.4
SR 1728	1/4/00	4	4.5	8.7
SR 1103	1/4/00	1	7.0	12.3

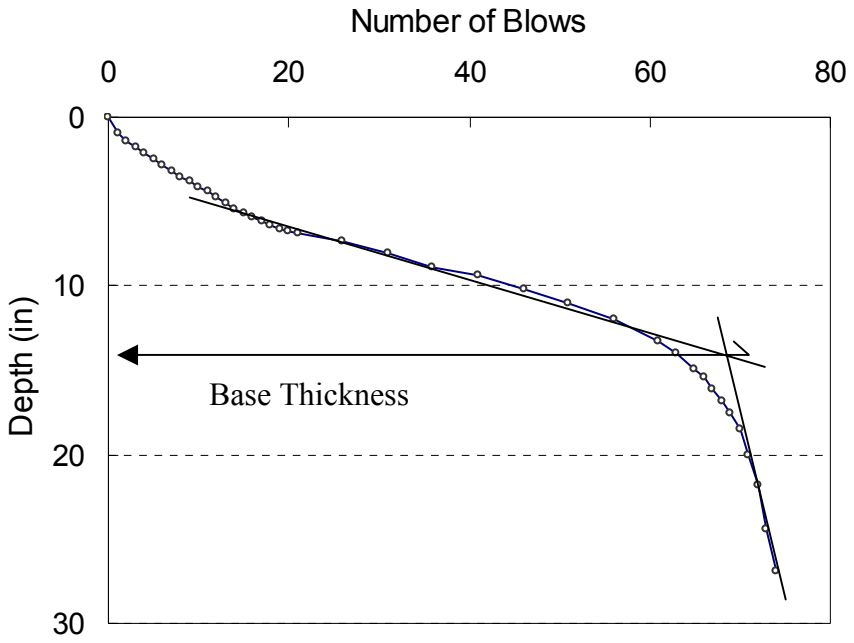

Figure 4.15. Determination of base layer thickness for the SR 2026 section.

For the base layer condition evaluation, the predicted condition indicators were plotted against the base CBR values in Figures 4.16 through 4.19. Figures 4.16 and 4.17 show the relationships between the adjusted BDI and DBDI values and the base CBR values. It is observed that the base CBR value decreases with an increase in the adjusted values of the indicator but the results show a larger variation. Garg and Thompson (1998) reported that the quality of the base layer has no significant effect on pavement surface deflections. Similar to full depth pavements, there is little difference in the R square values obtained from the BDI and DBDI approach, which indicates that deflection data under a 12 kip load level used in this study may not improve the accuracy in predicting the base layer condition evaluation.

The ε_{abc} and $d\varepsilon_{abc}$ values were also plotted against the base CBR values in Figures 4.18 and 4.19. It can be seen that the base CBR value decreases as the ε_{abc} and $d\varepsilon_{abc}$ values increase. The ε_{abc} and $d\varepsilon_{abc}$ show a slightly higher degree of correlation than the deflection basin parameters. Based on the NCDOT's condition criterion for marginal to poor stone base layers (CBR is less than 100), the criterion for each indicator has been established and is shown in Table 4.6. About 80 % of these pavement sections show marginal to poor quality of base layer based on the developed criteria.

Table 4.6. Criteria for Poor Base Layer in Aggregate Base Pavements

Base Condition Indicators	Criteria for Poor Base Layer
Adjusted BDI	3 mils
Adjusted DBDI	3.5 mils
Adjusted ε_{abc}	700 microstrain
Adjusted $d\varepsilon_{abc}$	500 microstrain

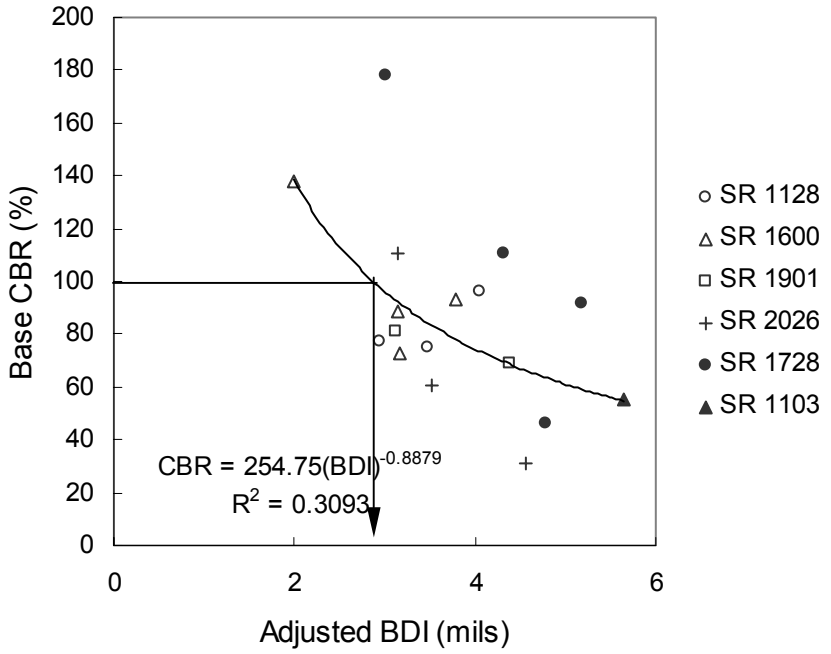

Figure 4.16. Adjusted BDI as a base condition indicator for aggregate base pavements.

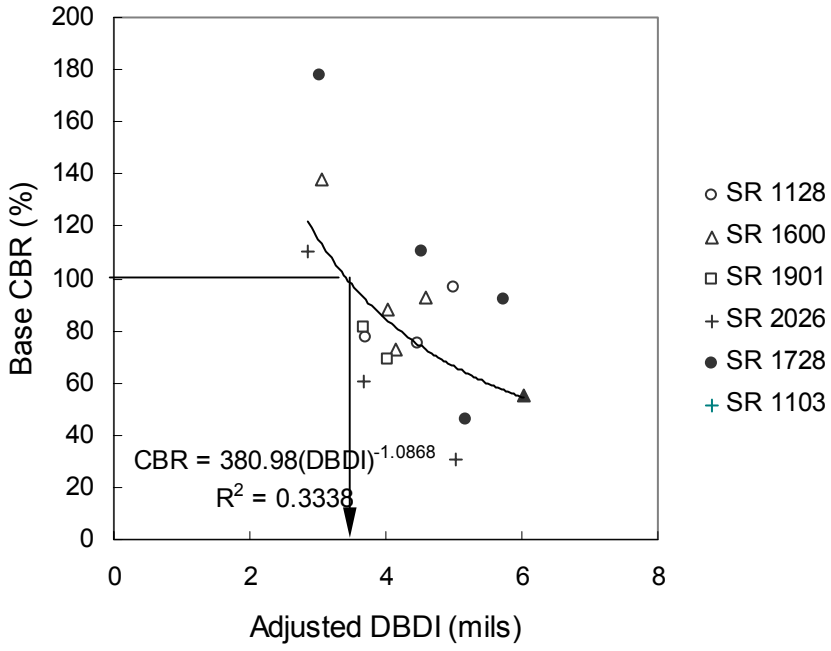

Figure 4.17. Adjusted DBDI as a base condition indicator for aggregate base pavements.

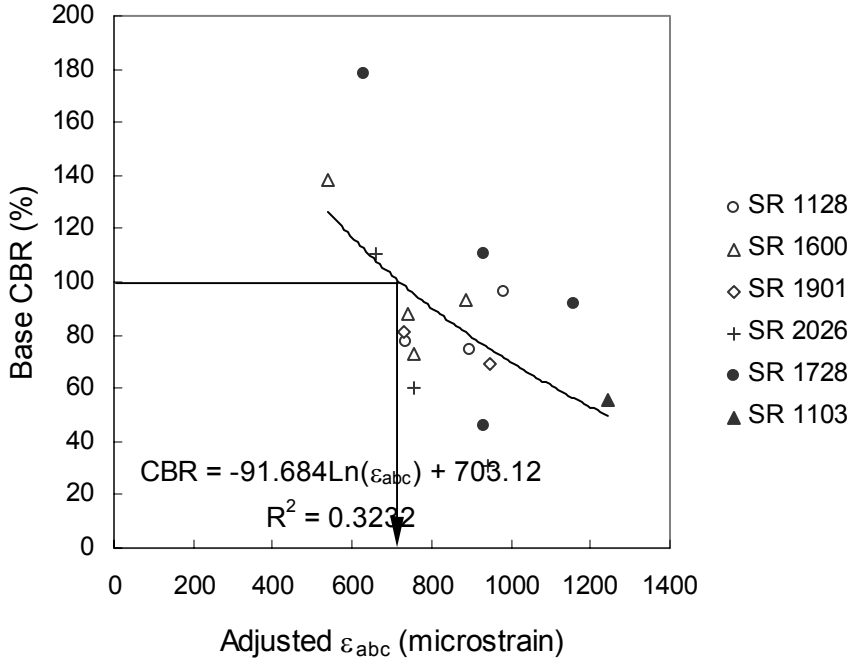

Figure 4.18. Adjusted ε_{abc} as a base condition indicator for aggregate base pavements.

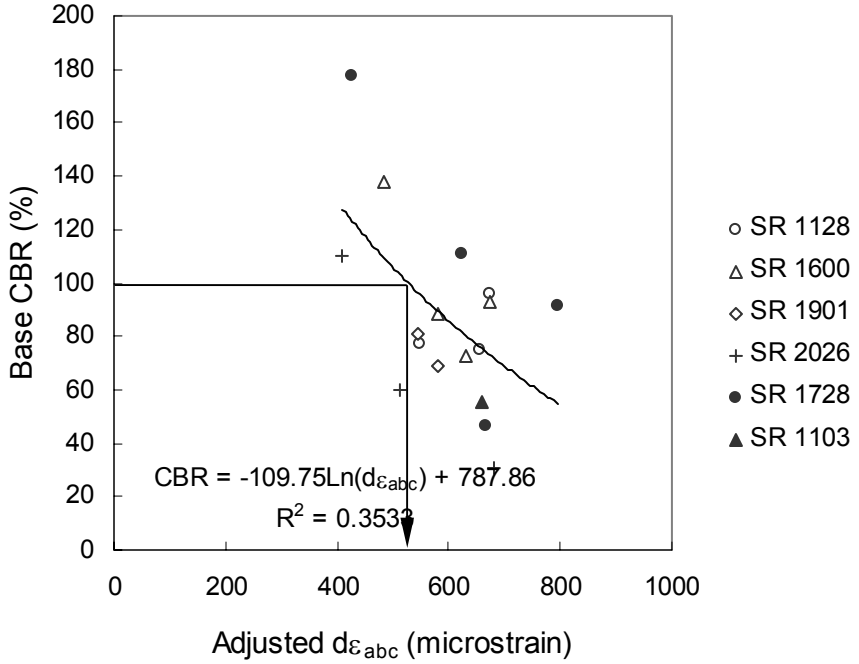

Figure 4.19. Adjusted $d\varepsilon_{abc}$ as a base condition indicator for aggregate base pavements.

4.2.3 Subgrade

Indicators for Subgrade Condition Evaluation

According to the sensitivity study, the Base Curvature Index (*BCI*) was found to be a good indicator for the condition of the subgrade in aggregate base pavements. The BCI is defined as the difference in deflections at 24 and 36 in. of the radial distance from the center of the load plate. The difference of BCI values (DBCI) obtained from deflections under different load levels was also investigated for condition assessment of the subgrade. In addition, the ε_{sg} and $d\varepsilon_{sg}$ were calculated using Equations 2.14.a and 2.14.b.

Structural Correction Procedure for Subgrade Condition Assessment

As described previously, each condition indicator is dependent on the pavement structure and, therefore, a structural correction procedure is needed. These indicators can be described in terms of structural and material parameters by the following equation:

$$\log(BCI) = -1.280 \log(H_{ac}) - 0.150 \log(H_{base}) - 0.406 \log(E_{ac}) - 0.167 \log(E_{ri}) + 3.385$$

$$R^2 = 0.889 \qquad SEE = 0.108 \tag{4.14}$$

$$\log(DBCI) = -1.254 \log(H_{ac}) - 0.162 \log(H_{base}) - 0.413 \log(E_{ac}) - 0.194 \log(E_{ri}) + 3.342$$

$$R^2 = 0.896 \qquad SEE = 0.104 \tag{4.15}$$

$$\log(\varepsilon_{sg}) = -1.330 \log(H_{ac}) - 0.571 \log(H_{base}) - 0.446 \log(E_{ac}) - 0.474 \log(E_{ri}) + 7.328$$

$$R^2 = 0.921 \qquad SEE = 0.105 \tag{4.16}$$

$$\log(d\varepsilon_{sg}) = -1.316 \log(H_{ac}) - 0.551 \log(H_{base}) - 0.454 \log(E_{ac}) - 0.495 \log(E_{ri}) + 7.263$$

$$R^2 = 0.909 \qquad SEE = 0.113 \tag{4.17}$$

Validation of Condition Assessment Procedure for Subgrade Layer

The adjusted subgrade condition indicators were plotted against the subgrade CBR values in Figures 4.20 through 4.23 for subgrade condition evaluation in aggregate base pavements. It is noted that the deflection data for a 9 kip load level used in the NCHRP 10-48 report (Kim et al., 2000) were also input to this procedure, and the results were plotted in Figures 4.20 and 4.22. It can be seen from Figure 4.20 that the subgrade CBR values decrease with increasing adjusted BCI values except for SR 1128 and SR 1600. The trend line between the adjusted BCI values and subgrade CBR values developed by Kim et al. (2000) was shifted to the left, thus the corrected relationship was established.

A similar trend can be observed in Figure 4.22 for the adjusted ε_{sg} values. Compared with Figures 4.2 and 4.4 for full depth pavements, which show close relationships between the DBDI and $d\varepsilon_{sg}$ values and the subgrade CBR values, larger variations were observed in aggregate base pavements (Figures 4.21 and 4.23). These poor correlations between condition indicators and subgrade strength in aggregate base pavement may be due to the fact that a 12 kip FWD load level is not large enough to induce the nonlinear behavior of subgrade soils, which may be related to the condition of the subgrade layer.

Kim et al. (2000) also developed a procedure for assessment of pavement layer conditions and found that the Subgrade Stress Ratio (SSR) and subgrade modulus (E_{sg}) are also good indicators of the condition of the subgrade for aggregate base pavements. The FWD deflection data used here were input to the artificial neural network algorithm developed by Kim et al. (2000) to predict the SSR and E_{sg} values. These values were plotted against the subgrade CBR values in Figures 4.24 and 4.25. It can be seen that a

reasonable correlation between each indicator and CBR values can be found. Based on the criterion that a subgrade CBR value less than 10 represents a poor subgrade condition, the criteria for the subgrade condition indicators are presented in Table 4.7. The subgrade layers in these pavements are in good condition based on the developed criteria.

Table 4.7. Criteria for Poor Subgrade Layer in Aggregate Base Pavements

Subgrade Condition Indicators	Criteria for Poor Subgrade
Adjusted BCI	3.7mils
Adjusted ε_{sg}	700 microstrain
SSR	0.53
Adjusted E_{sg}	5 ksi

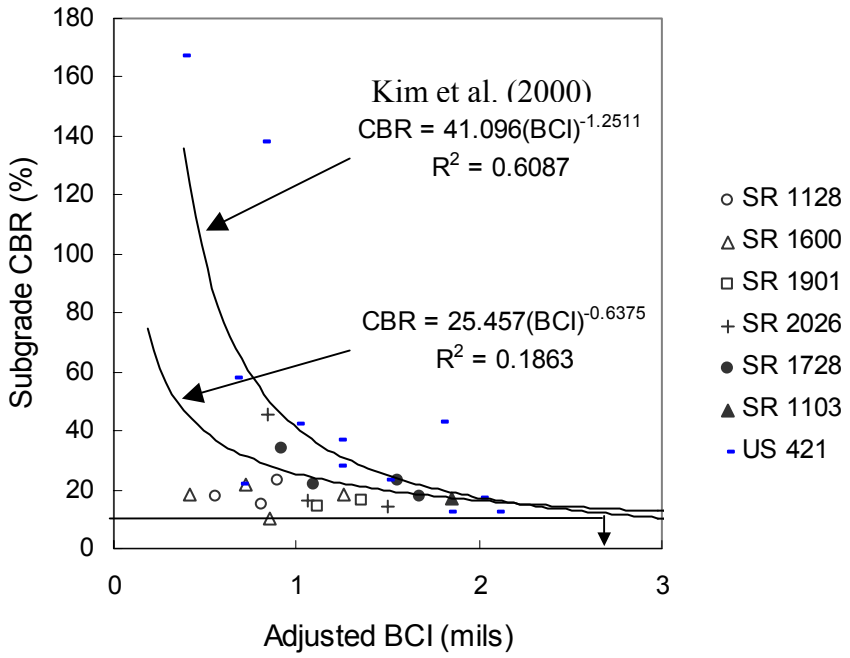

Figure 4.20. Adjusted BCI as a subgrade condition indicator for aggregate base pavements.

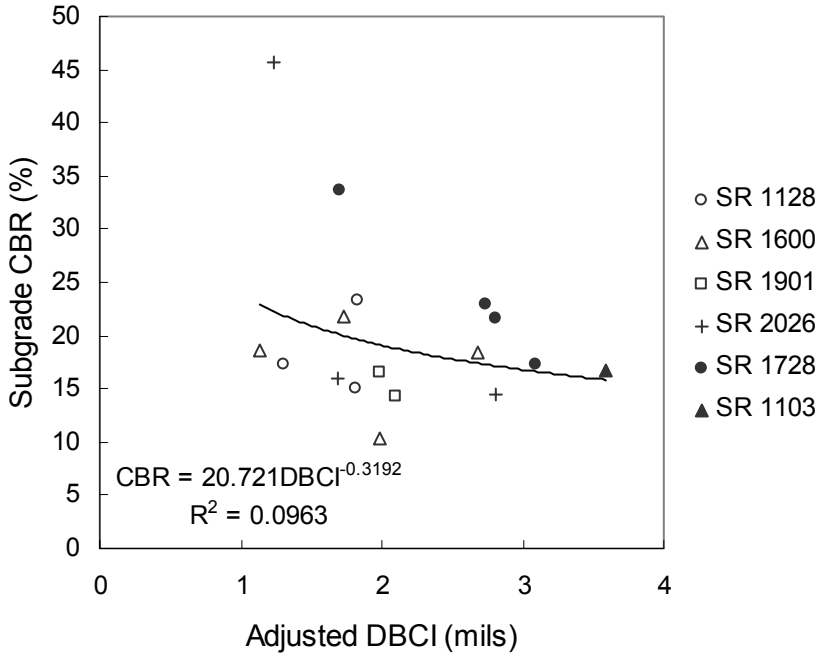

Figure 4.21. Adjusted DBCI as a subgrade condition indicator for aggregate base pavements.

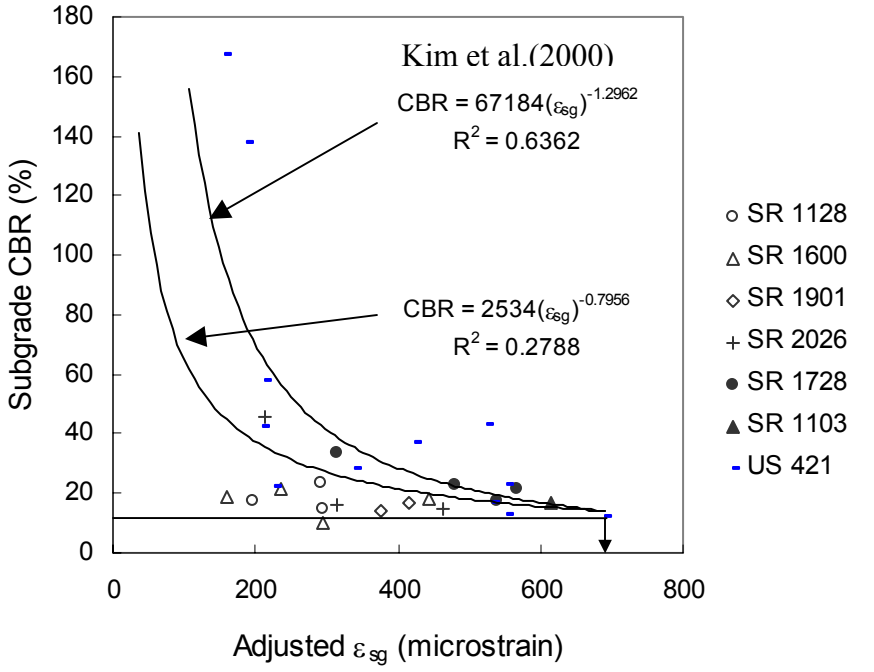

Figure 4.22. Adjusted ε_{sg} as a subgrade condition indicator for aggregate base pavements.

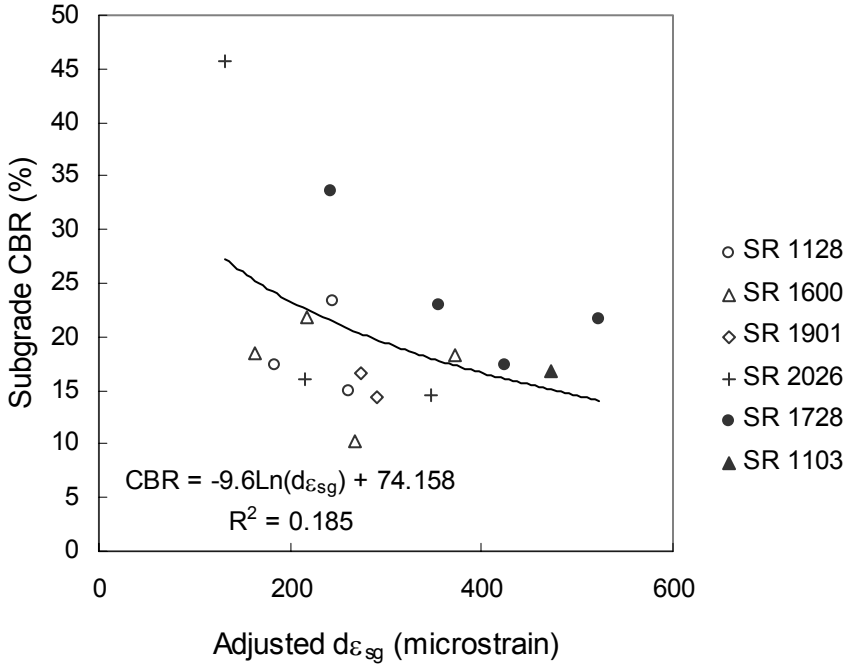

Figure 4.23. Adjusted $d\varepsilon_{sg}$ as a subgrade condition indicator for aggregate base pavements.

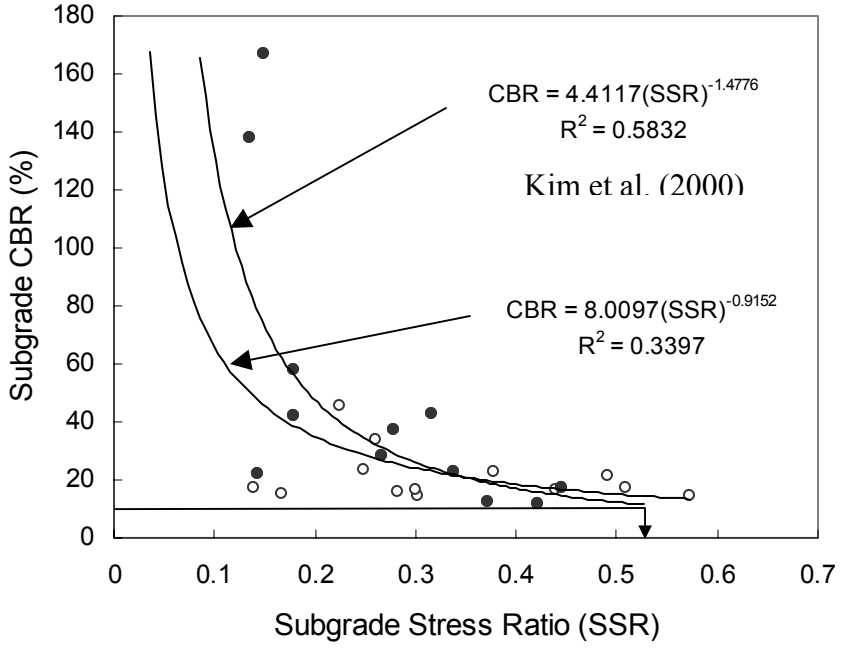

Figure 4.24. SSR as a subgrade condition indicator for aggregate base pavements.

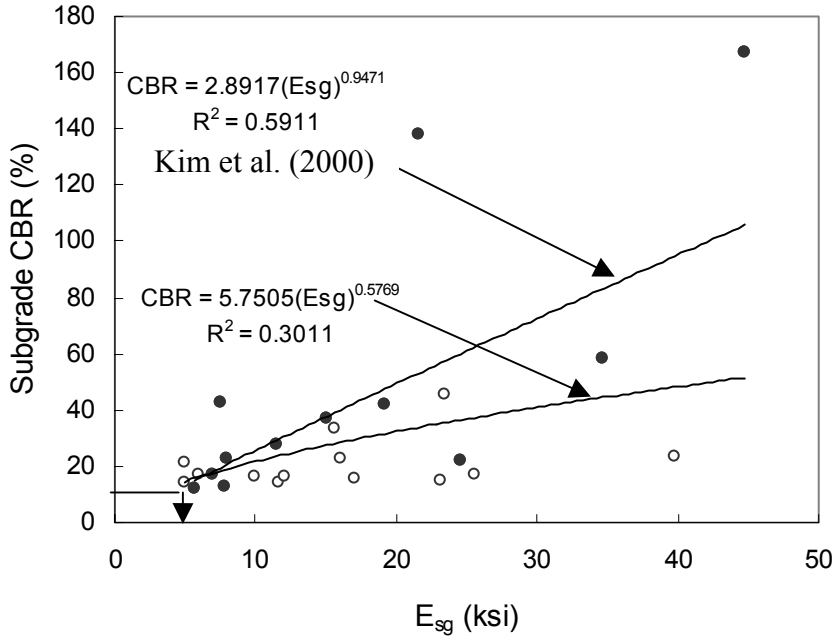

Figure 4.25. E_{sg} as a subgrade condition indicator for aggregate base pavements.

4.2.4 Validation of Condition Assessment Procedure Using NCDOT Data

During the previous NCDOT temperature correction project (23241-95-1), multi-load level FWD deflection data were collected from seven pavement sections in different climatic regions of North Carolina, all of which were in good condition at the time of testing (1995). Three pavement sections out of these were revisited in 2001 to check their current conditions. A visual distress survey was carried out to identify any noticeable deterioration in these pavements, and multi-load level FWD tests were performed on them at the same FWD test locations used in the previous project. Results of the visual distress survey are shown in Table 4.8.

Table 4.8. Results of Visual Distress Survey in NCDOT Test Sections

Route	County	Distress Survey Result
US 74	Polk	Continuous fatigue cracking in inside wheelpath. Low severity fatigue with longitudinal cracking in outside wheelpath
US 421	Wilkes	Light rutting with low severity longitudinal cracking
US 264	Pitt	Pavement condition is good. Very light rutting. No cracking

Figures 4.26 through 4.28 show the magnitude of pavement responses in both 1995 and 2001 for US 74, US 421, and US 264. It can be seen from Figure 4.26 that the ε_{ac} values for US 264 (no fatigue cracking) is slightly higher than those for US 74 (excessive level of fatigue cracking). The use of the magnitude of ε_{ac} values can hardly predict the severity of fatigue cracking in these pavement sections.

Another important question to this project is whether the difference in multi-load FWD deflections could predict the poor performance observed in US 74 in advance. The

percent increase in layer strains due to the increase in FWD load level from 6 kip to 15 kip is shown in Figures 4.29 to 4.31. In all three layers, the percent increase in strain estimated from US 264 was slightly higher than that from US 74. The trend shown in these figures does not support the hypothesis that the difference in multi-load deflections may yield information related to the future performance of pavements. However, it must be noted that the traffic loads applied to these two pavements between 1995 (FWD testing time) and 2001 (distress survey time) are different. Unfortunately, the research team does not have reliable traffic information for these two pavements for any further investigation.

However, the important point to be made is the increasing trend of the pavement responses as a function of time in all the pavement sections. The percent of increase in pavement responses between 1995 and 2001 is shown in Figures 4.32 to 4.34. This finding indicates the possible occurrence of distresses in pavement layers between 1995 and 2001. This trend is more noticeable in US 74 which has the most significant level of distresses such as fatigue cracking and rutting. Regardless of the load level, the percent of increase in pavement responses in US 74 is higher than that in US 264.

Another observation can be made by comparing the pavement responses of US 264 and US 74. The ε_{ac} and ε_{abc} values obtained from US 264 and US 74 were about the same in 2001. However, the ε_{sg} values obtained from US 74 are higher than those values obtained from US 264 in 2001. The significantly increasing trend of pavement response with time and higher ε_{sg} values in US 74 may result from various types of distress. Since the traffic monitoring data were not available in these pavement sections, it is difficult to estimate pavement performance accurately.

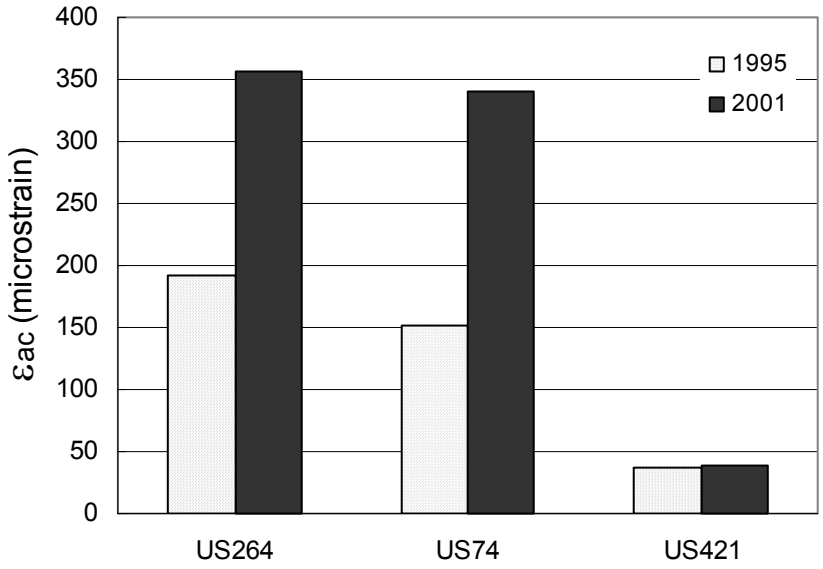

Figure 4.26. Magnitudes of ε_{ac} for the US 264, US 74, and US 421 sections in 1995 and 2001.

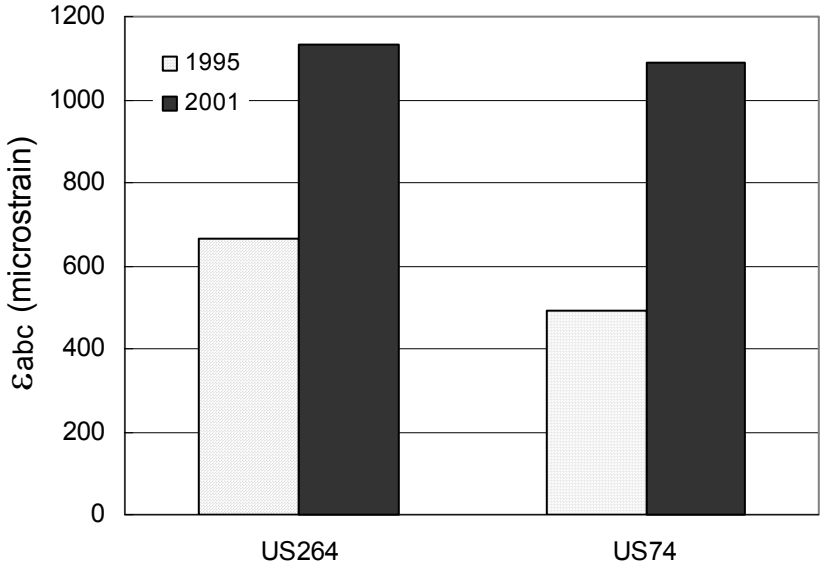

Figure 4.27. Magnitudes of ε_{abc} for the US 264 and US 74 sections in 1995 and 2001.

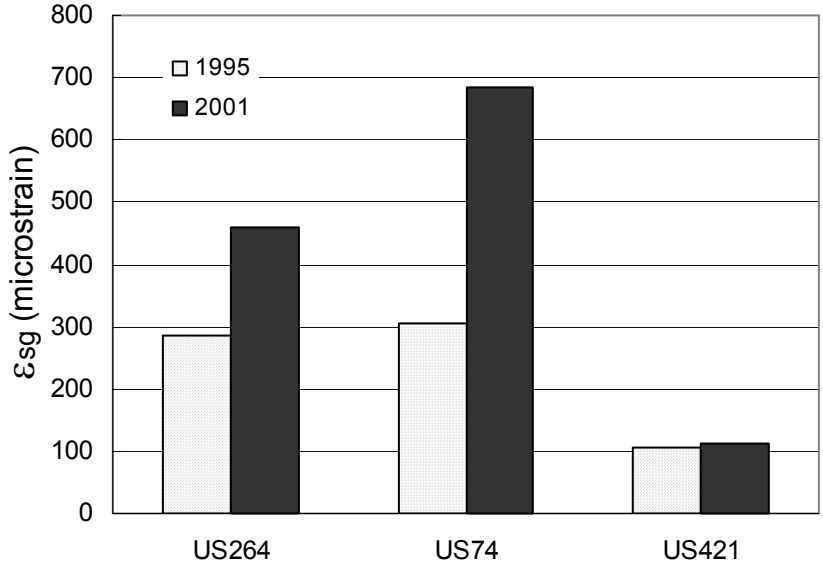

Figure 4.28. Magnitudes of ε_{sg} for the US 264, US 74, and US 421 sections in 1995 and 2001.

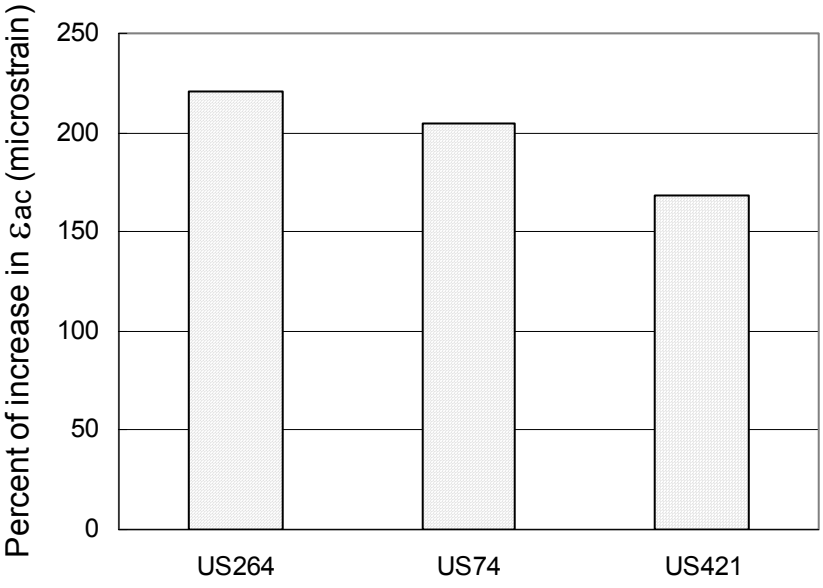

Figure 4.29. Percent increase in ε_{ac} due to increased load level estimated from FWD testing in 1995.

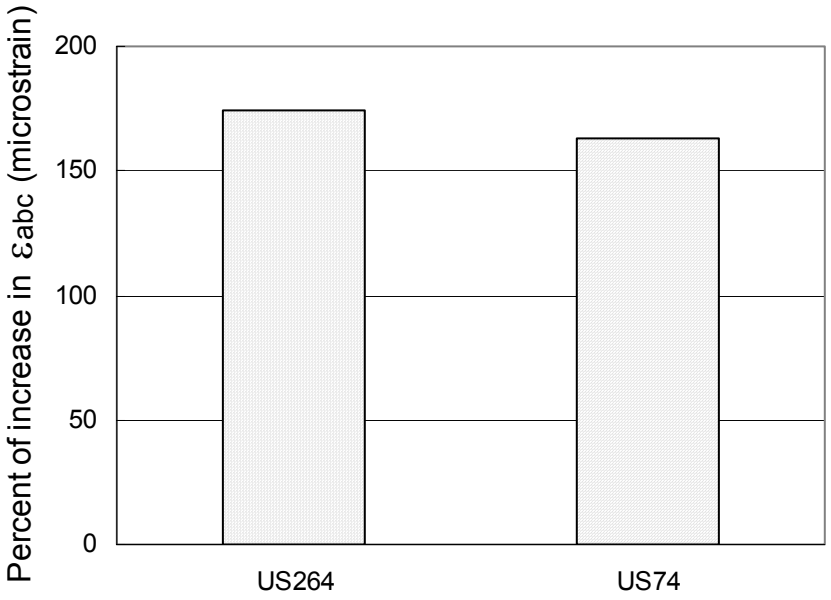

Figure 4.30. Percent increase in ε_{abc} due to increased load level estimated from FWD testing in 1995.

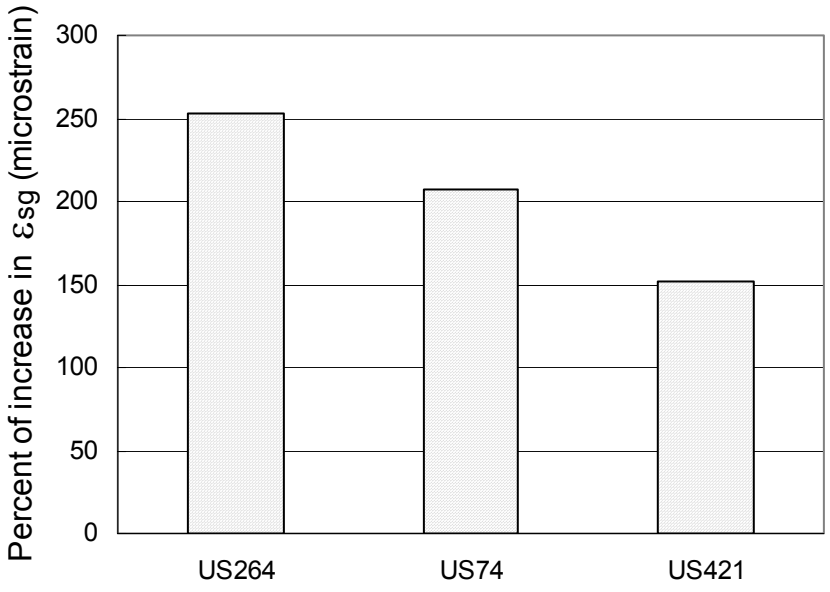

Figure 4.31. Percent increase in ε_{sg} due to increased load level estimated from FWD testing in 1995.

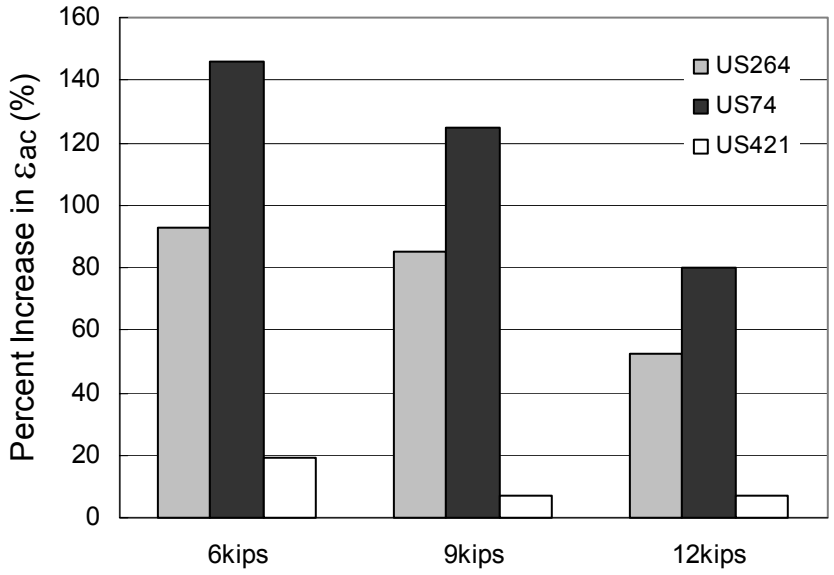

Figure 4.32. Percent of increase in ε_{ac} between 1995 and 2001 for the US 264, US 74, and US 421 sections.

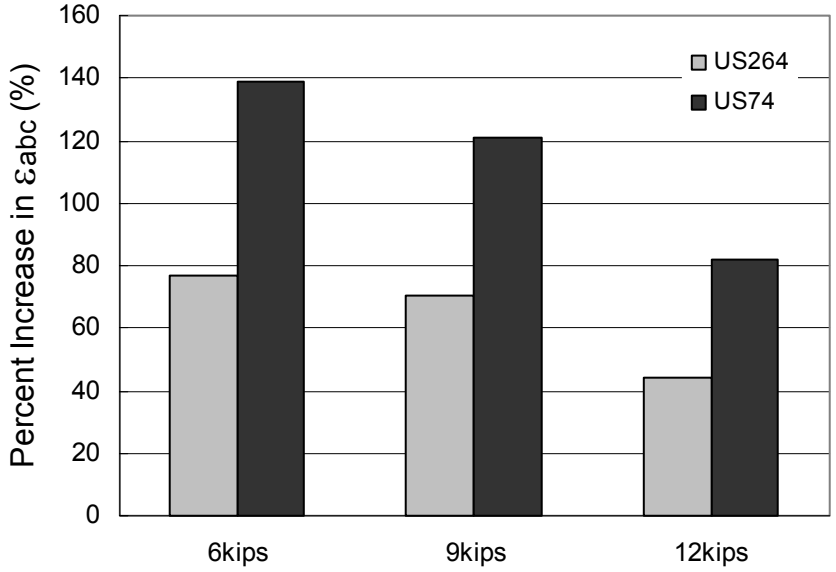

Figure 4.33. Percent of increase in ε_{abc} between 1995 and 2001 for the US 264 and US 74 sections.

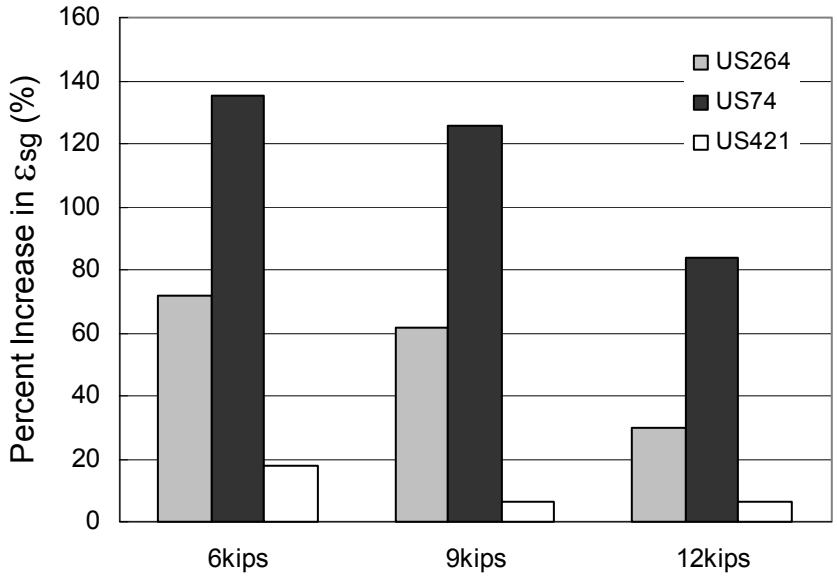

Figure 4.34. Percent of increase in ε_{sg} between 1995 and 2001 for the US 264, US 74, and US 421 sections.

4.2.5 Validation of Condition Assessment Procedure Using the LTPP Data

The LTPP data were used to validate the condition assessment procedures for the base and subgrade layers. Since North Carolina is located in the wet-no-freeze and wet-freeze regions, LTPP pavement sections in these regions were selected for this investigation. The LTPP data include the results of resilient modulus testing of base and subgrade materials and multi-load level FWD deflections. The average resilient moduli values of base and subgrade materials were measured for each sample cored from the LTPP test sections at selected confining pressures and deviator stresses. Table 4.9 shows the list of confining pressures and deviator stresses used in the resilient modulus testing. FWD deflections measured during the fall season of the year were used in this study.

Table 4.9 Confining pressures and deviator stresses used in the resilient modulus testing

Layer	Confining Pressure (psi)	Deviator Stress (psi)
Base	3	3, 6, 9
	5	5, 10, 15
	10	10, 20, 30
	15	10, 20, 30
	20	15, 20, 40
Subgrade	2	2, 4, 6, 8, 10
	4	2, 4, 6, 8, 10
	6	2, 4, 6, 8, 10

The measured resilient moduli and corresponding bulk and deviator stress values were input to the universal soil model (Equation A.1) to determine the coefficients, k_1, k_2, and k_3. In order to minimize the laboratory testing induced errors, the results of resilient modulus test were screened based on the criteria mentioned by Santha (1994). Santha suggests that the universal soil model is applicable only to subgrade soils having decreasing resilient modulus with increasing deviator stress at lower deviator stresses and having increasing resilient modulus with increasing confining pressure. The predicted coefficients using the regression analysis are shown in Tables 4.10 and 4.11 for the base and subgrade materials, respectively.

Table 4.10 Coefficients of the universal soil model for the base materials

State	SHRP ID	k_1 (psi)	k_2	k_3	Moisture Content (%)
GA (13)	1005	120.2	0.669	-0.147	6.8
GA (13)	1031	90.9	0.677	-0.248	6.1
MN (27)	6251	107.8	0.710	-0.031	5
MS (28)	1016	91.6	0.670	-0.119	10.4
MS (28)	1802	149.5	0.528	-0.140	6.5
TX (48)	1068	84.9	0.699	-0.021	6.7
TX (48)	1077	155.3	0.660	-0.038	6

Table 4.11. Coefficients of the universal soil model for the subgrade materials

State	SHRP ID	k_1 (psi)	k_2	k_3	Moisture Content (%)
AL (1)	0101	80.6	0.19	-0.17	19.9
AL (1)	0102	94.3	0.16	-0.14	21.6
GA (13)	1005	75.5	0.47	-0.09	12.5
GA (13)	1031	37.0	0.57	-0.27	10.9
MN (27)	6251	38.9	0.57	-0.23	7.4
TX (48)	1060	47.7	0.36	-0.30	21.5
TX (48)	1068	53.7	0.04	-0.21	18.8
TX (48)	1077	74.8	0.42	-0.14	10.7

Among these coefficients, the k_1 is selected as the best indicator for representing the stiffness characteristic of the base and subgrade layers. Jooste and Fernando (1995) also concluded that the k_1 is the most influential coefficient for the resilient modulus of unbound materials.

As a preliminary study, the changes in the deflection basin parameters with changing FWD testing time and location were investigated. Figures 4.35 and 4.36 show the surface deflections and deflection basin parameters at a particular drop location in the 48-1077 section at different FWD testing times of a day. It can be observed from these figures that the BCI, the condition indicator for the subgrade layer, is quite insensitive to the change in testing time. In Figure 4.37, the changes in deflection basin parameters at different FWD drop locations were presented. The point to be made from Figure 4.37 is that the BCI value is mostly constant regardless of test location. These observations suggest that the use of BCI values for the subgrade condition evaluation may not be affected by the time of day or testing location.

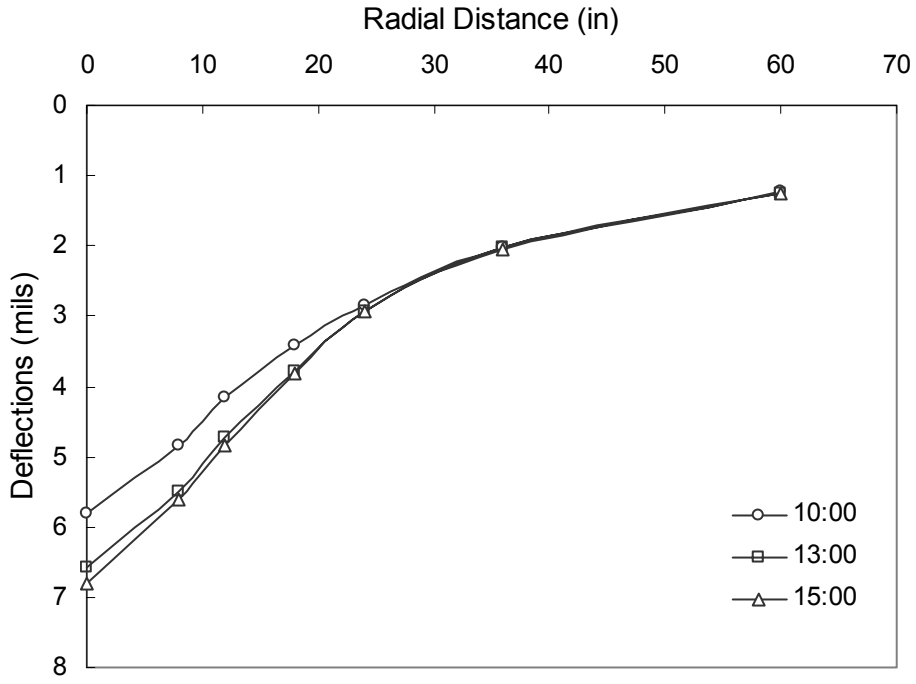

Figure 4.35. Surface deflections at different time of FWD testing for the 48-1077 section.

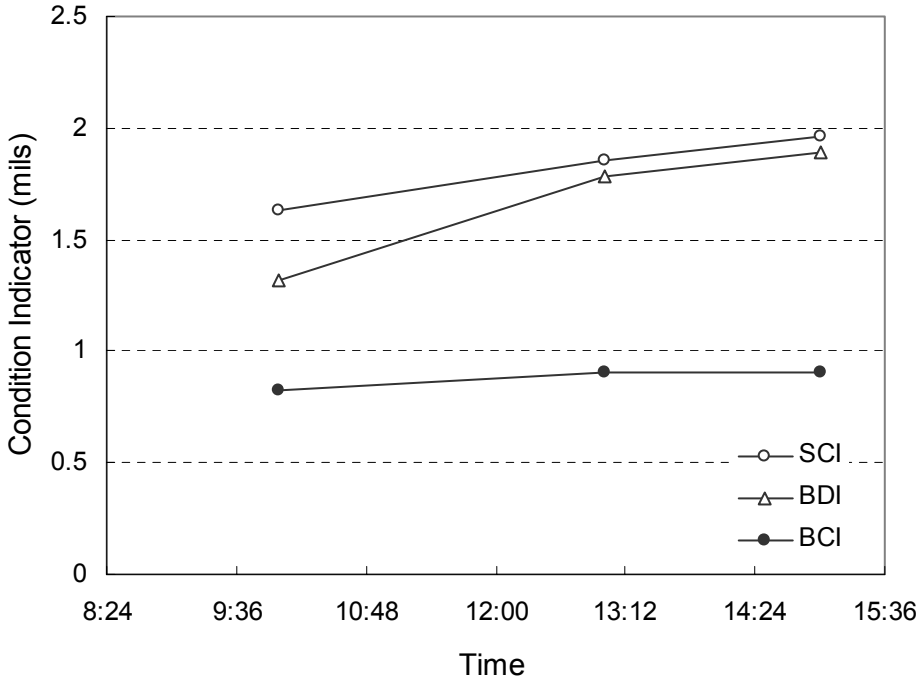

Figure 4.36. Variation of deflection basin parameters with time of FWD testing for the 48-1077 section.

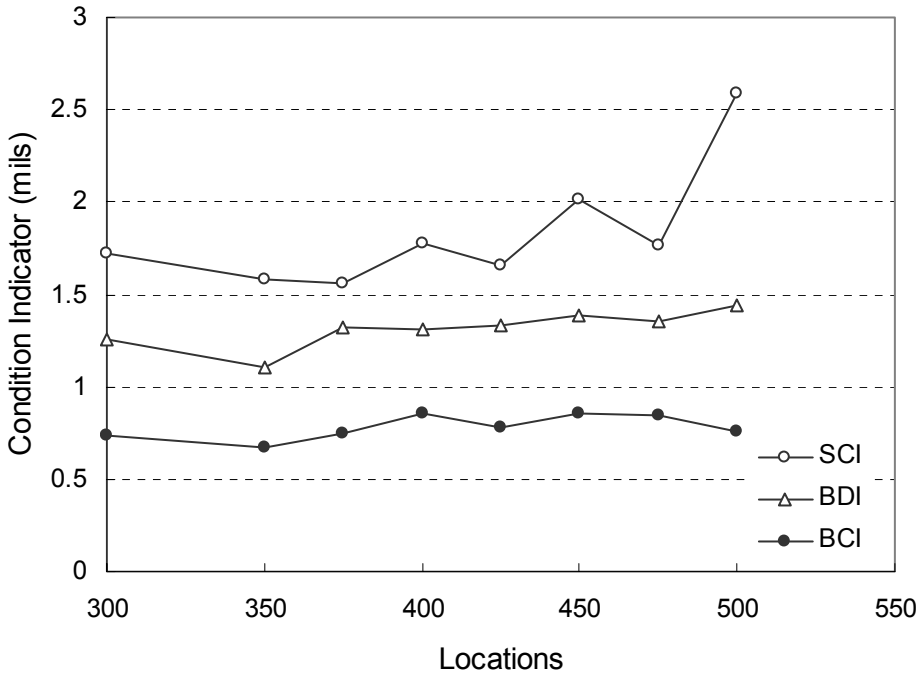

Figure 4.37. Variation of deflection basin parameters in the 48-1077 section.

For the base layer condition assessment, the BDI and DBDI values adjusted using the structural correction procedure were plotted against the k_1 values of the base materials in Figures 4.38 and 4.39. Although there are some errors due to location-specific variations in the stiffness of pavement materials, it is observed that the k_1 value decreases with an increase in the adjusted BDI and DBDI values with relatively good correlations.

Figures 4.40 and 4.41 present the relationships between the adjusted ε_{abc} and $d\varepsilon_{abc}$ values, and the k_1 values of the base materials respectively. It can be seen that the k_1 decreases as the ε_{abc} and $d\varepsilon_{abc}$ increase. The ε_{abc} and $d\varepsilon_{abc}$ result in a slightly lower degree of correlation than the BDI and DBDI. This trend may be due to the fact that there is an additional step of prediction (i.e., from deflections to pavement responses) involved in using the compressive strain as a condition indicator than using the deflection basin

parameters directly. This additional step causes more approximation and errors and therefore poorer correlations with actual layer condition. It is also noted by comparing Figures 4.40 and 4.41 that the $d\varepsilon_{abc}$ values, and therefore the use of multi-load deflections, negatively impact the correlation between the pavement response and k_1 parameter.

The BCI and DBCI values are plotted in Figures 4.42 and 4.43 against the k_1 values of the subgrade materials. It was found from Figure 4.42 that the k_1 decreases as the adjusted BCI increases with a reasonable degree of correlation. However, the adjusted DBCI in Figure 4.43 shows a much larger variation and may not be suitable for an indicator for the condition of subgrade. Figures 4.44 and 4.45 show the adjusted ε_{sg} and $d\varepsilon_{sg}$ values versus the k_1 values for the subgrade soils respectively. It can be found that the degrees of correlation using the subgrade strain are close to those using the deflection basin parameters.

In summary, the following conclusions can be made from Figures 4.38 to 4.45:

(1) structurally adjusted BDI and BCI seem to be the best indicators for the prediction of k_1 values of aggregate base and subgrade respectively;

(2) in general, the degree of correlation between k_1 and the deflection basin parameters is better than that with the compressive strain;

(3) the use of multi-load deflections does not improve the prediction accuracy for the k_1 values of aggregate base and subgrade layers.

The same type of investigation was conducted using the k_2 and k_3 parameters of aggregate base and subgrade materials and revealed that there exists no reliable relationship between condition indicators and k_2 and k_3 parameters.

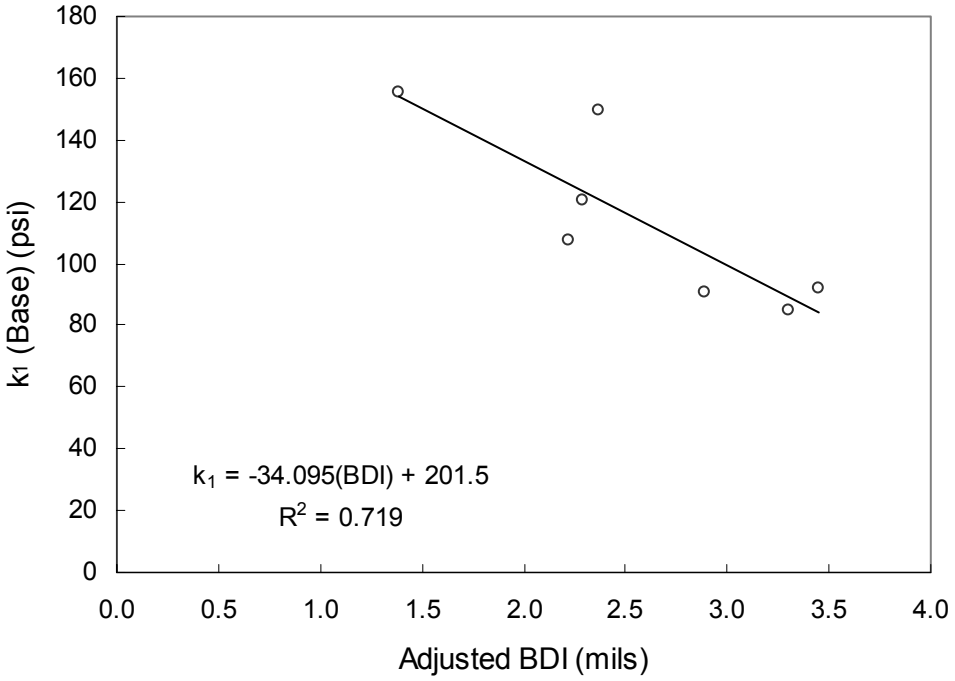

Figure 4.38. Adjusted BDI versus k_1 of aggregate base for LTPP test sections.

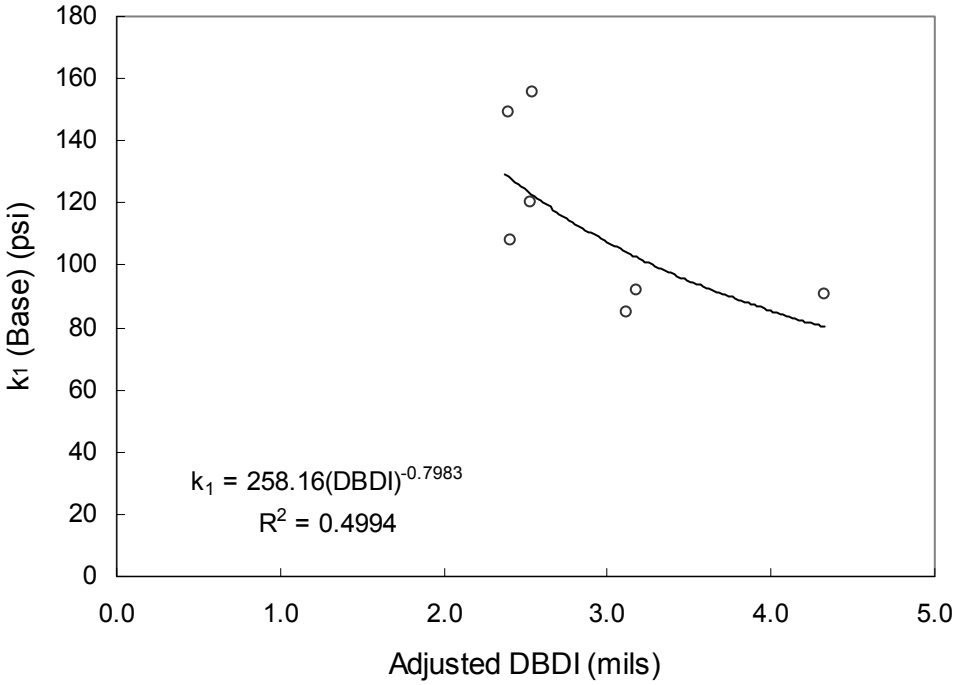

Figure 4.39. Adjusted DBDI versus k_1 of aggregate base for LTPP test sections.

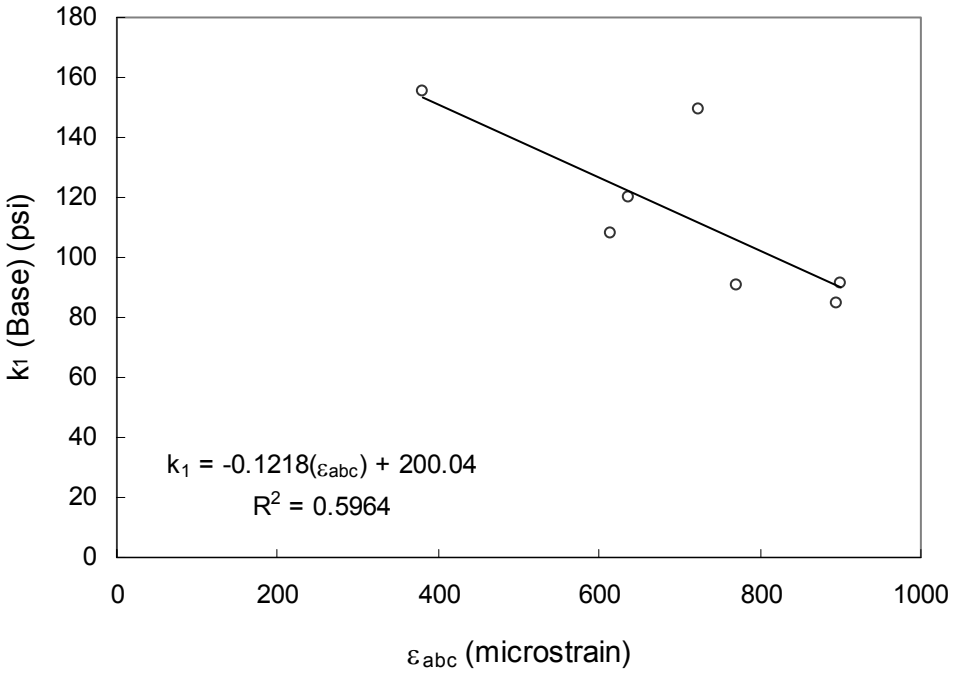

Figure 4.40. Adjusted ε_{abc} versus k_1 of aggregate base for LTPP test sections.

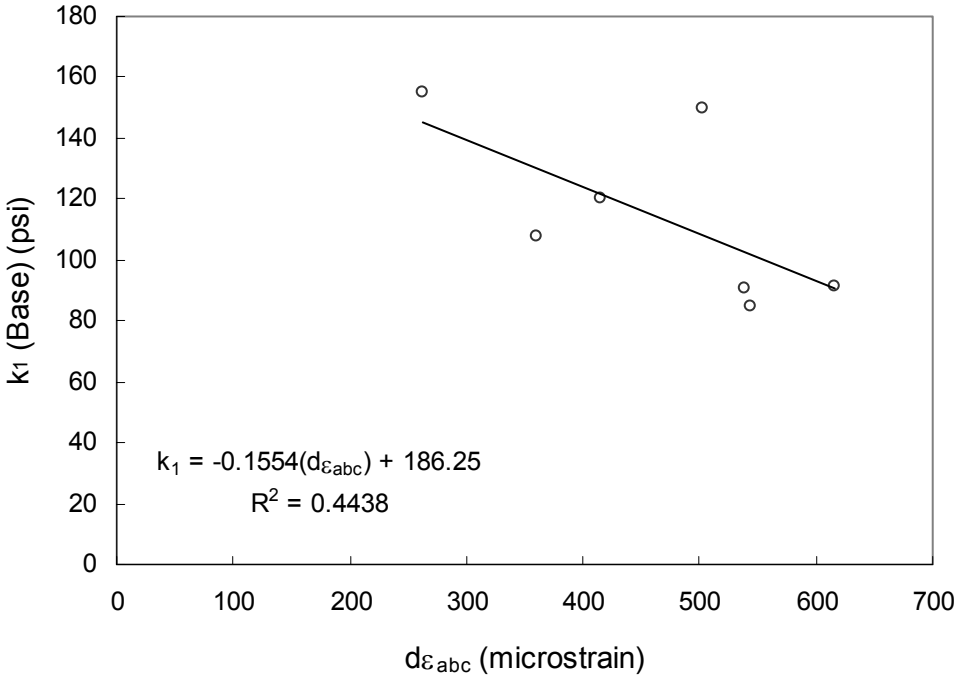

Figure 4.41. Adjusted $d\varepsilon_{abc}$ versus k_1 of aggregate base for LTPP test sections.

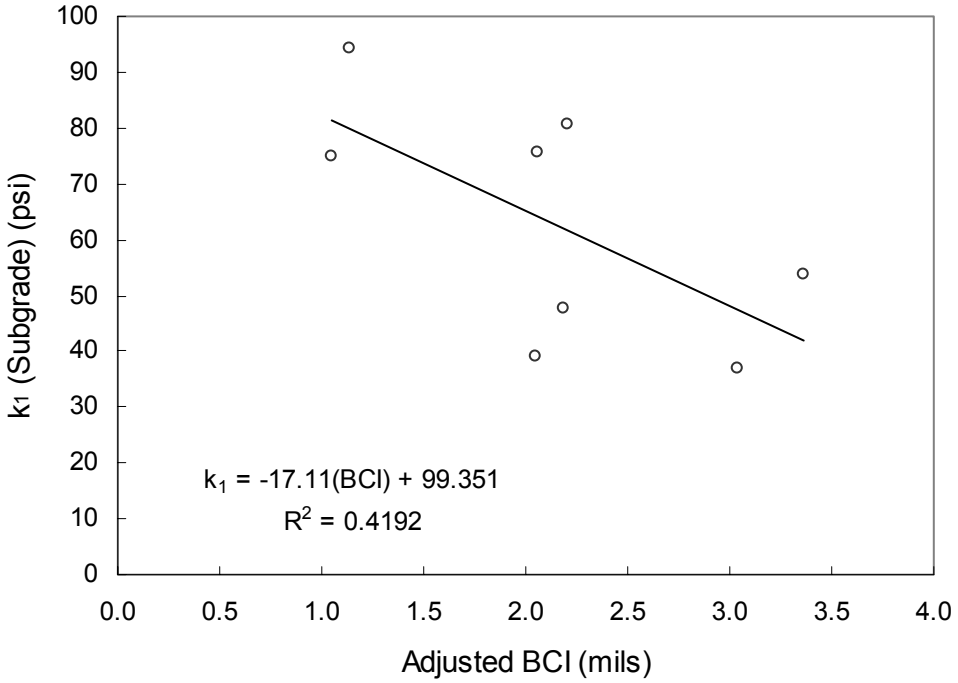

Figure 4.42. Adjusted BCI versus k_1 of subgrade for LTPP test sections.

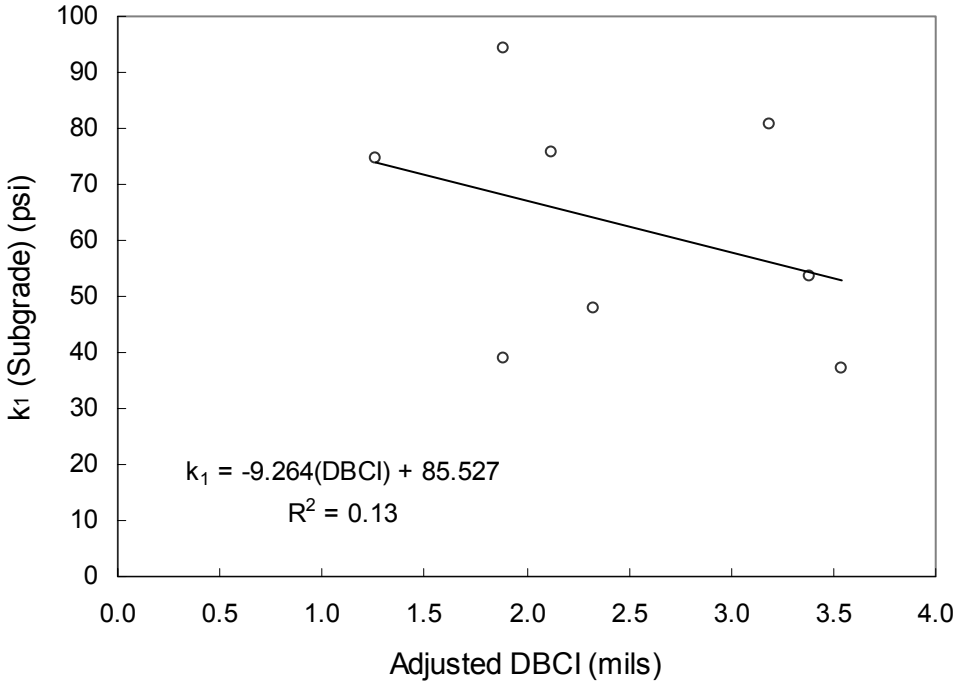

Figure 4.43. Adjusted DBCI versus k_1 of subgrade for LTPP test sections.

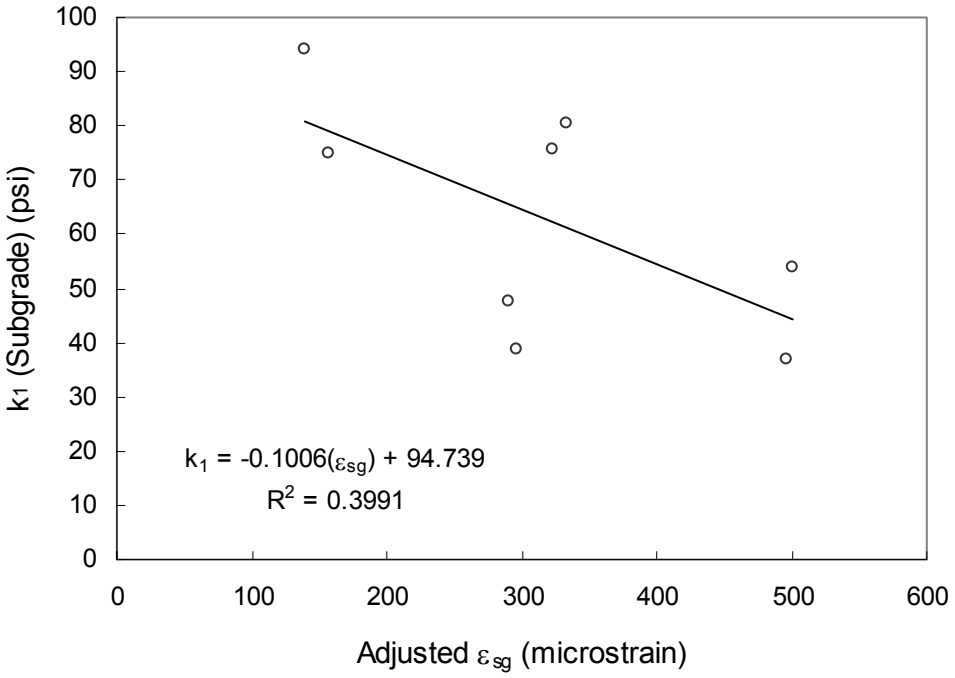

Figure 4.44. Adjusted ε_{sg} versus k_1 of subgrade for LTPP test sections.

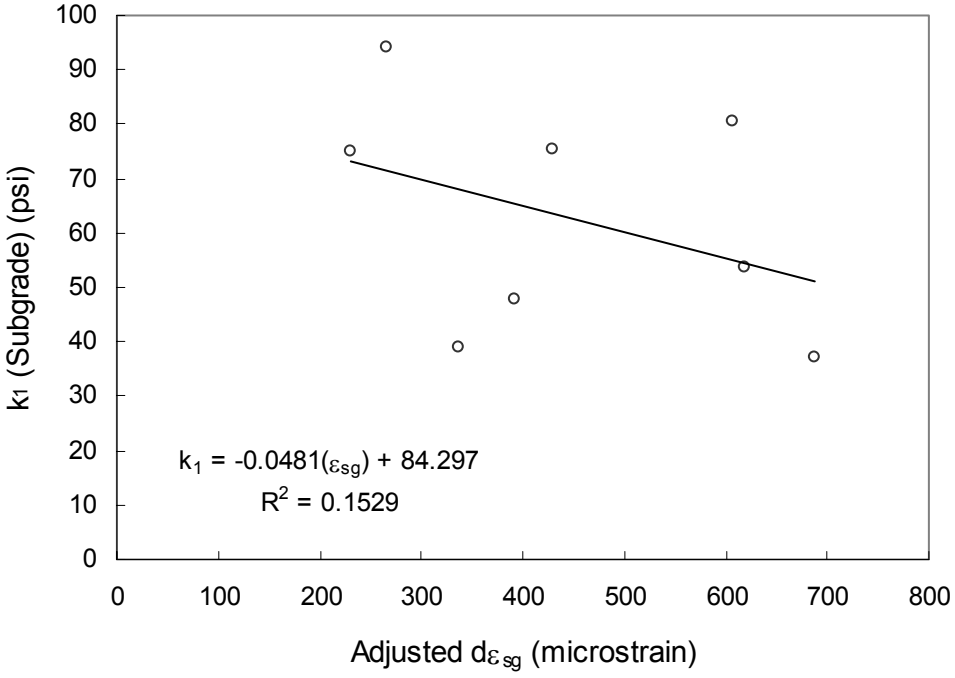

Figure 4.45. Adjusted $d\varepsilon_{sg}$ versus k_1 of subgrade for LTPP test sections.

4.2.6 The Effect of Load Level on the Nonlinear Behavior of a Pavement Structure

Surface deflections and base/subgrade CBR values measured from pavement sites in North Carolina (Tables 4.1 and 4.5) were incorporated to study the relationship between the degree of nonlinearity of a pavement structure and the strength of pavement materials. To check the nonlinearities for NC pavements, measured surface deflections were normalized with respect to a load level. For example, the normalized deflections against radial distances from the center of the load plate for SR 1125 and SR 1706 are plotted in Figures 4.46 and 4.47, respectively. The normalized center deflections are about the same in these pavements. It can be seen that normalized deflections from SR 1125 are the same for all the load levels, while those from SR 1706 increase as a load level increases. This finding indicates that only SR 1706 shows the possible existence of nonlinearities in a pavement structure. The difference in the asphalt layer thickness shown in Table 4.1 may explain this observation. That is, the thicker pavement structure (4.9 in.) in SR 1125 kept the subgrade strain small enough not to cause significant nonlinearities. On the other hand, the subgrade strain in SR 1706 is larger than that of SR 1125 because of the thin structure (3.2 in.) in this pavement.

To determine the degree of nonlinearity in a pavement structure, deflection ratios can be calculated by dividing the normalized deflections under a 12 kip load by the normalized deflections under a 6 kip load. Figure 4.48 presents the deflection ratio-subgrade CBR relationship for full depth pavements. As can be seen, deflection ratios decrease with increasing subgrade CBR values, but the correlation shows a large scatter. It is also noted that AC layer thickness has no effect on the deflection ratio-subgrade CBR relationship.

Attempts were made to correlate the deflection ratios with base/subgrade CBR values for aggregate base pavements (Figures 4.49 and 4.50). No unique relationship was observed between deflection ratios and base CBR values, indicating that the strength of the base layer may not affect the nonlinear behavior of a pavement structure. For the subgrade layer, a similar trend as in the full depth pavements was observed. It seems to be difficult to use material CBR values for estimating the degree of nonlinearity of pavement materials. Overall, a large number of pavements show the softening effect of a pavement structure because these pavements are for secondary roads and the quality of the pavement system is inferior.

The deflection ratio concept was applied to the FWD deflections obtained from test sections in DataPave 2.0. The deflection ratios are plotted against the AC mid-depth temperatures in Figures 4.51 through 4.53 for pavements with gravel, crushed stone, and hot mix asphalt concrete (HMAC) base layer. It is noted that the subgrade soils in these pavement sections are silty or granular sandy materials except for the 48-1068 section. For gravel and crushed stone base pavements, the deflection ratios are less than one at a wide range of temperatures, which demonstrates the possible hardening behavior of pavement materials. Compared with Figures 4.49 and 4.50 for aggregate base pavements in NC secondary roads, this result indicates a good quality of base and subgrade materials in these sections.

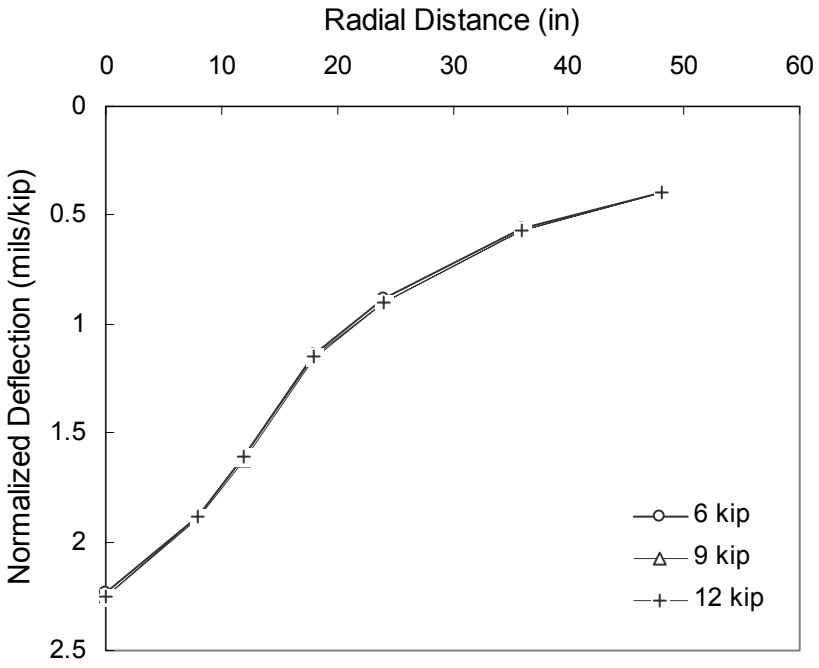

Figure 4.46. Normalized deflections at SR 1125.

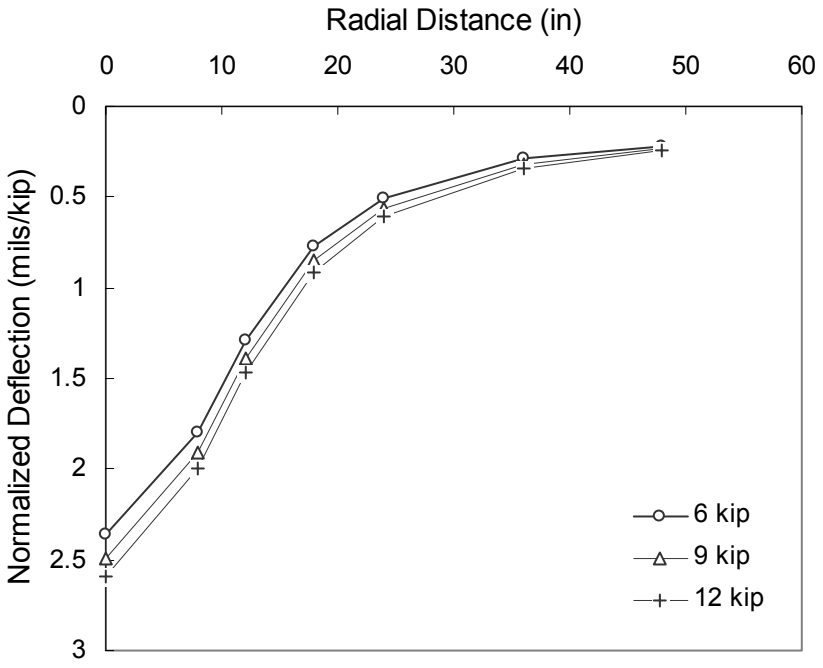

Figure 4.47. Normalized deflections at SR 1706.

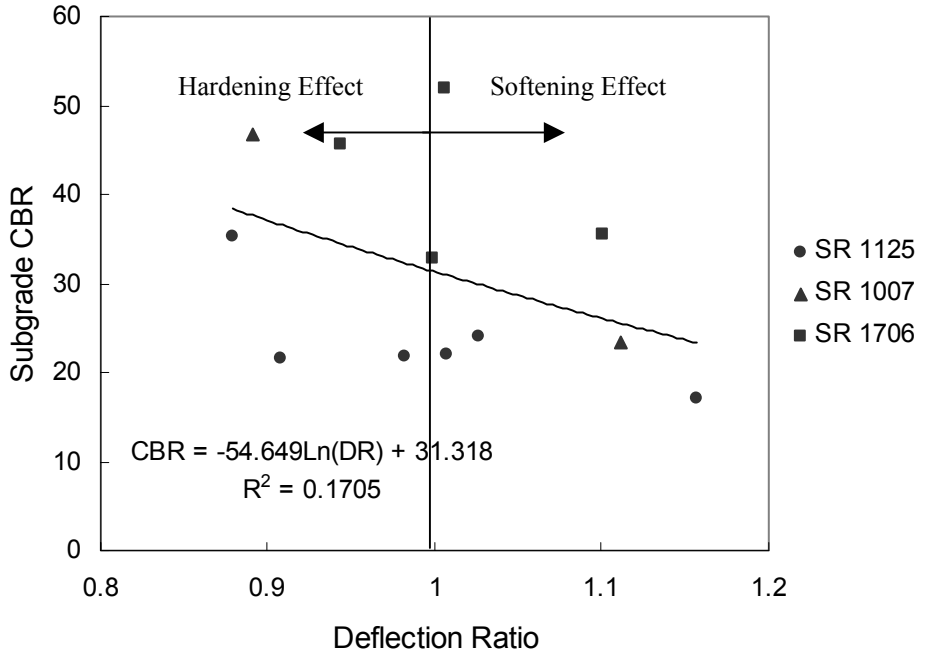

Figure 4.48. Subgrade CBR value versus deflection ratio for full depth pavements.

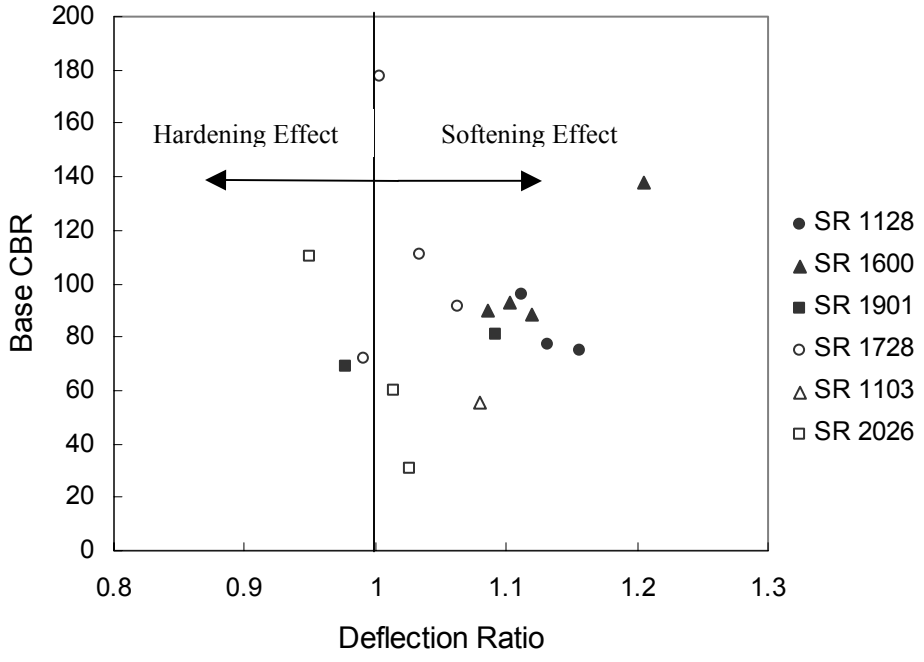

Figure 4.49. Base CBR value versus deflection ratio for aggregate base pavements.

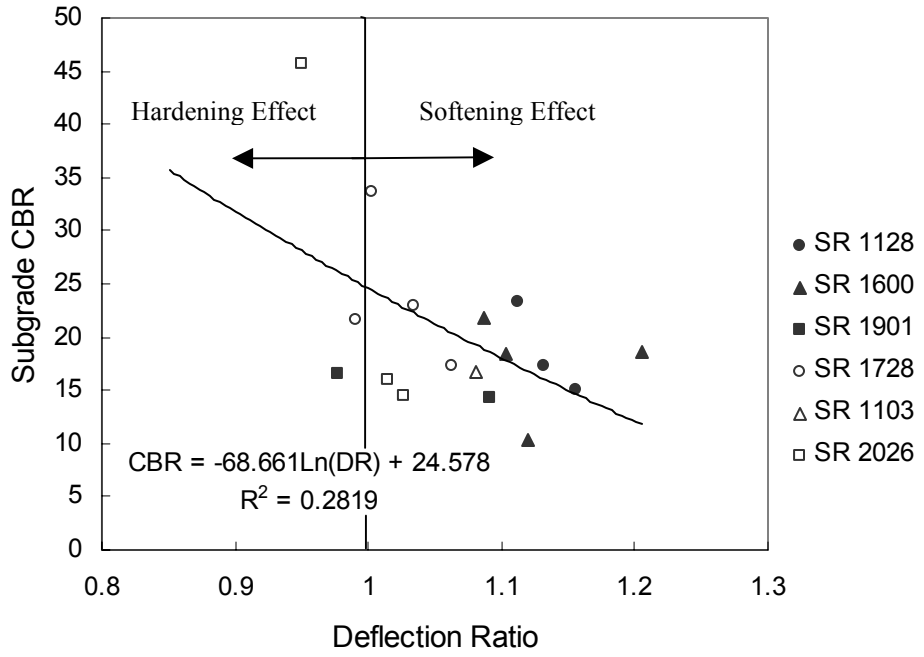

Figure 4.50. Subgrade CBR value versus deflection ratio for aggregate base pavements.

It is well known that as the AC mid-depth temperature increases, the AC modulus decreases, and then stress in the base and subgrade layers increases simultaneously. The modulus of granular materials increases as the stress increases (the hardening effect), whereas the reverse trend is observed in fine-grained soils (the softening effect). As shown in Figure 4.51, overall the deflection ratio of the gravel base pavements decreases as the AC mid-depth temperature increases. This trend can be explained by the well-known effect of bulk stress on the modulus of granular materials. However, as shown in Figure 4.52, the deflection ratios for crushed stone base pavements were relatively constant, regardless of the AC mid-depth temperature and subgrade soil type. This trend is because the modulus of crushed stone is very high and seems to be less sensitive to change in stresses.

Further investigation was conducted to determine the effect of subgrade soil type on the nonlinear behavior of a pavement structure. As shown in Table 4.3, the subgrade soils in the 31-0114 and 1-0102 sections are classified as CL, indicating a plastic clayey material, whereas the subgrade soils in the 25-1002 and 27-6251 sections are SP, which is a granular sandy material. It should be noted that the thickness of the AC and base layers and the type of base materials are almost the same in these sections. It is observed from Figure 4.54 that the deflection ratios in pavements with a CL soil are larger than one and increase with increasing AC mid-depth temperatures, while the deflection ratios in pavements with a SP soil are less than one and decrease with increasing AC mid-depth temperatures. This study concludes that the deflection ratio is a very useful parameter to predict the soil type in the subgrade layer.

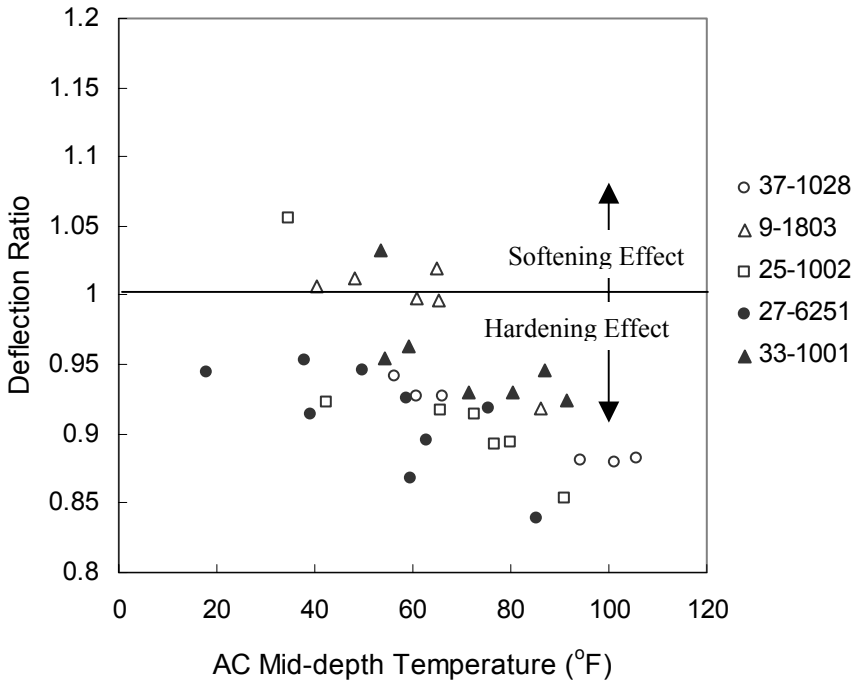

Figure 4.51. Deflection ratio versus AC mid-depth temperature for pavements with a gravel base layer.

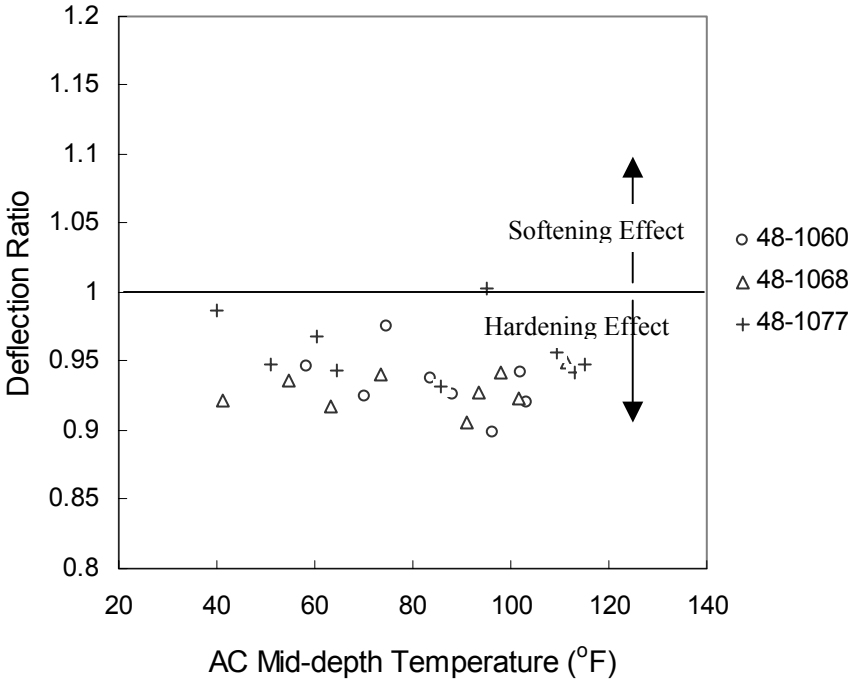

Figure 4.52. Deflection ratio versus AC mid-depth temperature for pavements with a crushed stone base layer.

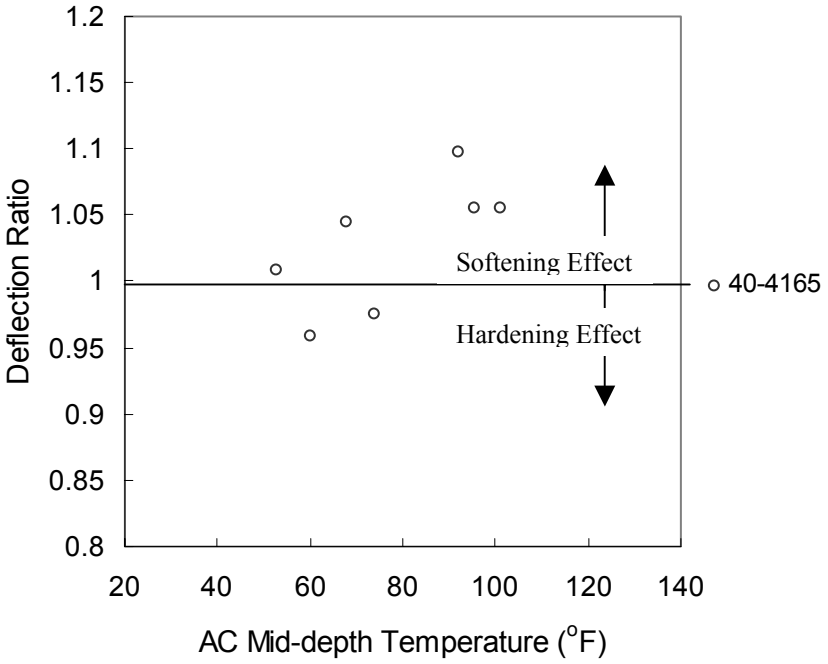

Figure 4.53. Deflection ratio versus AC mid-depth temperature for pavements with a HMAC base layer.

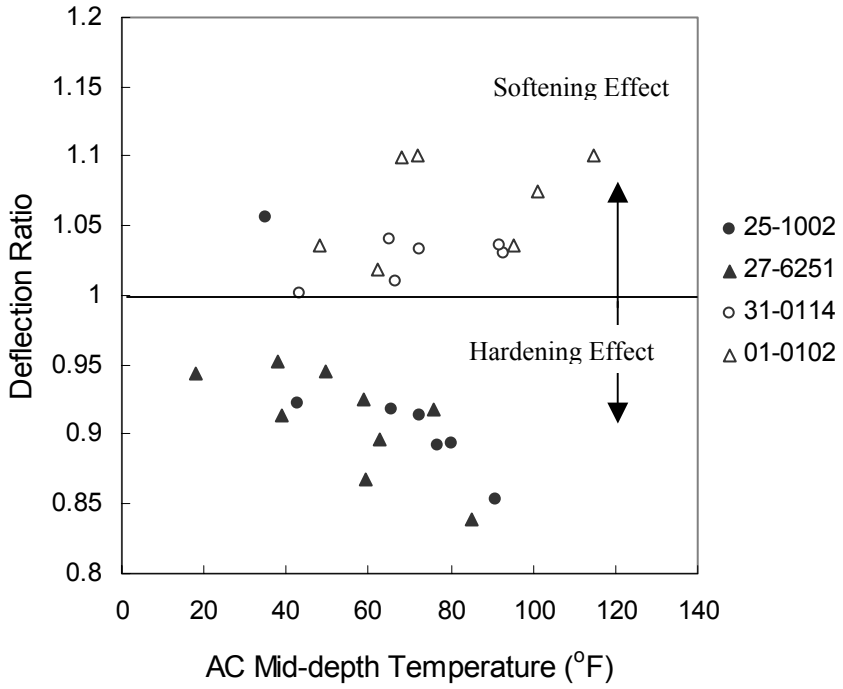

Figure 4.544 Effect of subgrade soil type on nonlinear behavior of a pavement structure.

4.3 Summary

The procedure for condition assessment of pavement layers using FWD multi-load level deflections is presented in this chapter. Figure 4.55 shows the flow chart of the procedure in determining the pavement layer conditions of aggregate base pavements. It is found from this study that the deflection basin parameters and the critical pavement responses are good condition indicators for pavement layers. For the full depth pavements, the BDI, DBDI, ε_{sg}, and $d\varepsilon_{sg}$ can be used to determine the condition of the subgrade layer. The results from this study indicate that the E_{ac}, ε_{ac}, and $d\varepsilon_{ac}$ are the most sensitive indicators for the AC layer conditions in the aggregate base pavements. The BDI, DBDI, ε_{abc}, and $d\varepsilon_{abc}$ are found to be good indicators for the base layer conditions. For the subgrade in aggregate base pavements, the BCI, ε_{sg}, SSR, E_{sg} seem to be good condition indicators. The study for nonlinear behavior of a pavement structure that the deflection ratio can be used to determine the quality and type of unbound layer materials.

Since the data used for the validation were collected from the secondary road pavements in North Carolina and the maximum FWD load level used here is 12 kip, it is difficult to predict the accurate pavement layer conditions. The better quality pavement performance data and the higher FWD load level would be necessary to validate the pavement layer condition procedure more reliably.

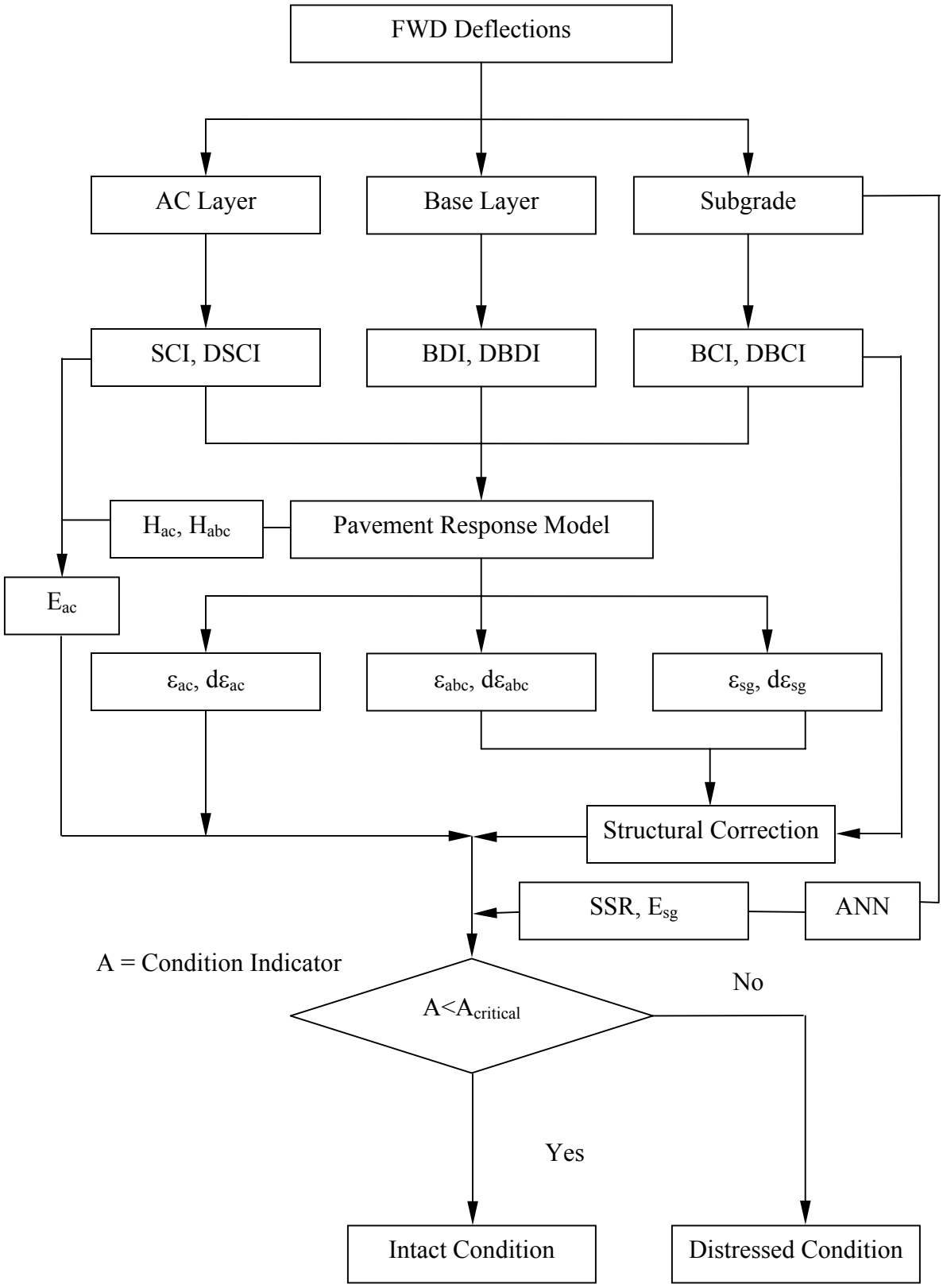

Figure 4.55 The flow chart of the procedure for assessment of the pavement layer conditions for aggregate base pavements.

CHAPTER 5

DEVELOPMENT OF REMAINING LIFE PREDICTION USING MULTI-LOAD LEVEL DEFLECTIONS

In this chapter, the remaining life prediction methods using multi-load level deflections are developed by employing the pavement response models and pavement performance models. The pavement response models were designed to predict critical pavement responses from surface deflections and deflection basin parameters. The critical pavement responses include tensile strain at the bottom of the AC layer for fatigue cracking, and compressive strain on the top of the base, as well as on the subgrade, for rutting potential. The pavement performance models were used to develop the relationships between critical pavement responses obtained from pavement response models and pavement performance. The fatigue cracking model developed by the Asphalt Institute (AI, 1981) and the VESYS rutting model (Kenis, 1978) were adopted as the pavement performance models. Pavement performance measures from the field database include cracking area, rut depth, and pavement condition rating from a visual distress survey.

5.1 Pavement Performance Model

5.1.1 Fatigue Cracking

The fatigue cracking of asphalt concrete is the phenomenon of load-induced cracking due to a repeated stress or strain level below that of the ultimate strength of the material. The

fatigue cracking characteristics obtained from laboratory fatigue testing can be expressed in terms of strain and number of load applications to failure.

$$N_f = K(\frac{1}{\varepsilon_t})^c \quad (5.1)$$

where

N_f = the number of load repetitions to failure due to fatigue cracking

ε_t = tensile strain at the bottom of the asphalt concrete specimen, and

K, c = regression constants.

Monismith and McLean (1972) have accounted for the effect of stiffness of the material on the fatigue cracking potential and established criteria for fatigue cracking associated with different mix properties. The Asphalt Institute (AI, 1981) suggested the pavement performance model for a standard mix with an asphalt volume of 11% and air void volume of 5%. The allowable number of load applications to control fatigue cracking can be expressed as:

$$N_f = 0.0796\varepsilon_t^{-3.291}\left|E^*\right|^{-0.854} \quad (5.2)$$

where

E* = the dynamic modulus of the asphalt mixture in psi.

It was reported that the use of this equation would result in fatigue cracking of 20% of the total area, as observed on selected sections of the AASHO Road Test. Equation 5.2 was adopted in this study as the fatigue cracking prediction model.

5.1.2 Permanent Deformation

The Asphalt Institute (1981) introduced the performance model for permanent deformation using the vertical compressive strain on the top of the subgrade. The number of load applications to failure can be expressed as:

$$N_f = 1.365 \times 10^{-9} (\varepsilon_c)^{-4.477} \tag{5.3}$$

where

N_f = the number of load applications to failure due to permanent deformation, and

ε_c = the vertical compressive strain on top of the subgrade.

According to the Manual Series No. 1 (AI, 1981), when good compaction of the pavement materials is obtained and the asphalt mixture is well designed, the use of this model should not result in rutting greater than 0.5 in. for the design traffic.

The VESYS method (Kenis, 1978) was developed from observations of repeated load tests. It is assumed that the permanent strain is proportional to the resilient strain. The permanent strain at the N^{th} load application can be expressed as follows:

$$\varepsilon_p(N) = \mu \varepsilon_r N^{-\alpha} \tag{5.4}$$

where

$\varepsilon_p(N)$ = the permanent strain due to a single load application,

ε_r = the resilient strain at the 200^{th} repetition,

N = the number of load applications, and

α and μ = the permanent deformation parameters.

The cumulative permanent deformation can be obtained by integrating Equation 5.4:

$$\varepsilon_p = \int_0^N \varepsilon_p(N)dN = \varepsilon_r \mu \frac{N^{1-\alpha}}{1-\alpha} \tag{5.5}$$

Incremental permanent strain for a single load application can be obtained by differentiating Equation 5.5:

$$\frac{\partial \varepsilon_p}{\partial N} = \varepsilon_r \mu N^{-\alpha} \tag{5.6}$$

F(N) is defined as the fractional increase of the total strain and is expressed as follows:

$$F(N) = \frac{\Delta \varepsilon_p}{\varepsilon_r + \Delta \varepsilon_p} \frac{1}{\partial N} = \frac{\Delta \varepsilon_p}{\varepsilon_r} \frac{1}{\partial N} = \mu N^{-\alpha} \tag{5.7}$$

The rut depth is:

$$RD(N) = \int_0^N \int_0^z \varepsilon_c(z) F(N) dz dN \tag{5.8}$$

where

z = the depth of the pavement layer, and

ε_c = the vertical compressive strain at depth z.

Using Equations 5.7 and 5.8, one can obtain:

$$RD(N) = \sum_{i=1}^{n} \left[\int_0^N \mu_i N^{-\alpha_i} dN \int_{d_{i-1}}^{d_i} \varepsilon_c(z) dz \right] = \sum_{i=1}^{n} \left[\frac{\mu_i N^{1-\alpha_i}}{1-\alpha_i} \int_{d_{i-1}}^{d_i} \varepsilon_c(z) dz \right] \tag{5.9}$$

Table 5.1 presents the ranges of α and μ for various materials used in flexible pavements.

Table 5.1. Typical Permanent Deformation Parameters for Flexible Pavement Materials (after Bonaquist, 1996)

Material	α	μ
Asphalt Concrete	0.45 – 0.90	0.10 - 0.50
Granular Base	0.85 – 0.95	0.10 – 0.40
Sandy Soil	0.80 – 0.95	0.05 – 0.10
Clay Soil	0.60 – 0.90	0.05 – 0.10

Tseng et al. (1989) proposed a model using three permanent deformation parameters for the permanent deformation potential in a pavement structure. It provides the regression technique for determining how these three parameters are affected by the material properties, environmental conditions, and stress state. The three-parameter model is developed by fitting a curve that relates permanent strains to loading cycles obtained from creep and recovery or repeated load triaxial tests. The curve describing the relationship between cumulative permanent strain versus number of load repetitions is expressed by:

$$\varepsilon_p = \varepsilon_0 e^{-(\rho/N)\beta} \tag{5.10}$$

The model of permanent deformation is based on an evaluation of the vertical resilient strain in each layer by the finite element method and on the fractional increase of total strains for each material layer of the pavement as determined by the three material properties, ε_0, ρ, and β. The finite element analysis is used to take into account the nonlinear stress-strain behavior of materials. Using Equations 5.4, 5.9 and 5.10, the rut depth, *RD(N)* at N^{th} load repetition, is defined as follows:

$$RD(N) = \sum_{i=1}^{n} \left\{ \left(\frac{\varepsilon_{0_i}}{\varepsilon_{r_i}} \right) e^{-\left(\frac{\rho_i}{N}\right)^{\beta_i}} \int_{d_{i-1}}^{d_i} \varepsilon_c(z)\,dz \right\} \tag{5.11}$$

where

n = number of pavement layers,

ε_{ri} = resilient strain imposed in the laboratory test to obtain the three parameters of the materials in the i^{th} layer,

N = expected number of load cycles,

d_i = depth of the i^{th} layer, and

ε_c = vertical resilient strain in the i^{th} layer from the finite element solution.

5.2 Remaining Life Prediction Method

5.2.1 Cumulative Damage Concept

The proposed method is based on the cumulative damage concept in which a damage factor is defined as the damage per pass caused to a specific pavement system by the load in question. According to Miner's hypothesis, damage is linearly cumulative; that is, damage at a particular point in time can be accumulated by adding together the damage from various load levels, as shown below:

$$S = \sum_{i=1}^{n} S_i \tag{5.12}$$

where

S = the damage due to n number of load groups,

n = the number of load groups, and

S_i = the damage ratio due to the ith load group.

The damage ratio (S_i) is defined as the ratio of the actual and allowable number of load repetitions of a specific load group. Therefore, the pavement fails when the damage is one. The damage ratio is obtained from:

$$S_i = \frac{N_i}{N_{f,i}} \tag{5.13}$$

where

N_i = actual number of load repetitions for load group i and

$N_{f,i}$ = allowable number of load repetitions for load group i.

Where multiple load groups exist, S_i indicates the contribution of the load group i to the overall damage in the pavement system under mixed traffic loading. The total damage can be expressed using Equations 5.12 and 5.13:

$$S = \sum_{i=1}^{n} \frac{N_i}{N_{f,i}} \tag{5.14}$$

To utilize Minor's hypothesis in the multi-load level data analysis, the damage factor (*DF*) is defined as the damage done by one pass of a load. Assuming that damage is accumulated linearly throughout the life of the pavement system, one obtains:

$$DF_i = \frac{1}{N_{f,i}} \tag{5.15}$$

where DF_i is the damage factor of load group *i*.

The pavement performance models for fatigue cracking and rutting are applied to determine the damage factor for load group *i*. Then the damage ratio caused to the pavement structure by a specific load group can be determined by multiplying the damage factor for the load group to the number of load repetitions for a given period. These damage ratios due to various load groups can be added to represent the damage caused to the pavement structure by the multiple load groups for the given period. When the sum of the damage ratios is equal to one, the pavement fails. The total damage (*S*) due to mixed loading groups for the remaining life (*Y*) is determined from:

$$S = \sum_{i=1}^{n} (P_i \times DF_i) \times Y \tag{5.16}$$

Knowing that the total damage is one when the pavement fails, and that all the factors in Equation 5.16 can be obtained from multi-load level FWD tests and traffic

information, the remaining life of a pavement can be predicted. The approach described above is illustrated in Table 5.2.

Table 5.2. Calculation of Damage due to Mixed Load Groups

Load Group	Load Level (kip)	No. of Load Repetitions per Year	Total No. of Repetitions for Remaining Life	Damage Factor	Damage Ratio
1	6	P_1	$P_1 \times Y$	DF_1	$P_1 \times Y \times DF_1$
2	9	P_2	$P_2 \times Y$	DF_2	$P_2 \times Y \times DF_2$
3	12	P_3	$P_3 \times Y$	DF_3	$P_3 \times Y \times DF_3$
4	15	P_4	$P_4 \times Y$	DF_4	$P_4 \times Y \times DF_4$
…	…	…	…	…	…
N	…	…	…	…	…

The prediction accuracy of the approach described above can be improved by accounting for seasonal effects and the difference between performance measured by laboratory tests and the actual performance of pavements. The seasonal effects can be accounted for by applying the approach described above to each season; that is, the damage factor and the traffic information are determined for each season. The total damage is modified as:

$$S = \sum_{i=1}^{n} \sum_{j=1}^{m} \left(P_{i,j} \times DF_{i,j} \right) \times Y \tag{5.17}$$

where

$P_{i,j}$ = the number of repetitions of the i^{th} load group during the j^{th} season,

$DF_{i,j}$ = the damage factor due to the i^{th} load group in the j^{th} season, and

n, m = the number of load groups and seasons, respectively.

The mechanistic approach described above, incorporating the seasonal adjustments and the shift factor, is schematically displayed in Figure 5.1.

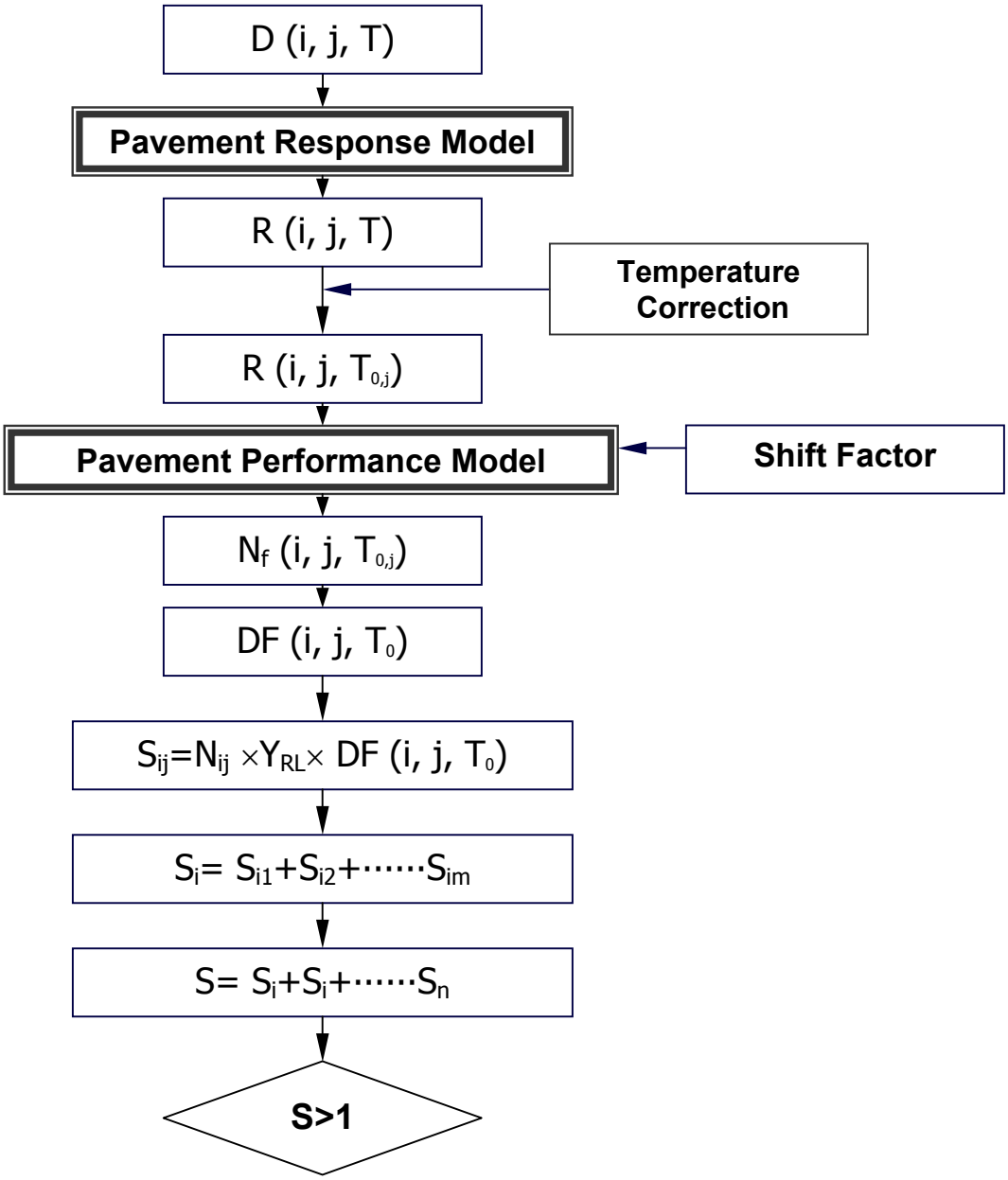

Note:

i = load level; j = season; m = number of seasons; n = number of load levels;
T = AC layer temperature; $T_{0,j}$ = reference temperature for season j;
D (i, j, T) = deflections under load level i in season j at temperature T;
R (i, j, T) = pavement response under load level i in season j at temperature T;
DF = damage factor; S_{ij} = damage ratio of load level i for season j;
N_{ij} = number of repetitions of load level i during season j;
Y_{RL} = remaining life in year; S_i = damage ratio of load level i; and
S = total damage due to traffic during the remaining life.

Figure 5.1. Conceptual flowchart of the multi-load level data analysis method for remaining life prediction.

5.2.2 Traffic Consideration

The performance prediction of existing pavements is significantly affected by traffic volume during the design period. The traffic monitoring data in Long Term Pavement Performance (LTPP) contain the number of axles corresponding to a particular axle load for a given period. To convert the actual traffic data to an 18 kip single-axle load, the equivalent single-axle load (ESAL) was calculated using the equivalent axle load factor (EALF), the lane distribution factor, the direction distribution factor, and the traffic growth factor. Based on the results of AASHTO road tests, an equivalent axle load factor (EALF) for a 18 kip single-axle load can be determined using the following equations:

$$\log\left(\frac{W_x^t}{W_s^t}\right) = 4.79\log(S+1) - 4.79\log(L_x + L_2) + 4.33\log L_2 + \frac{G_t}{\beta_x} - \frac{G_t}{\beta_{18}} \tag{5.18}$$

$$G_t = \log\left(\frac{4.2 - p_t}{4.2 - 1.5}\right) \tag{5.19}$$

$$\beta_x = 0.40 + \frac{0.081\left(L_x + L_2\right)^{3.23}}{\left(SN+1\right)^{5.19} L_2^{3.23}} \tag{5.20}$$

$$EALF = \frac{W_s^t}{W_x^t} \tag{5.21}$$

where

W_x^t = the number of *x*-axle load repetitions at the end of time *t*,

W_s^t = the number of *s*-kip standard single axle load repetitions to time *t*,

L_x = the load in kip on one single axle, one set of tandem axles, and one set of tridem axles,

L_2 = the axle code, 1 for single-axle, 2 for tandem axles, and 3 for tridem axles,

SN = the structural number, and

P_t = the terminal serviceability.

The EALFs with $p_t = 2.5$ and $SN = 5$ were used in this study. Assuming that the regression constants in Equations 5.18 to 5.20 are the same as the load level of a standard axle change, the EALFs for 12, 24, and 32 kip single axle load were also determined for multi-load deflection data. After computing the EALF's for multi-load level deflections, the equivalent single axle load for each individual standard load level can be obtained using the following equation:

$$ESAL = (\sum_{i=1}^{m} N_i F_i)(G)(D)(L)(Y) \quad (5.22)$$

N_i = the number of load repetitions for the ith load group,

F_i = the equivalent axle load factor for the ith load group,

G = the growth factor,

D = the directional distribution factor,

L = the lane distribution factor, and

Y = the design period in years.

5.2.3 Performance Prediction for Fatigue Cracking

Procedure for Performance Prediction of Fatigue Cracking

The procedure for performance prediction of fatigue cracking requires the determination of the horizontal tensile strain at the bottom of the AC layer (ε_{ac}) and the elastic modulus of asphalt concrete (E_{ac}) using multi-load level FWD deflection data. The ε_{ac} under different load levels can be predicted from pavement response models (Equation 2.8.a)

where the BDI value and the AC layer thickness are used as inputs. Based on the synthetic database developed from the dynamic, nonlinear finite element analysis, the following regression equation was derived to predict the E_{ac} value:

$$\log(E_{ac}) = -1.183 \log(H_{ac}) - 1.103 \log(SCI) + 4.356 \quad (5.23)$$

The predicted ε_{ac} and E_{ac} were input to the pavement performance model for fatigue cracking (Equation 5.2), after which the allowable number of load repetitions to failure for a given load group ($N_{f,i}$) may be estimated. The equivalent single axle load for a standard load level was used to estimate the actual number of load repetitions for a given load group (N_i). The damage ratio due to the fatigue cracking for each season and each corresponding load group was determined using the damage factor, the inverse value of the $N_{f,i}$, and N_i values. Total damage caused by the fatigue cracking was determined by adding the damage ratios at a given season and load level.

Verification of Fatigue Cracking Predictive Procedure Using LTPP Data

The LTPP data were used to test the accuracy of the procedure for performance prediction of fatigue cracking developed in this research. Details on the characteristics of pavement sections are shown in Chapter 4. Figures 5.2 to 5.3 show the area with fatigue cracking as a function of the date of the distress survey for each of the LTPP test sections. According to the study for various types of distresses using LTPP data reported in the FHWA TechBrief (2000), distresses related to cracking were categorized as a magnitude as shown in Table 5.3.

Table 5.3. Magnitude of Distress Related to Cracking for Each Category

Distress Type	Nominal	Moderate	Excessive
Area with fatigue cracking (ft^2)	11 – 111	122 – 667	> 667
Longitudinal cracking in the wheelpath (ft)	3 – 167	170 – 533	> 533
Longitudinal cracking not in the wheelpath (ft)	3 – 167	170 – 533	> 533
Transverse cracks (no)	1 – 10	11 – 50	> 50

Figure 5.2 shows the test sections with excessive levels of fatigue cracking whereas Figure 5.3 shows the test sections with nominal and moderate levels of fatigue cracking. The damage ratio for fatigue cracking can be determined by dividing the measured area with fatigue cracking shown in these figures by the wheelpath area. It should be noted that 20% of the fatigue cracking area is assumed to be a failure condition considering the damage ratio is equal to one.

The stepwise procedure described earlier was applied to the multi-load level FWD deflections for each season and load group to predict the damage ratio due to fatigue cracking. Other climatic and environmental factors influence the fatigue cracking performance of a pavement, such as the annual precipitation and the mean air temperature in the winter season. Figure 5.4 shows the relationship between the area with fatigue cracking and the annual precipitation for LTPP test sections. The effects of precipitation are accounted for by multiplying equation 5.2 by a factor, annual precipitation (*P)*, as follows:

$$N_f = 0.0796\varepsilon_t^{-3.291}\left|E^*\right|^{-0.854}\left(\frac{P}{0.3}\right)^{-0.3} \quad (5.24)$$

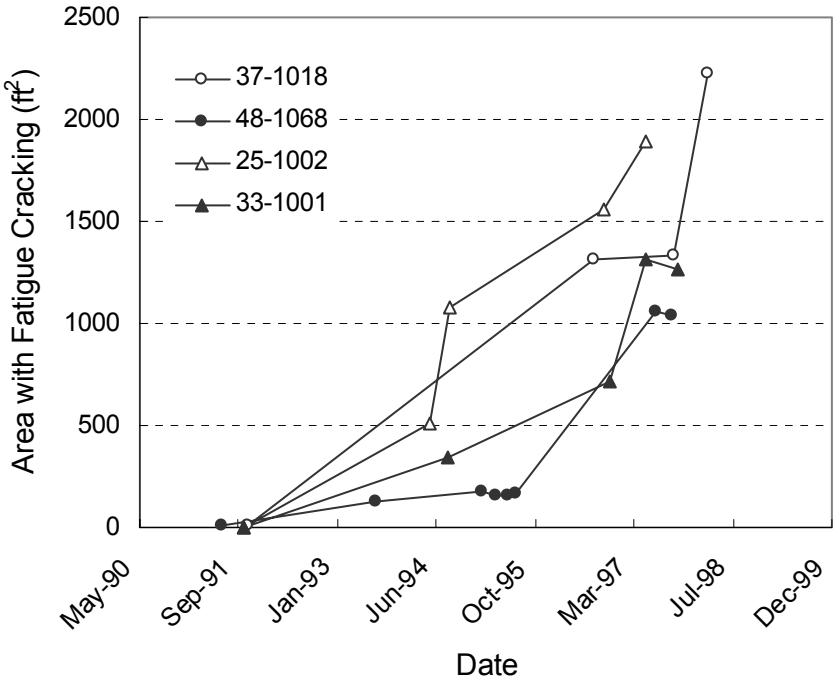

Figure 5.2. Change in area with fatigue cracking measured for pavement with excessive levels of fatigue cracking.

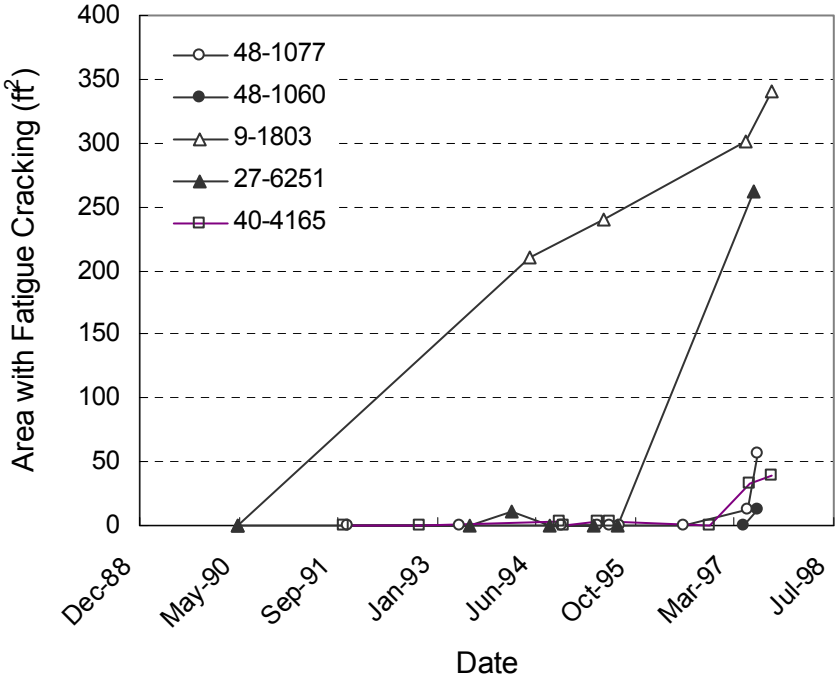

Figure 5.3. Change in area with fatigue cracking measured for pavement with nominal and moderate levels of fatigue cracking.

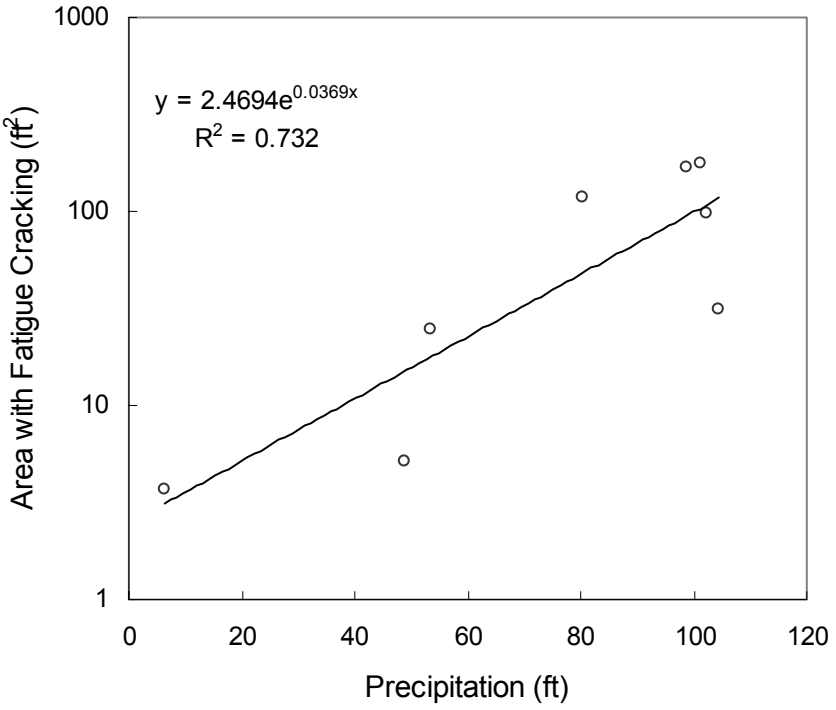

Figure 5.4. Relationship between area with fatigue cracking versus annual precipitation for LTPP test sections.

The predicted and measured damage ratios for fatigue cracking are plotted in Figures 5.5 through 5.8 against the date of the FWD testing and the distress survey for pavements with excessive levels of fatigue cracking. As shown in Figures 5.5 and 5.6, the predicted values agree quite well with the measured values for pavements in the wet no freeze region. However, it was found from Figures 5.7 and 5.8 that the proposed procedure underestimates the damage ratios for pavements in the wet freeze region. The drastically increasing trend in the damage ratio with time may be due to the low temperature cracking in this region. The same plots for pavements with nominal and moderate levels of fatigue cracking are shown in Figures 5.9 to 5.13. Although a large discrepancy was found in section 48-1077, generally the prediction of damage ratios for pavements with low severe fatigue cracking is satisfactory.

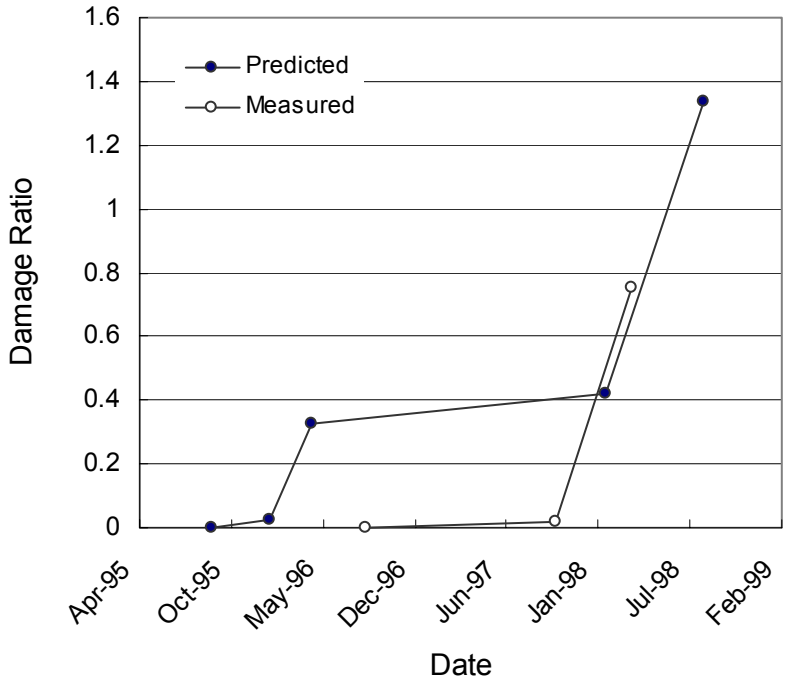

Figure 5.5. Predicted and measured damage ratios due to fatigue cracking for the 37-1028 section (wet no freeze region).

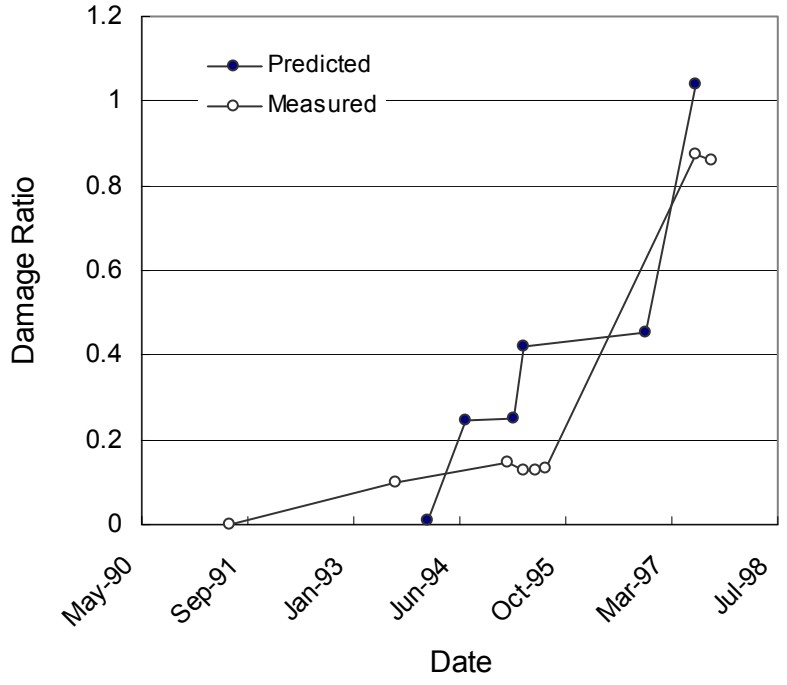

Figure 5.6. Predicted and measured damage ratios due to fatigue cracking for the 48-1068 section (wet no freeze region).

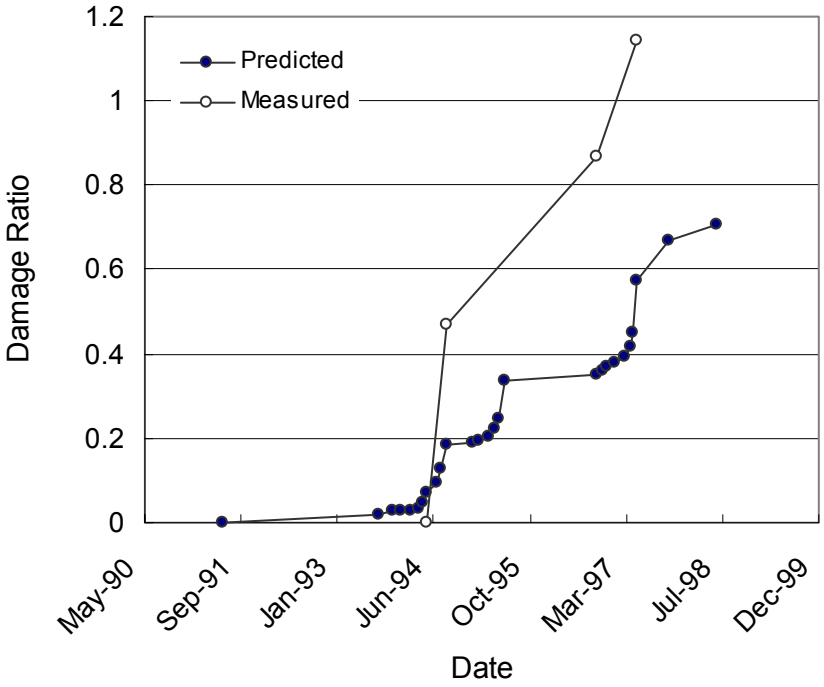

Figure 5.7. Predicted and measured damage ratios due to fatigue cracking for the 25-1002 section (wet freeze region).

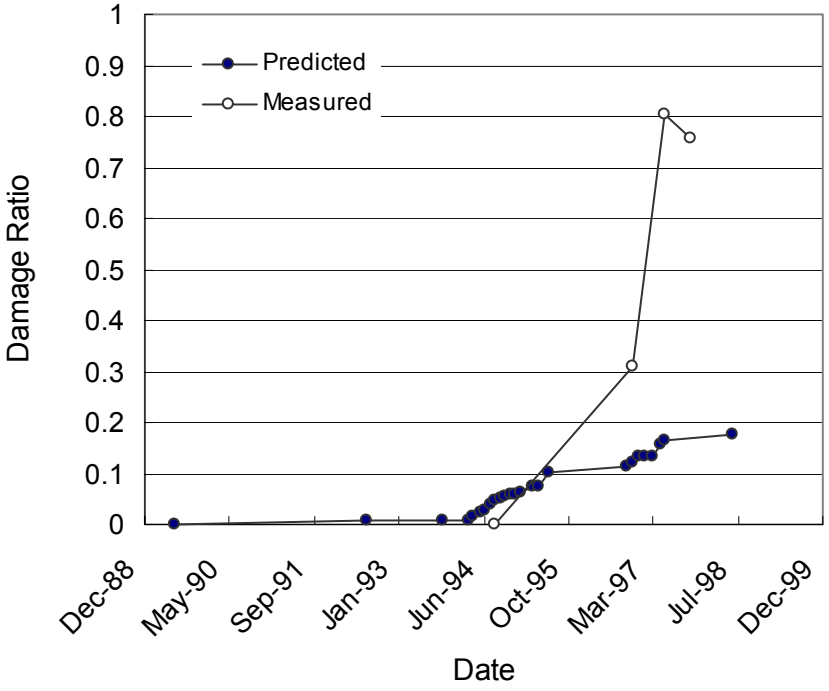

Figure 5.8. Predicted and measured damage ratios due to fatigue cracking for the 33-1001 section (wet freeze region).

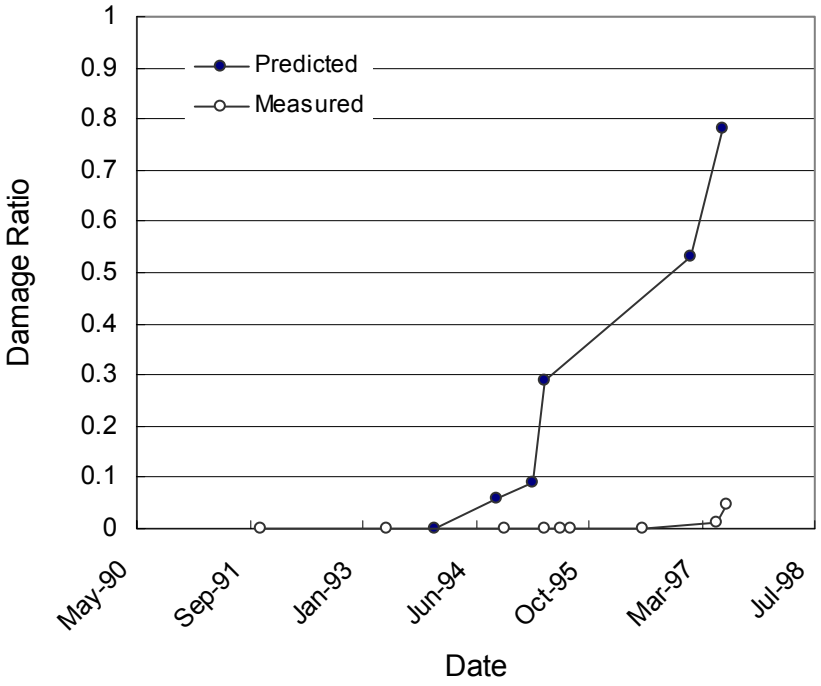

Figure 5.9. Predicted and measured damage ratios due to fatigue cracking for the 48-1077 section (wet no freeze region).

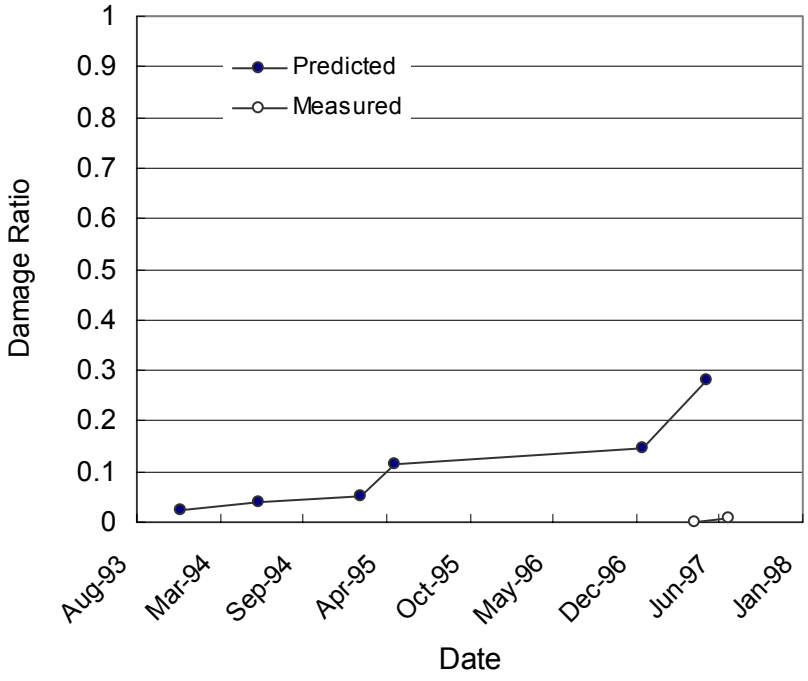

Figure 5.10. Predicted and measured damage ratios due to fatigue cracking for the 48-1060 section (wet no freeze region).

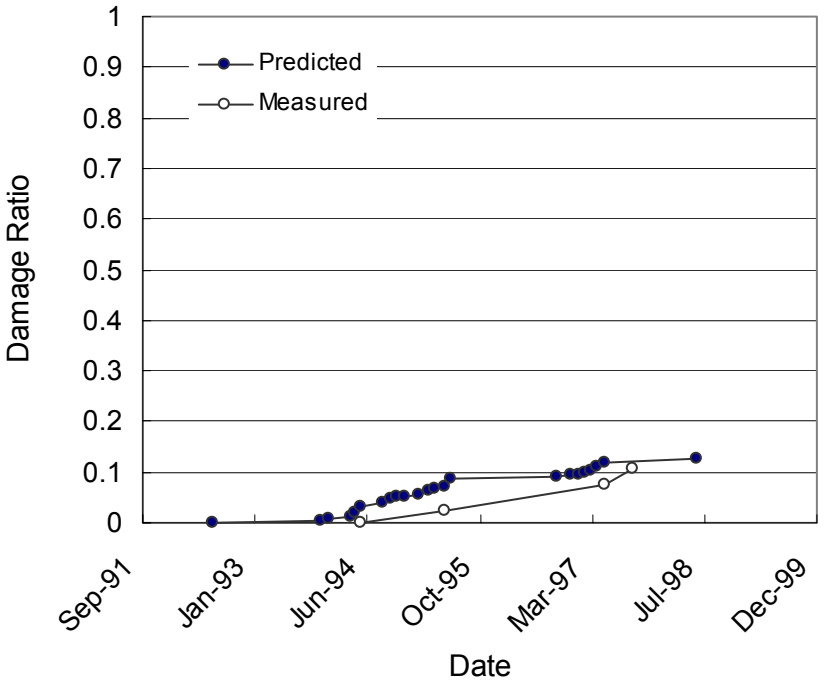

Figure 5.11. Predicted and measured damage ratios due to fatigue cracking for the 9-1803 section (wet freeze region).

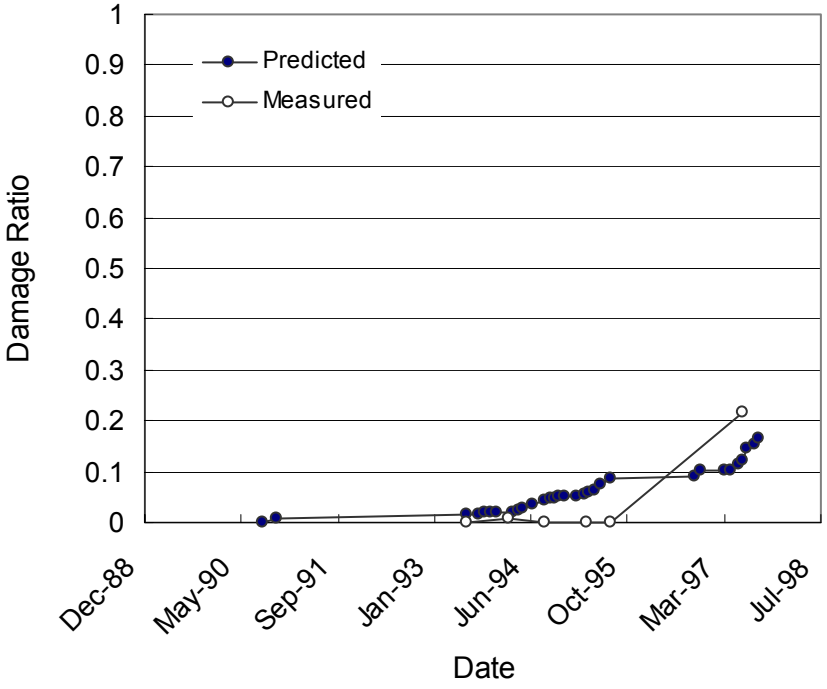

Figure 5.12. Predicted and measured damage ratios due to fatigue cracking for the 27-6251 section (wet freeze region).

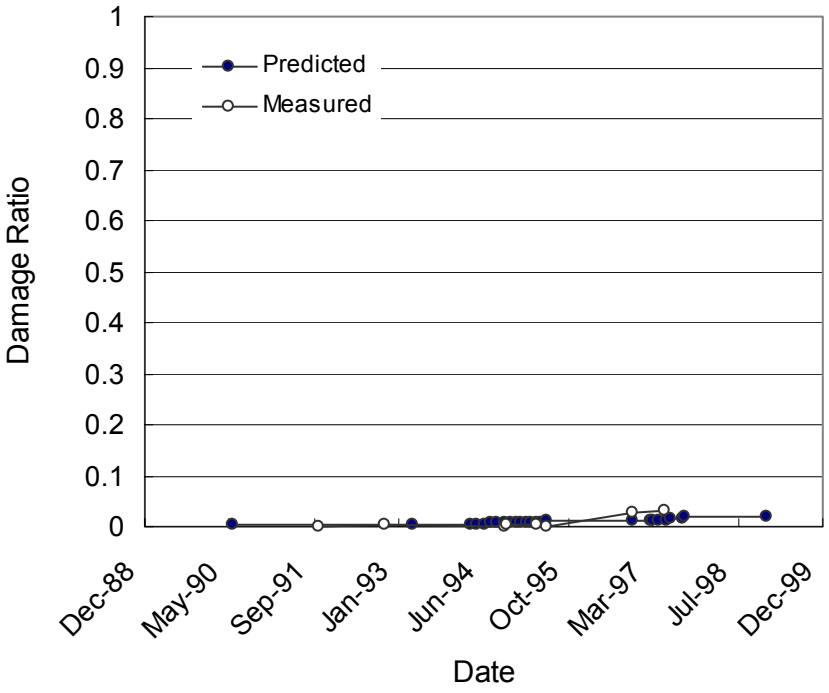

Figure 5.13. Predicted and measured damage ratios due to fatigue cracking for the 40-4165 section (wet freeze region).

5.2.4 Performance Prediction for Rutting

Procedure for Performance Prediction of Rutting

For the performance prediction of rutting in flexible pavements, the VESYS model (Equation 5.9) developed by the FHWA (Kenis, 1978) was used in this study. Since no laboratory tests for determining the VESYS rutting parameters were performed on the pavement materials in these test sections, those values were adopted from the work by Park (2000) for asphalt concrete and the paper by Kenis (1977) for base and subgrade materials. The rutting parameters for asphalt concrete were determined based on the measured AC mid-depth temperature. Table 5.4 shows the VESYS rutting parameters for each layer material.

Table 5.4. The VESYS Rutting Parameters (after Park, 2000, and Kenis, 1997)

Layer	Rutting Parameter	Temperature (^{o}F)			
		60	78	95	86
Asphalt Concrete	α	0.75	0.74	0.72	0.73
	μ	0.30	0.31	0.34	0.32
Base	α	0.75	0.75	0.75	0.75
	μ	0.28	0.28	0.28	0.28
Subgrade	α	0.75	0.75	0.75	0.75
	μ	0.02	0.02	0.02	0.02

The average compressive strain in the AC layer and the compressive strain on the top of the base and subgrade layers under different load levels were calculated from surface deflections using the pavement response models described in Chapter 2. It is noted that the average compressive strain in the AC layer was determined by dividing the difference in deflections between the top and bottom layers of the asphalt concrete by the thickness of the AC layer. The predicted compressive strain, the VESYS rutting parameters, and the ESALs were input to the VESYS rutting model to determine the rut depth for a given season and load group.

Verification of Procedure for Performance Prediction of Rutting Using LTPP Data

The same LTPP test sections used in the procedure for fatigue cracking performance prediction were selected for the verification of the rutting prediction procedure. It is well known that the rut depth in the AC layer becomes a function of the AC mid-depth temperature. Rut depth in the AC layer at a high temperature is more significant than that at a low temperature. For example, Figures 5.14 and 5.15 present the change in AC mid-depth temperatures recorded in 1994/1995 from the 48-1060 section. It is noted that a year is divided into two seasons such as fall/winter and spring/summer. Average AC

mid-depth temperatures in spring/summer and fall/winter are 95^{o}F and 68^{o}F, respectively. Although some variation in AC mid-depth temperatures was observed at each season, the FWD deflections at the average AC mid-depth temperature for each season were used in this study because temperature collection and FWD testing were not performed monthly. To verify the accuracy of this approach, the predicted rut depths using deflections at average seasonal and monthly AC mid-depth temperatures were plotted in Figures 5.16 and 5.17 against the date of the FWD testing. Since the discrepancies in total rut depths (less than 4 mils) are very small, the use of FWD deflection data at the average AC mid-depth temperature for each season seems to be acceptable in this study.

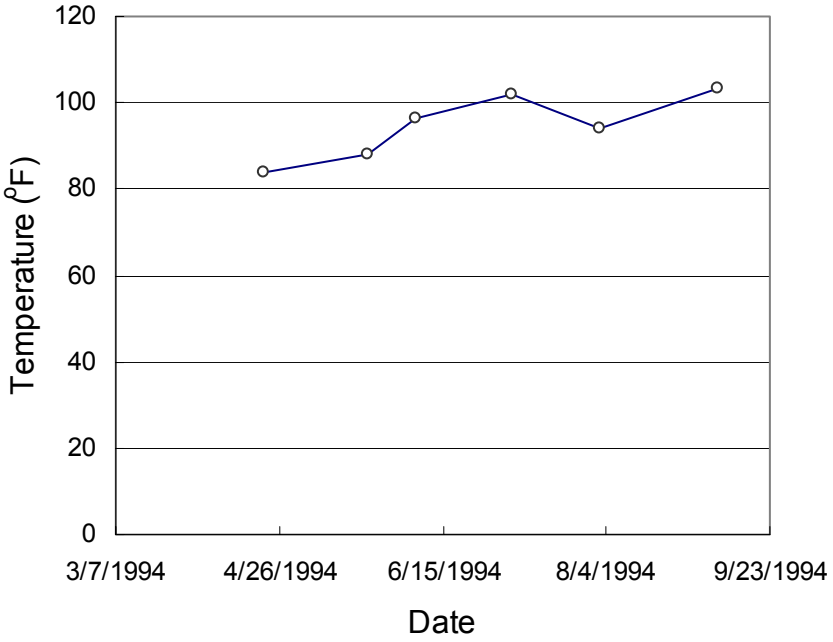

Figure 5.14. Change in AC mid-depth temperatures recorded in spring/summer season from the 48-1060 section.

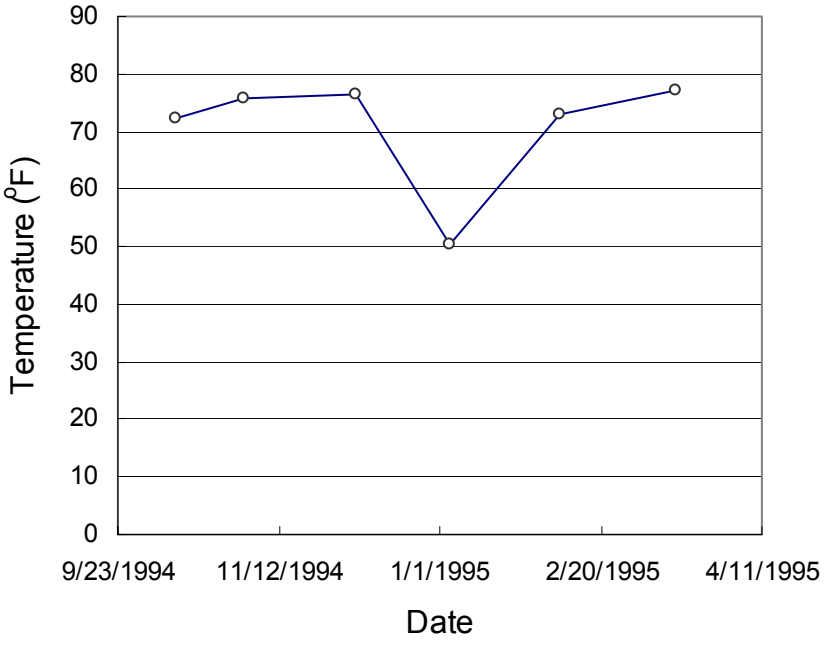

Figure 5.15. Change in AC mid-depth temperatures recorded in fall/winter season from the 48-1060 section.

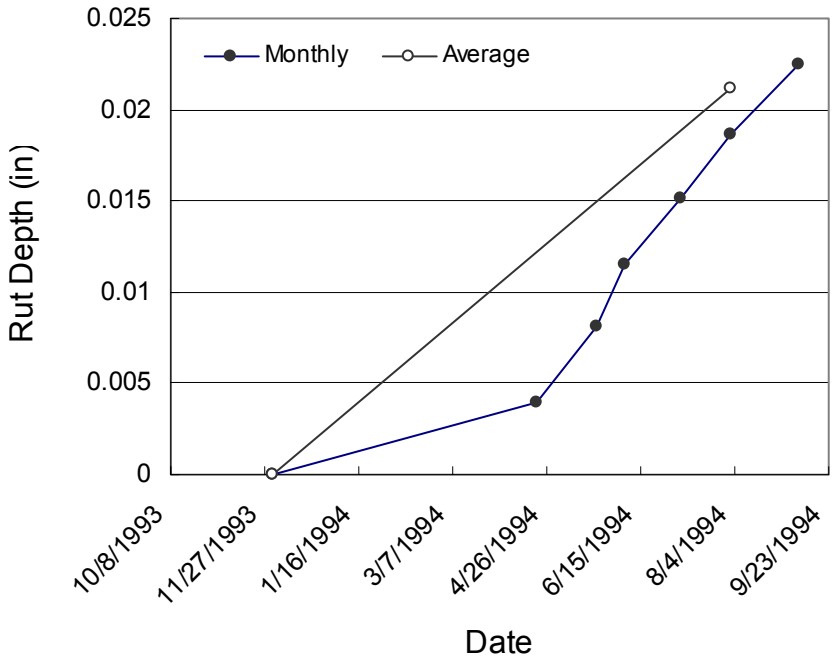

Figure 5.16. Predicted rut depths using the deflections at monthly and average spring/summer AC mid-depth temperatures for the 48-1060 section.

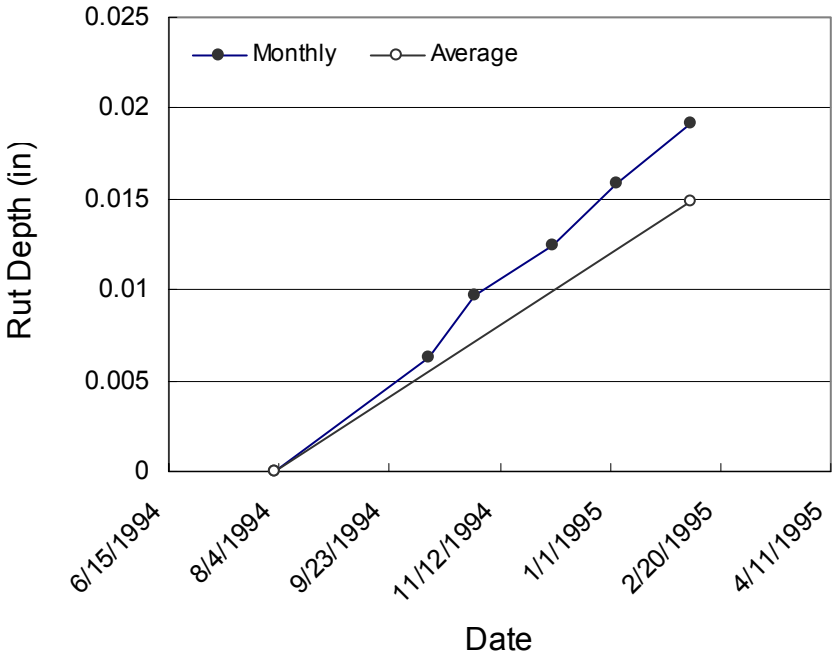

Figure 5.17. Predicted rut depths using the deflections at monthly and average fall/winter AC mid-depth temperatures for the 48-1060 section.

The wheelpath rut depth obtained using the Lane Width Wire Line Method is defined as the maximum distance for each wheelpath between a lane-width wire line placed across the lane and the pavement surface. The categorization of rutting related distresses is shown in Table 5.5, and the measured rut depths for the LTPP test sections are shown in Table 5.6. It can be seen that pavements in the wet no-freeze region show a higher severity of rutting than those in the wet freeze region. The main reason for this result may come from the effect of temperature. The average number of days above 90^{o}F in the wet no-freeze region is 74, whereas the number in the wet freeze region is 21.

Table 5.5. Magnitude of Distress Related to Rutting for Each Category

Distress Type	Nominal	Moderate	Excessive
Rutting (in)	< 0.27	0.27 – 0.78	> 0.78
Roughness, IRI, (ft/mile)	< 8.6	8.6 – 12.8	> 12.8

Table 5.6. Measured Rut Depths for LTPP Test Sections

Region	State	SHRP ID	Survey Date	Total Rut Depth (in)
Wet No Freeze	NC (37)	1028	9/29/98	0.55
	TX (48)	1077	3/26/98	0.67
	TX (48)	1068	3/9/95	0.28
	TX (48)	1060	1/5/99	0.47
Wet Freeze	CT (9)	1803	6/17/98	0.20
	MA (25)	1002	10/9/96	0.31
	MN (27)	6251	2/9/96	0.24
	NH (33)	1001	10/22/97	0.31
	OK (40)	4165	9/11/97	0.31

The developed procedure was applied to both single (9 kip) and multi-load level deflection data. The predicted and measured rut depths against the date of FWD testing

and a visual distress survey for each LTPP test section are plotted in Figures 5.18 through 5.26. Since the deflection data from these pavements before any trafficking was not available, the predicted rut depth before the time of the first FWD testing is assumed to be the same as the measured rut depth at the time of the first FWD testing. Overall, the predicted rut depths agree reasonably well with the field measurements considering that the rutting parameters used in the prediction did not reflect mixture-specific characteristics. The discrepancies may have also resulted from an inaccurate reading of traffic volume data, environmental factors, and other types of distresses. The accuracies of this method for single and multi-load level are demonstrated in Figures 5.27 and 5.28 by comparing the predicted rut depths with the measured values. Generally, predicted rut depths using single and multi-load level deflections have a good agreement with measured rut depths over a wide range of rutting potential. However, the procedure using single load level deflections consistently underpredicts the rut depths. This observation demonstrates that the rutting prediction procedure using multi-load level deflections can estimate an excessive level of rutting quite well and improve the quality of prediction for rutting potential in flexible pavements.

In addition to surface rut depth, it is necessary to check the layer rutting with respect to test date. This study can explain the proportion of total rut depth measurements contributed by each individual layer in flexible pavements. The predicted rut depths in each layer are plotted in Figures 5.29 to 5.32 against the dates of FWD testing for pavements in the wet no-freeze region. The results from the prediction of layer rutting on each test section are presented in Table 5.7. Most rutting was found in the base layer in sections 48-1077 and 48-1060. However, for sections 37-1028 and 48-

1068, more than 30% of the total rutting occurred in the AC layer. It is well known that rutting in the AC layer is accelerated at high temperatures. According to the study for condition assessment of the AC layer in Chapter 6, the AC moduli in the 37-1028 and 48-1068 sections are lower than those in the 48-1077 and 48-1060 sections at high temperatures. This fact supports the possible existence of a large amount of AC layer rutting in these two pavement sections.

Table 5.7. Predicted Layer Rut Depths for LTPP Test Sections

State	SHRP ID	Percent of AC Rut Depth (%)	Percent of Base Rut Depth (%)	Percent of Subgrade Rut Depth (%)	Total Rut Depth (in)
NC (37)	1028	36.31	58.09	5.59	0.55
TX (48)	1077	6.52	90.83	2.63	0.70
TX (48)	1068	32.95	60.90	6.14	0.27
TX (48)	1060	7.25	89.88	2.85	0.47

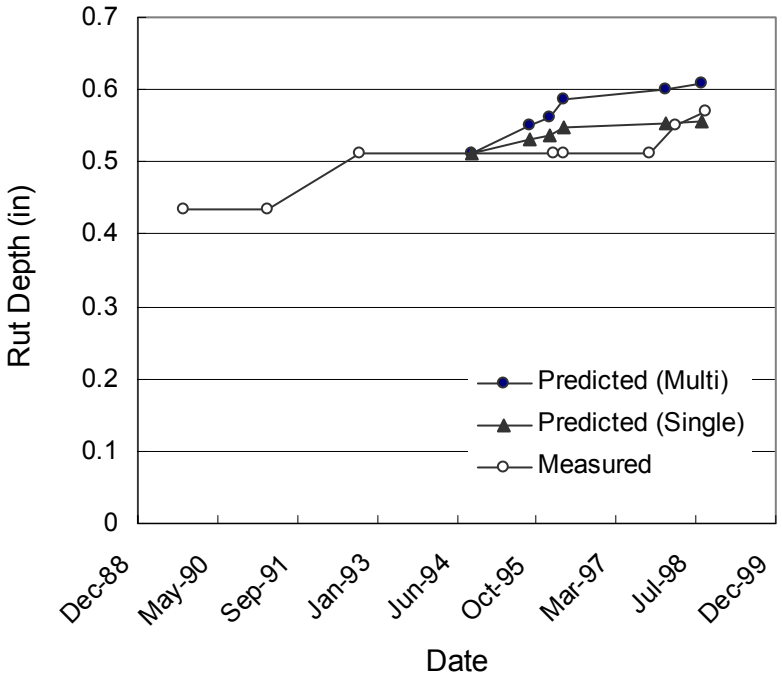

Figure 5.18. Predicted and measured total rut depths for the 37-1028 section.

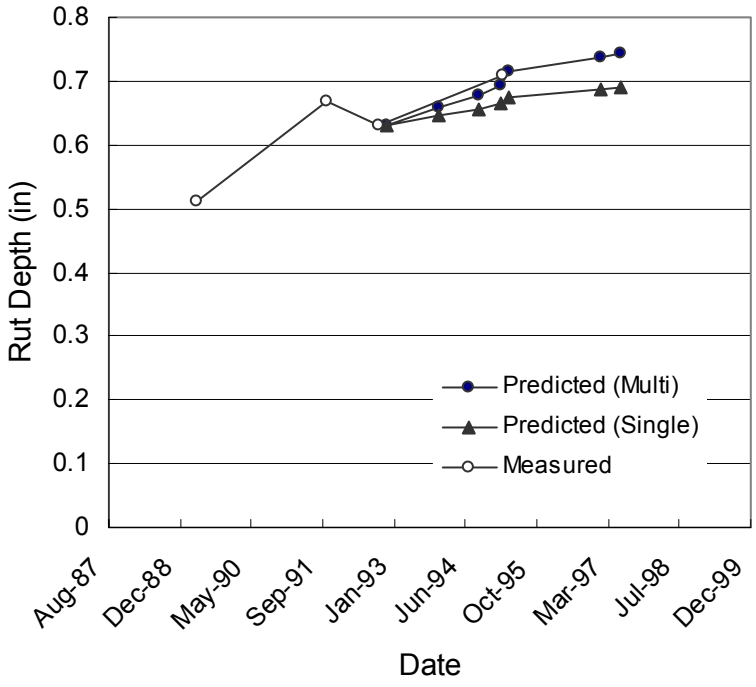

Figure 5.19. Predicted and measured total rut depths for the 48-1077 section.

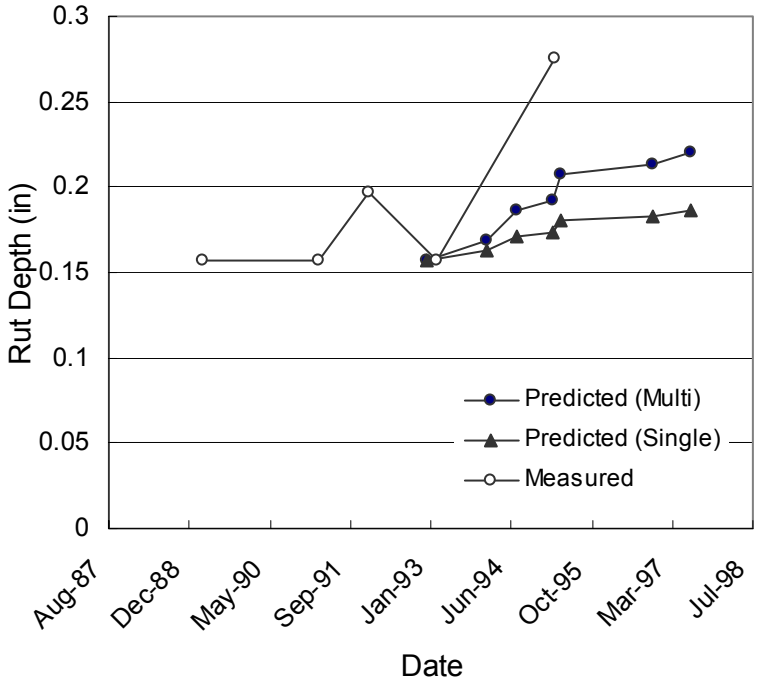

Figure 5.20. Predicted and measured total rut depths for the 48-1068 section.

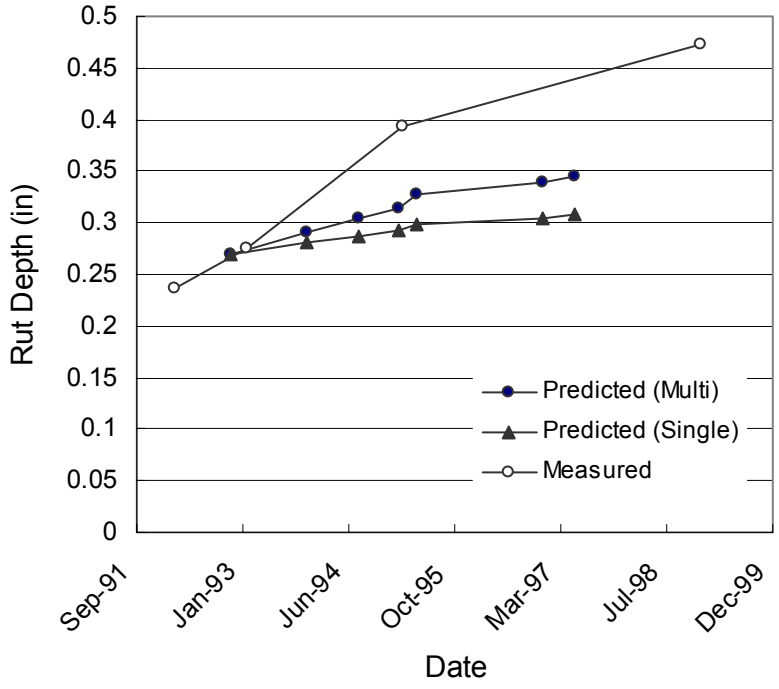

Figure 5.21. Predicted and measured total rut depths for the 48-1060 section.

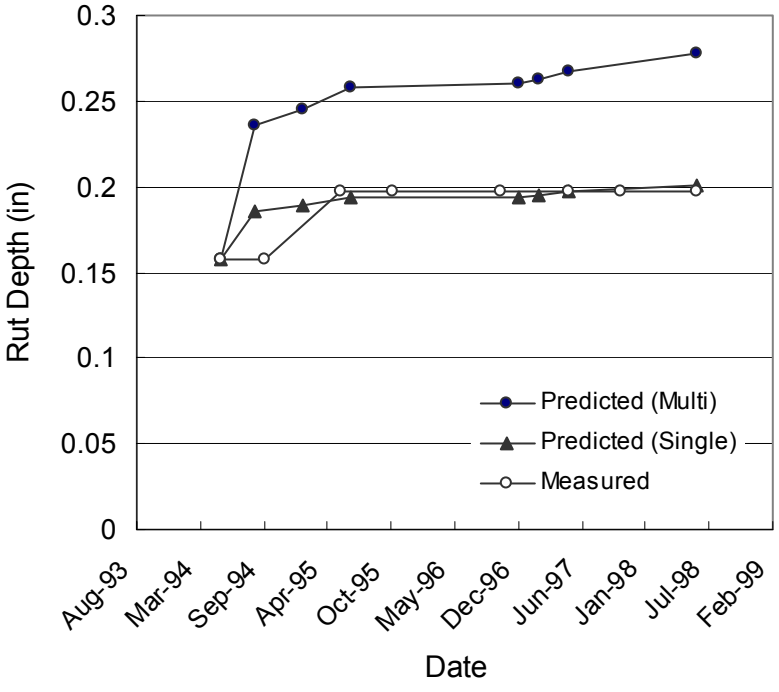

Figure 5.22. Predicted and measured total rut depths for the 9-1803 section.

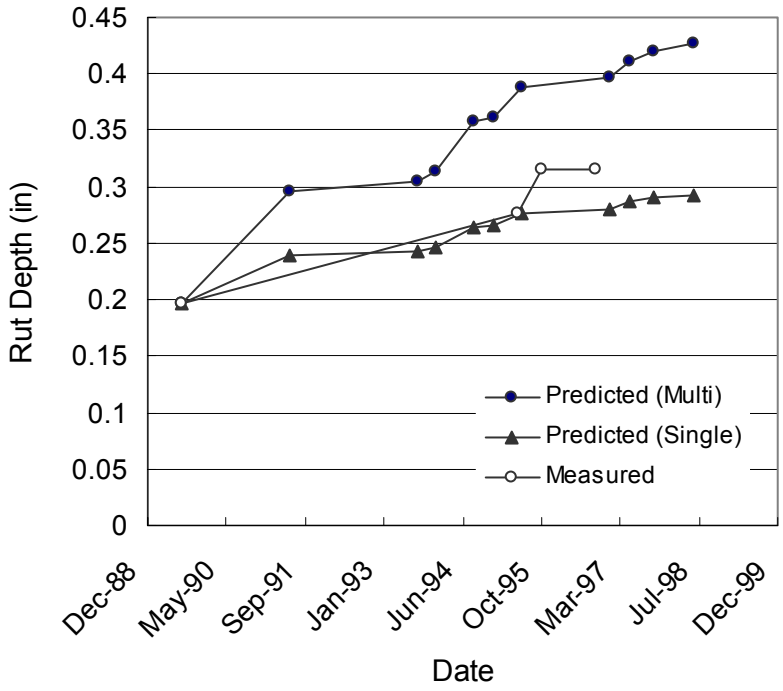

Figure 5.23. Predicted and measured total rut depths for the 25-1002 section.

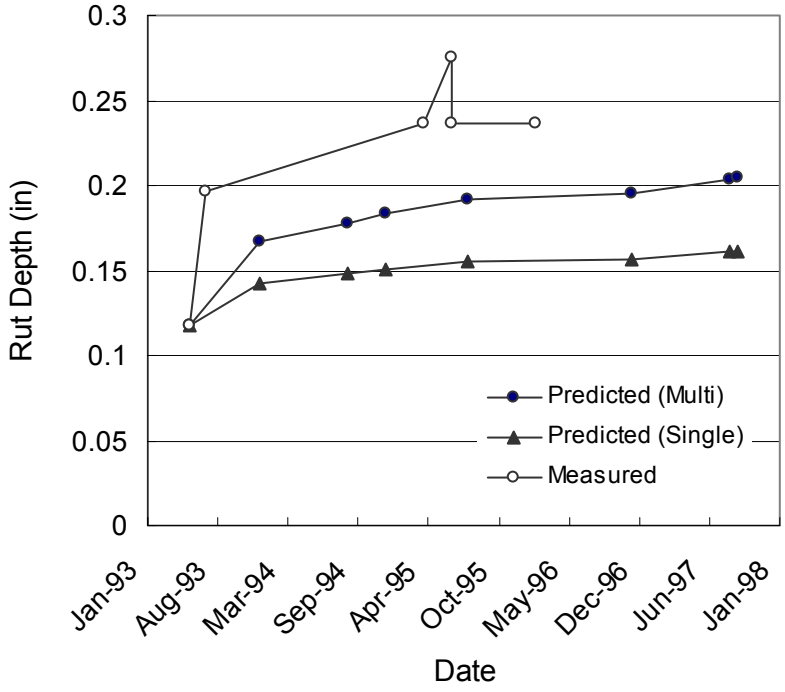

Figure 5.24. Predicted and measured total rut depths for the 27-6251 section.

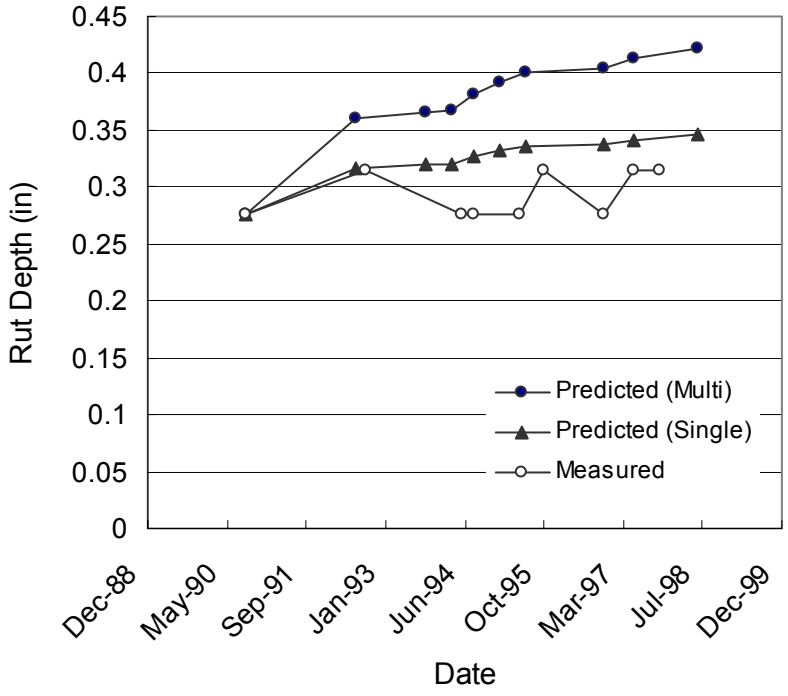

Figure 5.25. Predicted and measured total rut depths for the 33-1001 section.

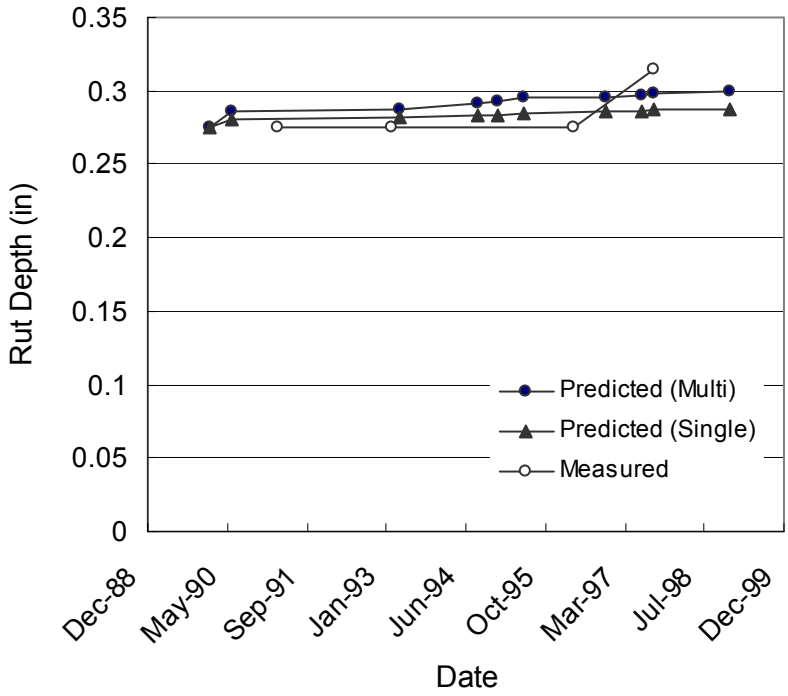

Figure 5.26. Predicted and measured total rut depths for the 40-4165 section.

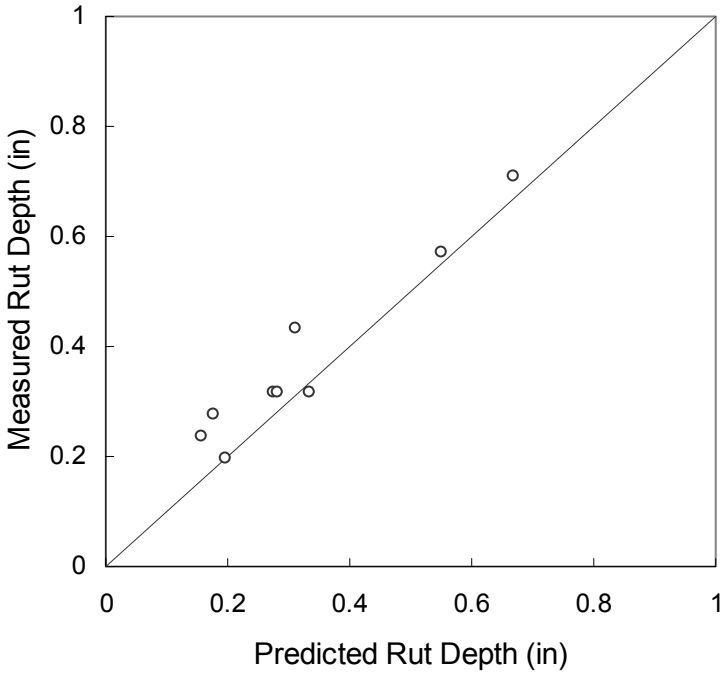

Figure 5.27. Comparison of predicted and measured rut depths for the LTPP test sections (single-load level).

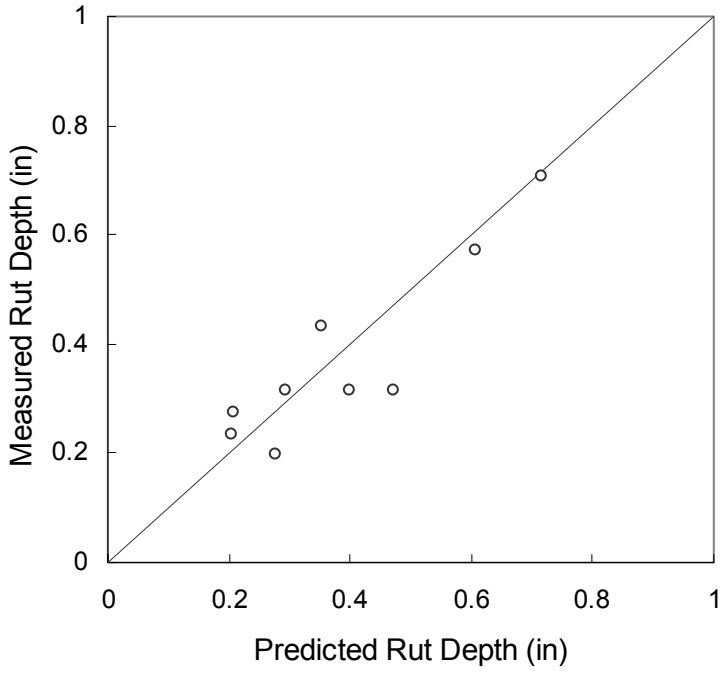

Figure 5.28. Comparison of predicted and measured rut depths for the LTPP test sections (multi-load level).

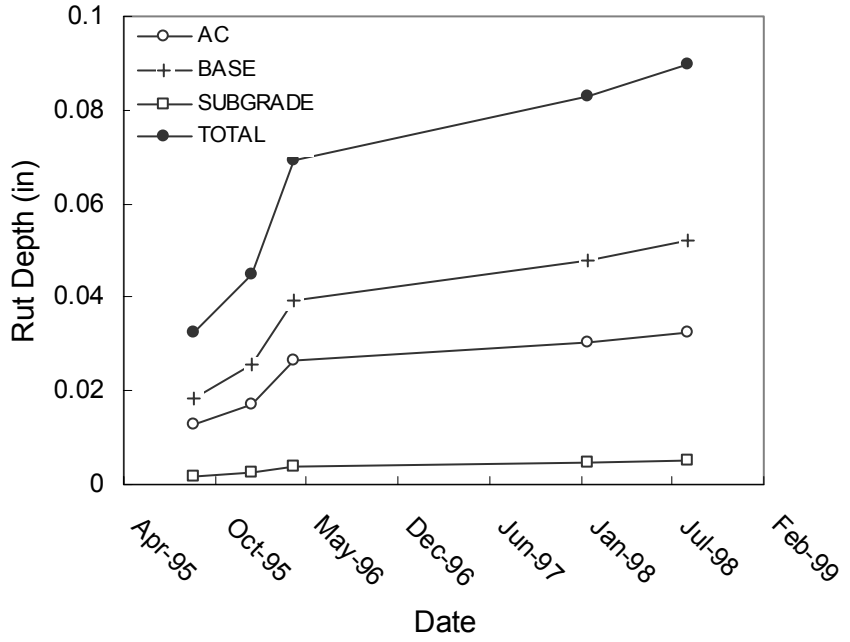

Figure 5.29. Predicted layer rut depths for the 37-1018 section.

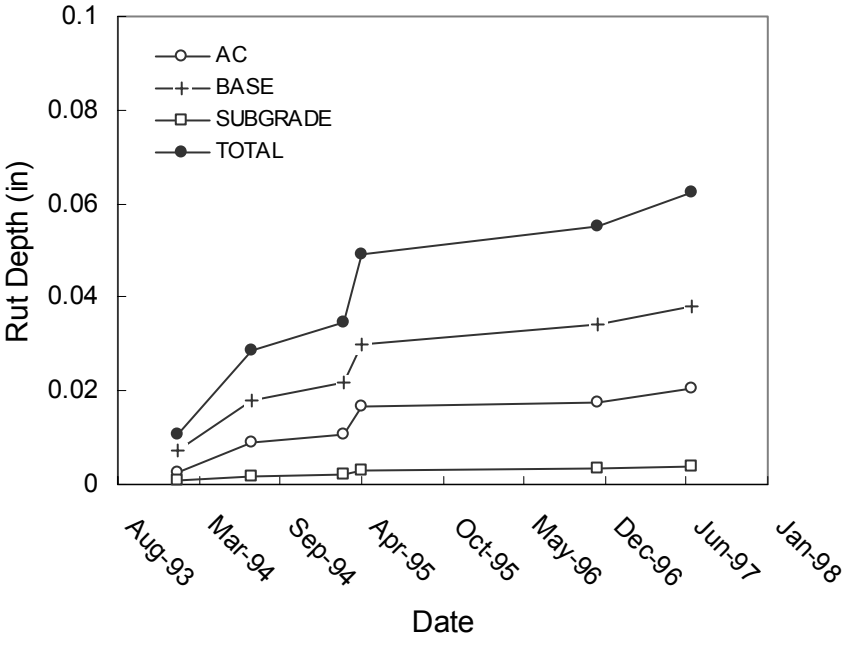

Figure 5.30. Predicted layer rut depths for the 48-1068 section.

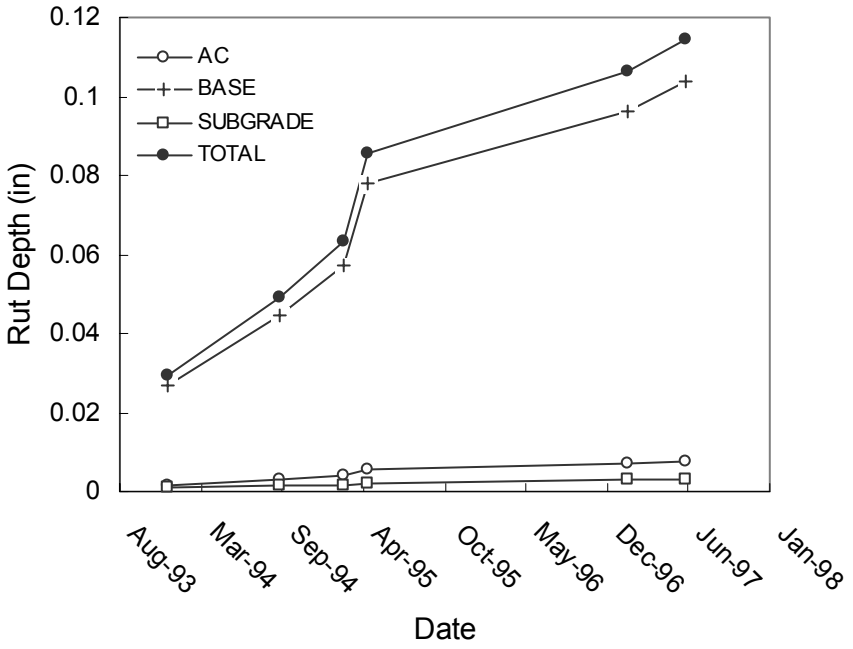

Figure 5.31. Predicted layer rut depths for the 48-1077 section.

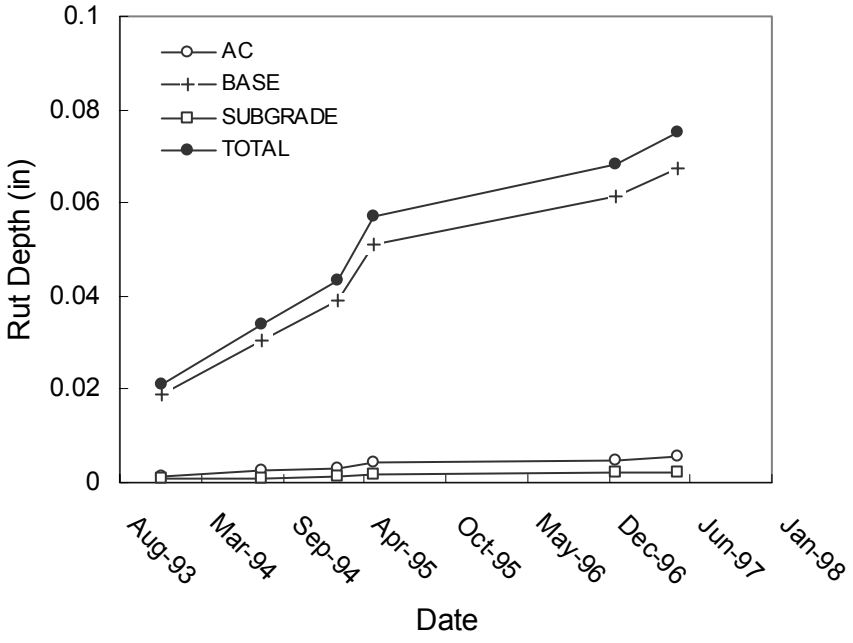

Figure 5.32. Predicted layer rut depths for the 48-1060 section.

5.3 Summary

The effort made in this chapter is to develop reliable procedures for remaining life prediction from the multi-load FWD deflections. The flow charts of the overall procedures for fatigue cracking and rutting are shown in Figures 5.33 and 5.34. In the following, the remaining life prediction procedure is described stepwise.

- Fatigue Cracking

1. Collect the surface deflections from a multi-load level FWD test.
2. Calculate SCI values from surface deflections for each load level.
3. Predict E_{ac} from the regression based backcalculation approach.
4. Predict ε_t using the pavement response model.
5. Determine the number of load applications to failure due to fatigue cracking using the pavement performance model.
6. Collect the actual number of load applications from the traffic monitoring.
7. Calculate the damage ratio for a given period and load level.
8. Calculate the total damage ratio by summing the damage ratio.
9. If the total damage ratio is greater than one, the AC layer is in a failure condition.

- Rutting Potential

1. Collect surface deflections from a multi-load level FWD test.
2. Calculate SCI values for the AC layer, BDI values for the base layer, and BCI values for the subgrade.
3. Predict ε_{cac}, ε_{abc}, and ε_{sg} based on the pavement response models.
4. Collect the actual number of load applications from the traffic monitoring.
5. Determine the rutting parameters for each layer.

6. Predict the layer rut depths using the pavement performance model.
7. Calculate the total rut depth by summing up the layer rut depths.
8. If the total rut depth is greater than the critical rut depth, the pavement is considered to be distressed.

Figures 5.35 and 5.36 give the worksheet for the calculation of each step mentioned above.

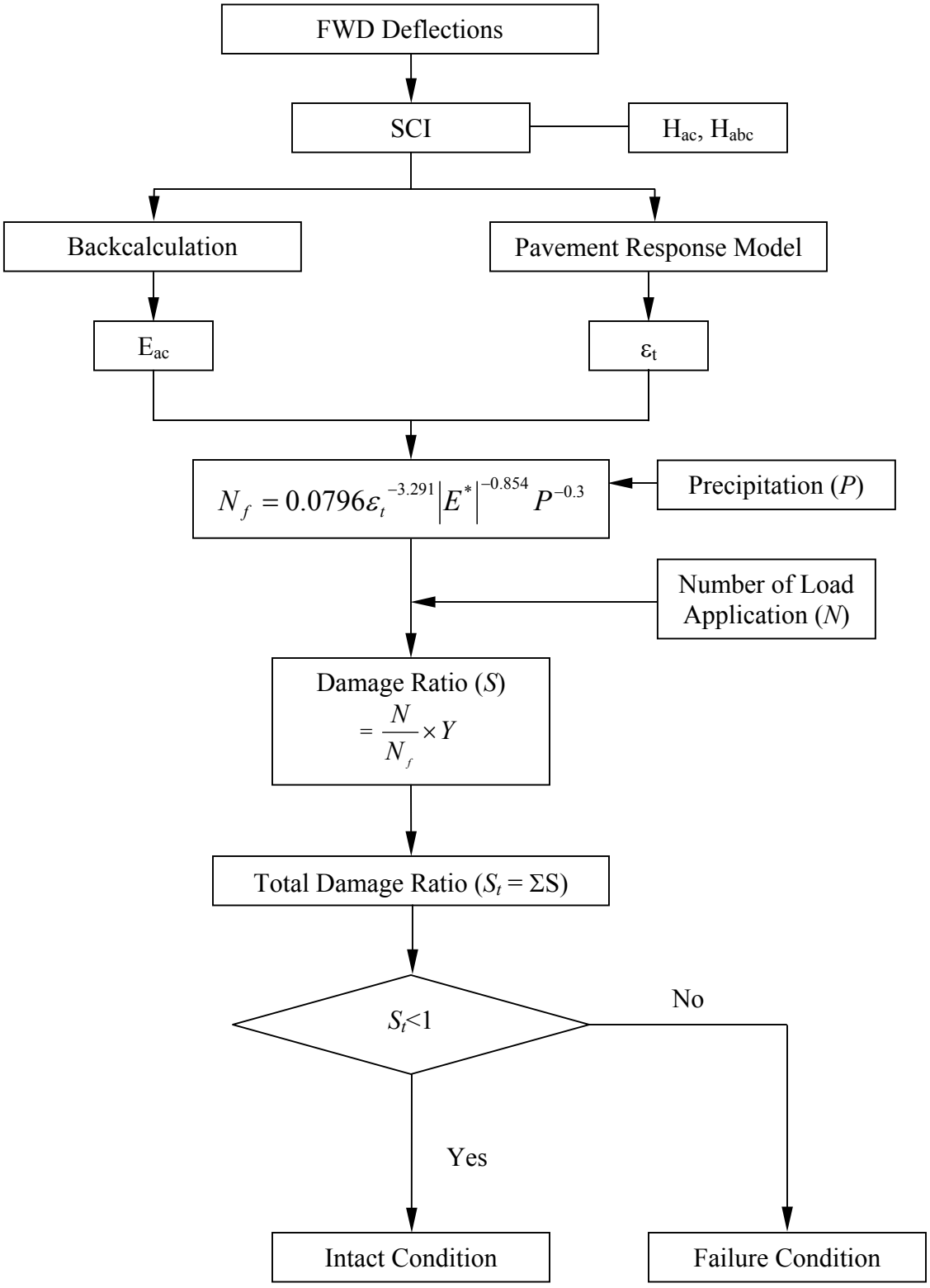

Figure 5.33. Flow chart for the remaining life prediction procedure for fatigue cracking.

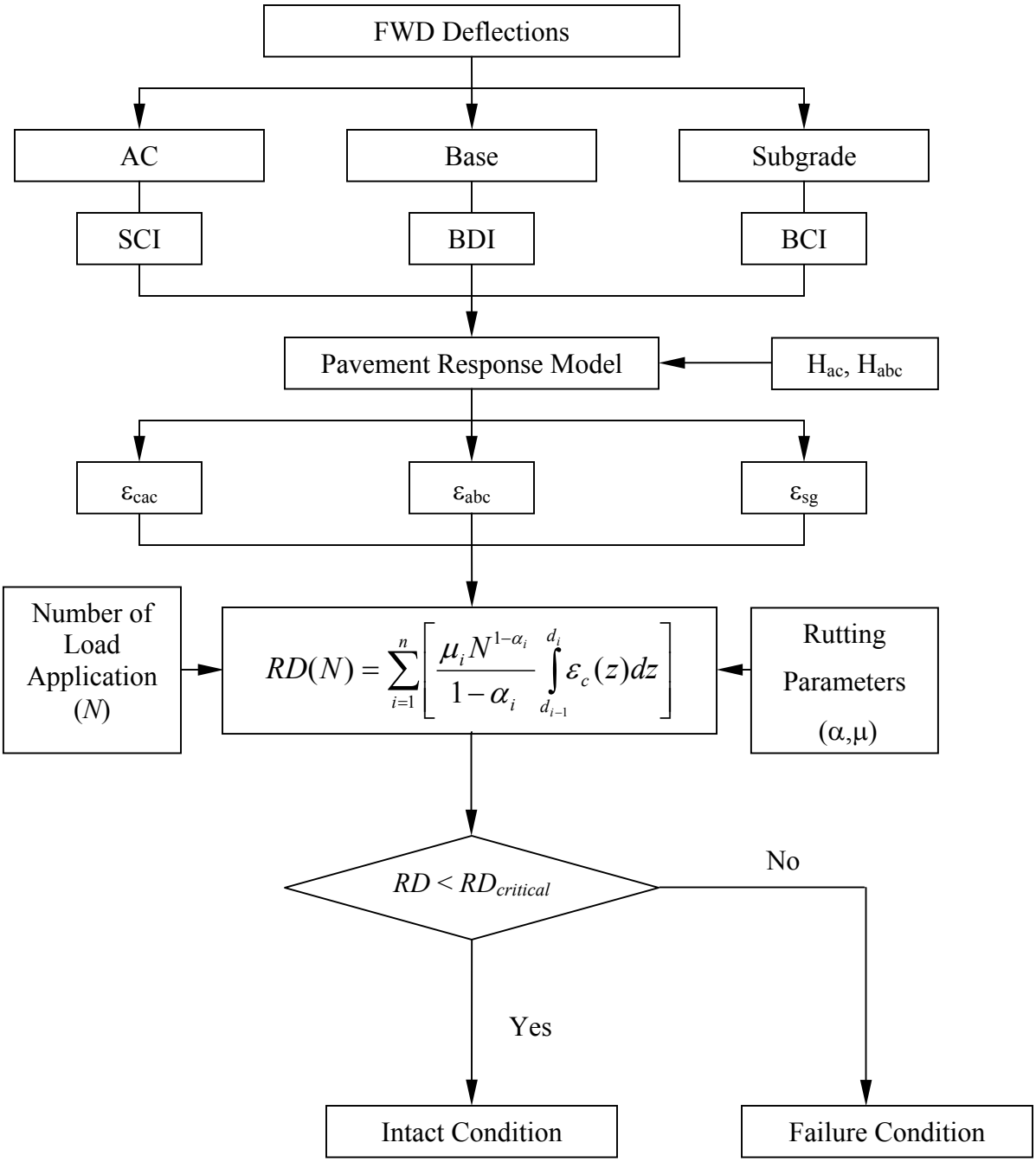

Figure 5.34. Flow chart for the remaining life prediction procedure for rutting.

1

Date	AC Mid depth Temperature (^oF)	SCI (mils)	Eac (ksi)
9/13/1995	101.48	5.23	225
1/18/1996	56.66	2.91	430
4/18/1996	77.54	3.93	308
1/20/1998	49.46	2.00	653
8/25/1998	91.76	3.38	364

2

Tensile strain at the bottom of the AC layer (ε_t)			
6 kips	9 kips	12 kips	15 kips
135.0	217.8	304.3	414.3
61.1	127.8	166.3	246.0
105.0	168.3	249.9	337.2
63.8	105.2	150.6	208.3
136.4	220.7	296.5	387.8

3

Number of load applications to failure (N_f)			
6 kips	9 kips	12 kips	15 kips
1387138	286959	95516	34577
10845665	957400	401928	110751
2420981	513611	139683	52105
6582071	1268635	389974	134107
889156	182392	69096	28560

4

Number of load applications (N)			
6 kips	9 kips	12 kips	15 kips
181415	25484	7251	11733
96186	13512	3844	6221
96186	13512	3844	6221
192741	27075	7704	12465
192741	27075	7704	12465

5

Damage Ratio (S)				**6**
6 kips	9 kips	12 kips	15 kips	Total Damage Ratio
0.065	0.044	0.038	0.170	0.317
0.068	0.049	0.041	0.187	0.344
0.124	0.085	0.079	0.354	0.642
0.141	0.098	0.091	0.409	0.740
0.358	0.247	0.203	0.846	**1.653**

Figure 5.35. The worksheet for the calculation of the damage ratios due to fatigue cracking for the 38-1018 section.

Date	Tac (°F)	SCI (mils)				BDI (mils)				BCI (mils)			
		6 kips	9 kips	12 kips	15 kips	6 kips	9 kips	12 kips	15 kips	6 kips	9 kips	12 kips	15 kips
9/13/1995	101.3	3.82	5.24	6.65	8.31	2.13	2.95	3.74	4.69	1.14	1.65	2.13	2.68
1/18/1996	56.66	2.13	2.91	3.86	4.76	1.22	2.01	2.44	3.23	1.02	1.22	1.81	2.24
4/18/1996	77.54	2.87	3.94	5.16	6.50	1.77	2.48	3.27	4.02	1.06	1.57	2.09	2.68
1/20/1998	49.28	1.38	2.01	2.68	3.43	1.22	1.77	2.28	2.87	0.91	1.34	1.73	2.17
8/25/1998	91.58	3.07	3.39	4.92	5.83	2.13	2.99	3.70	4.45	1.06	1.54	2.05	2.52

Compressive strain in the AC layer (ε_{cac})				Compressive strain on top of the base layer (ε_{abc})				Compressive strain on top of the subgrade (ε_{sg})			
6 kips	9 kips	12 kips	15 kips	6 kips	9 kips	12 kips	15 kips	6 kips	9 kips	12 kips	15 kips
89.0	124.6	160.6	204.7	300.8	413.8	516.9	634.9	185.4	273.9	352.0	446.7
47.4	66.4	89.2	112.7	177.5	290.1	345.7	448.7	166.1	198.6	298.4	370.6
65.6	91.8	122.2	157.1	254.6	348.4	453.4	553.6	172.4	258.4	347.6	446.1
29.9	44.2	60.1	78.3	182.7	254.9	323.6	401.6	145.6	219.8	287.4	360.3
69.7	78.0	116.3	139.0	303.0	417.5	508.0	607.5	171.2	252.7	336.6	419.2

Number of load applications (N)				Cumulative number of load applications				Rutting parameters					
								α	μ	α	μ	α	μ
8876	1836	871	810	8876	1836	871	810	0.74	0.31	0.75	0.28	0.75	0.02
8876	1836	871	810	17751	3671	1743	1620	0.74	0.31	0.75	0.28	0.75	0.02
17751	3671	1743	1620	26627	5507	2614	2430	0.73	0.32	0.75	0.28	0.75	0.02
26627	5507	2614	2430	53253	11013	5228	4859	0.74	0.31	0.75	0.28	0.75	0.02
8876	1836	871	810	62129	12849	6099	5669	0.73	0.32	0.75	0.28	0.75	0.02

Rut depth in the AC layer (in)					Rut depth in the base layer (in)					Rut depth in the subgrade (in)					Total Rut Depth (in)
6 kips	9 kips	12 kips	15 kips	Total	6 kips	9 kips	12 kips	15 kips	Total	6 kips	9 kips	12 kips	15 kips	Total	
0.003	0.003	0.003	0.004	0.013	0.004	0.004	0.004	0.005	0.018	0.0004	0.0004	0.0004	0.0005	0.0016	0.033
0.001	0.001	0.001	0.001	0.017	0.002	0.002	0.002	0.002	0.025	0.0002	0.0002	0.0002	0.0002	0.0024	0.045
0.002	0.002	0.002	0.003	0.027	0.003	0.003	0.003	0.004	0.039	0.0003	0.0003	0.0003	0.0004	0.0037	0.069
0.001	0.001	0.001	0.001	0.030	0.002	0.002	0.002	0.003	0.048	0.0002	0.0002	0.0002	0.0003	0.0047	0.083
0.001	0.000	0.001	0.001	0.033	0.001	0.001	0.001	0.001	0.052	0.0001	0.0001	0.0001	0.0001	0.0050	0.090

Figure 5.36. The worksheet for the calculation of the rut depth for the 38-1018 section.

CHAPTER 6

CONCLUSIONS AND RECOMMENDATIONS

6.1 Conclusions

This study discusses the use of multi-load level FWD deflections for layer condition assessment and performance prediction in flexible pavements. To simulate the actual pavement responses, the dynamic finite element program in conjunction with the stress-dependent soil model was developed as a forward modeling of pavement structure. Based on the synthetic database developed from a forward modeling program, an attempt was made to establish the pavement response models for specific types of distress. To estimate layer condition and remaining life of flexible pavements, the multi-load level deflection analysis methods were developed using pavement response models and pavement performances obtained from the various field databases. Based on the study, the following conclusions may be drawn:

1. The deflection basin parameters and critical pavement responses can be used to determine the strength of base and subgrade materials of a flexible pavement. A 12 kip of FWD load level, used as the maximum load level by the NCDOT, seems not large enough to improve the accuracy in assessing base and subgrade layer condition.
2. The predicted elastic modulus of the AC layer, E_{ac}, and critical pavement responses, ε_{ac} and $d\varepsilon_{ac}$, are capable of estimating the current condition of the AC layer.

3. Results from the study for nonlinear behavior of a pavement structure indicate that the deflection ratio obtained from multi-load level deflections can predict the type and quality of base/subgrade materials.
4. The performance of fatigue cracking can be predicted using the proposed procedure except for pavements with high and rapidly increasing cracking in wet freeze regions. Better prediction was achieved by employing climatic factors to this prediction algorithm.
5. The proposed procedure for rutting performance prediction was found to be accurate in estimating the actual rutting performance. The rutting performance prediction was validated with data collected from pavement sections in the LTPP database. Research efforts also were concentrated on accurately predicting the individual layer rutting.

6.2 Recommendations

More field data are needed to further validate the proposed procedures. The traffic monitoring data, climatic information, and detailed data on pavement materials should be collected by well controlled technique. The FWD load levels used in this study are limited up to 16 kip. The greater FWD load level deflection data is necessary in some strong pavements to yield more accurate and reliable prediction of pavement performance. Additional research effort is needed to investigate the effect of shift factors in the pavement performance models on the proposed procedures.

CHAPTER 7

IMPLEMENTATION AND TECHNOLOGY TRANSFER PLAN

The major products from this research project are the asphalt pavement layer condition assessment and remaining life prediction procedures displayed in Figures 4.55, 5.33, and 5.34. These procedures are programmed into APLCAP (Asphalt Pavement Layer Condition Assessment Program), a VisualBasic software developed at North Carolina State University for the NCHRP 10-48 project. The resulting product is an APLCAP version 2.0, for which the operational guideline is given in Appendix C.

In order for this program to be successfully implementd by the NCDOT, the program needs to be tested by PMU engineers for various field cases. Their feedback on the performance of the program is necessary to customize it to meet the needs for routine operation. Some parts of the program require further research and refinement, including: (1) traffic data analysis; (2) the effect of damage on the modulus of asphalt concrete; and (3) lab-to-field shift factors or transfer functions. Also, rigorous beta testing is necessary for the program to be used more widely.

APLCAP version 2.0 provides an excellent modular framework for layer condition assessment and remaining life prediction of asphalt pavements using single- and multi-load FWD deflections. It is recommended that other pavement design and rehabilitation procedures used by the PMU engineers be added to this program. The consolidation of deflection analysis algorithms into a single program has many advantages, including easy implementation of new research findings in this subject area,

consistency within the NCDOT in deflection analysis, and efficient evaluation of the effects of changing design parameters on pavement design and rehabilitation decisions.

When APLCAP version 2.0 is ready to be disseminated more widely within the NCDOT, one-day workshop on the background concepts and the use of the software may be beneficial to ensure a smooth start in the implementation effort.

REFERENCES

1. AASHTO (1993). *AASHTO Guide for Design of Pavement Structures*. American Association of State Highway and Transportation Officials, Washington D.C., 1993.
2. AI (1981), "Thickness Design – Asphalt Pavements for Highways and Streets", Manual Series No. 1, Asphalt Institute.
3. Bonaquist, R. F. (1996). "Development and Application of a Comprehensive Constitutive Model for Granular Materials in Flexible Pavement Structures." Ph. D. Dissertation, University of Maryland, College Park, MD.
4. Brown, S. F., Louch, S. C., and O'Reilly, M. P., (1987), "Repeated Loaded Loading of Fine Grained Soils," TRRL Contractors Report, CR72, School of Civil Engineering, University of Nottingham, Nottingham, England.
5. Brown, S. F. and Pappin, J.W., (1981), "Analysis of Pavements with Granular Bases", Transportation Research Record 810, TRB, Washington, D.C., pp. 17-23.
6. Chang, D. W. (1991). "Nonlinear Effects on Dynamic Response of Pavements Using the Non-Destructive Testing Techniques," Ph. D. Dissertation, University of Texas at Austin, Austin, TX.
7. Chen, D-H, Bilyeu, J;Lin, H-H, and Murphy, M. Temperature Correction on FWD Measurements. In *Transportation Research Record* 1716, TRB, National Research Council, Washington, D.C., 2000, pp. 30-39.

8. Elliot, R. P., and David, L., (1989), "Improved Characterization Model for Granular Bases", Transportation Research Record 1227, TRB, Washington, D.C., pp. 128-133.
9. Federal Highway Administration (2000), "Performance Trends of Rehabilitation AC Pavements" *Tech Brief No. FHWA-RD-00-165*, U.S. Department of Transportation, Washington, D. C.
10. Garg, N., and Thomson, M. R., (1998), "Triaxial Characterization of Mn/ROAD Granular Materials", Transportation Research Record 1577, TRB, Washington D. C., pp. 22-36.
11. Garg, N., and Thomson, M. R., (1998), *Mechanistic-Empirical Evaluation of the Mn/Road Low Volume Road Test Sections.* Final Report No. FHWA-IL-UI-262, the Illinois Department of Transportation, Springfield, IL.
12. Hicks, R. G. and C. L. Monismith. (1971). "Factors Influencing the Resilient Properties of Granular Materials," Transportation Research Record 345, TRB, Washington D. C., pp. 15-31.
13. Jung, F. (1988). "Direct Calculation of Maximum Curvature and Strain in Asphalt Concrete Layers of Pavements from Load Deflection Basin Measurements," Transportation Research Record 1196, TRB, Washington D.C.
14. Jooste, F. J. and Fernando, E. G. (1995). "Development of a Procedure for the Structural Evaluation of Superheavy Loads Routes." *Research Report 1335-3F*, Texas Transportation Institute, College Station, TX.
15. Kenis, W. J. (1978). "Predictive Design Procedure, VESYS User's Manual: An Interim Desigh Method for Flexible Pavement Using the VESYS Structural

Subsystem." *Final Report No. FHWA-RD-77-154*, Federal Highway Administration, U.S. Department of Transportation, Washington, D.C.

16. Kenis, W. J. and Wang, W. (1997). "Calibrating Mechanistic Flexible Pavement Rutting Models from Full Scale Accelerated Tests." *Proc. of the 8th International Conference on Asphalt Pavements*, Seattle, WA, 663-672.
17. Kim, Y. R., S. R. Ranjithan, J. D. Troxler, and B. Xu. *Assessing Pavement Layer Condition Using Deflection Data*. NCHRP Report 10-48, TRB, National Research Council, Washington, D. C., 2000.
18. Kim, Y. R., and H. M. Park. *Use of Falling Weight Deflectometer Multi-Load Data for Pavement Strength Estimation*. NCDOT Report (Project HWY-00-4), North Carolina State University, Raleigh, 2001.
19. Kim, Y. R., B. O. Hibbs, and Y. C. Lee. Temperature Correction of Deflections and Backcalculated Asphalt Concrete Moduli. In *Transportation Research Record* 1473, TRB, National Research Council, Washington, D.C., 1995, pp. 55-62.
20. Kim, Y. R., S. Park, and L. Shao. *Statewide Calibration of Asphalt Temperature Study from 1992 and 1993*. NCDOT Report (Project 23241-95-1), North Carolina State University, Raleigh, 1996.
21. Kim, Y. R., S. Park, and L. Shao, (1996), *Statewide Calibration of Asphalt Temperature Study from 1992 and 1993*. Final Report Submitted to the North Carolina Department of Transportation, North Carolina State University, Raleigh, NC.
22. Lee, Y. C. (1997). "Condition Assessment of Flexible Pavements using FWD Deflections." Ph. D. Dissertation, North Carolina State University, Raleigh, NC.

23. Lukanen, E. O., Stubstad, R. N., and Briggs, R. *Temperature Predictions and Adjustment Factors for Asphalt Pavement*. Report FHWA-RD-98-085. FHWA, U.S. Department of Transportation, 2000.
24. Mamlouk, M. S., (1987), "Dynamic Analysis of Multi-Layer Pavement Structures-Theory, Significance and Verification," *Proceedings, 6th International Conference on the Structural Design of Asphalt Pavements*, Vol. 1, pp. 466-474.
25. May, R. W., and Witczak, M. W., (1981), "Effective Granular Modulus to Model Pavement Responses", Transportation Research Record 810, TRB, Washington, D. C., pp. 1-9.
26. Monismith, C. L., and D. B. McLean (1972), "Structural Design Considerations," Proceedings, Association of Asphalt Paving Technologists, Cleveland, OH.
27. NCHRP, (1996) "Laboratory Determination of Resilient Modulus for Flexible Pavement Design", National Cooperative Highway Research Board, pp.75-82.
28. Park, S. W. (2000). "Evaluation of Accelerated Rut Development in Unbound Pavement Foundations and Load Limits on Load-Zoned Pavements," Ph. D. Dissertation, Texas A&M University, College Station, TX.
29. Park, S. and Y. R. Kim (1997), "Temperature Correction of Backcalculated Moduli and Deflections Using Linear Viscoelasticity and Time-Temperature Superposition", Transportation Research Record 1570, TRB, Washington, D.C., pp. 108-117.
30. Pezo, R. F., (1993), "A general Method of Reporting Resilient Modulus of Tests of Soils, A Pavement Engineer's Point of View", Paper presented at 72nd Annual Transportation Research Board Meeting, January.

31. Rada, G., and M. W. Witczak, (1981), "Comprehensive Evaluation of Laboratory Resilient Moduli Results for Granular Materials", Transportation Research Record 810, TRB, Washington, D.C., pp. 23-33.
32. Santha, B. L. (1994), "Resilient Modulus of Subgrade Soils: Comparison of Two Constitutive Equations", Transportation Research Record 1462, TRB, Washington, D.C., pp. 79-90.
33. Sowers, G. F. and Hedges, C. (1966). "Dynamic Cone for Shallow in-situ Penetration Testing," *Vane Shear and Cone Penetration Resistance Testing of in-situ Soils*, *ASTM STP 399*, ASTM, Philadelphia, PA, pp. 29-30.
34. Thadkamalla, G. B., and George, K. P., (1995), "Characterization of Subgrade Soils at Simulated Field Moisture", Transportation Research Record 1481, TRB, Washington, D. C., pp.21-27.
35. Thompson, M. R. (1989), "ILLI-PAVE Based NDT Analysis Procedures," In *Nondestructive Testing of Pavements and Backcalculation of Moduli*, ASTM STP 1026, A. J. Bush III and G. Y. Baladi, Eds., American Society for Testing and Materials, Philadelphia, pp. 229-244.
36. Thompson, M. R. (1989), "Area Under the Pavement Profile to Predict Strain," Informal Presentation at FWD Users Group Annual Meeting, Indianapolis, IN.
37. Thompson, M. R., and Elliot, R. P., (1985), "ILLI-PAVE-Based Response Algorithms for Design of Conventional Flexible Pavements", Transportation Research Record 1043, TRB, Washington, D. C., pp. 55-57.
38. Tseng, K. H. and Lytton, R. L. (1989), "Prediction of Permanent Deformation in Flexible Pavement materials,' Implication of Aggregates in the Design,

Construction, and Performance of Flexible Pavements, ASTM STP 1016, H. G. Schreuders and C. R. Marek, Eds., American Society for Testing and Materials, Philadelphia, pp. 154-172.

39. Tutumluer, Erol, and Thompson, M. R., (1997), "Anisotropic Modeling of Granular Bases in Flexible Pavements," Paper presented at 76th Annual Transportation Research Board Meeting, January.
40. Uzan, J., (1985), "Characterization of Granular Materials", Transportation Research Record 1022, TRB, Washington, D. C., pp. 52-59.
41. Witczak, M. W., and Uzan, J., (1988), "The Universal Airport Pavement Design System, Report I of V: Granular Material Characterization," University of Maryland.
42. Xu, B. (2001). "Assessment Pavement Layer Condition Using Deflection Data," Ph. D. Dissertation, North Carolina State University, Raleigh, NC.

APPENDIX A

FORWARD MODELING OF PAVEMENTS

A.1 General Description of the Finite Element Model

The two-dimensional finite element program, NCPAVE, was developed to compute pavement responses under static and dynamic loading. It considers the pavement as an axisymmetric solid of revolution and divides it into a set of finite elements connected at four nodal points. It is capable of automatically generating a finite element mesh for the analysis of a pavement structure and accommodating the stress-dependent soil model in the base and subgrade layer.

NCPAVE generates the mesh for the area around the FWD loading plate using finer elements with a 0.5 in. spacing in the radial direction. The elements become coarser laterally and vertically away from the load center. The mesh in the vertical direction is designed to match typical pavement layer thicknesses. A stiff layer with a modulus of 4000 ksi was located at the bottom of the subgrade. These combinations result in a finite element mesh of about 2,500 nodes and 2,200 elements for a typical flexible pavement structure.

The nodal points at the bottom boundary are fixed whereas those on the right boundary are constrained from moving in the radial direction. The nodal points on the centerline are designed to move only vertically because of the axisymmetric nature of the problem.

The program output consists of radial and axial displacements at each of the nodal points and the state of stress and strain at the centroid of each element. Quadrilateral stresses are calculated as the average value of the stresses at the four nodal points.

In the finite element analysis, a pavement structure was divided into four groups: surface layer, base layer, subgrade layer, and stiff layer. Although the behavior of asphalt concrete is time and temperature dependent, it is assumed to be an elastic material for this study. To account for the nonlinear behavior of the base and subgrade materials, Uzan's universal soil model is incorporated into the program using the following equation:

$$M_r = K_1 P_a \left(\frac{\theta}{P_a} \right)^{K_2} \left(\frac{\sigma_d}{P_a} \right)^{K_3} \tag{A.1}$$

where

θ = the sum of the principal stresses,

σ_d = the applied deviator stress,

P_a = atmosphere pressure, and

K_1, K_2, K_3 = regression constants.

Uzan's model is expressed in terms of both deviator and bulk stresses and, therefore, accounts for the effect of shear stress on the resilient modulus. For static analysis, an iterative procedure is used to calculate the stress-dependent modulus in each element of the unbound layers. Convergence is dependent on the difference between the new and old moduli values. A 2% of difference between the new and old modulus in each step is acceptable as a convergence criterion. To simulate the state of stress in the field more accurately, the initial geostatic stress is calculated for each element in the unbound material layers using the typical unit weight of these materials. The values of

unit weight used in this program are 145 lbf/ft^3 for granular materials, and 125 lbf/ft^3 for fine-grained soils.

A.2 Dynamic Finite Element Model

The dynamic nature of the FWD test is one of the most important factors affecting the pavement responses. Due to the inertia effect on a pavement system, the responses computed using the static finite element method are different from those measured from FWD testing. Mamlouk (1987) presented a computer program capable of considering the inertia effect and also indicated that this effect is most significant when a shallow stiff layer or frozen subgrade is encountered.

The equilibrium equation for the linear dynamic response of finite elements is as follows:

$$M\ddot{U} + C\dot{U} + KU = R \qquad \text{(A.2)}$$

where

M, C, and K = the mass, damping, and stiffness matrices;

U, $\dot{U}$ and $\ddot{U}$ = the displacement, velocity, and acceleration; and,

R = the external load.

To investigate the dynamic responses of a pavement structure to dynamic loading, the dynamic equilibrium equation is solved using the explicit integration scheme in which the displacement at time t+Δt is directly solved in terms of previous displacement and the dynamic equilibrium condition established at time t. As an explicit integration scheme, the central difference method was implemented in this program based on the following assumptions:

$$\ddot{U}^t = \frac{1}{\Delta t^2}\left(U^{t-\Delta t} - 2U^t + U^{t+\Delta t}\right) \tag{A.3}$$

$$\dot{U}^t = \frac{1}{2\Delta t}\left(U^{t+\Delta t} - U^{t-\Delta t}\right) \tag{A.4}$$

Substituting Equations A.3 and A.4 into A.2, one can obtain:

$$(\frac{1}{\Delta t^2}M + \frac{1}{2\Delta t}C)U^{t+\Delta t} = R^t - (K - \frac{2}{\Delta t^2}M)U^t - (\frac{1}{\Delta t^2}M - \frac{1}{2\Delta t}C)U^{t-\Delta t} \tag{A.5}$$

From this equation, one can solve for displacement at $t+\Delta t$. The following summarizes the time integration scheme using the central difference method (Bathe, 1982).

A. Initial calculations:

1. Form stiffness matrix, mass matrix, and damping matrix.
2. Initialize U^0, $\dot{U}^0$, and $\ddot{U}^0$.
3. Select time step Δt.
4. Calculate integration constants:

$$a_0 = \frac{1}{\Delta t^2}; \qquad a_1 = \frac{1}{2\Delta t}; \qquad a_2 = 2a_0; \qquad a_3 = \frac{1}{a_2}$$

5. Calculate $U^{-\Delta t} = U^0 - \Delta t\dot{U}^0 + a_3\ddot{U}^0$.
6. Form effective mass matrix $\hat{M} = a_0 M + a_1 C$.

B. For each time step:

1. Calculate effective loads at time t:

$$\hat{R}^t = R^t - (K - a_2 M)U^t - (a_0 M - a_1 C)U^{t-\Delta t}$$

2. Solve for displacements at time $t+\Delta t$:

$$\hat{M}U^{t+\Delta t} = \hat{R}^t$$

3. Evaluate accelerations and velocities at time t:

$$\ddot{U}^t = a_0\left(U^{t-\Delta t} - 2U^t + U^{t+\Delta t}\right)$$

$$\dot{U}^t = a_1\left(U^{t+\Delta t} - U^{t-\Delta t}\right)$$

An important consideration in using the central difference method is that it requires a small time step to ensure stability of the solution. The critical time step is expressed as:

$$\Delta t_{cr} = \frac{T_{\min}}{\pi} \qquad \text{(A.6)}$$

where

T_{min} = the smallest natural period of the system.

Material damping of 2%, 0.9%, and 3% obtained from dynamic laboratory tests are used for the AC layer, base course, and subgrade, respectively (Chang, 1991).

A.3 Verification of the Finite Element Model

For the static loading problem, the developed finite element program, NCPAVE, is verified by comparing the responses obtained from the finite element program for pavement analysis using ABAQUS (Kim et. al, 2000) and ILLIPAVE (Thompson, 1981). ILLIPAVE is a static finite element program for plane strain analysis of elastic solids with stress-dependent material properties. The verification study was conducted in two phases, the first phase with linear elastic material models for all the layers and the second with the nonlinear elastic model for the base and subgrade layers. Table A.1 presents layer thicknesses and material properties of the pavement structure used for verification purposes.

Table A.1. Layer Thicknesses and Material Properties for the Linear Elastic Analysis

Layer	Thickness (in)	Modulus (ksi)	Poisson's ratio
Surface	6	300.0725	0.35
Base	8	20.0145	0.4
Subgrade	100	5/10/15	0.45

The first case predicts the pavement responses under a 9 kip static load in two- and three-layer flexible pavements with linear elastic material properties. The surface deflections at seven sensors calculated using the NCPAVE and ABAQUS programs are shown in Figures A.1 and A.2. Comparisons indicate a difference of less than 1% between the results of the two programs. Regardless of the number of layers, layer thicknesses, and stiffness characteristics of pavement materials, surface deflections calculated using NCPAVE are in good agreement with those computed from ABAQUS in a linear elastic case.

In the second case, it is assumed that the moduli of granular base and cohesive subgrade materials are stress-dependent. Since there is no standard finite element program incorporating the universal soil model, a decision was made to compare the predictions with the ILLIPAVE program using the K-θ model. It is noted that the universal soil model reduces to the K-θ model, assuming that K_3 (the exponent of the σ_d term) is zero. Reasonable material coefficients were assumed for each layer on the basis of the Rada and Witczak study (1981). Table A.2 shows the coefficients of the K-θ model used for base and subgrade materials in this study.

Table A.2. The Coefficient of K-θ Model for the Nonlinear Elastic Analysis

Layer	K_1 (psi)	K_2
Base	7250	0.45
Subgrade	4500	0.53

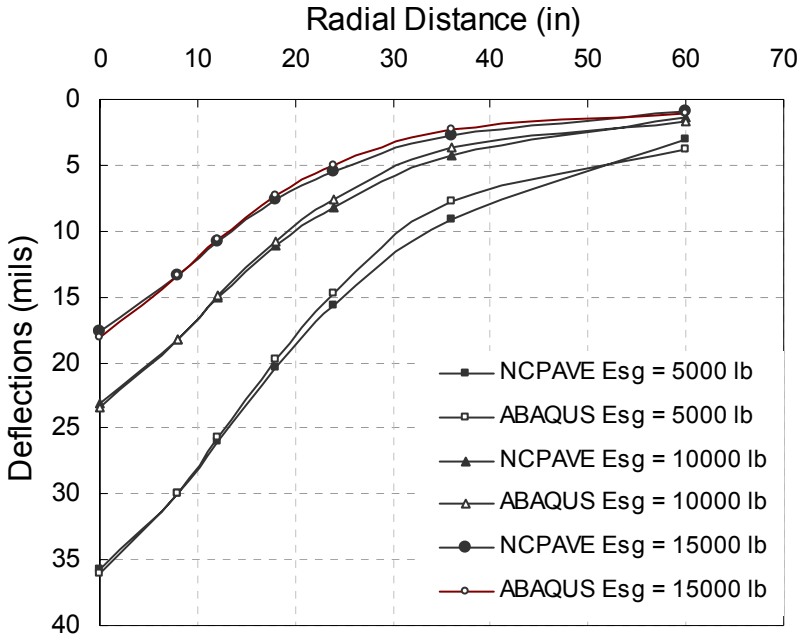

Figure A.1. Surface deflections in a two-layer pavement system.

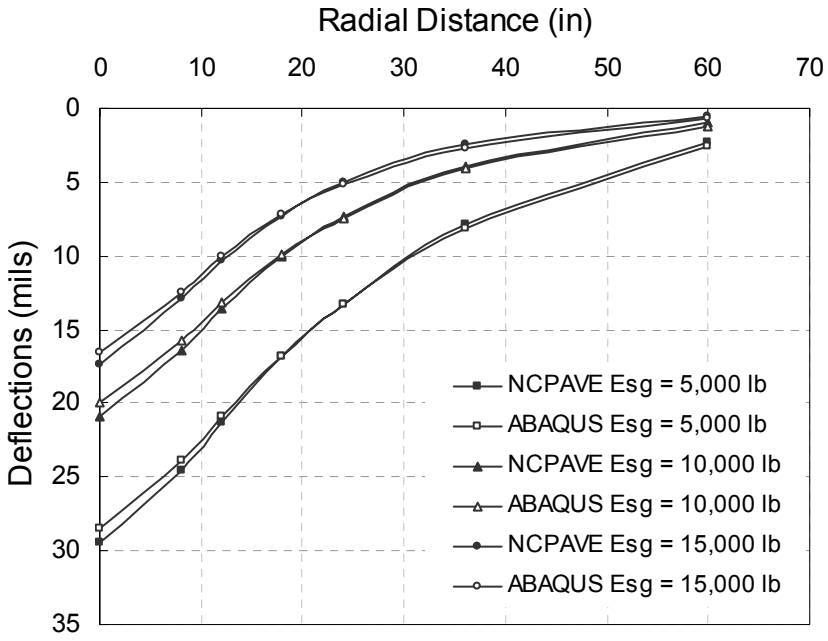

Figure A.2. Surface deflections in a three-layer pavement system.

This nonlinear analysis requires the stress-dependent moduli to be updated using the following iterative method. In the first step of iteration, initial stresses are calculated using the seed modulus assigned. The resilient modulus of each element is then calculated using the K-θ model. Another run is performed using the average value of the new and old resilient moduli, resulting in new stress values. The iteration continues until the moduli of both the base and subgrade elements converge to 2% of tolerance. Generally, a reasonable degree of convergence can be obtained after five or six iterations when the K-θ model is used.

The comparisons of pavement responses calculated using NCPAVE and ILLIPAVE are presented in Figures A.3 to A.6. Figure A.3 shows a comparison of surface deflections at the seven sensor locations. A slight difference can be observed between the two basins in this figure. There are several possibilities for the reasons that different results may occur in the nonlinear analysis:

1. The mesh size and element shape for the pavement structure has some effect on the results obtained.
2. The difference in the convergence criterion for the nonlinear analysis could yield different results.

As shown in Figure A.4, the variations of vertical stresses with depth are quite close between NCPAVE and ILLIPAVE. A slight difference can be observed in horizontal stresses (Figure A.5). About 0.14 psi of difference in horizontal stresses is negligible in the finite element method. All of the pavement responses calculated from NCPAVE appear to be in good agreement with those computed from ILLIPAVE. The values of modulus at the final iteration step are shown in Figure A.6.

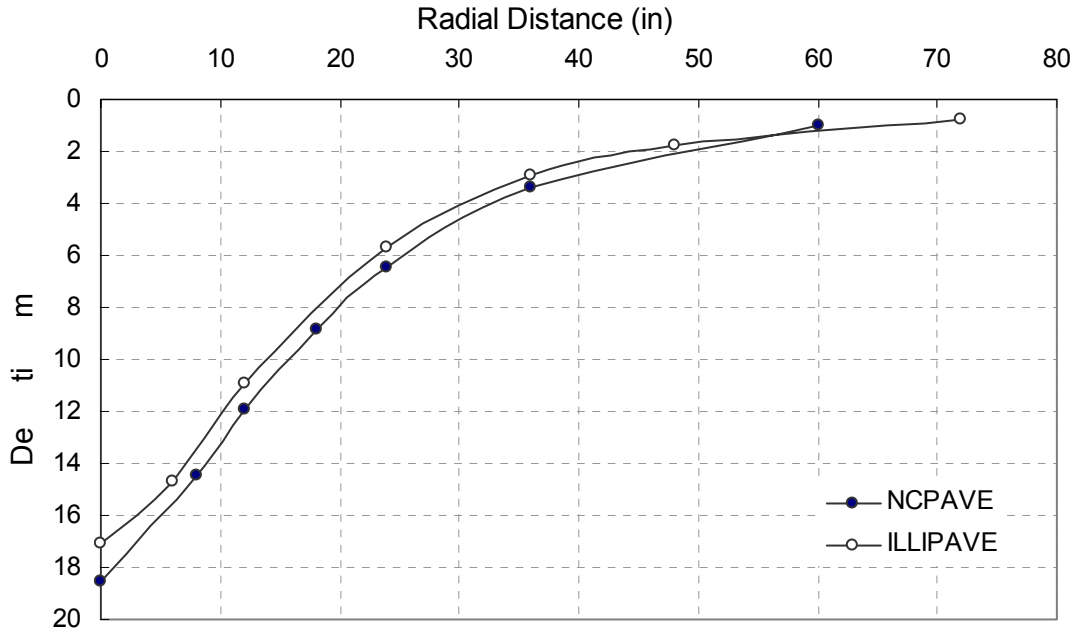

Figure A.3. Surface deflections in the nonlinear analysis.

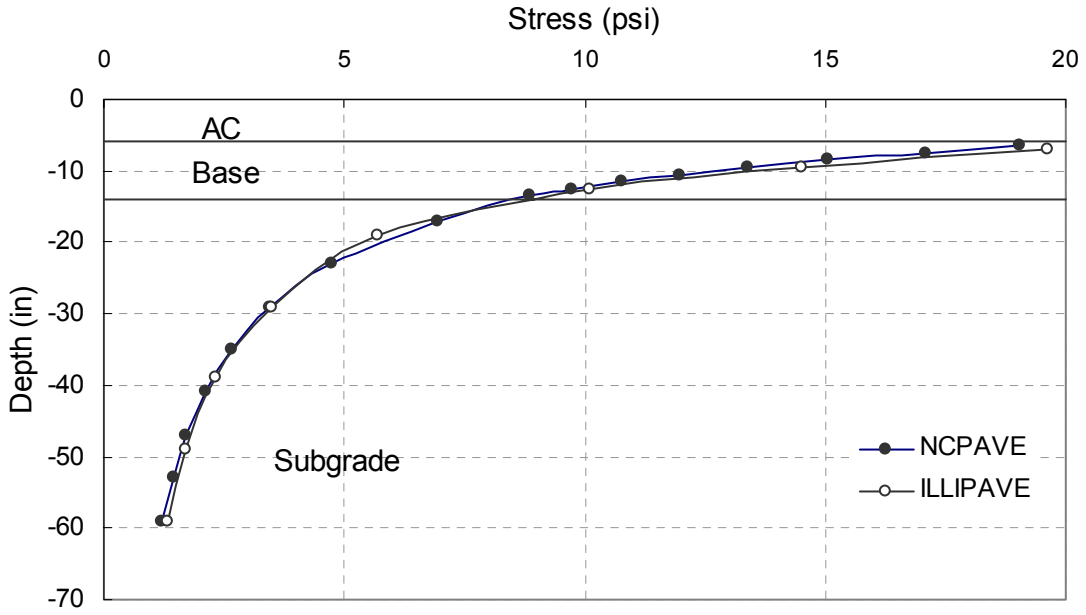

Figure A.4. Variations of vertical stress.

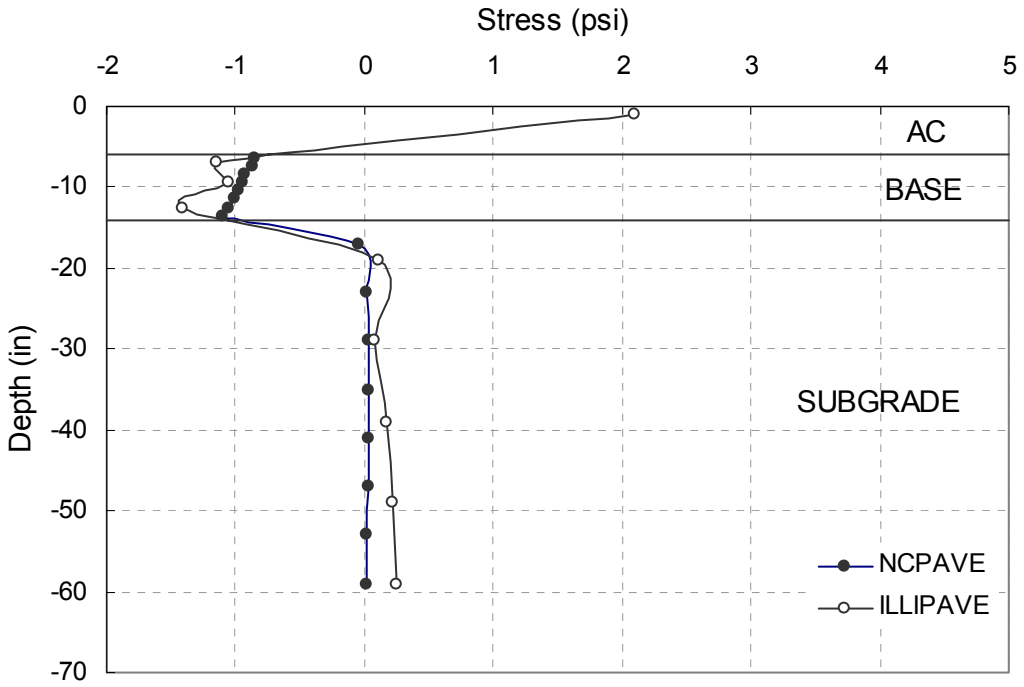

Figure A.5. Variations of horizontal stress.

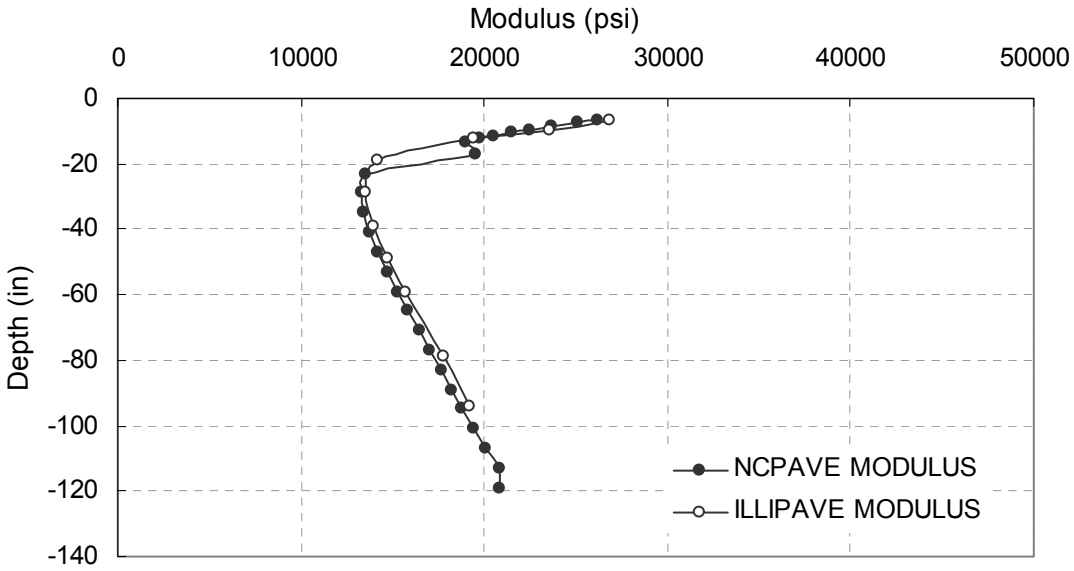

Figure A.6. Stress-dependent modulus distribution.

To verify the dynamic finite element program, 2×2 and 100×100 mesh-size specimens with 4-node axisymmetric isoparametric elements were estimated under a uniformly distributed load. The specimen geometry and the boundary conditions are shown in Figure A.7. All the materials were considered to be linear elastic. An impact load with a duration of 0.03 sec and peak pressure of 81 psi was applied to the top of the specimen. The time step used here is 10^{-6} sec. The shape of the impact load with time in this program is similar to that of a FWD test. In the case of the 2×2 mesh-size specimen, vertical displacements were recorded at the center location and compared with those obtained from ABAQUS (Figure A.8). Comparisons indicate excellent agreement in displacements between the two programs. Figure A.9 shows the displacement-time histories at different locations in the 100×100 mesh-size specimen. In order to investigate the dynamic response on a pavement structure, it was modeled as a three-layer linear elastic system. Layer thicknesses and material properties for each layer in the analysis are provided in Table A.3. The displacement-time histories for a pavement structure are shown in Figure A.10. Considering the maximum displacement within time duration to be an actual displacement, the deflection basin is plotted in Figure A.11.

Table A.3. Layer Thicknesses and Material Properties Used in Dynamic Finite Element Analysis

Pavement Layer	Thickness (in)	Modulus (ksi)	ν	γ (lb/ft^3)
Asphalt Concrete	1	500	0.35	135
Aggregate Base	2	25	0.4	125
Subgrade	100	15	0.45	110

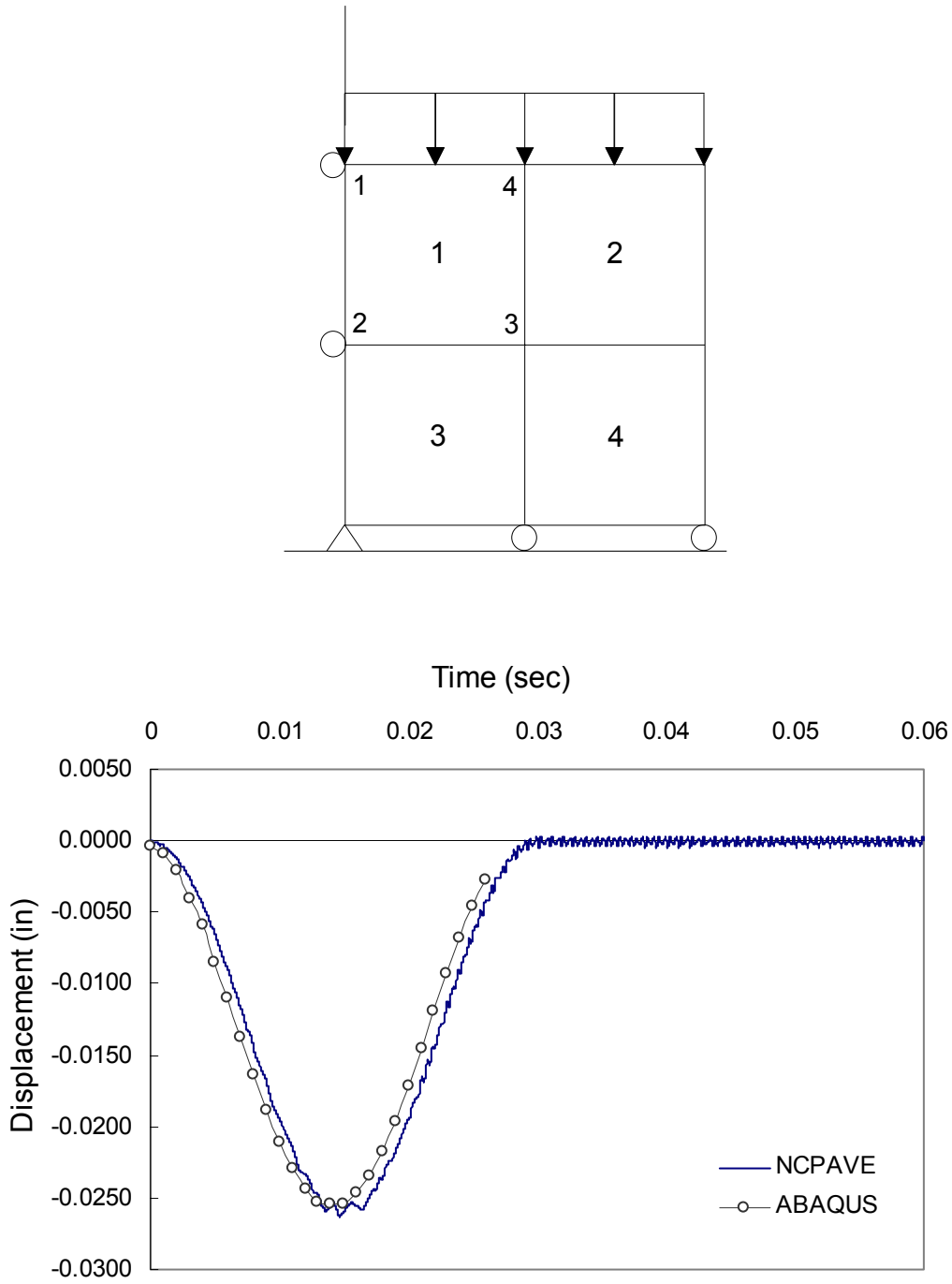

Figure A.8. Comparison of displacement-time histories obtained from NCPAVE and ABAQUS (2x2 mesh).

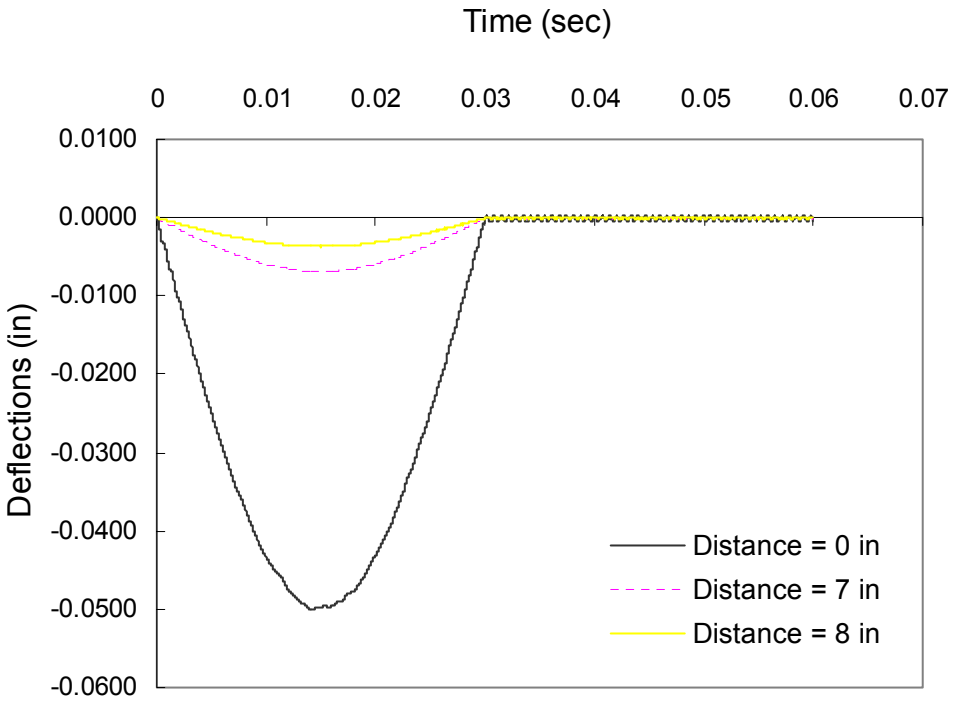

Figure A.9. Displacement-time histories in 100x100 mesh size specimen.

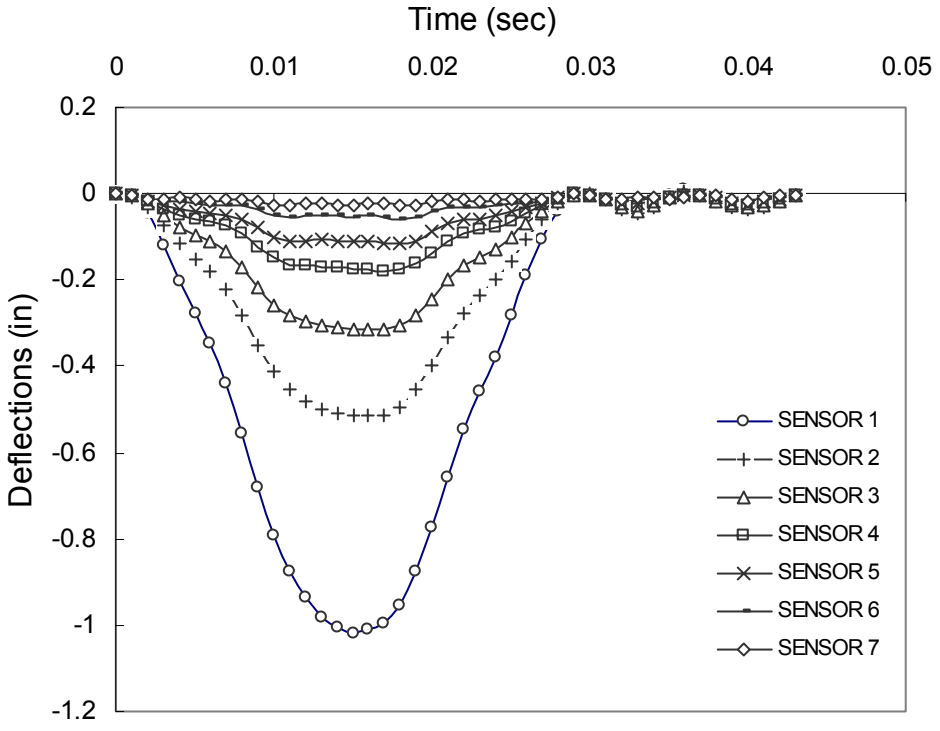

Figure A.10. Displacement - time histories of a pavement structure under FWD loading.

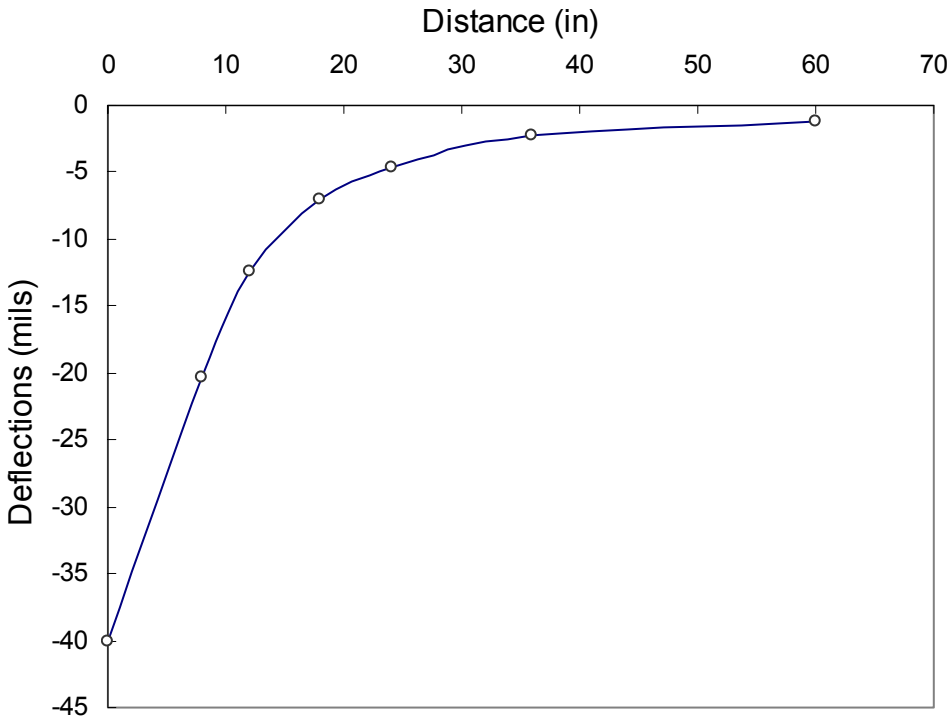

Figure A.11. Computed deflection basin.

APPENDIX B

EQUATIONS IN METRIC UNIT

$$\varepsilon_{ac} = \frac{H_{ac}}{2R} \tag{2.1.a}$$

$$R = \frac{-a}{2(D_0 - D_{edge})} \tag{2.1.b}$$

$$AUPP = \frac{1}{2}(5D_0 - 2D_1 - 2D_2 - D_3) \tag{2.2}$$

$$\log(\varepsilon_{ac}) = 1.024 \log(AUPP) + 2.625 \tag{2.3}$$

$$\log(\varepsilon_{ac}) = 0.821 \log(AUPP) + 2.583 \tag{2.4}$$

$$SSR = \frac{\sigma_{dsg}}{q_u} \tag{2.5}$$

$$\log(SSR) = 1.671 \log(D_0) - 2.876 \tag{2.6}$$

$$\log(\varepsilon_{ac}) = 1.078 \log(BDI) + 0.184 \log(H_{ac}) + 2.974 \tag{2.7.a}$$

$$\log(d\varepsilon_{ac}) = 1.086 \log(DBDI) + 0.238 \log(H_{ac}) + 2.860 \tag{2.7.b}$$

$$\log(\varepsilon_{ac}) = 1.082 \log(BDI) + 0.259 \log(H_{ac}) + 2.772 \tag{2.8.a}$$

$$\log(d\varepsilon_{ac}) = 1.089 \log(\mathrm{D}BDI) + 0.326 \log(H_{ac}) + 2.633 \tag{2.8.b}$$

$$\log(\varepsilon_{ac}) = 1.075 \log (AUPP) + 2.625 \tag{2.9}$$

$$\log(\varepsilon_{ac}) = 1.035 \log (AUPP) + 2.583 \tag{2.10}$$

$$\log(\varepsilon_{cac}) = 1.076 \log(SCI) + 1.122 \log(H_{ac}) + 0.315 \tag{2.11}$$

$$\log(\varepsilon_{abc}) = 0.938 \log(BDI) - 0.079 \log(H_{ac}) + 0.045 \log(H_{base}) + 3.826 \tag{2.12.a}$$

$$\log(d\varepsilon_{abc}) = 0.918 \log(DBDI) + 0.007 \log(H_{ac}) + 0.071 \log(H_{base}) + 3.386 \tag{2.12.b}$$

$$\log(\varepsilon_{sg}) = 0.999 \log(BDI) + 0.063 \log(H_{ac}) + 3.585 \tag{2.13.a}$$

$$\log(d\varepsilon_{sg}) = 1.000 \log(DBDI) + 0.103 \log(H_{ac}) + 3.668 \quad (2.13.b)$$

$$\log(\varepsilon_{sg}) = 1.017 \log(BCI) - 0.042 \log(H_{ac}) - 0.494 \log(H_{base}) + 5.072 \quad (2.14.a)$$

$$\log(d\varepsilon_{sg}) = 1.023 \log(DBCI) - 0.045 \log(H_{ac}) - 0.445 \log(H_{base}) + 4.928 \quad (2.14.b)$$

$$D_{eff} = 4.75\, H_{ac} - 413 \quad (3.1)$$

$$\lambda_w = \frac{w_{T_0}}{w_T} \quad (3.2)$$

$$\log w = b + nT \quad (3.3)$$

$$w = 10^{b+nT} \quad (3.4)$$

$$\lambda_w = 10^{-n(T-T_0)} \quad (3.5)$$

$$\lambda_w = 10^{-C(H_{ac})(T-T_0)} \quad (3.6)$$

$$C = -Ar + C_0 \quad (3.7)$$

$$\log(BDI) = -1.864 \log(H_{ac}) - 0.710 \log(E_{ac}) + 0.045 \log(E_{ri}) + 5.711 \quad (4.1)$$

$$\log(DBDI) = -1.910 \log(H_{ac}) - 0.724 \log(E_{ac}) + 0.040 \log(E_{ri}) + 5.727 \quad (4.2)$$

$$\log(\varepsilon_{sg}) = -1.782 \log(H_{ac}) - 0.750 \log(E_{ac}) + 0.035 \log(E_{ri}) + 9.411 \quad (4.3)$$

$$\log(d\varepsilon_{sg}) = -1.812 \log(H_{ac}) - 0.766 \log(E_{ac}) + 0.028 \log(E_{ri}) + 9.399 \quad (4.4)$$

$$Adjusted \quad BDI = \frac{Estimated \quad BDI}{\beta_1} \quad (4.5)$$

$$\beta_1 = \frac{BDI_m}{BDI_r} \quad (4.6)$$

$$\log(E_{ac}) = -1.059 \log(SCI) - 1.009 \log(H_{ac}) + 4.741 \quad (4.7)$$

$$\log(CBR) = 2.6 - 1.07 \log(PD) \quad (4.8)$$

$$\log(E_{ac}) = -1.183 \log(H_{ac}) - 1.103 \log(SCI) + 5.096 \quad (4.9)$$

$$\log(BDI) = -1.549 \log(H_{ac}) - 0.095 \log(H_{base}) - 0.572 \log(E_{ac}) - 0.013 \log(E_{ri}) + 4.702 \quad (4.10)$$

$$\log(DBDI) = -1.476 \log(H_{ac}) - 0.112 \log(H_{base}) - 0.559 \log(E_{ac}) - 0.018 \log(E_{ri}) + 4.352 \quad (4.11)$$

$$\log(\varepsilon_{abc}) = -1.583 \log(H_{ac}) + 0.001 \log(H_{base}) - 0.591 \log(E_{ac}) + 0.146 \log(E_{ri}) + 8.064 \quad (4.12)$$

$$\log(d\varepsilon_{abc}) = -1.362 \log(H_{ac}) + 0.010 \log(H_{base}) - 0.536 \log(E_{ac}) + 0.145 \log(E_{ri}) + 7.074 \quad (4.13)$$

$$\log(BCI) = -1.280 \log(H_{ac}) - 0.150 \log(H_{base}) - 0.406 \log(E_{ac}) - 0.167 \log(E_{ri}) + 3.778 \quad (4.14)$$

$$\log(DBCI) = -1.254 \log(H_{ac}) - 0.162 \log(H_{base}) - 0.413 \log(E_{ac}) - 0.194 \log(E_{ri}) + 3.665 \quad (4.15)$$

$$\log(\varepsilon_{sg}) = -1.330 \log(H_{ac}) - 0.571 \log(H_{base}) - 0.446 \log(E_{ac}) - 0.474 \log(E_{ri}) + 9.348 \quad (4.16)$$

$$\log(d\varepsilon_{sg}) = -1.316 \log(H_{ac}) - 0.551 \log(H_{base}) - 0.454 \log(E_{ac}) - 0.495 \log(E_{ri}) + 9.197 \quad (4.17)$$

$$N_f = K\left(\frac{1}{\varepsilon_t}\right)^c \quad (5.1)$$

$$N_f = 0.0796\varepsilon_t^{-3.291}\left|E^*\right|^{-0.854} \quad (5.2)$$

$$N_f = 1.365 \times 10^{-9}(\varepsilon_c)^{-4.477} \quad (5.3)$$

$$\varepsilon_p(N) = \mu\varepsilon_r N^{-\alpha} \quad (5.4)$$

$$\varepsilon_p = \int_0^N \varepsilon_p(N)dN = \varepsilon_r \mu \frac{N^{1-\alpha}}{1-\alpha} \tag{5.5}$$

$$\frac{\partial \varepsilon_p}{\partial N} = \varepsilon_r \mu N^{-\alpha} \tag{5.6}$$

$$F(N) = \frac{\Delta \varepsilon_p}{\varepsilon_r + \Delta \varepsilon_p} \frac{1}{\partial N} = \frac{\Delta \varepsilon_p}{\varepsilon_r} \frac{1}{\partial N} = \mu N^{-\alpha} \tag{5.7}$$

$$RD(N) = \int_0^N \int_0^z \varepsilon_c(z) F(N) dz dN \tag{5.8}$$

$$RD(N) = \sum_{i=1}^{n} \left[\int_0^N \mu_i N^{-\alpha_i} dN \int_{d_{i-1}}^{d_i} \varepsilon_c(z) dz \right] = \sum_{i=1}^{n} \left[\frac{\mu_i N^{1-\alpha_i}}{1-\alpha_i} \int_{d_{i-1}}^{d_i} \varepsilon_c(z) dz \right] \tag{5.9}$$

$$\varepsilon_p = \varepsilon_0 e^{-(\rho/N)\beta} \tag{5.10}$$

$$RD(N) = \sum_{i=1}^{n} \left\{ \left(\frac{\varepsilon_{0_i}}{\varepsilon_{r_i}} \right) e^{-\left(\frac{\rho_i}{N}\right)^{\beta_i}} \int_{d_{i-1}}^{d_i} \varepsilon_c(z) dz \right\} \tag{5.11}$$

$$S = \sum_{i=1}^{n} S_i \tag{5.12}$$

$$S_i = \frac{N_i}{N_{f,i}} \tag{5.13}$$

$$S = \sum_{i=1}^{n} \frac{N_i}{N_{f,i}} \tag{5.14}$$

$$DF_i = \frac{1}{N_{f,i}} \tag{5.15}$$

$$S = \sum_{i=1}^{n} (P_i \times DF_i) \times Y \tag{5.16}$$

$$S = \sum_{i=1}^{n} \sum_{j=1}^{m} \left(P_{i,j} \times DF_{i,j} \right) \times Y \tag{5.17}$$

$$\log\left(\frac{W_x^t}{W_s^t}\right) = 4.79\log(S+1) - 4.79\log(L_x + L_2) + 4.33\log L_2 + \frac{G_t}{\beta_x} - \frac{G_t}{\beta_{18}} \tag{5.18}$$

$$G_t = \log\left(\frac{4.2 - p_t}{4.2 - 1.5}\right) \tag{5.19}$$

$$\beta_x = 0.40 + \frac{0.081\left(L_x + L_2\right)^{3.23}}{\left(SN+1\right)^{5.19} L_2^{3.23}} \tag{5.20}$$

$$EALF = \frac{W_s^t}{W_x^t} \tag{5.21}$$

$$ESAL = (\sum_{i=1}^{m} N_i F_i)(G)(D)(L)(Y) \tag{5.22}$$

$$\log(E_{ac}) = \text{-}1.183\ \log(H_{ac}) - 1.103\ \log(SCI) + 5.096 \tag{5.23}$$

$$N_f = 0.0796\varepsilon_t^{-3.291}\left|E^*\right|^{-0.854}\left(P\right)^{-0.3} \tag{5.24}$$

APPENDIX C

PROGRAM GUIDE FOR APLCAP VERSION 2.0

INTRODUCTION

This manual provides an overview of the computer program that implements the condition evaluation procedures using 9000 lb FWD deflections described in the NCHRP 10-48 final report and the condition evaluation and remaining life prediction procedures using multi-load FWD deflections described in the main body of this final report. This software package is called APLCAP 2.0, which stands for Asphalt Pavement Layer Condition Assessment Program Version 2.0.

The prototype is implemented using MS Visual Basic (6.0) for MS Windows-based computing platforms. It is styled and structured similar to typical Windows-based applications. The compiled version of the executable binary file is designed to run as a stand-alone program on computers running MS Windows, and does not require the use of any proprietary software packages.

APLCAP should be viewed as a functional *prototype* of a software package that represents the key functions and features. Although some debugging, validation, and testing have been performed, like typical prototypes, it has not been subjected to rigorous QA/QC that is required of commercial quality software packages. Similarly, some help utilities to guide a user are provided, but could be improved in commercial distribution versions.

The following sections describe briefly the major components of APLCAP.

APLCAP OVERALL STRUCTURE

The program is implemented such that the user could access all the components of APLCAP via a set of menu options. The main menu items include: *File Menu, Analysis Menu, Results Display Menu,* and *Help Menu.* Each of these menu items is described below.

File Menu

This menu item includes the following options: *New File, Open File, Convert FWD File,* and *Exit.*

New File

This option allows the user to create a new condition assessment scenario by inputting new FWD data. Upon invoking this menu option, an Analysis Selection input interface (Figure C-1) is displayed, via which the user will select an option for analysis. Two options are available:

- Condition Assessment Using 9000 lb FWD Deflection Data;
- Condition Assessment Using Multi-load FWD Deflection Data.

a) Upon invoking "Condition Assessment Using 9000 lb FWD Deflection Data" menu option, a Pavement Specification A input interface (Figure C-2) is displayed, via which the user will input the following set of information.

Title – a unique name to identify the specific scenario.

Number of Test Locations – the number of locations at which the FWD data to be analyzed.

Pavement Type – select one of: Aggregate Base, Full Depth, and AC/Fractured PCC (PCC and CTB are not included in this version.)

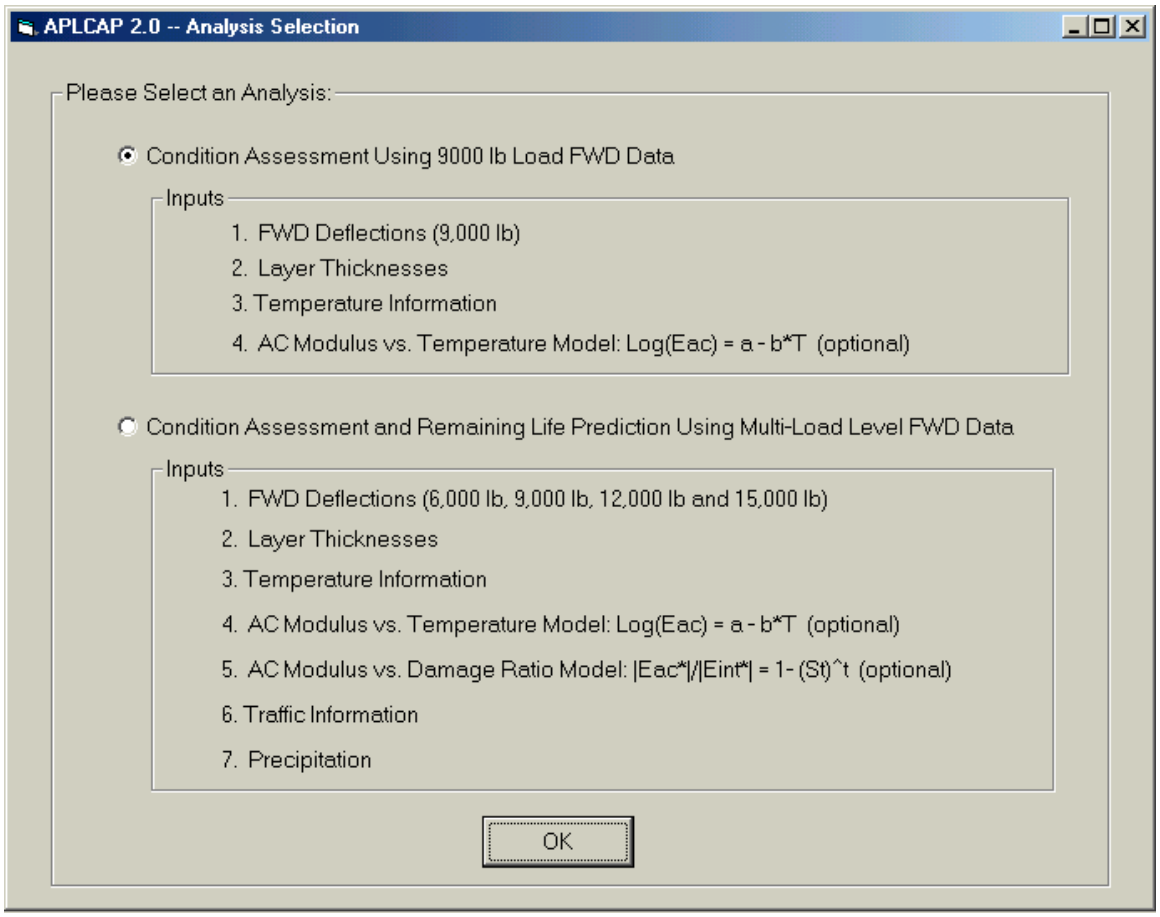

Figure C-1 Analysis Selection interface

Region – specify one of the regions (East, Central, West) in North Carolina. The corresponding values for the temperature correction constants *a* and *b* are assigned, and displayed in this interface.

Average Temperature One Day Before Test – the average (based on low and high) temperature on day of testing. (This value is used as the default value corresponding to each location, and could be modified later.)

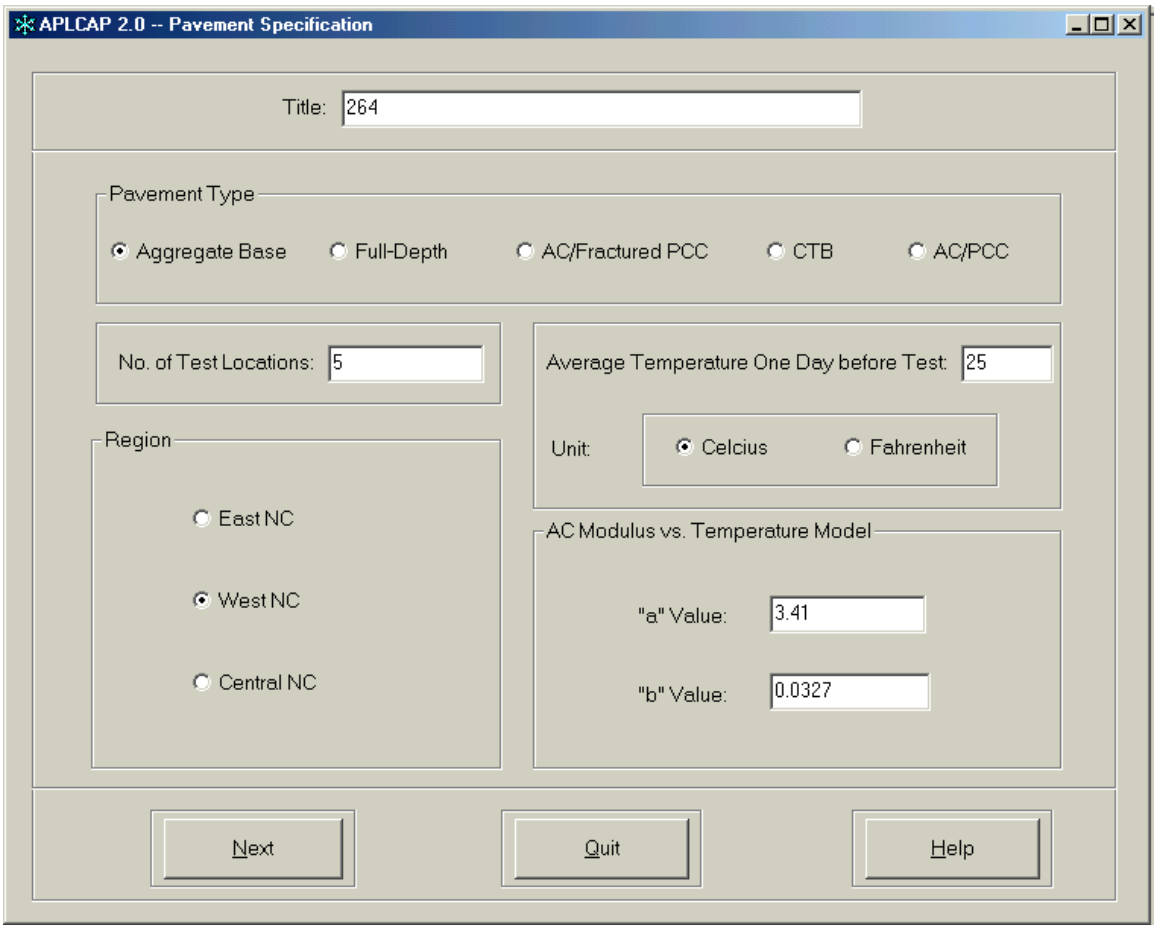

Figure C-2 Pavement Specification A interface

AC Modulus vs. Temperature Model Constants - Default values for the temperature correction constants are assigned based on the region where the FWD testing was conducted.

AC modulus vs. temperature model is expressed as:

$$\log(E_{ac}) = a - b * T \qquad (1)$$

b value is used to obtain temperature adjustment factors for various condition indicators.

The general expression of temperature adjustment factors can be written as:

$$\alpha = 10^{-f*b*(T_m - T_r)} \quad (2)$$

where *f* is the coefficient of temperature adjustment factor.

The *Next* button will invoke a series of Deflection Data Input A interfaces (Figure C-3) to input the FWD data at each location. Each interface allows the user to input the following information.

Title – a unique scenario specific name specified in the Pavement Specification A input interface is displayed.

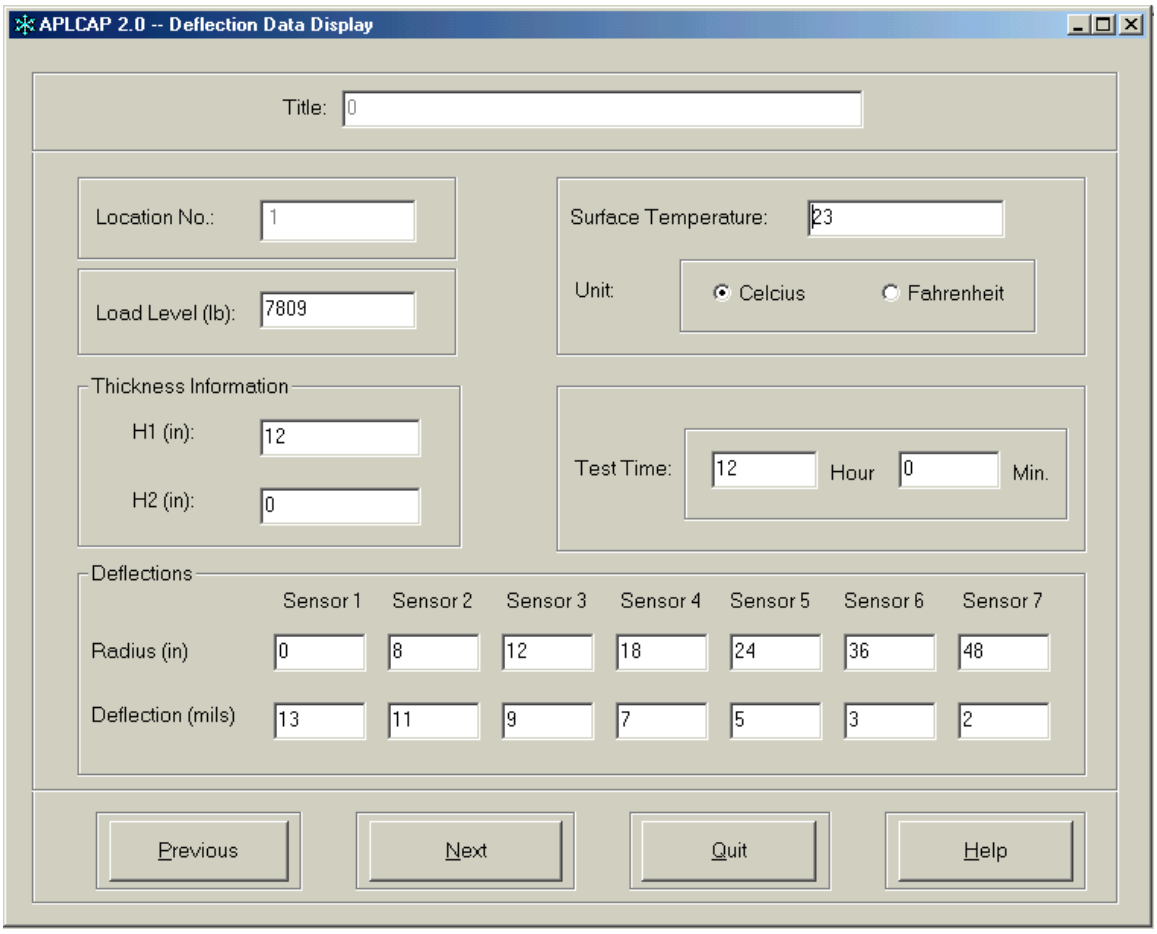

Figure C-3 Deflection Data Input A interface

Location Number – a unique number for each FWD test location. (An ascending series of numbers, starting with 1, is automatically assigned.)

Load Level – the weight used in the FWD testing. (This value is used as the default value corresponding to each location, and could be modified later.)

Thickness Information – the thickness information of pavement layer(s) corresponding to the test locations. (This is used as the default values corresponding to all other location, and could be modified later.)

Surface Temperature – the measured surface temperature at the test location.

Test Time – the time of day when the test was conducted.

FWD Measurements –

Radius (of Sensor Location) – the radial distance (in inches) from the load center to each sensor location. The sensor closest to the center must be specified first, and the farthest one last. (These spacing values are used as the default value corresponding to all other location, and could be modified later.)

Deflection – the deflection (in mils) at each sensor location.

The *Next* button invokes the Deflection Data Input A interface to input the FWD data at the next location. Once the data input for all locations is complete, the last Deflection Data Input A interface allows the user to *Save* the input information.

The Deflection Data Input A interfaces also provide the option via the *Previous* and *Next* buttons for a user to navigate through all Deflection Data Input A interfaces to view and modify the data before saving the file.

b) Upon invoking "Condition Assessment Using Multi-Load FWD Data" menu option, a Pavement Specification B input interface (Figure C-4) is displayed, via which the user

will input the following set of information.

Title – a unique name to identify the specific scenario.

Number of Test Locations – the number of locations at which the FWD data to be analyzed.

Pavement Type – select one of: Aggregate Base, Full Depth, and AC/Fractured PCC.

Region – specify one of the regions (East, Central, West) in North Carolina. The corresponding values for the temperature correction constants *a* and *b* are assigned, and displayed in this interface.

AC Mid-Depth Temperatures – Default values for average mid-depth temperature through each season at each region.

Average Temperature One Day before Test – the average (based on low and high) temperature on day of testing. (This value is used as the default value corresponding to each location, and could be modified later.)

AC Modulus vs. Temperature Model Constants - Default values for the temperature correction constants are assigned based on the region where the FWD testing was conducted.

Number of Load Applications Per Year – Annual load application values at load level 6000 lb, 9000 lb, 12000 lb, and 15000 lb. Upon clicking Calculation button, a traffic table will pop up as shown in Figure C-5. By filling in the daily traffic and clicking "Calculation" button afterwards, the annual load applications may be estimated automatically.

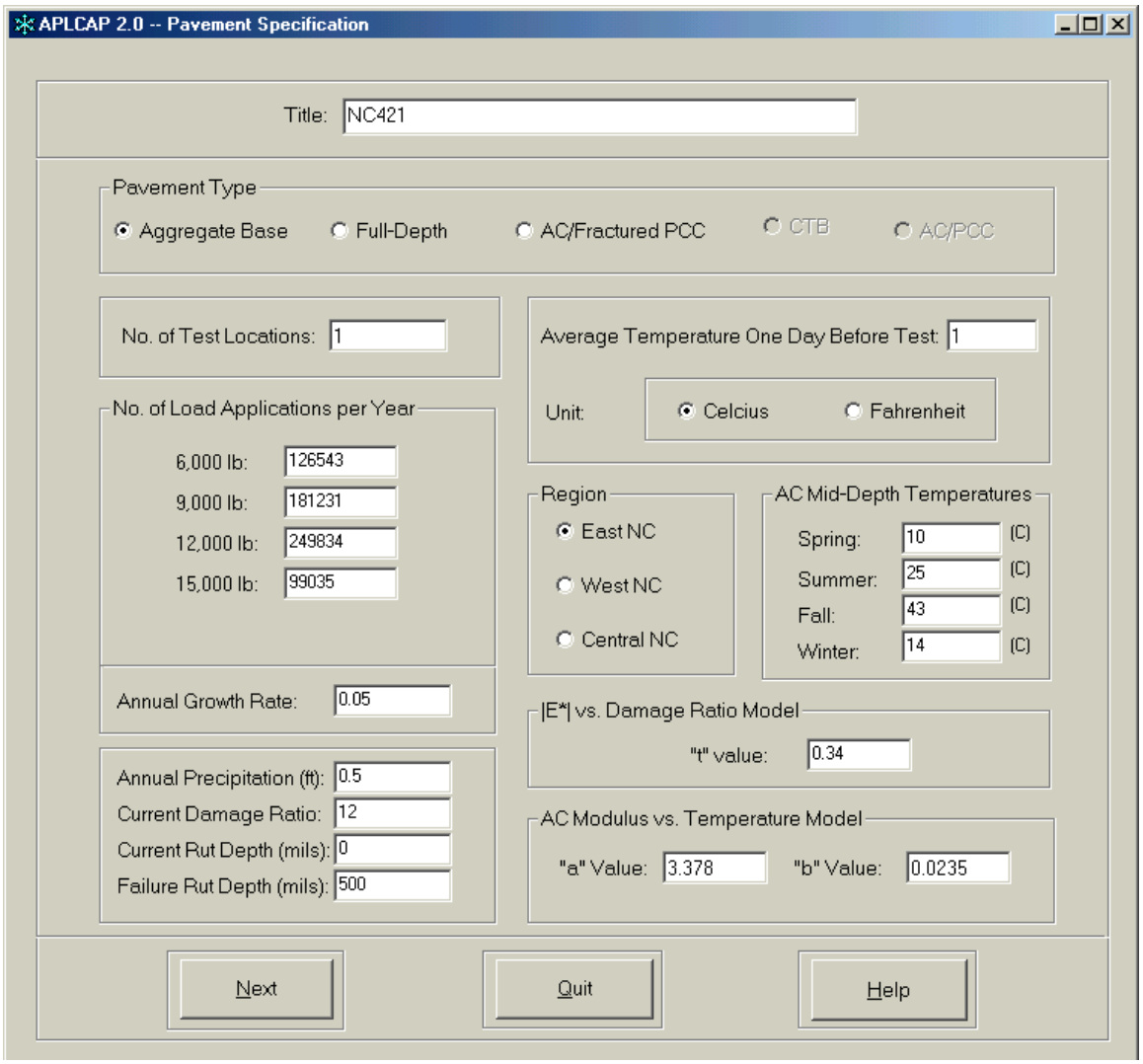

Figure C-4 Pavement Specification B interface

Annual Growth Rate – Default value for annual traffic growth rate.

Annual Precipitation – Default values for each selected *Region*.

Current Damage Ratio – Damage ratio measured before FWD test is displayed. This value can be estimated by calculating percentage of cracking area within a certain sample area.

Current Rut Depth – Value for measure rut depth before FWD test is displayed.

Failure Rut Depth – Value for which a pavement is considered as failure. Default value is 0.5 in.

|*E**| *vs. Damage Ratio Model* – AC effective dynamic modulus is a function of AC layer damage ratio. This relationship can be expressed as:

$$\frac{E^*}{E_0} = 1 - (S_t)^t \qquad (3)$$

where E* is dynamic AC modulus, E_0 is AC modulus when AC layer is intact, S_t is damage ratio, and *t* is a model constant.

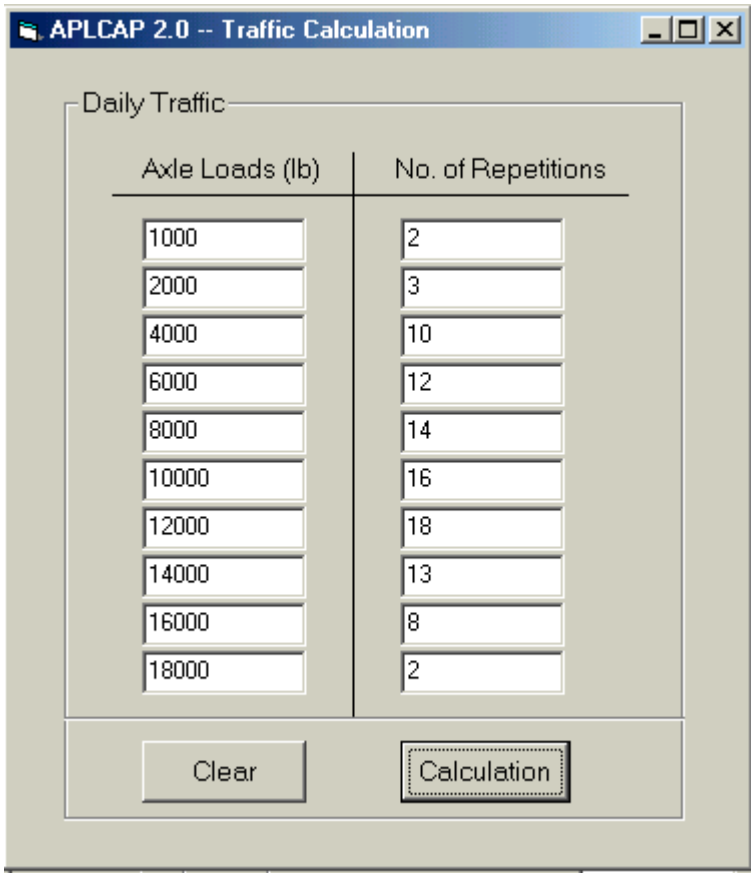

Figure C-5 Traffic Calculation interface

The *Next* button will invoke a series of Deflection Data Input B interfaces (Figure C-6) to input the FWD data at each location. Each interface allows the user to input the following information.

Title – a unique scenario specific name specified in the Pavement Specification B input interface is displayed.

Location Number – a unique number for each FWD test location. (An ascending series of numbers, starting with 1, is automatically assigned.)

No. of Locations – the total number of locations for analysis. (This value is used as the fixed value corresponding to total locations input before.)

Thickness Information – the thickness information of pavement layer(s) corresponding to the test locations. (This is used as the default values corresponding to all other location, and could be modified later.)

Surface Temperature – the measured surface temperature at the test location.

Test Time – the time of day when the test was conducted.

FWD Measurements –

Radius (of Sensor Location) – the radial distance (in inches) from the load center to each sensor location. The sensor closest to the center must be specified first, and the farthest one last. (These spacing values are used as the default value corresponding to all other location, and could be modified later.)

Load – weight used for FWD testing. Default values are 6000, 9000, 12000 and 15000 lb.

Deflection – the deflection (in mils) at each sensor location at each load level.

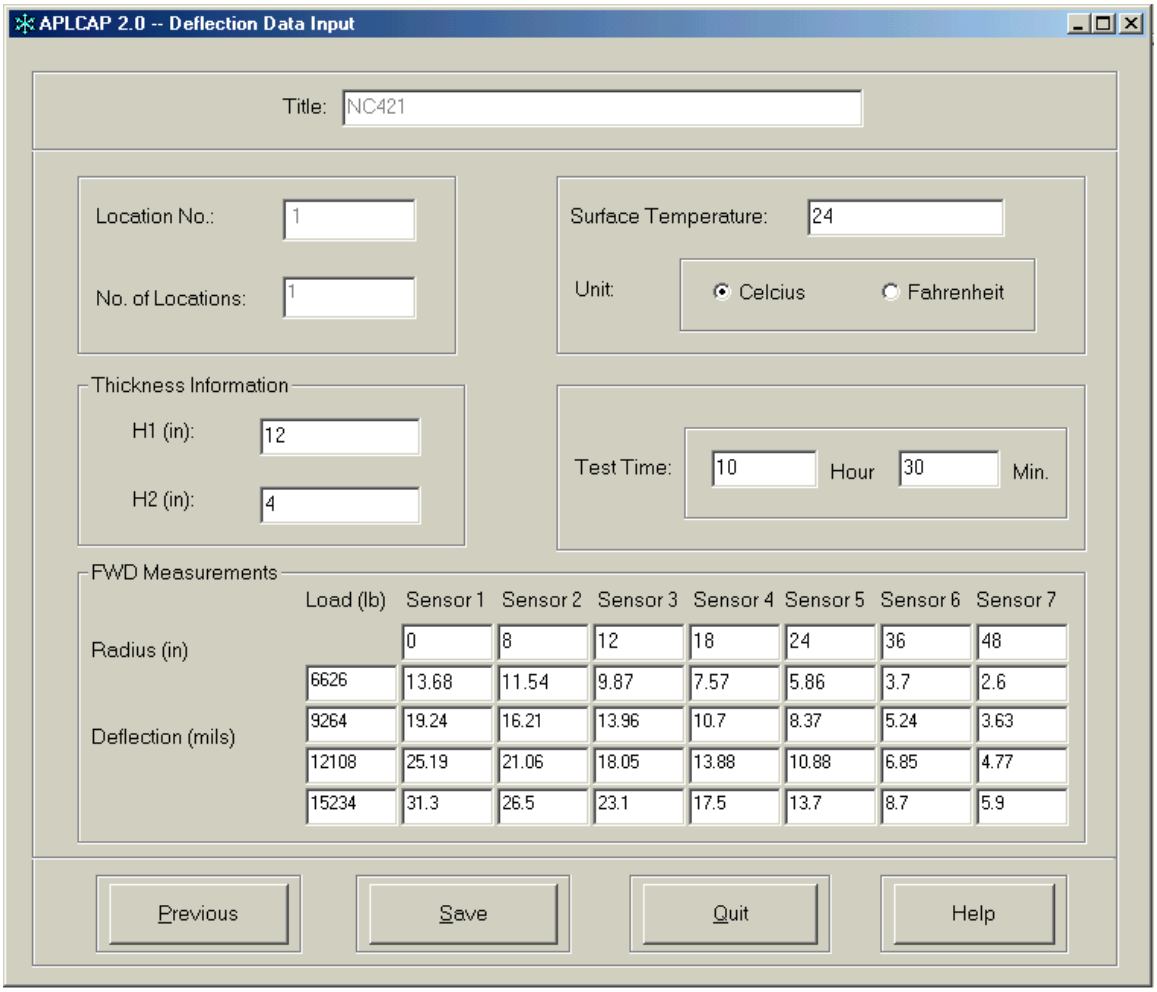

Figure C-6 Deflection Data Input B interface

The *Next* button invokes the Deflection Data Input B interface to input the FWD data at the next location. Once the data input for all locations is complete, the last Deflection Data Input B interface allows the user to *Save* the input information.

The Deflection Data Input B interfaces also provide the option via the *Previous* and *Next* buttons for a user to navigate through all Deflection Data Input B interfaces to view and modify the data before saving the file.

Open File

This option allows the user to open an already saved file from a previous session. Selecting this menu option displays a Windows File Dialog box from which the user can specify the desired file. After the file is selected, the user can view and modify the data via the input interfaces Pavement Specification and Deflection Data Input as described above in *New File* menu option.

Convert FWD File

This option enables the user to import FWD information gathered using the DYNATEST and KUAB procedure. On selection of this option, the user is prompted to specify the file containing the FWD information. Upon loading this file, the user is prompted also to input additional information (e.g., temperature, climate zone) that is needed for the condition evaluation procedures. A user specifies this information via the Pavement Specification interface and the Deflection Data Input interface.

Exit

Selecting this will close all files and the program.

Analysis Menu

This menu item includes the following options: *Screen Deflection Data* and *Analyze Deflection Data.*

Screen Deflection Data

This option allows the user to view and screen the deflection input data, to identify potentially erroneous measurement information, and to correct the data using the SLIC method.

When this menu option is selected and the analysis using 9000 lb FWD data is selected, the Deflection Data Screening A interface (Figure C-7) is displayed. This interface allows the user to select one test location at a time to view the deflection data. For each selected test location, three graphs showing the variation of deflection, surface modulus, and SLIC Method Information with sensor location are displayed. Also, an evaluation of the deflection data is provided on the top of the panel; this indicates any abnormality that may exist at any specific sensor location. The right hand side panel enables the user to select one sensor location where the deflection data may appear to be erroneous, and then apply the SLIC method. The modified deflection information is displayed before the user selects to accept or reject the modifications. If the modifications are accepted, this modified deflection information is used in all subsequent analyses.

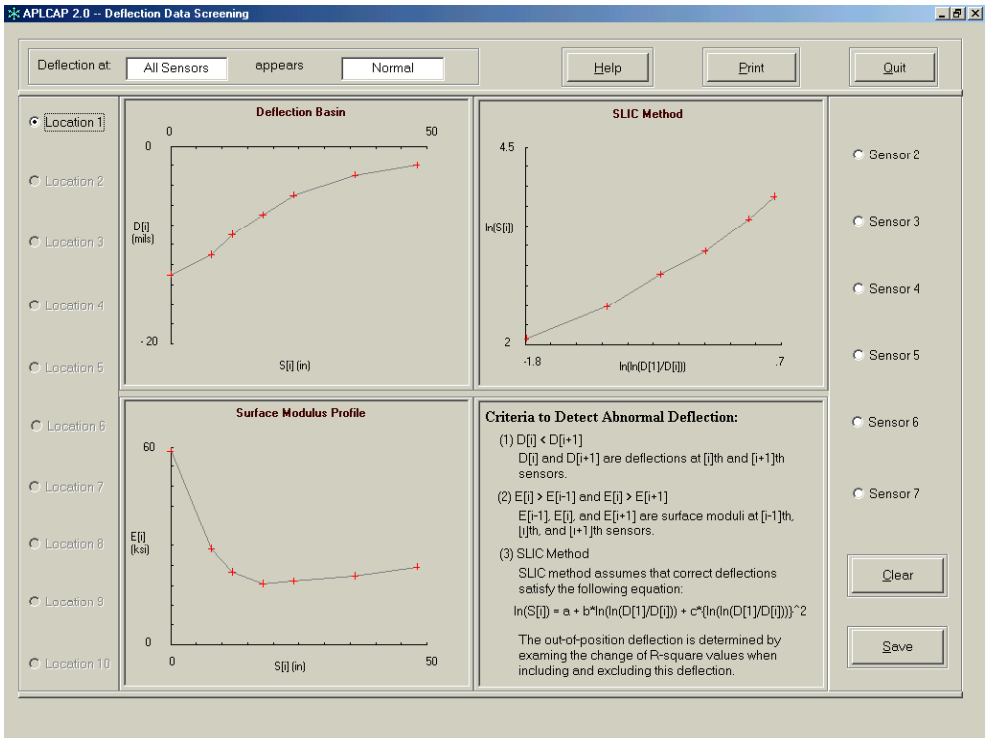

Figure C-7 Deflection Data Screening A interface

When this menu option is selected and the analysis using multi-load FWD data is selected, the Deflection Data Screening B interface (Figure C-8) is displayed. This interface allows the user to screen the deflection basin at each load level at a time.

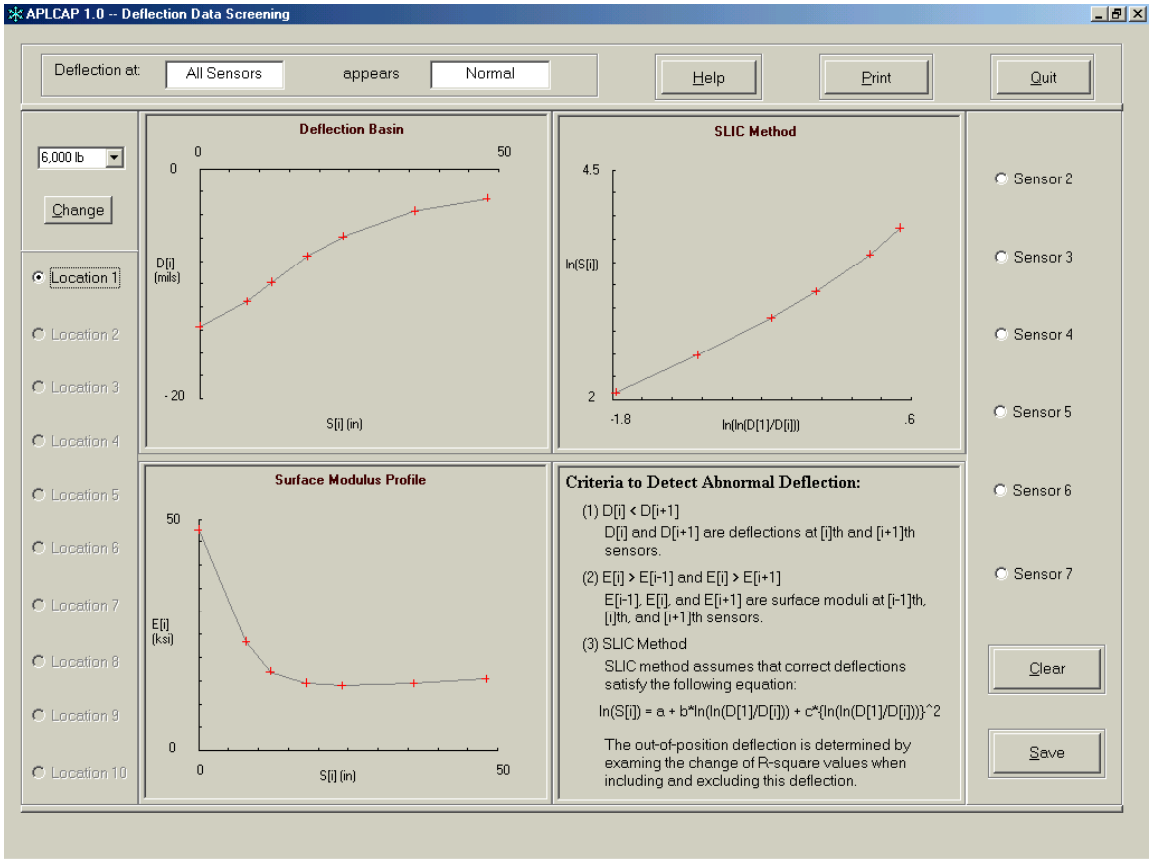

Figure C-8 Deflection Data Screening B interface

Analyze Deflection Data

Selecting this option invokes proper procedures presented in the flowcharts (Figures C-9, C-10, and C-11). An interface displayed in response to its selection shows the default output file names and the path names where they will be stored. Using the *Browse* button, the user may override these defaults.

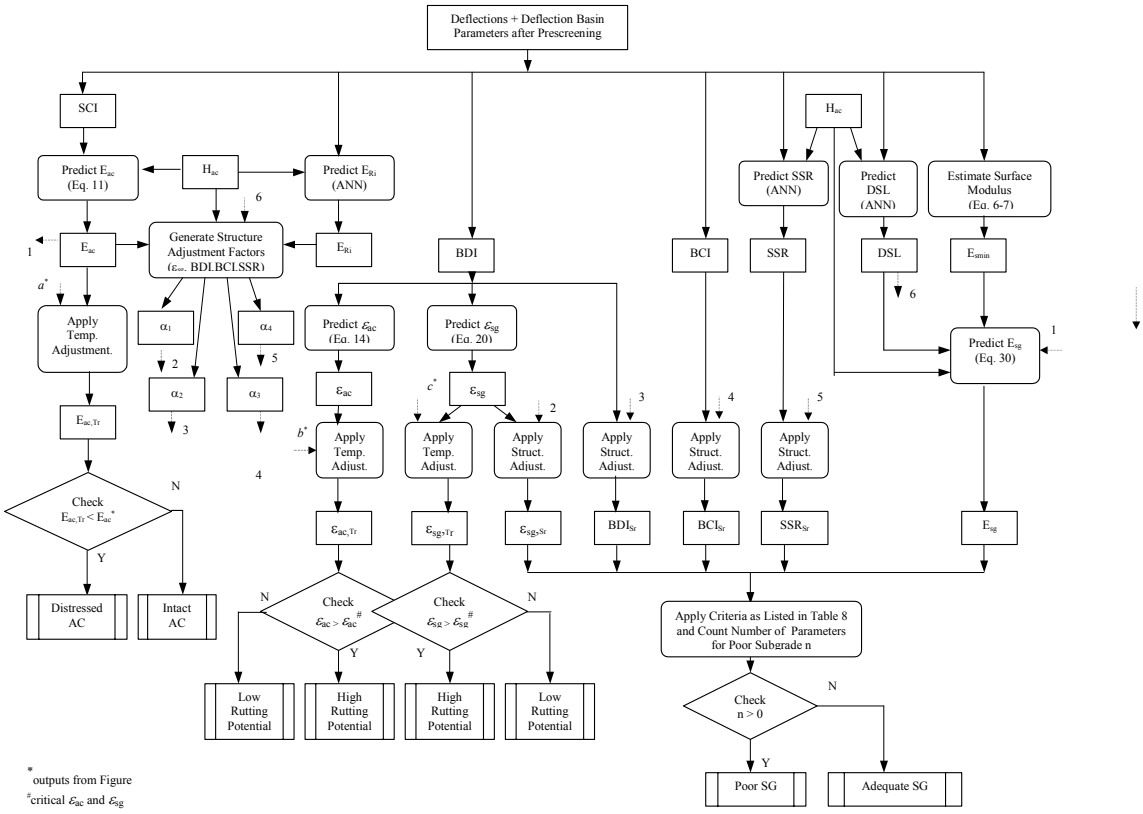

Figure C-9 Layer condition assessment procedure for aggregate base pavement

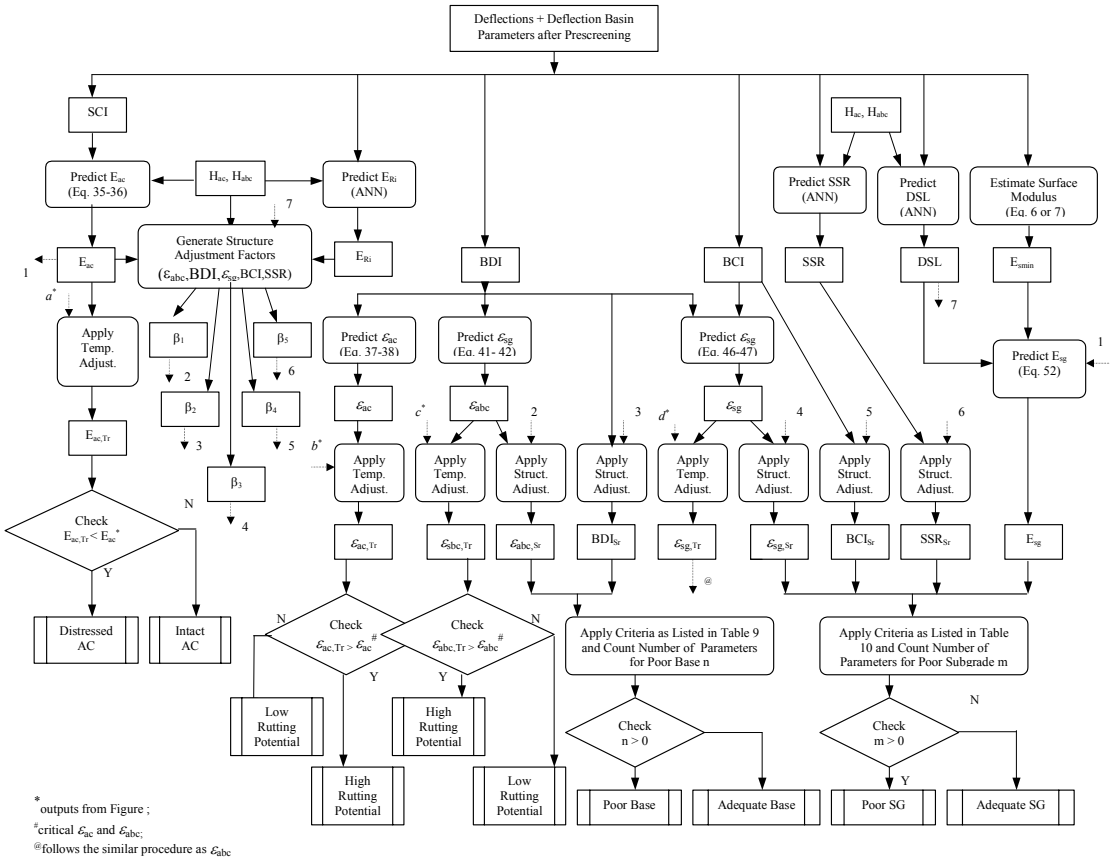

Figure C-10 Layer condition assessment procedure for full-depth pavement

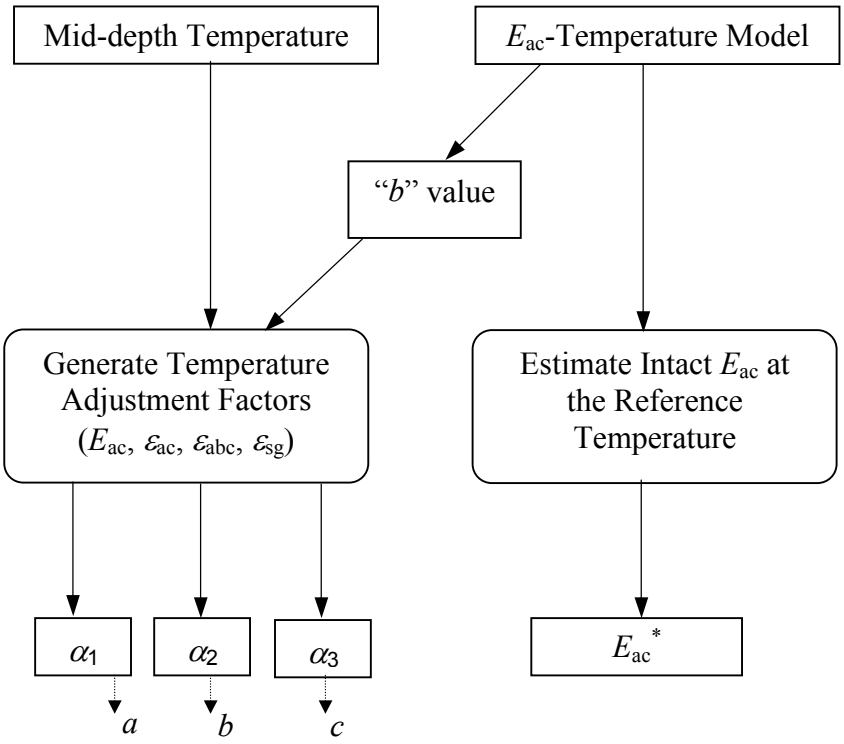

Figure C-11 Procedure for generating temperature adjustment factors for full-depth pavements

Results Display Menu

This menu item includes the following options: *Deflection Data, Output Figures, Output Tables,* and *Print Summary Output File.*

Deflection Data

This option allows the user to view the deflection data that was used in the analysis. Depending on the analysis chosen, Display Deflection Data A and Display Deflection Data B interface will be invoked. The Display Deflection Data interface, similar to the Deflection Data Screening interface described above, is used to display the

variation of deflection, surface modulus, and SLIC method information with sensor locations. A *Print* option allows the user to print the graphs.

Output Figures

Selecting this option displays the outputs from the analyses in a set of graphs. The graphical outputs are displayed in the Output Figures A (Figure C-12) or Output Figures B (Figure C-13) interface depending on the analysis applied. The difference between these two interfaces is that Output Figures B has more items (condition indicators) to display.

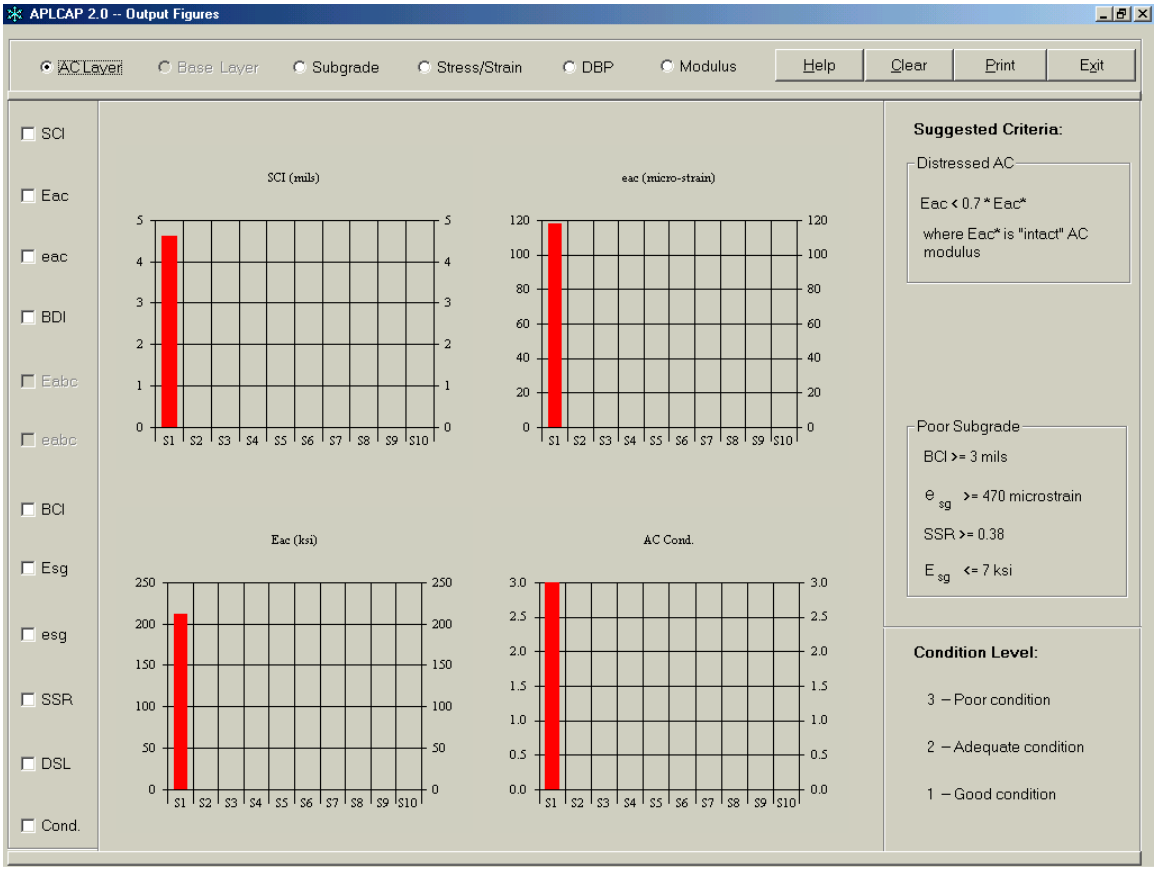

Figure C-12 Output Figures A interface

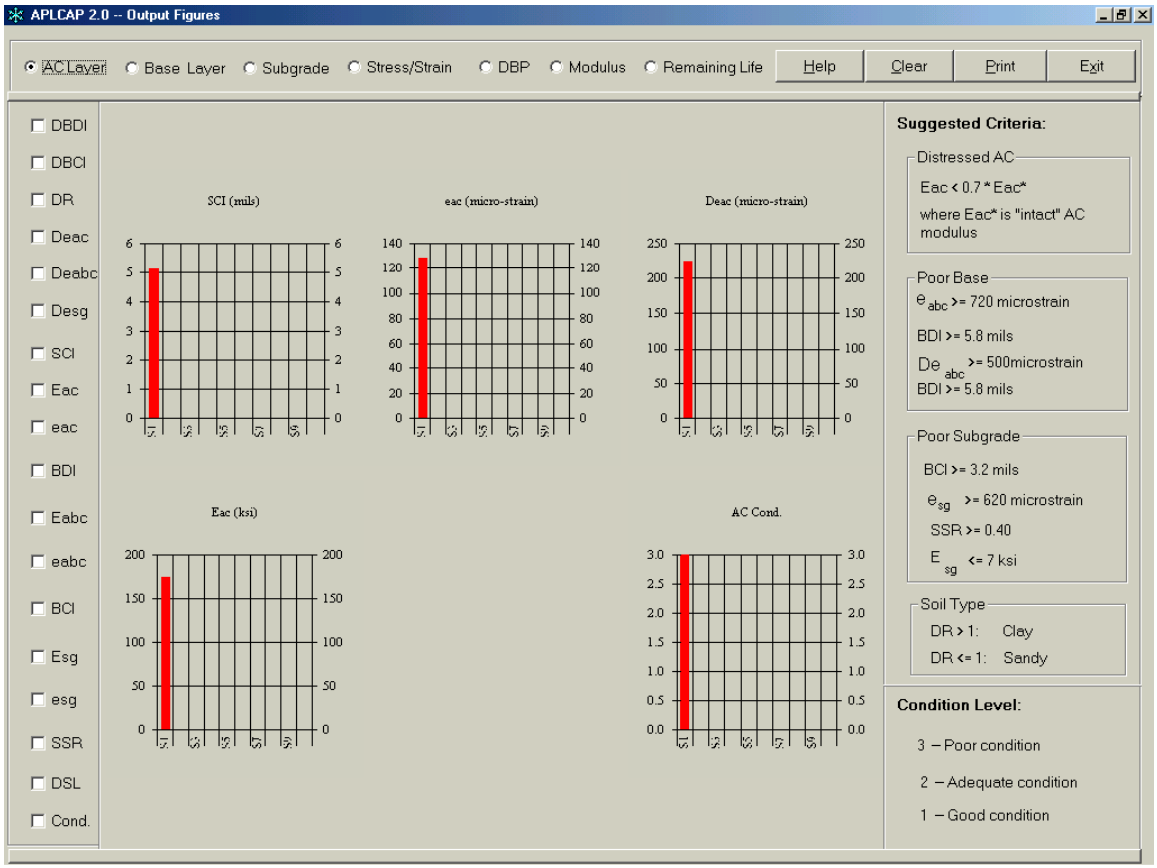

Figure C-13 Output Figures B interface

The center panel is used for displaying the selected graphs. The user may select the output(s) to display from the list of items shown in the left panel. To minimize crowding, a maximum of only four items could be displayed at a time. The top panel includes a set of preselected outputs grouped by different layers, as well as the final condition evaluation of distress levels of all layers. For example, the user could view all the relevant output graphs (e.g., SCI, surface layer modulus, condition evaluation) associated with the AC layer. Again, the *Print* option allows the user to send the screen display to a printer.

Output Tables

Selecting this option displays a table that summarizes all the outputs from the analyses. Outputs for all locations and condition evaluation parameters are shown in a single table in the Output Tables A (Figure C-14) or Output Tables B (Figure C-15) interface depending on the analysis. Again, the *Print* option allows the user to send the table to a printer.

Print Summary Output File

When the *Analyze FWD Data* menu option is invoked, all the outputs from the analyses are written to a summary file in ASCII format. By selecting this menu option, the user sends this file out to a printer.

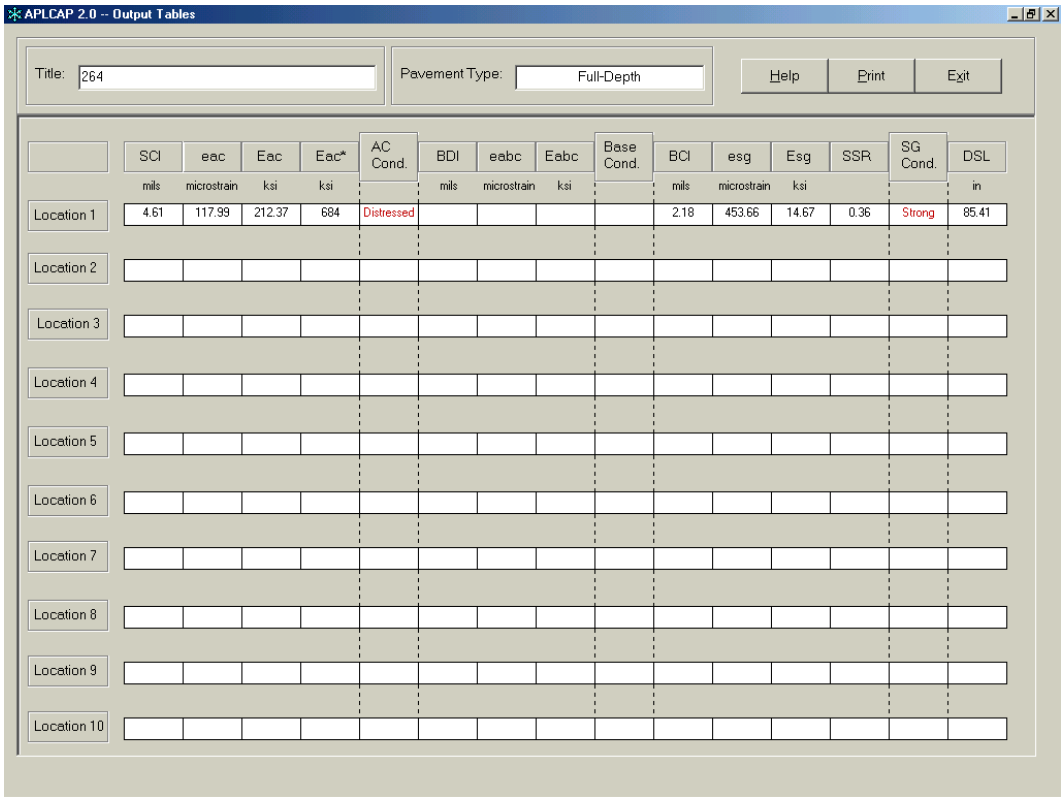

Figure C-14 Output Tables A interface

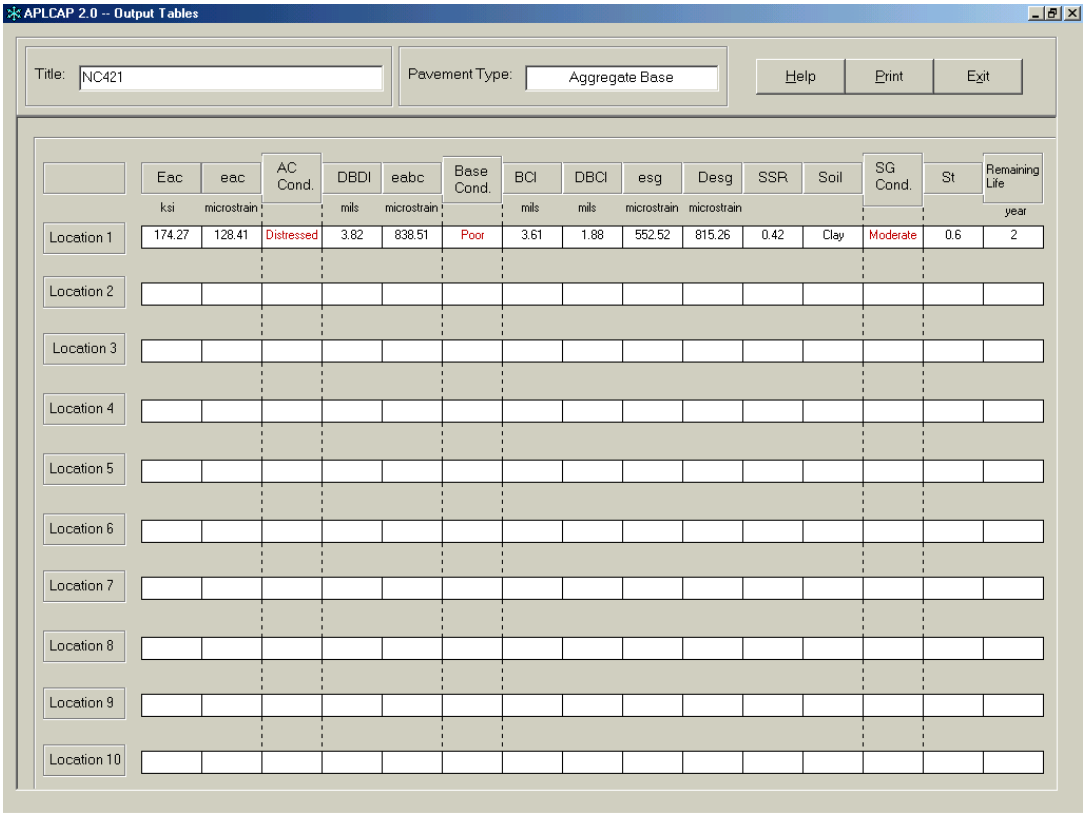

Figure C-15 Output Tables B interface

Help Menu

This menu item provides a summary help screen. Information in here is limited to providing an overview. More detailed help instructions are provided in each screen via a Help button. In addition, information about items displayed on the different interfaces is provided through Windows-style pop-up notes when the cursor is placed over an item.